Role of AMP-activated Protein Kinase (AMPK) in regulation of Perivascular Adipose Tissue (PVAT) function

Ali Abdulmajed Ali Al-Ferjani
MBChB, MSc

Thesis submitted in fulfilment of the requirements for the degree of Doctor of Philosophy in School of Cardiovascular and Metabolic Health

May 2024

School of Cardiovascular and Metabolic Health

College of Medical, Veterinary and Life Sciences

University of Glasgow

Abstract

Most blood vessels are surrounded by a layer of adipose tissue known as perivascular adipose tissue (PVAT). PVAT has an endocrine role, releasing a wide array of biologically active molecules, including adipokines, cytokines/chemokines, growth factors, reactive oxygen species, nitric oxide, and hydrogen sulphide (H_2S), and other factors yet undetermined. These molecules exert a profound influence on vascular function under both physiological and pathophysiological conditions. While some of these factors possess vasorelaxant properties, referred to as PVAT-derived relaxing factors (PVRFs), others influence vascular tone by inducing vasoconstriction.

The exact mechanism(s) underlying the anti-contractile effect of PVAT remain incompletely understood, although much evidence suggests that PVRFs may activate K^+ channels on vascular smooth muscle cells (VSMCs) or endothelial nitric oxide synthase (eNOS) in endothelial cells possibly via AMP-activated protein kinase (AMPK). AMPK is a serine/threonine kinase with many potential physiological functions, including regulation of energy haemostasis. AMPK is expressed in all layers of the blood vessel, including the PVAT, and it is known that activation of AMPK leads to vascular dilatation via both endothelium- and non-endothelium-dependent mechanisms.

A previous study in our laboratory has demonstrated that AMPK mediates the anticontractile effect of PVAT on VSMCs. Therefore, this project aimed to investigate the contribution of AMPK to the endothelium-dependent anticontractile effect of PVAT in two distinct anatomical locations: the thoracic and abdominal aorta.

Experiments were conducted using wild type (WT) and global AMPKα1 knockout (KO) mice aortae. The anti-contractile effect of PVAT was studied by measuring the relaxation response to AMPK-independent vasodilator cromakalim in vessels contracted with phenylephrine using wire myography. Whereas the secretory function of the PVAT was tested using an immunoblotting array and ELISA. Immunoblotting methods were used to test eNOS and AMPK activity in the cultured Human Umbilical Vein Endothelial Cells (HUVECs).

Endothelium-intact thoracic and abdominal aortic rings from WT and KO mice were mounted on a wire myograph in the presence and absence of PVAT. The responses to the AMPK-independent vasodilator cromakalim were subsequently assessed. Relaxation responses to cromakalim in the WT abdominal vessels were significantly higher compared to abdominal vessels from KO mice. However, no significant difference in response to cromakalim were reported in thoracic aortae of both genotypes.

Adipokine array and ELISA demonstrated that fibroblast growth factor-21 (FGF-21) release is significantly reduced in conditioned media (CM) from the abdominal-aortic PVAT of KO mice in comparison with WT CM. FGF-21, known for its impact on endothelial cells, did not induce alterations in eNOS activity or nitric oxide release in HUVECs or 3T3-L1 adipocytes. Moreover, addition of FGF-21 had no effect on the PE-induced contraction and did not alter acetylcholine-induced relaxation in WT vessels lacking PVAT. However, there are some considerations (as discussed later) that need to be addressed.

In conclusion, this study suggests that AMPKα1 plays a significant role in maintaining the anti-contractile effect of abdominal PVAT; potentially through regulating adipokine secretion. Although FGF-21 did not show a significant effect on eNOS phosphorylation and nitric oxide release, its expression and release by abdominal PVAT, and likely other white adipose tissue depots is regulated by AMPK. This finding could be of clinical importance as both AMPK and FGF-21 share a different metabolic profile and could be promising candidates for drug development targeting metabolic diseases such as type 2 diabetes and metabolic syndrome.

Table of contents

Abstract ii
Table of contents iv
List of Figures viii
List of Tables x
Acknowledgements xi
Author's Declaration xii
List of Abbreviations xiii
Published abstracts. 1
Chapter 1 Introduction 2
1.1 Anatomy of the cardiovascular system 3
1.1.1 Endothelium (Tunica intima) 4
1.1.2 Vascular smooth muscle layer (Tunica media) 5
1.1.3 Adventitia and Perivascular adipose tissue (tunica externa) 7
1.2 Adipose tissue (general features) 7
1.3 Perivascular adipose tissue (PVAT) 9
1.3.1 PVAT-derived mediators 10
1.3.2 Role of PVAT in regulating vascular tone 11
1.3.3 Mechanism of the anticontractile effect of PVAT 13
1.3.4 PVAT and metabolic diseases: 15
1.4 AMP-activated protein kinase (AMPK) 17
1.4.1 Overview of AMPK 17
1.4.2 Pharmacological Activators of AMPK 20
1.4.3 Role of AMPK in the Vasculature 21
1.5 Hypothesis and Aims 27
Chapter 2 Materials and Methods 29
2.1 Animals 30
2.2 List of materials and suppliers 30
2.2.1 List of materials 30
2.2.2 List of specialist equipment and suppliers 32
2.3 List of antibodies 32
2.3.1 Primary antibodies for Immunoblotting 32
2.3.2 Secondary antibodies for Immunoblotting 34
2.4 Standard solutions 34
Methods 36
2.5 Genotyping 36
2.5.1 DNA extraction 36

2.5.2 Polymerase Chain Reaction for AMPKα1 Wild type (WT) and AMPKα1 Knockout (KO) 37
2.5.3 Gel preparation and electrophoresis 37
2.6 Functional studies (wire myography) 37
2.6.1 Preparation of the vessels 37
2.6.2 Testing the viability of the endothelium 39
2.6.3 Cumulative Dose response curves 40
2.6.4 Effect of FGF-21 on vascular relaxation 40
2.6.5 Preparation of PVAT conditioned media for adipokine array 40
2.6.6 Mouse Adipokine Array (Proteome Profiler) 40
2.6.7 FGF-21 ELISA 41
2.7 Human umbilical vein endothelial cell (HUVEC) culture 42
2.7.1 Recovery of cryopreserved cell stocks from liquid nitrogen 42
2.7.2 Passaging of HUVECs 42
2.7.3 Preparation of HUVEC lysates 43
2.8 Determination of protein concentration 43
2.9 Western blotting of Proteins 44
2.9.1 SDS- polyacrylamide gel electrophoresis 44
2.9.2 Electrophoretic transfer of proteins from gels onto nitrocellulose membranes 44
2.9.3 Blocking of membranes and probing with primary antibodies 45
2.9.4 Secondary antibody and immunodetection of proteins 45
2.9.5 Stripping of nitrocellulose membranes 46
2.9.6 Densitometric quantification of protein bands 46
2.10 Determination of FGF-21 level in PVAT 46
2.11 RNA extraction and reverse transcription polymerase chain reaction (RT-PCR) 47
2.11.1 PVAT RNA extraction and purification 47
2.11.2 Reverse transcription 48
2.11.3 Quantitative real time Polymerase Chain Reaction (PCR) 48
2.12 NO measurement assay (Sievers NO meter) 48
2.12.1 Preparation of the PVAT conditioned medium for NO analysis. 48
2.12.2 Preparation of HUVEC conditioned media for NO analysis 49
2.12.3 Detection of nitric oxide (NO) 49
2.12.4 Statistical analysis 49
Chapter 3 Role of AMPKα1 in modulating PVAT function (functional study) 51
3.1 Introduction 52
3.2 Aims of the study 55
3.3 Results 56

3.3.1 Effects of AMPKα1 on phenylephrine-induced contraction in endothelium intact and denuded WT and KO thoracic aortic rings..... 56
3.3.2 Effect of PVAT on PE-induced vascular contraction in WT thoracic aortic rings..... 57
3.3.3 Effect of endothelium on PE-induced vascular contraction in WT and KO abdominal aortic rings 57
3.3.4 Effect of PVAT on PE-induced vascular contraction in abdominal aortic rings. 58
3.3.5 Effect of genotype on cromakalim-induced vascular relaxation in endothelium intact and denuded thoracic aortic rings. 59
3.3.6 Effect of PVAT on cromakalim-induced vascular relaxation in wild-type thoracic aortic rings. 60
3.3.7 Effect of genotype on cromakalim-induced vascular relaxation in endothelium-intact abdominal aortic rings in the presence or absence of PVAT. 61
3.3.8 Effect of PVAT on cromakalim-induced vascular relaxation in abdominal aortic rings. 63
3.3.9 Phenylephrine does not stimulate AMPK in HUVECs 64
3.3.10 Cromakalim and phenylephrine do not activate AMPK or increase eNOS phosphorylation in HUVECs. 65
3.4 Discussion 67
3.5 Conclusion..... 73
Chapter 4 Effect of AMPKα1 on PVAT secretory function 74
4.1 Introduction..... 75
4.2 Aims of the study..... 77
4.3 Results 78
4.3.1 PVAT weight in thoracic and abdominal region. 78
4.3.2 AMPKα1 knockout mouse PVAT has altered adipokine release. 78
4.3.3 Abdominal PVAT from AMPKα1 knockout mice releases less FGF-21 .. 82
4.3.4 AMPKα1 knockout PVAT has reduced FGF-21 levels..... 83
4.3.5 *Fgf21* mRNA levels were not altered in AMPKα1 knockout mice. 84
4.3.6 Serum FGF-21 levels are not altered in AMPKα1 knockout mice. 85
4.3.7 Nitric oxide release by PVAT 86
4.3.8 Effect of PVAT conditioned medium on AMPK activity in HUVECs. 87
4.3.9 Effect of PVAT conditioned medium on eNOS stimulation in HUVECs. 88
4.3.10 Effect of PVAT conditioned medium on Akt stimulation in HUVECs.. 89
4.3.11 Effect of PVAT conditioned medium on ERK1/2 stimulation in HUVECs. 90
4.4 Discussion 91
4.5 Conclusion..... 99
Chapter 5 The effect of FGF-21 on cell signalling, NO analysis and vasorelaxation 100

5.1 Background....101
5.2 FGF-21 and AMPK:....102
5.3 FGF-21 and adiponectin:....104
5.4 Association of FGF-21 with cardiovascular risk and atherosclerosis....104
5.4.1 Role of FGF-21 in atherosclerosis....105
5.5 Aims of the study....108
5.6 Results....109
5.6.1 Effect of FGF-21 on AMPK activity in HUVECs....109
5.6.2 Effect of FGF-21 on eNOS phosphorylation in HUVECs....110
5.6.3 Effect of FGF-21 on Akt phosphorylation in HUVECs....111
5.6.4 Effect of FGF-21 on ERK1/2 phosphorylation in HUVECs....112
5.6.5 Effect of FGF-21 on nitric oxide release by HUVECs....113
5.6.6 Validation of human FGF-21 protein....113
5.6.7 Klotho level in HUVECs....114
5.6.8 Effect of FGF-21 on eNOS, AMPK, Akt, and ERK1/2 phosphorylation in 3T3-L1 adipocytes....115
5.6.9 Effect of FGF-21 on nitric oxide release by 3T3-L1 adipocytes....118
5.6.10 Effect of FGF-21 on nitric oxide release by PVAT....118
5.6.11 Effects of FGF-21 on vascular contraction/relaxation in thoracic aortic rings....119
5.7 Discussion....121
5.8 Conclusion:....127
Chapter 6 General Discussion....128
6.1 Summary and Discussion of Results....129
6.2 Limitations:....144
6.3 Conclusion:....145
List of References....146

List of Figures

Figure 1-1 Structure of the vascular wall. 4

Figure 1-2 AMPK α, β, and γ subunits 18

Figure 1-3 AMPK activation by upstream kinases and metabolic outcomes..... 19

Figure 2-1 AMPKα1 genotyping. 37

Figure 2-2 An illustration of segmentation of mouse aorta into four segments namely the ascending aorta, the aortic arch, the thoracic aorta and the abdominal aorta. 38

Figure 2-3 The wire myograph..... 39

Figure 2-4 Testing the viability of endothelium 39

Figure 2-5 Protein transfer..... 45

Figure 3-1 Effects of AMPKα1 on phenylephrine-induced contraction in endothelium intact and denuded WT and KO thoracic aortic rings 56

Figure 3-2 Effect of PVAT on PE-induced vascular contraction in wild-type thoracic aortic rings..... 57

Figure 3-3 Effect of endothelium on PE-induced vascular contraction in wild-type and AMPKα1 knockout abdominal aortic rings 58

Figure 3-4 Effect of PVAT on PE-induced vascular contraction in abdominal aortic rings. 59

Figure 3-5 Effect of genotype on cromakalim-induced vascular relaxation in endothelium intact and denuded thoracic aorta. 60

Figure 3-6 Effect of PVAT on cromakalim-induced vascular relaxation in wild-type thoracic aorta..... 61

Figure 3-7 Effect of genotype on cromakalim-induced vascular relaxation in endothelium-intact abdominal aortic rings in the presence or absence of PVAT.62

Figure 3-8 Effect of genotype on cromakalim-induced vascular relaxation in abdominal aortic rings in the presence or absence of endothelium. 63

Figure 3-9 Effect of PVAT on cromakalim- induced vascular relaxation in abdominal aortic rings 64

Figure 3-10 Effect of phenylephrine on basal and stimulated AMPK activity in HUVECs..... 65

Figure 3-11 Effect of cromakalim and phenylephrine on AMPK and eNOS phosphorylation following different incubation times in HUVECs. 66

Figure 4-1 PVAT weight in thoracic and abdominal region 78

Figure 4-2 Adipokine levels in wild type and AMPKα1 KO thoracic PVAT conditioned medium. 80

Figure 4-3 Adipokine levels in wild type and AMPKα1 KO abdominal PVAT conditioned medium. 82

Figure 4-4 FGF-21 in wild type and AMPKα1 KO PVAT conditioned medium. 83

Figure 4-5 FGF-21 levels in abdominal PVAT 84

Figure 4-6 *Fgf21* mRNA expression in WT and AMPKα1 KO PVAT 85
Figure 4-7 Serum FGF-21 levels in wild type and AMPKα1 KO mice..... 85
Figure 4-8 NOx production by aortic PVAT of wild type and AMPKα1 KO mice... 86
Figure 4-9 Effect of PVAT conditioned medium on AMPK activity in HUVECs. ... 87
Figure 4-10 Effect of PVAT conditioned medium on eNOS stimulation in HUVECs. 88
Figure 4-11 Effect of PVAT conditioned medium on Akt stimulation in HUVECs. 89
Figure 4-12 Effect of PVAT conditioned medium on ERK1/2 stimulation in HUVECs..... 90
Figure 5-1 FGF-21/FGFR/ß-Klotho complex 102
Figure 5-2 Effect of FGF-21 on AMPK activity in HUVECs 109
Figure 5-3 Effect of FGF-21 on eNOS phosphorylation in HUVECs 110
Figure 5-4 Effect of FGF-21 on Akt phosphorylation in HUVECs 111
Figure 5-5 Effect of FGF-21 on ERK1/2 phosphorylation in HUVECs 112
Figure 5-6 Effect of FGF21 on nitric oxide release by HUVECs 113
Figure 5-7 Validation of human FGF-21 protein.....114
Figure 5-8 Klotho expression in HUVECs and 3T3-L1 adipocytes 114
Figure 5-9 Effect of FGF-21 on eNOS, AMPK, AKT, and ERK1/2 phosphorylation in 3T3-L1 adipocytes 117
Figure 5-10 Effect of FGF-21 on nitric oxide release by 3T3-L1 adipocytes 118
Figure 5-11 Effect of FGF-21 on nitric oxide release by PVAT 119
Figure 5-12 Effects of FGF-21 on vascular contraction/relaxation in thoracic aortic rings 120

List of Tables

Table 2-1. Primary antibodies for Western blotting..... 33
Table 2-2.Secondary antibodies for Western blotting 34
Table 2-3.Details of the primers and their sequences. 36
Table 2-4 Taqman probes 48

Acknowledgements

In the name of Allah, the Most Gracious and the Most Merciful. First and foremost, I would like to express my gratitude to Allah (God) for providing me the blessings to complete this work.

I extend my sincere appreciation to my esteemed supervisors, Prof. Simon Kennedy and Dr. Ian Salt, for their invaluable scientific guidance, unwavering support, encouragement, and patient responses to my inquiries. Additionally, I wish to express gratitude to the Libyan Ministry of Higher Education and Scientific Research and my University for their generous support and funding throughout this project.

There are many people whose help over the years has been invaluable and greatly appreciated, at the University of Glasgow. Special thanks to the members of Kennedy and Salt groups, past and present for helping me with just about everything. Thanks, should also go to the laboratory technician, John McAbney, for his invaluable support and guidance.

To my beloved wife: I am absolutely unable to comprehend your patience with me throughout my academic career; your love and unwavering support have made this success a reality.

To my kids, Abdulmomen, Abdulmuhaymin, Mohammed, and Mayan: with your beautiful smiling faces, you truly are the best gift I have ever received.

Finally, I would like to dedicate this work to my parents, I will remain forever unable to repay your loving kindness and compassion that began before I was born and continues unabated.

Author's Declaration

I declare that this thesis has been written solely by me with the research entirely generated by myself, unless otherwise stated. It is entirely of my own composition and has not, in whole or in part, been submitted for any other degree.

This project was under the supervision of Prof. Simon Kennedy and Dr. Ian Salt.

Ali Al-Ferjani

May 2024

List of Abbreviations

3T3-L1	Fibroblast cell line isolated from 3T3 mouse embryo
A769662	6,7-Dihydro-4-hydroxy-3-(2′-hydroxy[1,1′-biphenyl]-4-yl)-6-oxo- thieno[2,3-b]pyridine-5-carbonitrile
ACC	Acetyl-CoA Carboxylase
ADRF	Adipocyte-Derived Relaxing Factor
AICAR	5-Aminoimidazole-4-Carboxamide 1-ß-D-Ribonucleoside
AMPK	AMP-Activated Protein Kinase
Akt	Protein Kinase B
BAT	Brown Adipose Tissue
BSA	Bovine Serum Albumin
CaMKKß	Calcium/Calmodulin-dependent Protein Kinase Kinase ß
CBM	Carbohydrate-Binding Module
CBS	Cystathionine-ß-Synthase
cGMP	Cyclic Guanosine Monophosphate
CTD	C-terminal domain
CVD	Cardiovascular Diseases
DMEM	Dulbecco's Modified Eagle's Medium
DMSO	Dimethyl Sulfoxide
eNOS	Endothelial NO Synthase
ERK1/2	Extracellular signal–Regulated Kinases 1/2
PAGE	Polyacrylamide gel electrophoresis
PBS	Phosphate Buffered Saline
PBST	PBS + Tween 20
PCR	Polymerase Chain Reaction
PI3K	Phosphatidylinositol-3-kinase
PKA	Protein kinase A
PKB	Protein kinase B
PKC	Protein kinase C
PPARγ	Peroxisome Proliferator-Activated Receptor γ
PVAT	Perivascular Adipose Tissue
ROS	Reactive Oxygen Species
SAT	Subcutaneous Adipose Tissue
SDS	Sodium Dodecyl Sulphate
SDS-PAGE	SDS-polyacrylamide gel electrophoresis
siRNA	Small interfering RNA

T2DM	Type 2 Diabetes Mellitus
TEMED	N, N, N', N'-tetramethylenediamine
TNF-α	Tumour Necrosis Factor α
TZDs	Thiazolidinediones
UCP-1	Uncoupling Protein 1
VEGF-A	Vascular Endothelial Growth Factor A
VSMCs	Vascular Smooth Muscle Cells
VAT	Visceral adipose tissue
WAT	White Adipose Tissue
ZMP	5-aminoimidazole-4-carboxamide-1-ß-D-furanosyl 5'-monophosphate

Published abstracts.

1. Hwej, AS., Al-Ferjani, A., Salt, I., Kennedy, S. 2020. Role of perivascular adipose tissue AMP-activated protein kinase (AMPK α 1) in regulation endothelium function and NO release. *Heart Journal*- Scottish Cardiovascular Forum- 23rd annual meeting. *https://doi.org/10.1136/heartjnl-2020-SCF.21*

2. Al-Ferjani, A., Salt, I., Kennedy, S. 2021. Deletion of AMPKα1 attenuates the anticontractile effect of perivascular adipose tissue (PVAT) in endothelium-intact mouse aorta. Selected Abstracts from Pharmacology 2020. *Br J Pharmacol*, 178(2):381-486. https://doi.org/10.1111/bph.15316

3. Al-Ferjani, A., Salt, I., Kennedy, S. 2023. PVAT-secreted -FGF21 does not mediate the anticontractile function of PVAT. Abstracts of the 19th World Congress of Basic & Clinical Pharmacology 2023. *Br J Pharmacol*. *https://doi.org/10.1111/bph.16105*

Chapter 1 Introduction

1.1 Anatomy of the cardiovascular system

The cardiovascular system (circulatory system) consists of the heart, blood vessels, and blood. Its primary function is to transport nutrients and oxygen-rich blood to all parts of the body and to carry deoxygenated blood back to the lungs (Aaronson *et al.*, 2020). It consists of the heart and a closed system of blood vessels. The heart is a muscular pump that forces blood around the body. The blood vessels include arteries, arterioles, capillaries, venules, and veins. Arteries are vessels that carry blood from the heart to the tissues (Chaudhry *et al.*, 2023). Large, elastic arteries leave the heart and divide into medium-sized, muscular arteries that branch out into the various regions of the body. Medium-sized arteries then divide into smaller arteries called arterioles (Aaronson *et al.*, 2020). As the arterioles enter a tissue, they branch into countless microscopic vessels called capillaries. Before leaving the tissue, groups of capillaries unite to form small veins called venules (Chaudhry *et al.*, 2023). These in turn, merge to form progressively larger blood vessels called veins. Veins then convey blood from the tissues back to the heart. Since the cells within the walls of blood vessels require oxygen and nutrients just like other tissues of the body, they also have a system of tiny blood vessels, called vasa vasorum, in their own walls.

The walls of all blood vessels except capillaries have three layers Figure 1-1. The inner layer (tunica intima/interna) consists of flattened endothelial cells which provide a smooth lining over which the blood can flow easily (Aaronson *et al.*, 2020). The middle layer is composed of a circular layer of smooth muscle (tunica media) and the outer layer (tunica externa) consists of two layers: adventitia compacta, a layer of mainly fibroblasts, and perivascular adipose tissue (PVAT) which surrounds most blood vessels (Touyz *et al.*, 2018). Capillary walls are composed of only a single layer of cells (endothelium) and a basement membrane (Aaronson *et al.*, 2020). They have no tunica media or tunica externa. This structure of capillaries permits the exchange of nutrients and waste products between the blood and tissues.

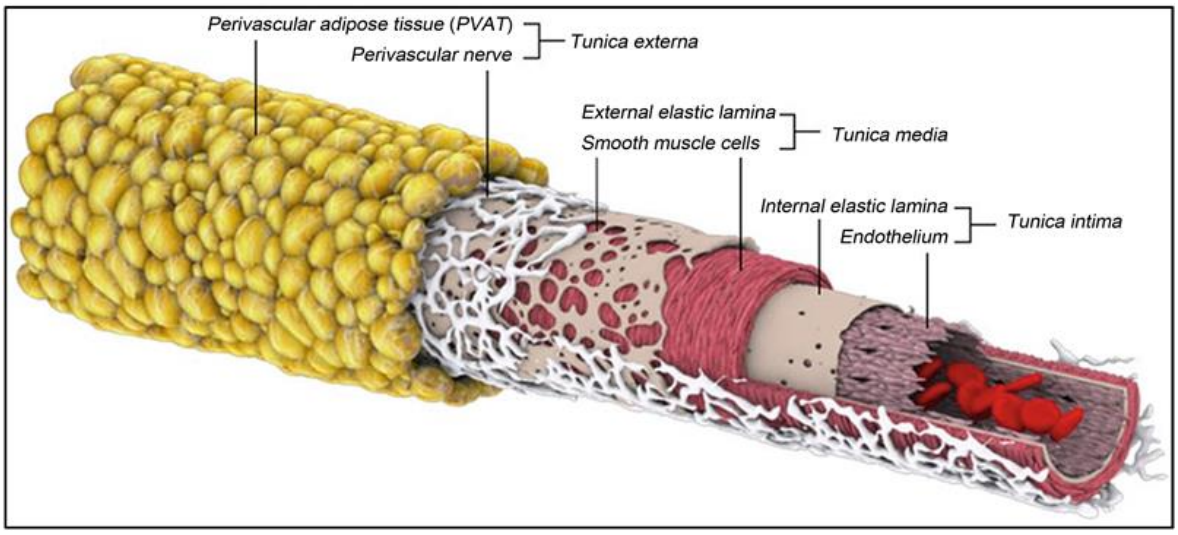

Figure 1-1 Structure of the vascular wall.

The vascular wall is composed of three layers: The endothelium (tunica intima), vascular smooth muscle cells (tunica media) and the adventitia (tunica externa), which contains perivascular adipose tissue cells, fibroblast cells, collagen fibers and nerve endings (Daly, 2019).

1.1.1 Endothelium (Tunica intima)

The vascular endothelium is a single layer of flattened endothelial cells (ECs) that line the lumen of all blood and lymphatic vessels, and structurally and metabolically separates the vascular wall and tissues from the circulating blood and its components (Luscher and Vanhoutte, 2020). The vascular endothelium, once considered a passive lining of arteries, is now recognized as a selective permeability barrier and a vital mediator in various biological processes. These include the regulation of vascular tone, haemostasis, immune responses, and inflammation (Luscher and Vanhoutte, 2020). The role of the endothelium in the regulation of vascular function was first recognised in 1980 when Furchgott and Zawadzki reported that the relaxations evoked by acetylcholine in the aorta and other arteries of the rabbit depend on the presence of ECs (Furchgott and Zawadzki, 1980).

The vascular endothelium synthesizes and secretes a multitude of vasoactive factors. Among them are vasoconstrictors like endothelin-1 (ET-1) and platelet-activating factor (PAF), along with vasorelaxant factors such as nitric oxide (NO), prostacyclin (PGI_2), and endothelium-derived hyperpolarizing factor (EDHF) (Sandoo *et al.*, 2010). Additionally, healthy endothelium acts as a gatekeeper for organ/tissue homeostasis and blood pressure regulation by supplying antioxidant,

anti-inflammatory, and antithrombotic activity as well as supporting the preservation of vascular tone (Eelen *et al.*, 2015). Maintaining a delicate equilibrium between the endothelium-derived relaxing and contracting factors is crucial for tightly regulating vascular function. Disruption of this balance indicates endothelial dysfunction, a significant contributor to chronic cardiometabolic disorders such as obesity, diabetes, hypertension, dyslipidaemia, and atherosclerotic vascular diseases (Wang *et al.*, 2022). Endothelial dysfunction is marked by vasoconstriction, increased cell proliferation, and a shift towards a proinflammatory and prothrombotic state (Gallo *et al.*, 2021). Among the various proposed cellular and molecular mechanisms contributing to endothelial dysfunction, oxidative stress and inflammation emerge as pivotal players, making them natural targets for intervention in patients with cardiovascular and metabolic diseases (Wang *et al.*, 2022).

1.1.1.1 Nitric oxide and regulation of vascular tone

Nitric oxide (NO) is an endogenously synthesised gaseous signaling molecule that has important functions in vascular relaxation and is an important regulator of many physiological processes across various systems. It is synthesised from the amino acid L-arginine, in the presence of molecular oxygen and NADPH, by a class of enzymes called nitric oxide synthases (NOS), one of which, eNOS is expressed mainly in vascular endothelial cells (Su, 2014). NO diffuses into vascular smooth muscle cells (VSMCs) and activates guanylyl cyclase, which increases cGMP production. cGMP causes VSMC relaxation by reducing intracellular Ca^{2+} levels (Krawutschke *et al.*, 2015). The activation of guanylyl cyclase by NO and the subsequent increase in cGMP levels leads to the inhibition of smooth muscle contraction, resulting in vasorelaxation and increased blood flow. This mechanism is a key component of the regulation of vascular tone and blood pressure.

1.1.2 Vascular smooth muscle layer (Tunica media)

This medial layer is composed principally of several layers of VSMCs and elastic fibres. VSMCs are key determinants of the properties of vessels throughout the arterial tree. VSMC contraction is largely responsible for modulating arterial diameter in muscular arteries and arterioles, and VSMC-derived elastin is crucial for elastic recoil in large elastic arteries such as the aorta (Basatemur *et al.*,

2019). The media of smaller arteries and arterioles (resistance vessels) is composed of VSMCs with relatively few elastic fibres, and these vessels play a key role in regulating blood flow from arteries into capillaries through changes in peripheral vascular resistance.

The contraction and relaxation of the VSMCs plays a fundamental role in blood flow and blood pressure regulation. When they contract the vessels then shrink, leading to an increase in blood pressure. Contractions of VSMCs in response to mechanical, humoral, or neural stimuli is mediated by increases in the intracellular calcium (Ca^{2+}) concentration either by influx into the cell following opening of calcium channels in the plasma membrane or by release from internal stores (sarcoplasmic reticulum, SR) (Zhao *et al.*, 2015b; Touyz *et al.*, 2018). The intracellular free calcium ions interact with calmodulin and the calcium-calmodulin complex activates myosin light chain kinase (MLCK). Activated MLCK phosphorylates the myosin light chain (MLC), leading to smooth muscle contraction (Zhao *et al.*, 2015b).

On the other hand, VSMCs relaxation is initiated when cytosolic Ca^{2+} concentration is reduced. This is mediated by inactivation of L-type voltage-dependent Ca^{2+} channels with reduced calcium influx, activation of the sodium–calcium exchanger with increased calcium efflux and stimulation of calcium reuptake into the sarcoplasmic reticulum through the activation of sarcoplasmic/endoplasmic reticulum Ca^{2+}ATPase (SERCA)(Touyz *et al.*, 2018). Reduction of intracellular Ca^{2+} leads to activation of MLC phosphatase, MLC dephosphorylation and inhibition of MLC kinase (Brozovich *et al.*, 2016).

The major physiological regulators of VSMC contraction are endothelium-derived relaxing factors and the neurohumoral stimuli (Touyz *et al.*, 2018). Endothelium releases NO, PGI_2, and EDHFs which cause VSMC relaxation mainly by reducing intracellular Ca^{2+}. Autonomic nerves release vasoconstrictors like norepinephrine (from sympathetic nerve endings) and vasodilators like acetylcholine (from parasympathetic nerve endings). These act on receptors on VSMCs to either raise or lower intracellular Ca^{2+}, causing contraction or relaxation. The key hormones that regulate VSMC contraction are part of the renin-angiotensin-aldosterone system, catecholamines (norepinephrine/epinephrine), endothelin-1 (ET-1), vasopressin, and oxytocin. These hormones trigger VSMC contraction by G protein-

coupled receptor signaling that ultimately increases intracellular calcium levels in VSMCs.

Membrane potential controls the contraction and relaxation of VSMCs. The opening of L-type voltage-dependent Ca^{2+} channels, Ca^{2+} inflow, and cell contraction are all linked to the depolarization of the cell membrane. Nonetheless, hyperpolarisation reduces L-type Ca^{2+} channel opening, and the cell remains relaxed. Hyperpolarisation of the cell membrane is mediated by opening of K^+ channels in the cell membrane allowing K^+ efflux. There are four different types of K^+ channels known: ATP-sensitive (K_{ATP}), voltage-dependent (K_v), inward rectifying (K_{ir}), and Ca^{2+}-activated (K_{Ca}).

1.1.3 Adventitia and Perivascular adipose tissue (tunica externa)

The adventitia contains connective tissues and elastic fibres. Perivascular adipose tissue (PVAT) is an adipose tissue which surrounds most systemic blood vessels, except capillaries, pulmonary and cerebral blood vessels, with variable amounts (Brown *et al.*, 2014; Hillock-Watling and Gotlieb, 2022). The structure and function of the PVAT will be discussed in detail in section 1.3.

1.2 Adipose tissue (general features)

Adipose tissue (AT) is mainly composed of adipocytes as well as several other cell types including endothelial cells, fibroblasts, pericytes, preadipocytes, macrophages and several types of immune cells. These non-adipocyte cell types are commonly referred to as the AT stromal vascular fraction (SVF) (Richard *et al.*, 2020). AT secretes an array of signalling molecules, termed adipocytokines, which function as circulating hormones to communicate with other organs to regulate many aspects of human health including: energy homeostasis, lipid/glucose metabolism, reproduction and immune function (Coelho *et al.*, 2013; Koenen *et al.*, 2021)

AT is generally classified into two main types with distinct functions, phenotypes, and anatomical localisations and these are: brown adipose tissue (BAT) and white adipose tissue (WAT) (Li *et al.*, 2022). BAT uses energy for non-shivering heat production, which is critical for body temperature maintenance. WAT is critical

for energy storage, endocrine communication, and insulin sensitivity, and comprises the largest AT volume in most mammals including humans (Koenen *et al.*, 2021). There is also a third type of AT, termed the "beige" or "brite" (brown-in-white) adipose tissue (Stanek *et al.*, 2021). It has a brown-like phenotype interspersed within WAT and also has thermogenic capacity (Richard *et al.*, 2020; Li *et al.*, 2022). These three types of AT also have endocrine functions and play important roles in systemic metabolic processes, especially in obesity and its comorbidities, such as cardiovascular diseases (CVDs).

Histologically, WAT is characterised by adipocytes with single large lipid droplets and few mitochondria (Cinti, 2011; Koenen *et al.*, 2021). BAT is characterised by adipocytes with multiple small lipid droplets and abundant mitochondria containing uncoupling protein 1 (UCP-1; a brown fat marker)(Koenen *et al.*, 2021). Beige or mixed AT displays the morphological features of BAT with lower expression of UCP-1 (Fitzgibbons *et al.*, 2011; Pilkington *et al.*, 2021). Anatomically, AT is divided into visceral and subcutaneous AT. Visceral AT surrounds most internal organs and has been considered as a metabolically active depot, while subcutaneous AT is the fatty layer underneath the skin which acts as a buffering system for excess nutrient and fat accumulation (Lee *et al.*, 2013).

Historically, AT was considered as a passive reservoir for energy storage, as well as a supportive and thermoregulatory organ. In recent years however, AT has emerged as a major endocrine organ which releases a large number of adipokines, cytokines, and chemokines into the blood, affecting the functions of other organs (Qi *et al.*, 2018).

In cases of central obesity, WAT expands and secretes proinflammatory cytokines that have been strongly linked to the development of many metabolic diseases including insulin resistance, CVDs, and metabolic syndrome. This expansion is characterized by an increase in adipocyte size (hypertrophy) and number (hyperplasia), as well as increasing the number of macrophages resulting in the secretion and release of inflammatory mediators, including interleukin-6 (IL-6), interleukin 1ß, tumor necrosis factor-α (TNF-α), leptin, and stimulation of monocyte chemoattractant protein-1 (MCP-1), which subsequently reduce the production of adiponectin thereby initiating a proinflammatory state (Kwaifa *et al.*, 2020; Koenen *et al.*, 2021). The alterations in WAT which are linked to obesity

also impair endothelial function in blood vessels, encouraging the development of atherosclerotic plaque (Kwaifa *et al.*, 2020). Unlike WAT, BAT can take-up lipids to produce heat by uncoupling oxidation on the mitochondrial electron transport chain, which contributes to clearance of plasma lipids and prevents storage of lipids in WAT and other organs (Qi *et al.*, 2018). Dysfunctional WAT might be positively associated with atherosclerosis development, whereas activation of BAT, such as through cold exposure, decreases cholesterol and triglyceride levels, providing protection against the development of atherosclerosis. (Berbée *et al.*, 2015; Khedoe *et al.*, 2015; van Dam *et al.*, 2017).

The distribution of WAT and BAT depots are, to a large extent different depending on genetic background, age, gender, and environmental status (temperature, diet, exercise). Generally, WAT depots can be broadly classified as either subcutaneous or intra-abdominal. Subcutaneous WAT is located superficially just beneath the skin and is the predominant location in a normal weight individual, accounting for approximately 80% of all body fat (Ibrahim, 2010; Berryman and List, 2017). Intra-abdominal WAT can be further divided into visceral or non-visceral and collectively accounts for up to 10–20% of total fat in men and 5–8% in women (Berryman and List, 2017). In mice, the most prominent BAT depot is located in the interscapular region (between the shoulder blades) and it is often used as a model for studying BAT (Lidell *et al.*, 2013).

1.3 Perivascular adipose tissue (PVAT)

Perivascular adipose tissue (PVAT) is an AT that surrounds most systemic blood vessels including the aorta and arteries such as the carotids, coronaries and mesenteric vessels (Kim *et al.*, 2020). PVAT has been considered as an active component of the blood vessel walls, and is involved in vascular homeostasis through adipokine release (Szasz and Webb, 2012). Compared to subcutaneous and visceral AT, PVAT expresses lower levels of adipocyte-associated genes including genes encoding for PPARγ, C/EBPα, and FABP4, along with reduced lipid droplet formation (Chatterjee *et al.*, 2009). Similar to different types of adipose tissue in different depots, PVAT shows divergent types depending on the species, anatomic location and vascular bed, and understanding the modulatory role of these localised fat depots in CVDs has attracted much interest (Kim *et al.*, 2020). In rodents, which are used in the majority of experimental studies, PVAT surrounding

the thoracic aorta is similar to BAT (Fitzgibbons *et al.*, 2011; Almabrouk *et al.*, 2017; van Dam *et al.*, 2017), while PVAT surrounding abdominal, mesenteric, and carotid artery is more like WAT (Police *et al.*, 2009; Cinti, 2011; van Dam *et al.*, 2017). Compared with thoracic PVAT, abdominal PVAT expresses greater levels of inflammatory genes and markers of immune cell infiltration, and it is highly responsive to high-fat diet (HFD), suggesting that the WAT phenotype is more atherogenic and pro-inflammatory than the BAT phenotype in PVAT (Padilla *et al.*, 2013; Reynés *et al.*, 2019). In addition, histological analysis indicates a structural similarity between thoracic PVAT and BAT and between abdominal PVAT and visceral WAT (Padilla *et al.*, 2013).

Similar to AT, PVAT contains many types of cells (eg, mature adipocytes, preadipocytes, mesenchymal stem cells, and immune cells), which produce and secrete adipokines, cytokines and other undetermined factors which locally modulate PVAT metabolism and vascular function (Chang *et al.*, 2020; Kim *et al.*, 2020). PVAT secretes a wide variety of active adipocytokines with various endocrine, vasocrine and paracrine effects. Some of these active molecules originate from adipocytes, such as adiponectin, H_2S, leptin and omentin, while others are secreted from stromal inflammatory cells in the PVAT such as TNF-α and IL-6 (Akoumianakis *et al.*, 2017).

PVAT differs from other adipose tissue in its secretory profile. PVAT has been demonstrated to release higher levels of pro-inflammatory cytokines including IL-8, IL-6, and monocyte chemoattractant protein-1 (MCP-1), and lower levels of adiponectin and leptin compared to subcutaneous and visceral AT (Chatterjee *et al.*, 2009). PVAT is also distinguishable from classical BAT and WAT in terms of vessel-tone controlling function. Li *et al.* reported that mouse thoracic aortic PVAT, but not BAT and WAT extracts induced resting tone vasodilation and further attenuated phenylephrine-induced vasoconstriction (Li *et al.*, 2022). This highlights the role of PVAT in regulating vascular function compared to other adipose tissues.

1.3.1 PVAT-derived mediators

PVAT is an endocrine organ that releases a wide range of biologically active molecules (Chang *et al.*, 2020). Research suggests that these factors have a

profound influence in the vasculature under physiological or pathophysiological conditions (Xia and Li, 2017). Although the identity of all of these factors has not been completely defined, an extensive range of adipocytokines have been characterised, for instance adiponectin (Fésüs *et al.*, 2007; Almabrouk *et al.*, 2017), leptin (Vecchione *et al.*, 2002), resistin (Park *et al.*, 2014), visfatin (Wang *et al.*, 2009), chemerin (Watts *et al.*, 2013), hydrogen sulfide (H_2S) (Fang *et al.*, 2009), nitric oxide (NO) (Gil-Ortega *et al.*, 2010; Victorio *et al.*, 2016), and hydrogen peroxide (Gao *et al.*, 2007). PVAT also secretes inflammatory cytokines such as IL-8, IL-6, MCP-1 (Chatterjee *et al.*, 2009; Siegel-Axel *et al.*, 2014). These adipose tissue-secreted factors can be classified as proinflammatory, such as leptin, and anti-inflammatory, such as adiponectin (Man *et al.*, 2020).

In addition, PVAT also expresses and secretes high amounts of various growth factors, including thrombospondin-1, serpin-E1, TGF-ß, VEGF (vascular endothelial growth factor), bFGF (basic fibroblast growth factor), aFGF (acidic fibroblast growth factor), platelet-derived growth factor (PDGF)-BB, PLGF (placental growth factor), HGF (hepatocyte growth factor), and ILGFBP-3 (insulin-like growth factor-binding protein- 3) (Rittig *et al.*, 2012; Siegel-Axel *et al.*, 2014). These growth factors have well-defined effects in stimulation of VSMC proliferation and migration (Chang *et al.*, 2020). VSMC proliferation and migration play major roles in vascular disease pathology and remodeling processes which occur in conditions such as hypertension, atherosclerosis, and vascular aneurysm formation.

1.3.2 Role of PVAT in regulating vascular tone

Traditionally PVAT was thought to act merely as a mechanical support for the blood vessels and protect them against neighbouring tissues, and therefore it was removed and discarded by most investigators as it was thought to impair diffusion of exogenous substances. Consequently, its role on vasculature was not recognised for many years. Nowadays, convincing data from clinical and experimental animal models indicates that PVAT is involved in paracrine crosstalk with blood vessels and also in the physiological homeostasis and pathological changes of the cardiovascular system (Lian and Gollasch, 2016; Chang *et al.*, 2020). The direct contact of PVAT with the vascular wall permits it to communicate easily with the underlying vascular smooth muscle cells (VSMCs) and endothelial cells (ECs) by

releasing a plethora of vasoactive substances which promote either vasoconstriction or vasodilation via paracrine activities (Kim *et al.*, 2020). To study the role of PVAT on the vasoactivities of the blood vessels, rings from thoracic aorta, abdominal aorta, mesenteric, carotid, or coronary arteries with and without PVAT (or by incubation of vessel rings with PVAT extracts or with a conditioned buffer from an intact piece of PVAT) have been studied using *in vitro* organ bath or wire myograph techniques.

The paracrine effects of PVAT on blood vessels was first demonstrated in 1991 when Soltis and Cassis reported a significantly diminished response to norepinephrine in isolated endothelium-intact rat aortic rings with intact PVAT compared to PVAT-free vessel rings (Soltis and Cassis, 1991). They suggested that this anticontractile effect is due to increased norepinephrine reuptake by PVAT which has a dense sympathetic innervation. Eleven years later, Lohn *et al.* (2002) demonstrated an attenuation of the contractile response to angiotensin II, serotonin, and phenylephrine in intact vessels compared to PVAT-removed vessels (Löhn *et al.*, 2002). Unlike norepinephrine, these substances are not subject to adrenergic neuronal reuptake mechanisms (Löhn *et al.*, 2002). They found that this anticontractile effect is due to release of transferable factors from perivascular adventitia and these factors act through activation of potassium channels and tyrosine kinase in vascular smooth muscle cells and this action is not dependent on nitric oxide (NO) synthesis. Therefore, they suggested that perivascular adventitial adipose tissue releases what they termed an 'adventitium-derived relaxing factor' (ADRF). Later on, it became clear that these factors are released by PVAT and not by adventitia, and eventually the term PVAT-derived relaxing factors (PVRFs) was coined. PVAT not only produces PVRFs but also induces the secretion of PVAT-derived contracting factors (PVCFs) to maintain homeostasis and contribute to the microenvironment of PVAT (Meyer *et al.*, 2013; Li *et al.*, 2022).

Studies have suggested that potential PVRFs include: adiponectin (Fésüs *et al.*, 2007; Weston *et al.*, 2013; Almabrouk *et al.*, 2017), leptin (Gálvez-Prieto *et al.*, 2012), omentin, nitric oxide (NO) (Victorio *et al.*, 2016), angiotensin 1–7 (Lee *et al.*, 2009), hydrogen sulfide (Fang *et al.*, 2009; Liu *et al.*, 2022), hydrogen peroxide (H_2O_2) (Thengchaisri and Kuo, 2003; Gao *et al.*, 2007; Friederich-Persson

et al., 2017), prostacyclin (Chang *et al.*, 2012a), and methyl palmitate (Lee *et al.*, 2011). These factors are counteracted by PVCFs, such as superoxide anion (Gao *et al.*, 2006), tumour necrosis factor-α, prostaglandins (Chang *et al.*, 2012b; Mendizábal *et al.*, 2013), calpastatin (Owen *et al.*, 2013), catecholamines (Ayala-Lopez *et al.*, 2014; Kumar *et al.*, 2019), chemerin (Ferland *et al.*, 2017), and COX-derived vasoconstrictor prostanoids and thromboxane A_2 (Meyer *et al.*, 2013). Some of the mediators, such as H_2O_2, leptin, H_2S and prostanoids, have both contractile and relaxant actions on blood vessels depending on their concentrations, vessel type, contractile status, disease conditions, and animal species through a variety of mechanisms (Hayabuchi *et al.*, 1998; Gao and Lee, 2001; Quehenberger *et al.*, 2002; Gao and Lee, 2005; Cacanyiova *et al.*, 2019).

Thus, the majority of literature suggests that an overall "anticontractility" mediated by PVAT-derived substances is the major characteristic of PVAT vasoactivity. However, the ultimate regulatory effect on vascular tone is reflected by the balance of PVAT-derived vasoconstrictor and vasodilator factors.

1.3.3 Mechanism of the anticontractile effect of PVAT

Paracrine vasorelaxant effects induced by PVAT-derived factors have been intensively studied. However, the detailed mechanisms of how PVRFs exert their effects on the blood vessel remain unclear, and it varies depending on anatomical location and animal species (Agabiti-Rosei *et al.*, 2018). It is hypothesised that PVAT modulates vascular function through two distinct mechanisms: endothelium-dependent and endothelium-independent pathways.

1.3.3.1 PVRF regulates anticontractile effects through endothelium-dependent mechanisms.

The endothelium plays essential roles in modulating the tone of underlying VSMC by releasing vasodilatory factors such as nitric oxide (NO), prostacyclin (PGI_2), and endothelium derived hyperpolarising factor (EDHF) or vasoconstrictive factors such as thromboxane (TXA_2) and endothelin-1 (ET-1) (Khaddaj Mallat *et al.*, 2017; Shimokawa and Godo, 2020). Endothelium-derived NO, one of the most potent vascular dilators, stimulates guanylate cyclase in VSMCs, resulting in an increase of cyclic GMP and activation of signaling cascades to induce blood vessel relaxation

(Kim *et al.*, 2020). The generation of vasoprotective NO is mediated by endothelial nitric oxide synthase (eNOS).

The endothelium-dependent anticontractile effects of PVAT on blood vessels might be mediated by PVAT-derived NO, or by release of PVRFs, such as adiponectin, leptin, and Ang-(1–7), which can induce an endothelium-dependent vasorelaxation (Gao *et al.*, 2007; Lee *et al.*, 2009; Gálvez-Prieto *et al.*, 2012; Lynch *et al.*, 2013; Victorio *et al.*, 2016; Sena *et al.*, 2017). PVAT produces NO primarily through the activity of eNOS, which is expressed in both the endothelial cells and adipocytes within PVAT. PVRFs may induce relaxation by indirect hyperpolarisation of the VSMC via stimulation of endothelial release of NO which stimulates different K^+ channels, in particular ATP–dependent and voltage-gated K^+ channels, in a Ca^{2+}-dependent manner (Dubrovska *et al.*, 2004; Lee *et al.*, 2009).

1.3.3.2 PVRF regulates anticontractile effects through VSMC-mediated mechanisms.

Numerous studies have demonstrated that PVAT induces relaxation in endothelium-denuded vessels, which suggests that PVRFs can directly target VSMCs. Indeed, studies have demonstrated that the anticontractile effects of PVAT from different locations (ie, thoracic aorta, abdominal aorta, or mesenteric artery) are mediated through distinct activation of potassium channels in VSMCs. However, results to date regarding the specific types of K^+ channels involved vary depending on the tissue and animal species.

In 2002, Lohn *et al*. demonstrated that blocking of ATP-dependent K^+ channels with glibenclamide or inhibition of tyrosine kinase with genistein in thoracic aorta of male Sprague-Dawley rats completely abolished the relaxant effect of PVRFs to serotonin, while blocking other K^+ channels, i.e. large-conductance Ca^{2+}-activated K^+ channels and delayed rectifier K^+ channels was either less effective or not effective at all (Löhn *et al.*, 2002). Moreover, they found that mechanical removal of endothelium or inhibition of endothelial NO did not affect the anticontractile effect of PVRFs to serotonin. Interestingly, they found that relaxation in intact PVAT rings was abolished when incubated in Ca^{2+}-free solution. Therefore, they concluded that PVAT induces relaxation through release of transferable factors

that act through activation of K^+_{ATP} channels and tyrosine kinase in a Ca^{2+}-dependent and endothelium-independent manner. In contrast, Gao and his group found that in thoracic aortic rings of Wistar rats the PVRF-induced NO relaxation is mediated by activation of calcium-dependent K^+ channels (K_{Ca}), as blockade of K_{Ca} channels, but not blockers of delayed rectifier potassium channels (K_V) and K_{ATP} channels, inhibited the relaxation response induced by donor solution from PVAT-intact vessels. In addition, they also found that PVAT induces endothelium-independent vasorelaxation via generation of H_2O_2 and subsequent activation of smooth muscle sGC (Gao *et al.*, 2007).

Other studies reported that PVAT-induced VSMCs relaxation is mediated by delayed rectifier potassium channels (K_v) in the mesenteric arteries of Sprague–Dawley rats (Verlohren *et al.*, 2004; Fésüs *et al.*, 2007), voltage-dependent K^+ channels in thoracic aorta of Wistar Kyoto rats (Lee *et al.*, 2011), and K_{Ca} channels in the internal thoracic arteries of humans (Gao *et al.*, 2005). In mouse mesenteric vessels, the vasorelaxant effect of adiponectin was found to be mediated by delayed rectifier K^+ (K_r) channel (Fésüs *et al.*, 2007) and large-conductance Ca^{2+}-activated K^+ (BK_{Ca}) channel (Lynch *et al.*, 2013). The reason behind this diversity in K_+ channel subtypes activated by PVRF is not clear, but it may be related to differences in the distribution of these K^+ channels among different vessels or different species.

1.3.4 PVAT and metabolic diseases:

Obesity and its associated vascular complications such as hypertension and T2DM are the major risk factors associated with CVDs (reviewed by (Saxton *et al.*, 2019). In obesity the distribution of fat depots is important in determining the adverse effects of adiposity. For instance, increased visceral AT is strongly associated with insulin resistance, dyslipidaemia, and hypertension (Koenen *et al.*, 2021). PVAT plays a beneficial role in maintaining the vasculature in a normal functional status as long as the PVAT-adipokine levels with opposing properties remain in equilibrium. Obesity induces increased oxidative stress, an inflammatory state and hypoxia, which contribute to PVAT dysfunction (Greenstein *et al.*, 2009; Stanek *et al.*, 2021). In obesity, PVAT can undergo significant changes and the equilibrium of PVAT-released adipocytokines is impaired in favour of proinflammatory or constriction-inducing agents, and PVAT becomes dysfunctional and exerts

detrimental effects with regard to vascular homeostasis (Sowka and Dobrzyn, 2021).

Excessive accumulation of dysfunctional PVAT has been strongly linked to the development of CVDs such as atherosclerosis and hypertension. Importantly, PVAT expands (hypertrophy) in obesity and is capable of responding to atherogenic stimuli and interacting with inflammatory cells, the nervous system, and vascular cells to promote or modulate vascular disease (Kim *et al.*, 2020). It has been demonstrated that the alteration in the secretory function of dysfunctional PVAT leads to vascular disorders, partially through its effect on the underlying VSMCs and ECs (Chang *et al.*, 2020). For example, it can promote endothelial cell dysfunction, recruit proinflammatory immune cells, and induce VSMC proliferation. In human epicardial adipose tissue the expression of adiponectin is decreased while inflammatory gene expression is markedly increased in patients with coronary artery disease (Iacobellis *et al.*, 2005; Baker *et al.*, 2006). Moreover, it has been reported that during obesity, dysfunctional PVAT secretes less vasodilatory and more pro-contractile adipokines, thus promoting vasoconstriction. This dual nature of PVAT has thus been called a “double-edged sword” (Saxton *et al.*, 2019).

The results from animal studies have indicated that HFD feeding significantly increased PVAT mass along with loss of its anticontractile effects. This loss of the anticontractile effect of PVAT is proposed to be due to an inability to produce the vasodilatory substances. Almabrouk *et al.* (2018) reported that in mice fed a HFD for 12 weeks, the anticontractile effect of PVAT is reduced along with a 70% decrease in adiponectin secretion. Similarly, the anticontractile effects of human PVAT in the subcutaneous small artery regions were lost in obese patients compared with healthy volunteers and were restored 6 months after bariatric surgery (Aghamohammadzadeh *et al.*, 2013). The same study reported that the PVAT anticontractile function was rescued with superoxide dismutase and catalase, suggesting that local oxidative stress and inflammation may contribute to the impaired anticontractile effects of PVAT in obese subjects. In addition, an improvement in anticontractile effects after bariatric surgery was accompanied by increased PVAT-derived adiponectin and nitric oxide bioavailability and reduced macrophage infiltration and inflammation (Aghamohammadzadeh *et al.*,

2013). Similarly, it has been demonstrated that diet-induced weight loss reverses obesity-induced dysfunctional PVAT through a mechanism involving reduced inflammation and increased nitric oxide synthase activity within PVAT (Bussey *et al.*, 2016).

Understanding the role of dysfunctional PVAT in obesity-related cardiovascular complications is a critical area of research. Therapies aimed at restoring healthy PVAT function and mitigating the effects of inflammation and oxidative stress may hold promise in reducing cardiovascular risks in obese individuals. Lifestyle modifications, such as weight loss, exercise, and a healthy diet, are also important strategies for improving PVAT function and overall cardiovascular health in individuals with obesity.

1.4 AMP-activated protein kinase (AMPK)

1.4.1 Overview of AMPK

AMP-activated protein kinase (AMPK) is the downstream component of a protein kinase cascade that acts as an intracellular energy sensor and is involved in the regulation of cellular and whole-body metabolism (Salt and Hardie, 2017). AMPK is sensitive to cellular energy levels and is activated in response to increases in AMP (or ADP) relative to ATP, resulting from such stimuli as hypoxia, nutrient deprivation, and ischaemia (Hardie, 2011; Carling, 2017). Once activated, AMPK stimulates ATP synthesis by stimulating ATP-producing pathways, such as FA oxidation, and attenuates ATP utilisation by inhibiting ATP-consuming pathways, such as lipogenesis, cholesterol synthesis, protein synthesis, and gluconeogenesis, thereby maintaining energy balance (Carling, 2017; Palmer and Salt, 2021).

AMPK is a heterotrimeric complex composed of α-catalytic subunit and regulatory ß- and γ-subunits (Figure 1-2). Each subunit has two or more isoforms (α1, α2, ß1, ß2, γ1, γ2, and γ3), generating up to 12 possible combinations (Hardie, 2011). Expression levels of the different subunit isoforms vary between tissues. In endothelium and adipose tissue, the predominant catalytic subunit isoform is α1, while the α2 catalytic subunit is most commonly found in skeletal and cardiac muscle (Salt and Hardie, 2017).

The catalytic α subunit is composed of an N-terminal catalytic serine/threonine kinase domain, which contains a conserved threonine residue at position 172, linked to a C-terminal regulatory domain by an autoinhibitory domain (AID) (Salt and Hardie, 2017). The ß subunit is composed of a C-terminal region which acts as a scaffold, interacting with the γ subunit and the C-terminal region of the α subunit (Juszczak *et al.*, 2020). The ß subunit also contains a region termed the carbohydrate binding module (CBM), sometimes referred to as the glycogen binding domain (GBD) (Carling, 2017). The γ subunit contains four cystathionine-ß-synthase (CBS) motifs which are required for binding the regulatory adenine nucleotides AMP, ADP and ATP, and are therefore important in allosterically regulating the AMPK complex (Ross *et al.*, 2016).

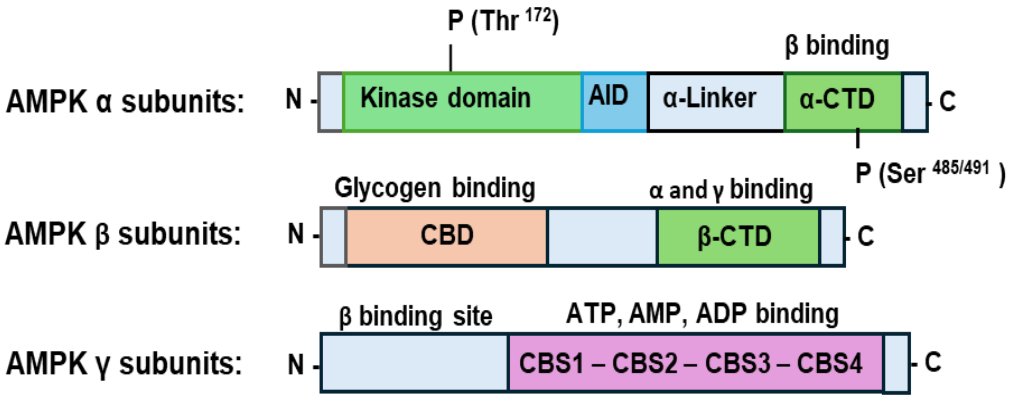

Figure 1-2 AMPK α, β, and γ subunits

The N-terminus of the AMPKα subunits has a serine/threonine kinase domain that is phosphorylated at residue Thr^{172} by upstream kinases. This domain is followed immediately by an autoinhibition domain (AID) that keeps the kinase domain inactive when AMP is not present, and a C-terminus domain (α-CTD) that engages in interactions with the β subunits. Phosphorylation of Ser $^{485/491}$ residues on the α-CTD negatively regulates AMPK. The AMPKβ subunits have an α and γ subunit interaction domain (β-CTD) and glycogen-binding domain (CBD). The AMPKγ subunits have four cystathionine-β-synthase (CBS) domains (CBS1-4) that can bind to ATP, AMP, and ADP. AMP binding initiates the allosteric activation of AMPK and promotes phosphorylation of AMPK by upstream kinases.

AMPK activation involves binding of AMP and/or ADP to cystathionine-ß-synthase (CBS) domains of the regulatory γ-subunit, which causes conformational changes to AMPK which promotes a subsequent net increase in phosphorylation of AMPKα on Thr^{172} by upstream kinases, leading to at least 100-fold activation (Towler and Hardie, 2007; Carling, 2017). At the same time, AMP inhibits Thr^{172} dephosphorylation by protein phosphatases (Davies *et al.*, 1995; Salt and Hardie, 2017). In addition to the AMP allosteric activation, AMPK can be activated at Thr^{172} on the catalytic α subunit by upstream kinases (Figure 1-3). Two major AMPK

kinases have been identified and they are liver kinase B1 (LKB1) and Ca^{2+}/calmodulin-dependent protein kinase kinase 2 (CaMKK2) (Shaw *et al.*, 2004; Hawley *et al.*, 2005; Woods *et al.*, 2005). LKB1 activates AMPK in response to low energy states (e.g., exercise, starvation) (Herzig and Shaw, 2018), while CaMKK2 is activated by increases in intracellular Ca^{2+} which occurs in response to many hormones including hormones that act on the endothelial cells, such as thrombin (Stahmann *et al.*, 2006) and vascular endothelial cell growth factor (VEGF) (Stahmann *et al.*, 2010; Hardie, 2018).

Numerous pharmacological agents, natural compounds, and hormones are known to activate AMPK, either directly or indirectly – some of which (for example, metformin and thiazolidinediones) are currently used to treat T2D.

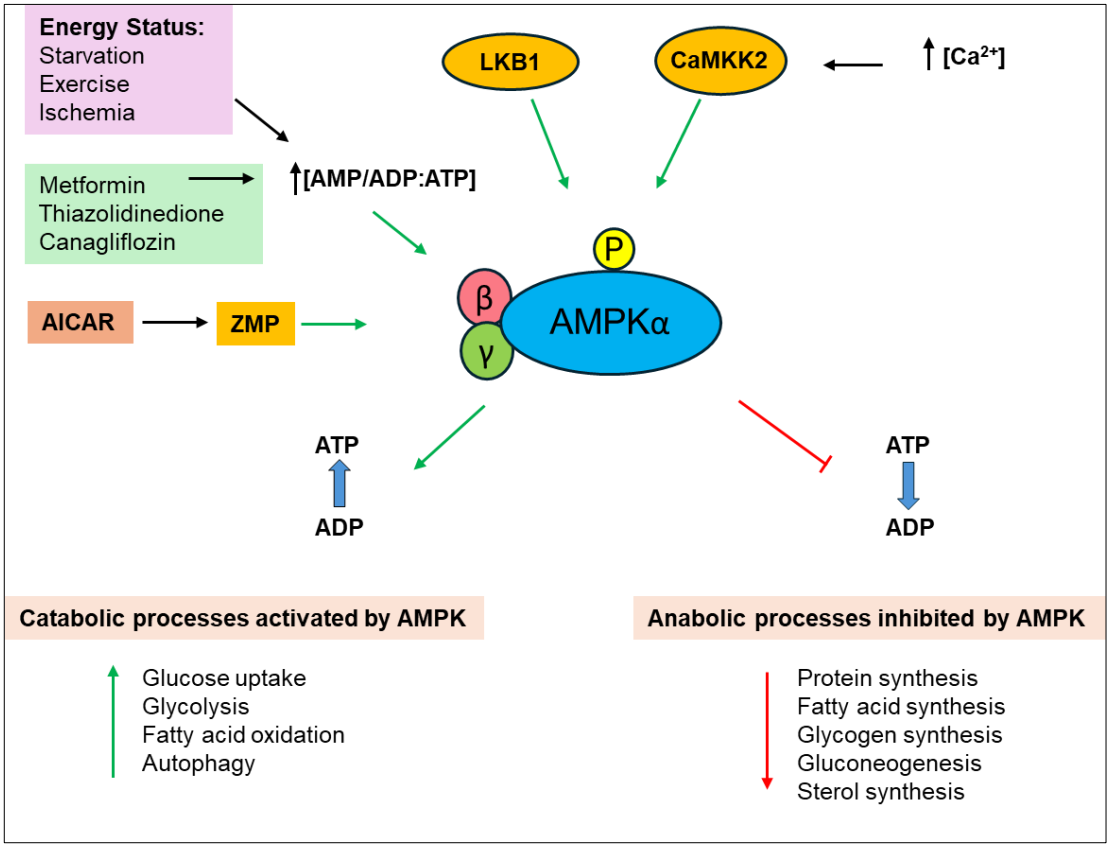

Figure 1-3 AMPK activation by upstream kinases and metabolic outcomes

AMPK is a heterotrimer of an α catalytic subunit complexed with β and γ regulatory subunits. Under ATP depletion, AMPK kinase undergoes allosteric transition and is phosphorylated at Thr^{172} by upstream kinases, such as CaMKK2 and LKB1, leading AMPK activation. AICAR is phosphorylated to ZMP, which mimics the effect of AMP. AMPKα Thr^{172} can also be phosphorylated by CaMKK2 independent of AMP levels in response to increased intracellular Ca2+ concentrations. AMPK activation restores ATP levels by suppressing ATP-consuming anabolic processes and stimulating catabolism and ATP generation.

1.4.2 Pharmacological Activators of AMPK

A variety of compounds with different structures have been used experimentally to activate AMPK. One the of AMPK activator classes consist of pro-drugs that are converted inside cells into an AMP analogue by cellular enzymes. The commonly used compound of this class is AICAR (5-aminoimidazole-4-carboxamide ribonucleoside), an adenosine analogue. AICAR is taken up into cells by adenosine transporters, and phosphorylated by adenosine kinase into ZMP, an AMP mimetic (Grahame Hardie, 2016). Since ZMP is an analogue of AMP, it binds to AMPK at the same sites as AMP and mimics all of the effects of AMP on the AMPK system without altering adenine nucleotide ratios, although it is less potent than AMP itself (Grahame Hardie, 2016; Salt and Hardie, 2017). AICAR has been widely used to activate AMPK in intact cells, tissues, and animals. However, AICAR has limited specificity, and several off-target effects have been reported (Kopietz *et al.*, 2021; Ahwazi *et al.*, 2021). Another compound that acts as a prodrug to activate AMPK is compound 13 (C13). Similar to AICAR, C13 is a phosphonate diester that is taken up into cells and converted by cellular esterases to compound 2 (C2) (Gómez-Galeno *et al.*, 2010). C2 is an AMP analogue which was shown to activate AMPK more potently than AMP or ZMP (Gómez-Galeno *et al.*, 2010; Salt and Hardie, 2017).

In addition to regulation by adenine nucleotides, a number of specific allosteric AMPK activators have recently been synthesised. These include A769662, a thienopyridone compound, and 991, a benzimidazole derivate (Cool *et al.*, 2006; Calabrese *et al.*, 2014). Both of these compounds activate AMPK by binding to the allosteric drug and metabolite (ADaM) site, located between the β-CBM and the N-lobe on the α subunit (Xiao *et al.*, 2013). Both compounds, A769662 and 991, showed marked selectivity for AMPK complexes containing β1 rather than β2 (Xiao *et al.*, 2013).

The selectivity of A769662 for β1 rather than β2 complexes of AMPK was confirmed by data showing that its effects are abolished by an S108A mutation in β1 that prevents the phosphorylation of that serine residue (Willows *et al.*, 2017). Similar to A769662, compound 991 shows some selectivity for β1 complexes since its effects are not abolished but significantly reduced in AMPK complexes harbouring β1(S108A) compared with AMPK containing wild type β1 (Willows *et al.*, 2017).

1.4.3 Role of AMPK in the Vasculature

Investigations have demonstrated the key role of AMPK in the regulation of endothelial and vascular smooth muscle cell function.

1.4.3.1 Role of AMPK in the vascular endothelium

Endothelium plays a critical role in modulating vascular tone and maintaining a laminar blood flow through releasing different vasoactive molecules including NO. Both AMPKα1 and α2 isoforms are expressed in the endothelial cells, although the α1 isoform is the predominant catalytic subunit in these cells (Morrow *et al.*, 2003; Goirand *et al.*, 2007). However, it has been reported that both AMPKα1 and AMPKα2 might be equally important in maintaining endothelial function. AMPKα2 plays a critical role in protecting the endothelial cells and maintaining them in a normal, non-atherogenic and non-inflammatory phenotype, and deletion of AMPKα2 causes accelerated oxidative stress and endothelial dysfunction (Wang *et al.*, 2010).

Activation of endothelial AMPK has been reported by a variety of physiological stimuli that result in low ATP, including hypoxia, low glucose, shear stress, and by elevation of intracellular calcium by agonists and hormones such as adiponectin, angiotensin II, and ghrelin (Nagata *et al.*, 2003; Ouchi *et al.*, 2004; Zhang *et al.*, 2006; Chen *et al.*, 2009; Wang *et al.*, 2012; Salt and Hardie, 2017). Additionally, several widely used hypoglycaemic drugs, such as metformin (Hattori *et al.*, 2006; Yu *et al.*, 2016), thiazolidinediones (Boyle *et al.*, 2008) and an SGLT2 inhibitor (canagliflozin) (Mancini *et al.*, 2018) and hypocholesterolaemic drugs, such as statins (Sun *et al.*, 2006) and fenofibrate (Murakami *et al.*, 2006), have been observed to activate AMPK in endothelial cells.

AMPK is one of the protein kinases, along with the phosphatidylinositol-3-kinase/protein kinase B (PI3K/Akt) pathway, implicated in the process of eNOS phosphorylation and NO production (Rodríguez *et al.*, 2021). Several studies have shown increased eNOS activity concomitant with increased AMPK Thr^{172} phosphorylation and AMPK activity in endothelial cells. AMPK-dependent phosphorylation of eNOS (on Ser^{1177}) has been reported following the exposure of cultured endothelial cells to agonists such as adiponectin (Cheng *et al.*, 2007),

VEGF (Reihill *et al.*, 2007), or pharmacological agents including statins (Rossoni *et al.*, 2011) and peroxisome proliferator-activated receptor (PPAR) agonists (Boyle *et al.*, 2008). Similar reports were also published using AMPK activators such as AICAR (Morrow *et al.*, 2003) and metformin (Davis *et al.*, 2006). AMPK activation causes endothelium-dependent relaxations in conduit and resistance arteries of both mice and humans by stimulating eNOS to produce NO (Ford and Rush, 2011; Dolinsky *et al.*, 2013; Chen *et al.*, 2019). In human aortic endothelial cells (HAECs), endothelial AMPK activation using AICAR caused an increase in eNOS Ser^{1177} phosphorylation and NO production (Morrow *et al.*, 2003). AMPK activation mediates shear stress and adiponectin-induced NO bioavailability through increased eNOS Ser^{1177} and Ser^{633} phosphorylation in the endothelial cells (Chen *et al.*, 2009).

Adiponectin is an adipokine with anti-inflammatory and anti-diabetic properties. A low adiponectin level (hypoadiponectinaemia) is associated with insulin resistance, endothelial dysfunction, and metabolic and cardiovascular diseases. Adiponectin has been reported to be an important physiological activator of AMPK in endothelial cells and exerts cardioprotective actions partially through AMPK activation and eNOS phosphorylation at Ser^{1177} (Zhao *et al.*, 2015a; Rodríguez *et al.*, 2021). It has also been demonstrated that endothelial AMPK can be activated independently of the cellular AMP/ATP ratio by peroxynitrite ($ONOO^-$), a potent oxidant formed by the combination of superoxide anions and NO. Peroxynitrite is reported to activate protein kinase C zeta (PKCζ) and leads to LKB1 activation and subsequent AMPK phosphorylation (Xie *et al.*, 2006). Moreover, oestrogen has been reported to activate AMPK and cause phosphorylation of acetyl coenzyme A carboxylase (ACC) and eNOS in human ECs via CaMKK2 (Yang and Wang, 2015).

Besides its beneficial role in endothelium-dependent vasodilation, endothelial AMPK has also been shown to play role in protecting against endothelial dysfunction and atherosclerosis. Activation of endothelial AMPK is implicated in the regulation of other important physiological functions such as reduction of oxidative stress and regulation of vascular inflammation (Colombo and Moncada, 2009; Jansen *et al.*, 2020), inhibition of apoptosis (Kim *et al.*, 2010), enhancing angiogenesis (Nagata *et al.*, 2003), and suppression of endoplasmic reticulum (ER) stress (Dong *et al.*, 2010). Inflammatory cell adhesion and endothelial dysfunction

are one of the earliest events in atherosclerosis, and AMPK appears to be involved in both these events. In HUVECs, activation of AMPK reduces inflammatory cell adhesion and migration, an essential step in initiation and progression of atherosclerotic lesions (Ewart *et al.*, 2008). AMPK exerts its anti-inflammatory effects on ECs by suppressing the nuclear factor-κB (NF-κB) signaling pathway and thus reducing levels of cytokines such as TNF-α and adhesion molecules such as intracellular adhesion molecule 1 (ICAM-1), vascular cell adhesion molecule 1 (VCAM-1), and E-selectin (Hattori *et al.*, 2006; Ewart *et al.*, 2008; Katerelos *et al.*, 2010). Furthermore, in cultured human endothelial cells canagliflozin, a hypoglycaemic drug was found to inhibit endothelial interleukin-1ß-stimulated pro-inflammatory chemokine/cytokine secretion partially by AMPK activation (Mancini *et al.*, 2018).

1.4.3.2 Role of AMPK in vascular smooth muscle cells

Vascular smooth muscle cells produce vasoconstriction or vasodilation in response to physiological or pathological stimuli. AMPK has been shown to be an important regulator of VSMCs function and its dysfunction leads to development of vascular diseases such as hypertension and atherosclerosis. As in the endothelium, α1 and α2 AMPK subunits are both expressed in VSMCs with α1-subunit being the more predominant isoform (Goirand *et al.*, 2007). VSMCs also express both ß1 and ß2 subunits, yet AMPKß1 is reported to be the predominant isoform contributing to activity (Rodríguez *et al.*, 2021).

Several studies demonstrated that in both large and small arteries, AMPK is involved in endothelium-independent vasodilation (Goirand *et al.*, 2007; Schneider *et al.*, 2015; Almabrouk *et al.*, 2017). In mouse aorta, activation of AMPKα1 by AICAR was demonstrated to induce a potent relaxation in an endothelium- and eNOS-independent manner (Goirand *et al.*, 2007; Almabrouk *et al.*, 2017). In mouse mesenteric arteries, AMPK activation using A769662 induced a pronounced endothelium-independent vasodilation by a decrease of intracellular-free calcium $[Ca^{2+}]_I$, which is achieved by calcium sequestration via sarcoplasmic reticulum (SR) Ca^{2+}-ATPase (SERCA) activation, as well as activation of BK_{Ca} channels in VSMCs (Schneider *et al.*, 2015). Similarly, in isolated human and rat renal resistance arteries, activation of AMPK with A769662 induced potent relaxations through both endothelium-dependent mechanisms involving nitric

oxide (NO) and intermediate-conductance calcium-activated potassium (IK_{Ca}) channels, as well as activation of SERCA in VSMCs (Rodríguez *et al.*, 2020).

AMPK has also been demonstrated to attenuate phenylephrine-induced VSMC contraction via phosphorylating and inactivating myosin light chain kinase (MLCK) (Horman *et al.*, 2008). Moreover, acetylcholine (Lee and Choi, 2013) and reactive oxygen species (ROS) such as H_2O_2 (Zhang *et al.*, 2008a) have been reported to induce endothelium-independent vascular relaxation by stimulating a AMPK-LKB1-dependent mechanism. LKB1-activated AMPK inhibits MLCK and decreases phosphorylation of myosin light chain which might attenuate vasoconstriction (Lee and Choi, 2013).

1.4.3.3 Role of AMPK in perivascular adipose tissue

PVAT has been recognized as an active contributor to vascular function due to its paracrine effects on the underlying VSMCs and EC. AMPK is expressed in PVAT as well as in the VSMCs and EC. AMPK activation in the ECs and VSMCs has been shown to play a role in vascular contractility as well as in maintaining vascular homeostasis. Many studies have proposed that AMPK exerts multiple beneficial/regulatory effects on several tissue and cell types, including endothelial cells and adipose tissue (Ewart *et al.*, 2008; Bijland *et al.*, 2013; Mancini *et al.*, 2017). The role of AMPK in PVAT or the actions of PVAT has not been widely investigated compared to the other types of adipose tissue.

A previous study in our lab demonstrated that morphologically there were no gross differences in PVAT or other fat depots between WT and AMPKα1 KO mice but KO PVAT had more infiltrating macrophages (Almabrouk *et al.*, 2017). The study also reported that a global deletion of AMPKα1 significantly attenuated the anticontractile effect of PVAT in endothelium denuded mouse aortic vessels (Almabrouk *et al.*, 2017). Moreover, several lines of evidence demonstrate that AMPK regulates production and secretion of adiponectin (Lihn *et al.*, 2004; Giri *et al.*, 2006), the main vascular mediator released by PVAT, suggesting that AMPK may regulate PVAT function via regulation of adiponectin production and secretion. Indeed, Almabrouk *et al*. found an impairment in adiponectin secretion by PVAT in the AMPKα1 knockout mice, and addition of adiponectin to either KO or WT aortic rings without PVAT augmented relaxation. However, the use of global

AMPKα1 KO models complicates the identification of AMPK's specific role in regulating vascular function within PVAT. This challenge arises because AMPKα1 is absent not only in PVAT but also in the endothelium and VSMCs, leading to broader metabolic and physiological issues. Therefore to better understand PVAT-AMPK's role in vascular regulation, it is important to develop experimental models that specifically KO AMPKα1 in PVAT while maintaining its expression in endothelial cells and VSMCs. Previous studies have used targeted knockout models to explore AMPK's role in adipose tissue metabolism, and creating a similar PVAT-specific knockout model could clarify AMPK's function in vascular homeostasis (Kim *et al.*, 2016).

Other studies reported that treatment of rat PVAT with palmitic acid (PA) resulted in reduced AMPK activity concomitant with inflammation and dysregulation of adipokine expression in PVAT (Sun *et al.*, 2014; Chen *et al.*, 2016; Ma *et al.*, 2017). However, pre-treatment of PVAT with several AMPK activators including metformin, AICAR, salicylate, and resveratrol (Sun *et al.*, 2014), with diosgenin, a steroidal sapogenin (Chen *et al.*, 2016), or with methotrexate (Ma *et al.*, 2017), inhibited NF-κB p65 phosphorylation and suppressed gene expression of pro-inflammatory adipocytokines, and upregulated adiponectin and PPARγ expression. Moreover, conditioned medium (CM) collected from PA-stimulated PVAT impaired endothelium-dependent vasodilation in response to acetylcholine (ACh), an effect that was restored when PVAT was pre-treated with AMPK-activating agents (Sun *et al.*, 2014; Chen *et al.*, 2016; Ma *et al.*, 2017).

Obesity is an independent risk factor for the development of cardiovascular diseases including coronary artery disease, hypertension, atherosclerosis. Obesity is associated with an increased PVAT mass along with structural and functional changes which contribute to PVAT dysfunction (Stanek *et al.*, 2021). Previous studies showed that AMPK acts as a protective mechanism against PVAT dysfunction resulting from diet-induced obesity. A study from our laboratory showed that HFD induced an inflammatory infiltrate, reduced AMPK phosphorylation as well as reducing adiponectin secretion and attenuating the anticontractile effect of mouse aortic PVAT (Almabrouk *et al.*, 2018). Interestingly, they found that thoracic PVAT of AMPKα1 knockout mice phenocopy many of the changes in wild-type aortic PVAT after HFD, suggesting that AMPK

within the PVAT is likely to have a protective role against deleterious changes in response to HFD.

Chen *et al*. also demonstrated that HFD-fed rats exhibited dysfunctional PVAT evidenced by increased IKKß and decreased AMPK phosphorylation, in addition to a significant elevation in serum level of TNF-α, while the level of adiponectin was reduced (Chen *et al*., 2016). This deleterious effect of HFD was efficiently restored via AMPK activation using diosgenin.

Taken together, these studies indicate that activation of AMPK in dysfunctional PVAT restores normal PVAT function and positively regulates vascular function

1.5 Hypothesis and Aims

Perivascular adipose tissue (PVAT) is an almost ubiquitous layer surrounding the blood vessels, exerting a profound influence on vascular function through the secretion of various vasoactive substances. PVAT has been acknowledged to confer a net anticontractile effect in healthy vascular physiology. Recent investigations have unveiled that PVAT exhibits distinct phenotypic variations depending on its anatomical location, thereby contributing to heterogeneous functional outcomes. While existing literature postulates that PVAT-induced vascular relaxation occurs through both endothelium-dependent and endothelium-independent mechanisms, the precise mechanisms remain elusive. The adenosine monophosphate-activated protein kinase (AMPK) has emerged as a pivotal regulator in the modulation of vascular smooth muscle cells (VSMCs) and endothelial function. Previous studies conducted within our research group have provided evidence of AMPK expression within PVAT and its involvement in mediating the endothelium-independent anticontractile actions of thoracic PVAT . Building upon this foundation, the central hypothesis of this doctoral thesis posits that AMPK also plays an indispensable role in the endothelium-dependent anti-contractile effects exerted by PVAT. To rigorously address this hypothesis, the current study aims to achieve the following objectives:

- Investigate the contribution of AMPK to the endothelium-dependent anticontractile effect of PVAT in two distinct anatomical locations, namely the thoracic and abdominal aorta. Despite both being conducting vessels, the PVAT surrounding the thoracic and abdominal aortae differs in both gross appearance and function, as detailed in Chapter 1. Mesenteric vessels were not included in this study due to their smaller size, which requires significant practice to handle and mount effectively. Additionally, this research builds on previous work that did not investigate mesenteric vessels, ensuring continuity and comparability of the results. Furthermore, although the current study utilized the same global AMPKα1 KO model as the previous research (the available model in our lab), it would be valuable to use a PVAT-specific AMPKα1 KO model to investigate the precise role of AMPKα1 in regulating vascular function within PVAT.

- Explore the influence of AMPK on the secretory function of PVAT, which underlies its paracrine signaling and potential vaso-modulatory capabilities.

- Assess the impact of AMPK on nitric oxide release from PVAT, elucidating its involvement in the endothelium-dependent mechanisms of PVAT-induced vascular relaxation.

Chapter 2 Materials and Methods

2.1 Animals

Wild type (Sv129) mice were originally purchased from Harlan Laboratories (Oxon, UK). AMPKα1 knockout mice were kindly supplied by Benoit Viollet (Institute Cochin, Paris, France). Mice were housed at the Central Research Facility at the University of Glasgow and maintained on 12 h cycles of light and dark. Mice were fed a standard chow diet and allowed free access to both food and water. All experiments were conducted in accordance with the United Kingdom Animals (Scientific Procedure) Act of 1986. Mouse breeding was performed under the project license numbers 70/8572 and PP1756142, held by Prof Simon Kennedy (University of Glasgow, U.K.).

2.2 List of materials and suppliers

2.2.1 List of materials

Abcam, Cambridge, UK

A769662 (6,7-Dihydro-4-hydroxy-3-(2'-hydroxy[1,1'-biphenyl]-4-yl)-6-oxo-thieno[2,3-b] pyridine-5-carbonitrile).

Anachem, Leicester, UK

DNAreleasy.

Fisher scientific UK Ltd Loughborough, UK

Phosphate buffered saline (PBS) Gibco™; Trypsin-EDTA Gibco™ (0.05 % (v/v); Bovine serum albumin (BSA); Primers for genotyping (Wild-type and AMPKα1 Knockout); Pierce™ BCA protein assay kit; High-Capacity cDNA Reverse Transcription Kit; TaqMan® Fast Advanced Master Mix; Corning tissue culture T75 flasks, 6-well plates.

GE Healthcare, Little Chalfont, Buckinghamshire, UK

3MM Whatman filter paper

Invitrogen (Life Technologies Ltd), Paisley, UK

SYBR™ Safe DNA Gel Stain; Agarose.

LI-COR, Biosciences, USA

Revert total protein staining.

MRC Technology, London, UK

Compound 991.

New England Biolabs Inc, UK

Blue Prestained Protein Standard, Broad Range (11-250 kDa).

Pall Corporation, USA

Nitrocellulose transfer membrane.

Promega, Southampton, UK

TAQ(GO) Hot Start Green Mastermix. DNA Ladder (100 bp); Gel loading dye (6x).

Promocell, Heidelberg, Germany

Endothelial Cell Growth Medium MV2.

Human umbilical vein endothelial cells (HUVECs).

Qiagen Ltd, Crawley, West Sussex, UK

RNeasy Mini Kit; QIAzol lysis reagent; RNase-free DNase set.

Sigma-Aldrich, Poole, UK

Acrylamide; Cromakalim; Ethylenediaminetetraacetic acid (EDTA); N,N,N',N'-tetramethylethylenediamine (TEMED); Ponceau stain; Triton X-100; Tween-20, Phenylephrine, Acetylcholine

Toronto Research Chemicals, Canada

5-Aminoimidazole-4-carboxamide-1-b-D-ribofuranoside (AICAR).

2.2.2 List of specialist equipment and suppliers

ADInstruments, Oxford, UK

Chart™ 8 Pro software.

Alpha Innotech, San Leandro, CA, USA

AlphaImager™ Gel Imaging System.

Bio-Rad Laboratories Ltd, UK

Agarose gel casting equipment

Mini Trans-Blot Electrophoretic Transfer Cell+ Power pack.

Gel Doc XR+ Gel Documentation System.

BMG Labtech, Ortenberg, Germany

FLUORstar OPTIMA Microplate Reader.

Camlab, Cambridge, UK

Jenway 6305 UV/Visible range Spectrophotometer.

Danish Myo Technology, Aarhus, Denmark

Four-channel small vessel wire myograph.

LI-COR Biotechnology, USA

LI-COR Odyssey® Sa infrared imaging system and Software.

Thermo Scientific, Waltham, MA, USA

Nanodrop spectrophotometer

2.3 List of antibodies

2.3.1 Primary antibodies for Immunoblotting

Table 2-1. Primary antibodies for Western blotting

Epitope (Clone)	Molecular weight	Host Species	Dilution	Secondary antibody dilution	Manufacturer and product number
AMPKα	62 kDa	Rabbit	1:1000	1:10000	Cell Signaling Technology #2532
Phospho-AMPKα (Thr^{172})	62 kDa	Rabbit	1:1000	1:10000	Cell Signaling Technology #2535
ACC	280 kDa	Rabbit	1:1000	1:10000	Cell Signaling Technology #3676
Phospho-ACC (Ser^{79})	280 kDa	Rabbit	1:1000	1:10000	Cell Signaling Technology #3661
eNOS	140 kDa	Rabbit	1:1000	1:10000	Sigma-Aldrich #N2643
Phospho-eNOS (Ser^{1177})	140 kDa	Rabbit	1:1000	1:10000	Cell Signaling Technology #9570
Akt	60 kDa	Mouse	1:1000	1:10000	Cell Signaling Technology #2920
Phospho-Akt (Ser^{473})	60 kDa	Rabbit	1:1000	1:10000	Cell Signaling Technology #4060
p44/42 MAPK (Erk1/2)	42,44 kDa	Rabbit	1:1000	1:10000	Cell Signaling Technology #9102
Phospho-p44/42 MAPK (Erk1/2) (Tyr^{202}/Tyr^{204})	42,44 kDa	Mouse	1:1000	1:10000	Cell Signaling Technology #5726
Klotho	62,116 kDa	Rabbit	1:1000	1:10000	Abcam #ab181373
Human Klotho beta	130-140 kDa	Mouse	1:1000	1:10000	R&D Systems # MAB5889
Mouse Klotho beta	130-140 kDa	Goat	1:1000	1:10000	R&D Systems # AF2619-SP
FGF-21	22 kDa	Rabbit	1:1000	1:10000	Abcam # ab171941

2.3.2 Secondary antibodies for Immunoblotting

Table 2-2.Secondary antibodies for Western blotting

Conjugate	Epitope	Host species	Dilution	Supplier (Cat #)
IRDye® 800CW	Rabbit	Donkey	1:10000	LI-COR Biosciences, USA (# 926-32213)
IRDye® 680CW	Rabbit	Donkey	1:10000	LI-COR Biosciences, USA (# 926-68073).
IRDye® 800CW	Mouse	Donkey	1:10000	LI-COR Biosciences, USA (# 926-32212)
IRDye® 680CW	Mouse	Donkey	1:10000	LI-COR Biosciences, USA (# 925-68072).
IRDye® 680LT	Goat	Donkey	1:10000	LI-COR Biosciences, USA (# 926-68024).

2.4 Standard solutions

Except when stated otherwise, all solutions and reagents were made up with distilled water.

Blocking buffer

5% Nonfat milk in TBST

High Potassium Physiological Salt Solution (KPSS)

1.2 mM $MgSO_4$, 62.5 mM KCl, 24.9 mM $NaHCO_3$, 1.2 mM KH_2PO_4, 2.5 mM $CaCl_2$, 11.1 mM glucose.

Krebs-Henseleit-HEPES Buffer (KHHB)

119.0 mM NaCl, 4.7 mM KCl, 1.2 mM $MgSO_4$, 24.9 mM $NaHCO_3$, 1.2 mM KH_2PO_4, 11.1 mM Glucose and 2.5 mM $CaCl_2$, 20 mM HEPES-NaOH, pH 7.4.

Lysis Buffer

50 mM Tris-HCl pH 7.4, 50 mM NaF, 1 mM Na pyrophosphate, 1 mM EGTA, 1 mM EDTA, 1% (v/v) Triton X-100, 250 mM mannitol, 1 mM dithiothreitol (DTT), 1 mM

benzamidine, 0.1 mM phenylmethylsulphonyl fluoride (PMSF), 1 mM Na vanadate and 5 µg/mL soybean trypsin inhibitor.

Physiological Salt Solution (PSS)

119.0 mM NaCl, 4.7 mM KCl, 1.2 mM $MgSO_4$, 24.9 mM $NaHCO_3$, 1.2 mM KH_2PO_4, 11.1 mM Glucose, 2.5 mM $CaCl_2$.

RIPA lysis buffer (1X)

50 mM Tris-HCl pH 7.4, 50 mM NaF, 1 mM Na pyrophosphate, 1 mM EGTA, 1 mM EDTA, 150 mM NaCl, 1.0% (v/v) Nonidet P-40 (NP-40), 1% (w/v) sodium deoxycholate, 0.1% (w/v) SDS, 250 mM mannitol, 1 mM DTT, 1 mM benzamidine, 0.1 mM PMSF, 1 mM Na vanadate, 5 µg/mL soybean trypsin inhibitor.

Running buffer

25 mM Tris, 192 mM glycine, 0.1% (w/v) SDS

Sample buffer

50 mM Tris-HCl pH 6.8, 2 % (w/v) SDS, 10 % (v/v) glycerol, 0.1 % (w/v) bromophenol blue, 200 mM DTT.

Transfer buffer

25 mM Tris, 192 mM glycine, 20% (v/v) ethanol.

Tris-acetate-EDTA (TAE) buffer

40 mM Tris, 1 mM EDTA, 20 mM acetic acid.

Tris-Buffered Saline (TBS)

20 mM Tris-HCl pH 7.5, 150 mM NaCl.

Tris-Buffered Saline Tween (TBST)

20 mM Tris-HCl pH 7.5, 150 mM NaCl, 0.1% (v/v) Tween 20.

Methods

2.5 Genotyping

The genotype of all wild type (WT) (Sv129) and AMPKα1 knockout (KO) mice was confirmed by reverse transcription polymerase chain reaction (RT-PCR) using the Go Taq amplification system (Promega, Southampton, U.K.). This comprised of DNA extraction and amplification from ear notches, followed by gel electrophoresis to separate DNA by mass/length and fluorescent staining of the amplified sequence. Details of the technique are outlined below:

2.5.1 DNA extraction

At 8 weeks of age ear notches were obtained from mice by staff from the Central Research Facility and animals were assigned identification numbers. Samples were stored at -20ºC until DNA was ready to be extracted. Ear notches were first transferred into PCR tubes and 10 µL DNAreleasy was added to each tube. Samples were then heated at 75˚C for 5 min, 96ºC for 2 min, and then kept at 20ºC until needed. Nuclease-free dH_2O (90 µL) was then added to each sample. Genotyping was performed by RT-PCR using the Go Taq amplification system as per the manufacturer's protocol. The reaction mixture for each sample consisted of the following:

- 13.75 µL TAQ(GO) Hot Start Green Mastermix which contains GoTaq® G2 DNA Polymerase, dNTPs (to expand the growing DNA strand with the help of Taq DNA polymerase), $MgCl_2$ (to enhance the DNA amplification by boosting the activity of Taq DNA polymerase), and load dye.
- Forward and reverse primers for either WT or KO sequence (Table 2-3).
- dH_2O

Table 2-3.Details of the primers and their sequences.

Target	Primer	Type	Sequence (5´ -3´)
AMPKα1	WT	Forward primer	AGCCGACTTTGGTAAAGGATG
		Reverse primer	CCCACTTTCCATTTTCTCCA
	KO	Forward primer	GGGCTGCAGGAATTCGATATCAAGC
		Reverse primer	CCTTCCTGAAATGACTTCTG

2.5.2 Polymerase Chain Reaction for AMPKα1 Wild type (WT) and AMPKα1 Knockout (KO)

A prepared DNA sample (2 µL) was added to 23 µL of the reaction mixture in a PCR tube. PCR was performed as follows: a hot-start at 95ºC for 5 min (enzyme activation), followed by 40 cycles of 95ºC for 30 seconds (DNA denaturation), 58ºC for 40 seconds and 72ºC for 1 min (primer binding). Samples were then subjected to 72ºC for 10 min (primer extension) and then stored at 4ºC until needed.

2.5.3 Gel preparation and electrophoresis

A 2% (w/v) agarose/TAE gel was prepared with ethidium bromide or SYBR™ Safe DNA Gel stain. Samples (10 µL) were loaded into each well along with 6 µL of a 100 bp DNA ladder in one well and electrophoresis (100 V for 15 min) was performed. UV fluorescence of DNA was then visualized using an AlphaImager™ gel imaging system. The presence or absence of a targeted sequence was used to identify wild-type and knockout mice (Figure 2-1).

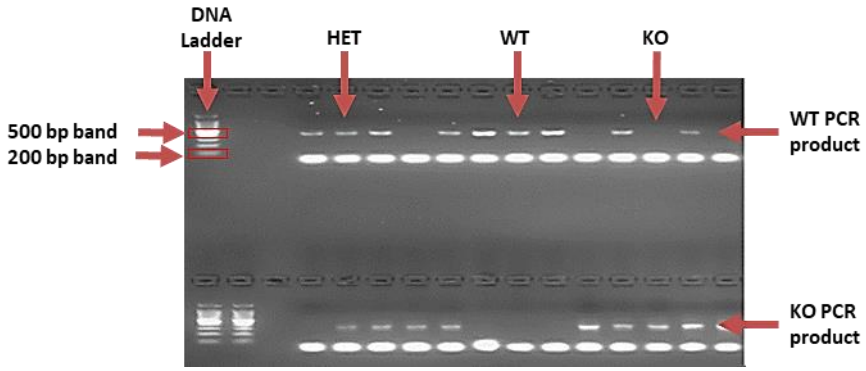

Figure 2-1 AMPKα1 genotyping.

Amplified PCR DNA products from mice ear notches were loaded on a 2% agarose gel. A 100 bp DNA ladder was loaded into the first well on the left. The upper row of wells was loaded with DNA products from PCR reactions using primers targeting WT alleles. The lower row was loaded with DNA products from PCR reactions using primers targeting KO alleles. Examples of WT, KO, and heterozygote (HET) mice are indicated.

2.6 Functional studies (wire myography)

2.6.1 Preparation of the vessels

Mice (males and females) were obtained at 12-20 weeks of age and were euthanized by a rising concentration of CO_2. After dissection, thoracic and

abdominal aortae were excised quickly and placed in an ice-cold PSS gassed with 95% O_2, 5% CO_2. Thoracic aorta is located above the diaphragm, within the thoracic cavity, and extends from the aortic arch down to the diaphragm. While abdominal aorta is located below the diaphragm, within the abdominal cavity and extends down to where it bifurcates into the common iliac arteries **Figure 2-2**. The aortae were cut into small ring sections approximately 1-2 mm long. Some rings were left with surrounding PVAT intact and in others, PVAT was removed. In some experiments the endothelium was removed by gently rubbing the interior of the vessel with a piece of fine wire. Two wires of 2 cm in length and 40 µm in diameter were passed through the lumen of the rings. The segments were mounted between two stainless steel jaws in the organ baths of a four-channel small vessel wire myograph (Figure 2-3). One jaw was connected to a force transducer that records the isometric tension developed by the vessel, while the other was connected to an adjustable micrometer that allows the operator to set up the initial isometric force. Vessels were incubated at 37 ^{0}C in PSS, gassed continuously with 95% O_2, 5 % CO_2 and allowed to equilibrate at a resting tension of 0 mN for 30 minutes. After equilibration, the vessels were stretched in a stepwise manner until the required optimum tension (9.81 mN) was reached. Chart™ 8 Pro software was used to record and measure vessel responses to different reagents.

In each experiment, to establish the viability of the segments, and to sensitise them before other pharmacological agents were added, the vessels were first challenged by replacing the PSS in the bath with 5 mL high potassium physiological salt solution (KPSS).

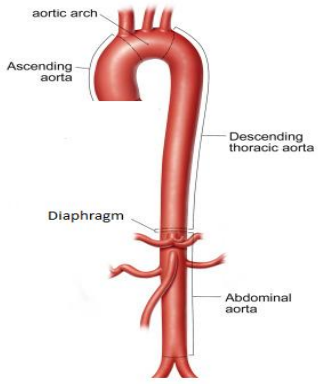

Figure 2-2 An illustration of segmentation of mouse aorta into four segments namely the ascending aorta, the aortic arch, the thoracic aorta and the abdominal aorta.

2.6.2 Testing the viability of the endothelium

Vessels were contracted in response to phenylephrine (PE) (1 μM) until a plateau was achieved. The presence of endothelium was confirmed by obtaining ≥ 50% relaxation in response to acetylcholine (ACh, 10 μM) in pre-contracted rings. When the relaxation response to ACh was ≤ 20% the vessel was considered as denuded of endothelium and the experiment was continued to compare the results with that of intact endothelium (Figure 2-4).

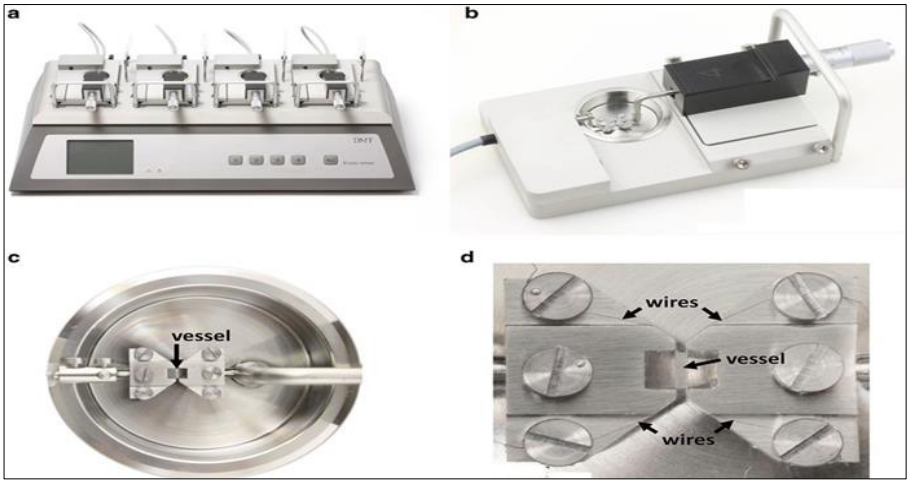

Figure 2-3 The wire myograph.

Danish Myo Technology (DMT) multi-chamber wire myograph (a). The wire myograph has four myograph units. (b) Each myograph unit contains a force transducer (left) and a micrometer (right), which are both connected to corresponding jaws to support the vessel inside the chamber. (c, d) Chamber with the jaws and a mounted vessel segment. From Danish Myo Technology A/S (adapted from www.dmt.dk).

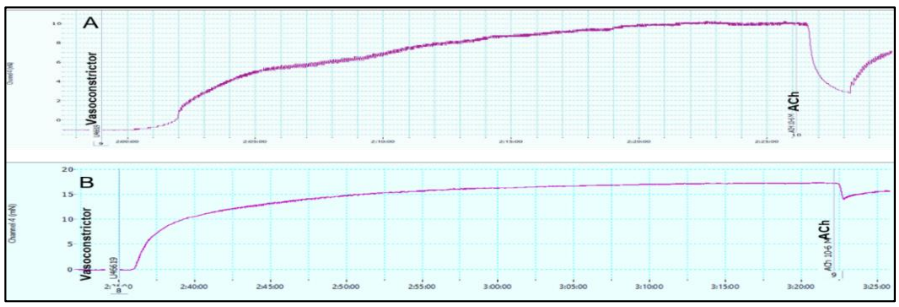

Figure 2-4 Testing the viability of endothelium

Vessels were mounted in the myograph baths and contracted with a vasoconstrictor (PE). Once tension reached a steady state, an endothelium-dependent vasodilator (acetylcholine, ACh) was added. (A) Vessels with ≥ 50% relaxation to ACh were considered endothelium-intact rings, while (B) vessels with ≤ 20% relaxation were considered endothelium-denuded rings.

2.6.3 Cumulative Dose response curves

Initially, aortic rings were contracted with PE (1 μM). Following a steady state of contraction being reached, cumulative concentration-response curves to the potassium-channel opener cromakalim were constructed by addition of increasing concentrations (1 nM to 10 μM) at 10 min intervals. Data are expressed as a percentage reduction in the vascular tone induced by PE.

2.6.4 Effect of FGF-21 on vascular relaxation

To test whether FGF-21 is involved in mediating the anticontractile effect of PVAT, mouse FGF-21 (100ng/mL) was added to the bath 10 min before vessels were contracted with PE. The aortic rings were then contracted with PE (1 μM) and cumulative concentration-response curves to a cromakalim (1 nM to 10 μM) or acetylcholine (1 nM to 30 μM) were constructed as described above.

2.6.5 Preparation of PVAT conditioned media for adipokine array

Thoracic and abdominal PVAT from both mouse strains was carefully dissected and weighed. The dissected samples were then incubated in 1 mL preoxygenated PSS at 37^{0}C for 1 h with continuous oxygenation. PVAT was then removed, and the conditioned media was stored at -80^{0}C.

2.6.6 Mouse Adipokine Array (Proteome Profiler)

Adipokine profiling was undertaken using a commercial adipokine array (ARY-013, R&D systems, Minneapolis, MN). The proteome profiler adipokine array is able to detect 38 adipokines in duplicates that are captured by specific antibodies on nitrocellulose membranes with the manufacturer's protocol summarised below.

Membranes were incubated with a supplied blocking buffer for 1 hour on a rocking platform shaker. Then 1 mL of PVAT conditioned medium was mixed with a 0.5 mL of supplied array buffer and 15 μL of reconstituted Mouse Adipokine Detection Antibody Cocktail and incubated at room temperature for 1 h. Blocking buffer was then aspirated, and sample/antibody mixture was added to the membrane and incubated overnight at 2-8 ^{0}C on a rocking platform shaker. Membranes were washed with washing buffer twice and then incubated with 2 mL of IRDye 800CW

Streptavidin (1:2000 dilution) at room temperature for 30 min on a rocking shaker. Membrane images were collected with a LiCor Sa Odyssey Imager.

The resultant images were imported to Image Studio software (LI-COR, USA) and signal intensity of each adipokine was measured. Data were normalized against an internal control, and final values were calculated and analysed using GraphPad Prism 8.0 software (California, U.S.A.). Six arrays for each genotype (3 thoracic and 3 abdominal) were analysed.

2.6.7 FGF-21 ELISA

FGF-21 concentration in serum and PVAT conditioned media was determined using a Mouse/Rat FGF-21 Quantikine ELISA Kit (MF2100, R&D systems, Minneapolis, MN).

2.6.7.1 Serum sample preparation

Blood samples from wild type and AMPKα1 knockout mice were collected at time of dissection and allowed to clot for 2 h at room temperature before centrifuging for 20 min at 2000 x g. Serum was then aspirated and stored at -20^{0}C. For analysis, serum samples were diluted 2-fold with a supplied calibrator diluent prior to FGF-21 ELISA.

2.6.7.2 PVAT conditioned media preparation for FGF-21 ELISA

Thoracic and abdominal PVAT from AMPKα1 KO mice and their wild type littermates was carefully dissected and weighed. The dissected samples were then incubated in 300 µL PSS at 37^{0}C for 1 h with continuous oxygenation. PVAT was then removed, and the conditioned media was stored at -80^{0}C.

2.6.7.3 FGF-21 ELISA protocol

Following the protocol provided by the manufacturer, the FGF-21 concentration in the sample was determined. Briefly, assay diluent (50 µL) was added to each well in the microplate. Standards, control, serum, or conditioned media (50 µL) were then added to each well. All standards, control, and samples were assayed in duplicate. The plate was then sealed and incubated for 2 h at room temperature. After incubation, the solution was aspirated completely, and wells

were washed 4 times with wash buffer (400 µL/well). After the last wash, the plate was inverted and blotted against clean paper towels. Anti-mouse/Rat FGF-21 antibody conjugate (100 µL) was then added to each well, which were covered with a new adhesive strip, and then incubated for 2 h at RT. The solution was then aspirated and washed 4 times with 400 µL/well wash buffer prior to adding 100 µL substrate solution for 30 min at RT; this step and all subsequent steps were protected from light. Finally, 100 µL of stop solution was added to each well and the plate gently tapped to ensure thorough mixing. The absorbance at 485 nm was determined within 30 min using a FLUOstar OPTIMA microplate reader (BMG Labtech, Germany). The FGF-21 concentration was determined by comparison of the mean absorbance from each sample relative to the standard curve.

2.7 Human umbilical vein endothelial cell (HUVEC) culture

2.7.1 Recovery of cryopreserved cell stocks from liquid nitrogen

HUVECs from pooled donors (Promocell) cryopreserved at passage 2 in liquid nitrogen were used. Cryovials were removed from liquid nitrogen and thawed in a water bath (37ºC) for 2 min. Cells were then transferred to a Corning T75 flask containing 12 mL pre-warmed Endothelial Cell Growth Medium MV 2 (Promocell-) (basal medium mixed with Supplement Mix). Final supplement concentrations (after addition to the medium) were as follows: foetal calf serum 5% (v/v); epidermal growth factor (recombinant human) 5 ng/mL; basic fibroblast growth factor (recombinant human) 10 ng/mL; insulin-like growth factor (Long R3 IGF-1) 20 ng/mL; vascular endothelial growth factor 165 (recombinant human) 0.5 ng/mL; ascorbic acid 1 µg/mL; hydrocortisone 0.2 µg/mL.

Cells were then incubated overnight in an incubator at 37ºC in 5 % CO_2. On the following day, the medium was aspirated to remove cryoprotective agents and cell debris and was replaced with fresh MV2 medium.

2.7.2 Passaging of HUVECs

Medium was replaced every two days and cells were sub-cultured when they reached 70-80% confluence. For sub-culturing, medium was aspirated, and cells

were washed with phosphate buffered saline (PBS). Then 2mL of sterile trypsin/EDTA (0.05% (v/v)) was added to each T75 flask to detach the cells. Flasks were then incubated at 37ºC for 1-2 min. When the cells started to detach, as observed under a 10x binocular microscope, flasks were gently tapped from the side to loosen the remaining cells. Trypsin was then neutralised by adding an appropriate volume of MV2 medium. The cell suspension was then divided into new T75 flasks (12 mL) and 6-well plates (2 mL/well).

2.7.3 Preparation of HUVEC lysates

HUVECs were utilised at passage 4, 5 or 6 when cell confluence reached ≥ 80% in 6-well plates. In each experiment the medium was discarded, cells were washed with PBS and then incubated in medium 199 for 2 h. Cells were then incubated with the relevant substances for various durations, after which, plates were transferred onto a tray of ice, medium was aspirated, and 100 µL/well lysis buffer was added. After scraping, cell lysates were collected into chilled microcentrifuge tubes and incubated on ice for 10 min. Tubes were then centrifuged in a pre-chilled bench top refrigerated microcentrifuge (17,000 x g 3 min, 4ºC). At the end, supernatants were collected into fresh chilled microfuge tubes and stored at -20ºC until needed.

2.8 Determination of protein concentration

Bicinchoninic acid method (BCA method) was used to assess the protein concentration of HUVEC and tissue lysates. In 96 well plates, standard dilutions of BSA ranging from 0.2 mg/mL to 2 mg/mL were used to generate a standard protein curve with distilled water as a blank. Lysates (2 µL, in duplicate) were added to other wells and then made up to 10 µL with distilled water. A working reagent (WR) was prepared by mixing BCA Reagent A with BCA Reagent B (50:1, Reagent A: B) (Pierce™ BCA Protein Assay Kit, Thermo Scientific™, UK). WR (200 µL) was added to all samples and reference standards. The plate was covered and incubated at 37ºC for 30 min. Absorbance was measured at 595 nm using a FLUOstar OPTIMA microplate reader (BMG Labtech, Germany). The mean absorbance from each sample was generated in duplicate and the protein concentration was determined by comparison with the BSA standard curve.

2.9 Western blotting of Proteins

2.9.1 SDS- polyacrylamide gel electrophoresis

Cell lysates were mixed with 4X sample buffer in a ratio of 3:1 and heated to 95^{0}C for 5 min in a heating block. In each well of a polyacrylamide gel, equal amounts of cell lysate protein were loaded along with blue pre-stained broad range markers. Gels were electrophoresed, using a Bio-Rad Mini-PROTEAN Tetra Cell system containing running buffer, initially at 80 V to allow stacking followed by 130 V until the dye front had eluted from the bottom of each gel.

2.9.2 Electrophoretic transfer of proteins from gels onto nitrocellulose membranes

Once separation had been completed, gels were removed from the plates and placed on nitrocellulose membranes (Pall Corporation; USA) pre-wetted with transfer buffer. Both the gel and nitrocellulose membrane were placed between two sheets of 3MM Whatman filter paper and transfer sponges forming a 'sandwich-like' structure (Figure 2-5). The sandwich was then placed between the two plates of a Bio-Rad mini protean transfer cassette and placed in the transfer tank which was topped up with transfer buffer. Then proteins were transferred onto the nitrocellulose membrane at 60 V for 135 minutes. Once completed, the nitrocellulose membranes were removed from the cassette and transferred into a container containing TBS.

In some experiments when total protein staining and quantifying used as an internal control, membranes were immediately stained with REVERT total protein stain for 5 min. Staining solution was removed and gels were washed three times with TBS (3 x 5 min) prior to imaging. Imaging was performed using LI-COR instrument with the detection of protein blue staining in red channel (700 nm). Quantification of the levels of protein loaded in each was performed by densitometry using Image Studio™ Acquisition Software. After REVERT staining, Membranes were then stripped with 0.2 M NaOH for 5 min, followed by washing in TBS (3 x 5 min).

2.9.3 Blocking of membranes and probing with primary antibodies

Following protein transfer, nitrocellulose membranes were blocked by incubation in 5% (w/v) milk powder prepared in TBS for 30 min at room temperature with continuous shaking. Membranes were then washed with TBS (3 x 5 min) and incubated, overnight with gentle shaking at 4ºC, with primary antibodies of interest diluted in TBST (TBS + 0.1% (v/v) Tween-20) supplemented with 5% (w/v) BSA at a dilution of 1:1000.

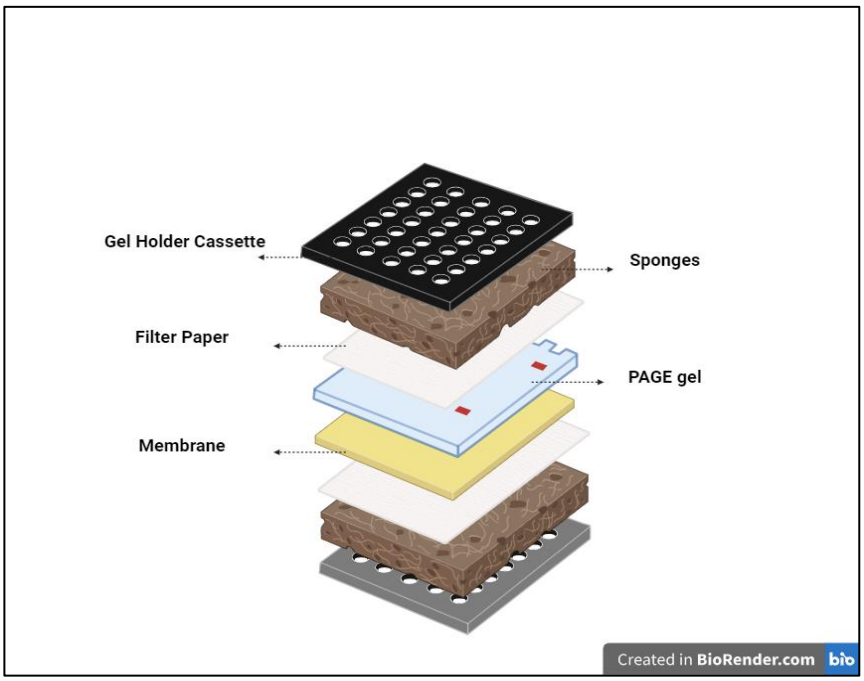

Figure 2-5 Protein transfer

After SDS-PAGE protein separation, gels were removed from the plates and placed on pre-wetted nitrocellulose membrane and together fitted between two layers of filter paper and transfer sponges forming a sandwich-like structure. This structure was placed between the plates of the transfer cassette with the gels toward the cathode and the membranes toward the anode. Created with BioRender.com

2.9.4 Secondary antibody and immunodetection of proteins

Following overnight incubation, membranes were then washed with TBST (3 x 5 min) and incubated, in the dark with gentle shaking for 1 hour at room temperature, with IRDye-labelled donkey anti-rabbit or anti-mouse IgG secondary antibodies diluted in TBST supplemented with 5% (w/v) BSA at a dilution of 1:10000. Thereafter, membranes were washed with TBST (3 x 5 min) and visualised using an Odyssey Sa Infrared Imaging System linked with Odyssey Sa Infrared

Imaging System software. A summary of the primary and secondary antibodies used along with dilutions are listed in Table 2-1 and Table 2-2.

2.9.5 Stripping of nitrocellulose membranes

Nitrocellulose membranes were incubated in stripping buffer (0.2 M NaOH) at RT for 15 min with shaking. Membranes were then washed (3 x 5 min) in TBS.

2.9.6 Densitometric quantification of protein bands

Images from the LI-COR Odyssey® Sa imaging program were imported into Image Studio™ Acquisition Software (LI-COR Biotechnology, USA). Protein band intensity was measured using either Image Studio™ Acquisition Software or Empiria Studio® Software (LI-COR Biotechnology, USA). Protein band quantification was typically expressed as a ratio of phospho/total immunoreactivity or immunoreactivity compared to an independent loading control.

2.10 Determination of FGF-21 level in PVAT

Abdominal and thoracic PVAT from both mouse strains was carefully dissected, weighed, snap-frozen in liquid nitrogen and stored at –80ºC. Tissues were then homogenised by adding 250 µL ice-cold RIPA (Radio-Immunoprecipitation Assay) lysis buffer and grinding using a battery-operated pestle motor mixer (Sigma-Aldrich, UK). Further homogenisation was obtained by sonication for 20 seconds. The homogenates were then vortex-mixed and placed on ice for 15 min. Lysates were then centrifuged (17,000x g, 10 min, 4ºC), and the supernatants collected and stored at -20ºC. Protein concentration of lysates was determined using BCA method, as described in 2.8. Equal amounts of PVAT lysate proteins were resolved by SDS-PAGE and transferred to nitrocellulose membranes. Membranes were then stained with REVERT total protein stain (Li-Cor Biosciences) prior to being visualised using an Odyssey Sa Infrared Imaging System. Total protein stain was washed off, and membranes were blocked by incubation in 5% (w/v) milk powder and immunoblotted with anti-FGF-21 antibody as described in section 2.9.3. Membranes were visualised using an Odyssey Sa Infrared Imaging System linked with Odyssey Sa Infrared Imaging System software. Quantification of the levels of FGF-21 relative to total lysate protein was assessed using into Image Studio™ Acquisition Software.

2.11 RNA extraction and reverse transcription polymerase chain reaction (RT-PCR)

2.11.1 PVAT RNA extraction and purification

Total RNA was isolated according to the RNeasy Lipid Tissue Mini Kit centrifugation protocol (Qiagen). Briefly, PVAT was transferred into 2 mL collection tubes and 1 mL/tube QIAzol lysis reagent and two stainless steel beads (5 mm mean diameter) were added. Tissue was lysed and homogenised using a Tissue Lyser LT (Qiagen) for 10 min. Homogenates were then placed on the benchtop at room temperature (15–25˚C) for 5 min prior to adding 200 µL chloroform to each and shaking vigorously for 15 sec. Tubes containing the homogenates were placed on the benchtop at room temperature for 2–3 min prior to being centrifuged at 12,000 x g for 15 min at 4ºC. After centrifugation, the sample separates into three phases: an upper, colourless, aqueous phase containing RNA; a white interphase; and a lower, red, organic phase. The upper, aqueous phase was transferred to a new tube and 1 volume of 70% ethanol was added and the mixture was mixed thoroughly by vortexing. The sample was transferred to a RNeasy Mini spin column placed in a 2 mL collection tube and centrifuged for 15 sec at 8000 x g at room temperature.

Buffer RW1 (350 µL) was added to the RNeasy Mini spin column and centrifuged for 15 sec at 8000 x g to wash the membrane. To ensure no DNA was present in samples, RNase-free DNase solution (Qiagen) was prepared and 80 µL was added directly to the RNeasy Mini spin column membrane, and placed on the benchtop for 15 min. Buffer RW1 (350 µL) was added to the RNeasy Mini spin column and centrifuged for 15 sec at 8000 x g. The spin column membrane was then washed twice by adding 500 µL Buffer RPE and centrifuging for 15 sec at 8000 x g. After centrifugation, the RNeasy Mini spin column was removed and placed in a fresh 2 mL collection tube to eliminate any possible carryover of buffer RPE or if residual flowthrough remains on the outside of the RNeasy Mini spin column. To elute the RNA, the column was placed in a fresh 1.5 mL collection tube, 30 µL RNase-free water was added directly to the spin column membrane and centrifuged for 1 min at 8000 x g. The RNA concentration was determined using a NanoDrop™ 1000 spectrophotometer (Thermo Scientific) prior to storage at -80ºC.

2.11.2 Reverse transcription

For cDNA synthesis, DNase treated RNA (1 µg) was reverse transcribed with a High Capacity cDNA Reverse Transcription kit containing 10X reverse transcription buffer, 25XdNTP Mix, 10X random primers, multiscribe reverse transcriptase and RNasefree water. Reverse transcription was performed in a thermocycler (Eppendorf® Mastercycler®) using the following parameters: 10 min at 25ºC, 120 min at 37ºC, and 5 min at 85ºC. Samples were then stored at -20ºC.

2.11.3 Quantitative real time Polymerase Chain Reaction (PCR)

Real time PCR was carried out on a QuantStudio™ 12K Flex Real-Time PCR System with application of the 384-Well Block Module (Applied Biosystems™ Applied, Life Technologies) using gene specific TaqMan probes (Table 2-4) to quantify the relative abundance of each gene with TaqMan™ Universal PCR Master Mix (Applied Biosystems) as the fluorescent molecule. PCR was performed in triplicate for each sample and gene expression was normalised to TATA binding protein (*Tbp*).

Table 2-4 Taqman probes

Taqman gene probes (mRNA)	Catalogue number
FGF-21 (*Fgf21*)	Mm07297622_g1
TATA-box binding protein (*Tbp*)	Mm01277042_m1
adiponectin (*Adipoq)*	Mm01343606_m1
eNOS (*Nos3)*	Mm00435217_m1

2.12 NO measurement assay (Sievers NO meter)

2.12.1 Preparation of the PVAT conditioned medium for NO analysis.

PVAT conditioned media was prepared as follows: thoracic and abdominal PVAT from both mouse strains was carefully dissected. PVAT from three mice was pooled and weighed then incubated in 1 mL preoxygenated KHHB at 37ºC for 1 h with

continuous oxygenation. In some experiments, FGF-21 (100ng/mL) or compound 991 (50 μM) was added. PVAT was then removed, and the conditioned media was stored at -80^{0}C. Samples (50 μL) were mixed with 200 μL of methanol, centrifuged (13,000 x g, 4^{0}C, 20 min), and supernatants were collected and stored at -20^{0}C.

2.12.2 Preparation of HUVEC conditioned media for NO analysis

HUVECs at passage 4, 5 or 6 were washed with PBS and then incubated in medium 199 for 2 h. Cells were then incubated with the relevant substances for various durations, after which, plates were transferred onto a tray of ice, medium was aspirated into fresh chilled microfuge tubes and samples (50 μL) mixed with 200 μL of methanol, centrifuged (13,000 x g, 4^{0}C, 20 min), and supernatants were collected and stored at -20^{0}C.

2.12.3 Detection of nitric oxide (NO)

NO concentration was determined using a Sievers Nitric Oxide Analyzer (NOA 280i). The NO analyser calculates NO present in the samples from the amount of nitrite (NO_2^-), which is formed by the reaction between NO and dissolved oxygen. To set up the NO analyser, a reflux mixture of acetic acid and NaI was added to the purge vessel. Iodide reacts with nitrite and converts it back to NO which reacts with O_2 to produce NO_2 (nitrogen dioxide), which is detected by chemiluminescence, and the signal was converted to an electrical potential by the NO analyser. Prior to each experiment, a nitrite standard calibration curve was obtained by injecting 20 μL of 100 μM, 50 μM, 10 μM, 1 μM, 500 nM, 100 nM and 50 nM KNO_2. Samples (20 μL) were then injected at regular intervals with time to allow the output curve to return to baseline. The output in mV was then related to the amount of NO_2^- present in the sample using the NO_2^- standard curve constructed on that day. All samples and standard solutions were measured in duplicate. Values were corrected for NO_2^- present in media in the absence of cells or tissue.

2.12.4 Statistical analysis

All results are expressed as mean ± standard error of the mean (SEM) where *n* represents the number of experiments performed or number of mice used. Data were analysed with GraphPad Prism 8.0 software (California, U.S.A.). When

comparing different groups, t-test, one-way or two-way ANOVA (analysis of variance) tests followed by appropriate post-hoc tests were used. The appropriate post-hoc test was automatically determined by Prism. The log EC50 was first calculated for each experiment, and group comparisons were then performed using a t-test in GraphPad Prism. In all cases, a *P* value of less than 0.05 was considered statistically significant.

Chapter 3 Role of AMPKα1 in modulating PVAT function (functional study)

3.1 Introduction

Perivascular adipose tissue (PVAT) surrounds most systemic blood vessels and, depending on the anatomical location, it can share characteristics of either BAT, WAT, or both. In mice, thoracic PVAT is morphologically similar to BAT (Fitzgibbons *et al.*, 2011; Almabrouk *et al.*, 2017), while mesenteric (Cinti, 2011), and abdominal (Police *et al.*, 2009) PVAT are similar to white adipose tissue (WAT). The phenotypic discrepancies between thoracic and abdominal PVAT appears to be clinically important, as abdominal aortae are more susceptible to atherosclerosis and the development of aortic aneurysms than thoracic aortae (Padilla *et al.*, 2013; Yap *et al.*, 2021). It has also been demonstrated that abdominal PVAT is more susceptible to inflammation, as indicated by greater expression of inflammatory genes and immune cell infiltration markers in abdominal PVAT relative to thoracic PVAT (Padilla *et al.*, 2013). PVAT secretes a wide variety of active adipocytokines with various endocrine, vasocrine and paracrine effects.

In addition to its supportive function, PVAT has been demonstrated to regulate vascular contractility due to secretion of some vasoactive molecules and its proximity to the blood vessel (Soltis and Cassis, 1991; Löhn *et al.*, 2002). These factors are called PVAT-derived relaxing factors (PVRFs). The exact mechanism(s) by which PVAT influences vascular contractility and relaxation is complex and not clearly understood. Many studies on the anticontractile properties of PVAT have demonstrated that this effect is not due to mechanical and physical interference since the transfer of a PVAT-derived CM to PVAT-free vessel preparations is sufficient to augmented relaxation (Almabrouk *et al.*, 2017). This further suggests that PVAT releases transmissible factor(s) which modulate the vascular tone of the underlying VSMCs and endothelium. It has been reported that PVAT influences endothelium and VSMCs function through release of PVAT-nitric oxide (Gil-Ortega *et al.*, 2010; Victorio *et al.*, 2016), or through release of other adipokines, such as adiponectin (Sena *et al.*, 2017), which stimulates endothelial nitric oxide synthase (eNOS) phosphorylation with subsequent nitric oxide release.

As thoracic and abdominal PVAT exhibit divergent phenotypes, their anti-contractile and secretory function is likely to be different. Indeed, Victorio *et al* demonstrated that anticontractile function of PVAT is lost in the abdominal aorta

along with a reduction in eNOS-derived NO production compared with the thoracic aorta (Victorio *et al.*, 2016). These findings highlight the roles of different PVAT depots in the control of vascular function and that could drive differences in susceptibility to vascular injury.

AMPK is a heterotrimeric complex composed of α, ß, and γ subunits, and each subunit has two or more isoforms (α1, α2, ß1, ß2, γ1, γ2, and γ3) (Hardie, 2011). The α subunit of AMPK contains the catalytic domain and exists in 2 isoforms, α1 and α2 (Salt and Hardie, 2017). In the endothelium and adipose tissue, the predominant catalytic subunit isoform is α1, while the α2 catalytic subunit is most commonly found in skeletal and cardiac muscle (Cheung *et al.*, 2000; Goirand *et al.*, 2007). AMPK activation leads to phosphorylation of several key proteins and mediates numerous downstream pathways that are involved in metabolic regulation (Hardie, 2011).

AMPK function is not limited to energy homeostasis, but also acts to regulate cardiac metabolism and contractile function, as well as promoting anticontractile, anti-inflammatory, and antiatherogenic actions in blood vessels (Salt and Hardie, 2017). It has been shown that direct AMPK activation in endothelial cells stimulates NO production via phosphorylation of eNOS at Ser^{1177} (Morrow et al., 2003). Similarly, activation of AMPKα1 in mouse aortic VSMCs was reported to induce vasorelaxation (Goirand *et al.*, 2007). Moreover, secretion of adiponectin and activation of AMPK complexes containing the α2 catalytic subunit in blood vessels has been reported to induce vasodilatation in mesenteric arteries (Meijer *et al.*, 2013). However, the role of AMPK in regulating PVAT-anticontractile function is not well defined.

A recent study in our laboratory investigated the role of AMPK in regulating PVAT-anticontractile function in endothelium denuded vessels. The study demonstrated that the anticontractile effect of PVAT was lost in AMPK α1 knockout mice compared to wild type mice (Almabrouk *et al.*, 2017). The study also reported a diminished adiponectin release from the PVAT of AMPK α1 knockout mice. Therefore, it has been suggested that AMPK influences vascular contractility by modulating adiponectin secretion by PVAT. PVAT-derived adiponectin was also reported to modulate endothelial function, partly by enhancing eNOS phosphorylation in the endothelium (Sena *et al.*, 2017).

The role of AMPK on PVAT-mediated endothelial function has not been well studied. We hypothesise that AMPK in PVAT is an important mediator of the effects of PVAT on endothelial function.

3.2 Aims of the study

The primary objective of the current investigations is to extend our understanding of how AMPKα1 plays a role in modulating the influence of PVAT on endothelial function. This aim is motivated by the findings of a preceding study within our laboratory, which revealed a diminution in the anticontractile influence of PVAT in arteries lacking endothelium. Additionally, these studies seek to investigate potential differences in the vasodilatory capacities of PVAT derived from distinct anatomical locations. A particular emphasis is placed on unravelling the role of AMPKα1 in both abdominal and thoracic PVAT, recognising the phenotypic distinctions between these adipose depots and the existing ambiguity regarding the anticontractile properties of abdominal PVAT. The histological analysis of WT and KO PVAT from different anatomical locations has been previously conducted and documented in our lab, as outlined in section 1.4.3.3.

3.3 Results

3.3.1 Effects of AMPKα1 on phenylephrine-induced contraction in endothelium intact and denuded WT and KO thoracic aortic rings

To test whether lack of AMPKα1 alters the contractile response of thoracic aortic vessels in the presence and absence of endothelium, the contractile response to phenylephrine (PE, 1 μM) was measured in PVAT-intact vessels. As seen in Figure 3-1, there was no significant difference in contraction between genotypes in both endothelium-intact and denuded rings. In endothelium-intact vessels, the magnitude of the PE-induced contraction was similar in both WT and KO aortic rings (Figure 3-1 A). WT vessels contracted 11.18 ± 0.54 mN (*n*=7) versus 10.9 ± 0.7 mN for AMPKα1 KO vessels (*n*=7). Similar results were observed in endothelium-denuded vessels: WT 11.64 ± 1.8 (*n*=5) versus KO 11.6 ± 0.6 (*n*=5) (Figure 3-1 B). The magnitude of the PE-induced contraction was not significantly different between endothelium-intact and endothelium-denuded aortic rings in either genotype.

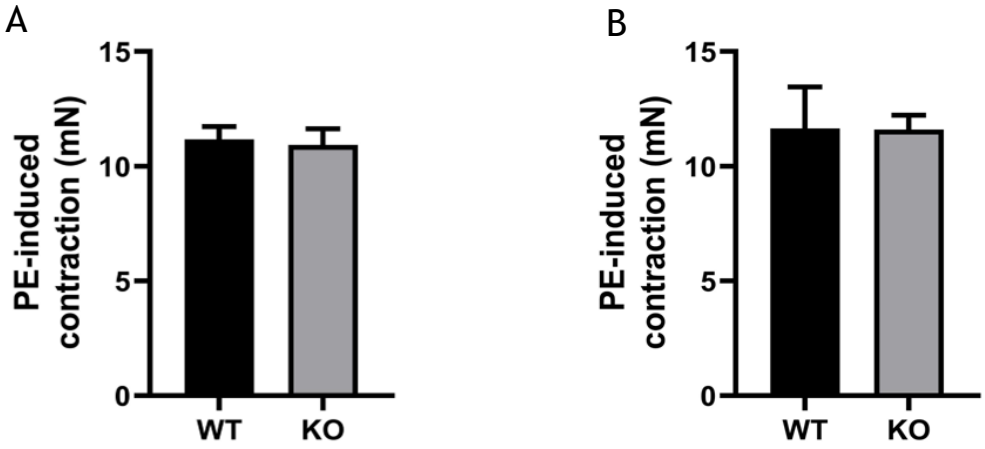

Figure 3-1 Effects of AMPKα1 on phenylephrine-induced contraction in endothelium intact and denuded WT and KO thoracic aortic rings

Endothelium-intact (A) and denuded (B) thoracic aortic rings from WT and KO mice with intact PVAT were mounted in a wire myograph and constricted with phenylephrine (PE, 1 μM). Maximum contraction was recorded using Lab Chart software. Data shown represent the mean ± SEM maximum contraction in mN (*n*= 7 and 5 for WT, and 7 and 5 for KO, in the presence or absence of endothelium respectively) (unpaired t test).

3.3.2 Effect of PVAT on PE-induced vascular contraction in WT thoracic aortic rings

To test the effect of PVAT on the contractile response of WT thoracic aortic vessels, the contractile response to PE (1 μM) was measured in endothelium-intact and endothelium-denuded rings. As reported above, in endothelium-intact aortic rings, the magnitude of the PE-induced contraction was 11.18 ± 0.54, (*n*=7) in PVAT-intact (PVAT+) vessels while in vessels without PVAT (PVAT-) it was 12.16 ± 0.8, (*n*=6) (Figure 3-2 A). In endothelium-denuded vessels, the PE-induced contraction was smaller, though not significantly so in vessels without PVAT (8.6 ± 1.4, n=5) compared to PVAT-intact vessels (11.6 ± 1.8, *n*=5) (Figure 3-2 B).

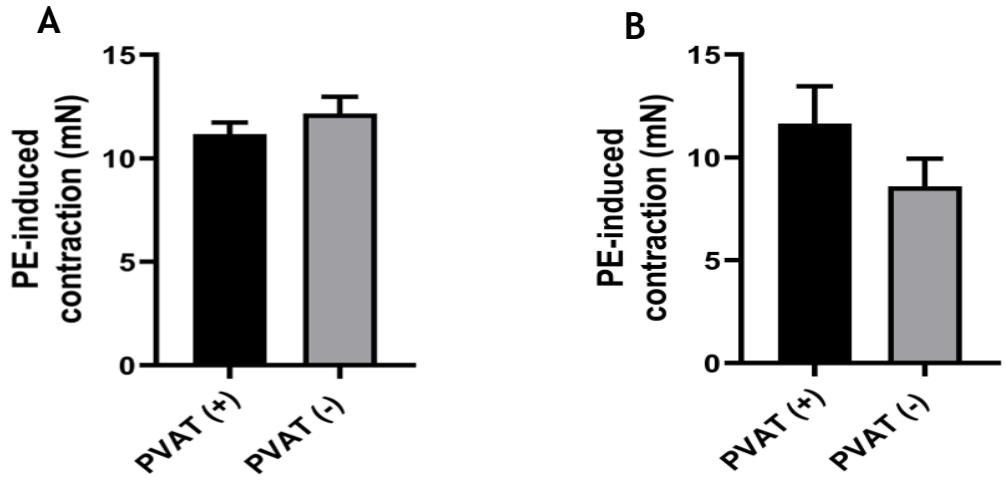

Figure 3-2 Effect of PVAT on PE-induced vascular contraction in wild-type thoracic aortic rings

Endothelium-intact (A) and denuded (B) WT thoracic aortic rings with and without PVAT were mounted in a wire myograph and constricted with phenylephrine (PE, 1 μM). Maximum contraction (in mN) was recorded using Lab Chart software. Data shown represent the mean ± SEM maximum contraction in mN (*n*=7 and 5 for PVAT-intact, and 6 and 5 for PVAT-removed vessels, in the presence or absence of endothelium respectively). (unpaired t test).

3.3.3 Effect of endothelium on PE-induced vascular contraction in WT and KO abdominal aortic rings

A previous study reported a difference in the anticontractile function between thoracic and abdominal PVAT (Victorio *et al.*, 2016) and so in addition to studying the phenotypic difference between thoracic and abdominal PVAT, this study examined whether a global lack of AMPKα1 alters the influence of the endothelium on contraction in PVAT-intact abdominal aortic vessels. Contractile response to PE (1 μM) was measured in PVAT-intact vessels in the presence and absence of

endothelium. In endothelium-intact vessels, the magnitude of the PE-induced contraction was similar in both WT and AMPKα1 KO aortic rings (Figure 3-3 A); WT vessels contracted 10.94 ± 0.78 mN (*n*=10) versus 9.31 ± 0.77 mN for AMPKα1 knockout vessels (*n*=9). Similar results were observed in endothelium-denuded vessels: WT 8.08 ± 0.96 (*n*=5) in WT versus 9.24 ± 0.31 (*n*=5) in KO rings (Figure 3-3 B).

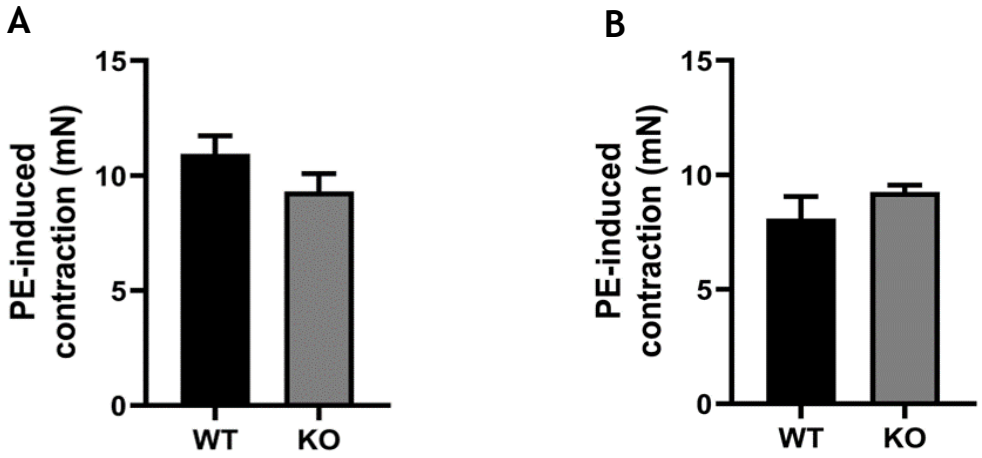

Figure 3-3 Effect of endothelium on PE-induced vascular contraction in wild-type and AMPKα1 knockout abdominal aortic rings

Abdominal aortic rings from WT and KO mice were mounted on a wire myograph and constricted with phenylephrine (PE, 1 μM). Maximum contraction was recorded using Lab Chart software. Data shown represent the mean ± SEM maximum contraction in mN from: (A) Endothelium and PVAT-intact aortic rings (*n*=10 for WT and 9 for KO). (B) Endothelium-denuded and PVAT-intact aortic rings (*n*=5 for both groups). (unpaired t test).

3.3.4 Effect of PVAT on PE-induced vascular contraction in abdominal aortic rings.

To examine the effect of PVAT in abdominal aortae on the contractile response, PE (1 μM)- induced contraction were measured in endothelium-intact WT and KO abdominal aorta rings with PVAT (PVAT+) and without PVAT (PVAT-). The results are summarised in Figure 3-4. In WT vessels (Figure 3-4 A), the magnitude of the PE-induced contraction was significantly different between PVAT-intact (10.94 ± 0.78, *n*=10) and PVAT-removed vessels (6.92 ± 0.87, *n*=8) ($P<0.05$). In KO mice (Figure 3 4 B), there was no significant difference between PVAT-intact and PVAT-removed vessels (9.31 ± 0.77, *n*=9 vs 7.58 ± 1.1, *n*=7)

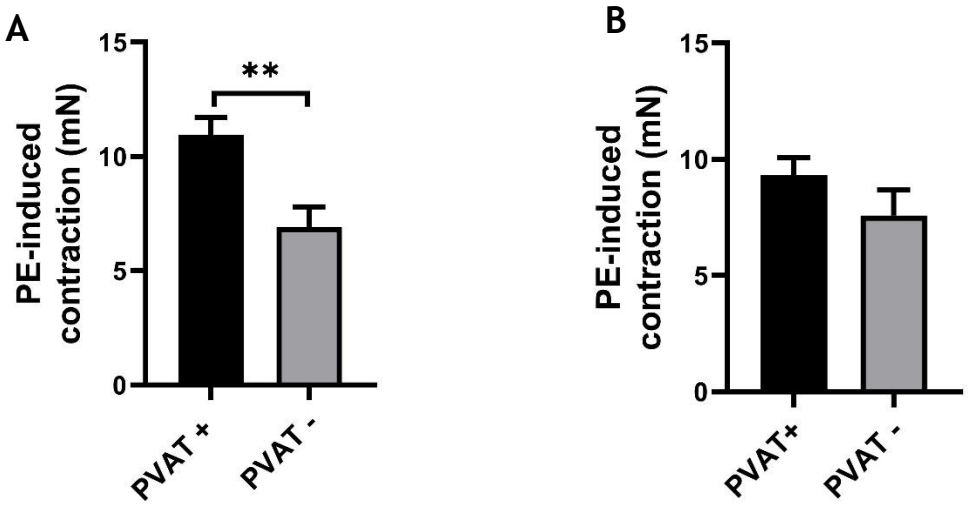

Figure 3-4 Effect of PVAT on PE-induced vascular contraction in abdominal aortic rings.

Endothelium-intact abdominal aortic rings with or without PVAT from (A) WT and (B) KO mice were mounted on a wire myograph and preconstricted with phenylephrine (PE, 1 μM). Maximum contraction was recorded using Lab Chart software. Data shown represent the mean ± SEM maximum contraction in mN. $^{**}P < 0.01$ (unpaired t-test).

3.3.5 Effect of genotype on cromakalim-induced vascular relaxation in endothelium intact and denuded thoracic aortic rings.

As a previous study in our lab demonstrated an attenuation in the anticontractile effect of KO PVAT relative to WT PVAT in endothelium-denuded thoracic aortic rings, the vasorelaxant effect of thoracic PVAT was examined in endothelium-intact thoracic aortic rings from WT and KO mice. Dose-response curves to cromakalim (1 nM – 10 μM) were constructed in endothelium-intact and endothelium-denuded thoracic aorta precontracted to phenylephrine (1 μM). Cromakalim is a potassium channel opener which induces vascular relaxation via hyperpolarisation of the vascular smooth muscle membrane. The results are summarised in Figure 3-5. In endothelium-intact vessels (Figure 3-5 A), the log EC50 and the maximum response to cromakalim (Emax) were not significantly different between WT (70.7 ± 7.3 %, *n*=7) and KO vessels (76.4 ± 7.0 %, *n*=7). Similarly, in endothelium-denuded vessels (Figure 3-5 B), the log EC50 and the Emax to cromakalim in WT vessels (49.6 ± 9.6 %, *n*=5) were not different from that of KO vessels (54.5 ± 6.2 %, *n*=5).

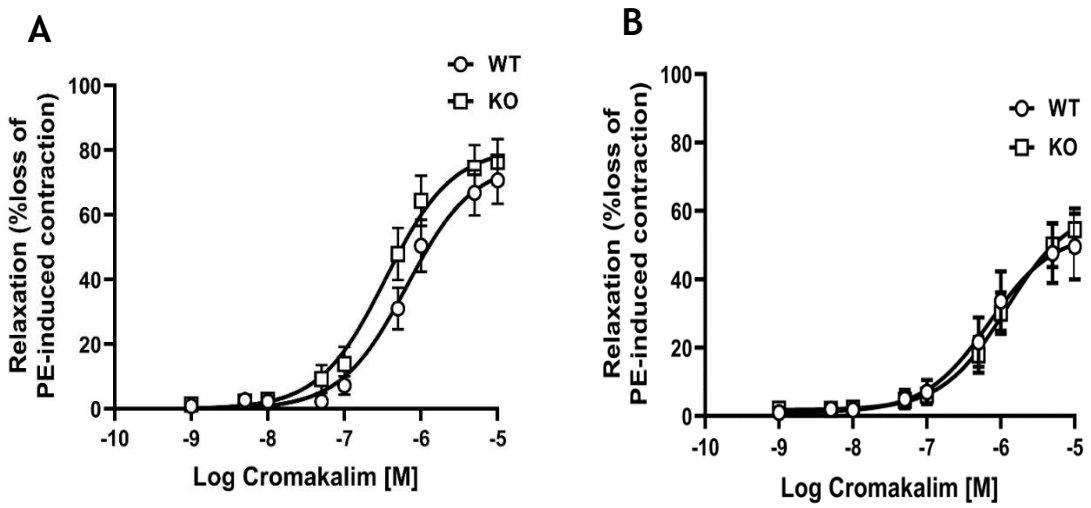

Figure 3-5 Effect of genotype on cromakalim-induced vascular relaxation in endothelium intact and denuded thoracic aorta.

Endothelium-intact (A) and denuded (B) thoracic aortic rings from WT and KO mice with intact PVAT were mounted on a wire myograph, preconstricted with phenylephrine (PE, 1 μM) and, once a steady state of contraction was achieved, it relaxed with increasing concentrations of cromakalim (1 nM – 10 μM). Data shown represent the mean ± SEM % relaxation (*n* = 7 and 5 for WT, and 7 and 5 for KO, in the presence or absence of endothelium respectively). (Two-way ANOVA).

3.3.6 Effect of PVAT on cromakalim-induced vascular relaxation in wild-type thoracic aortic rings.

To test whether thoracic PVAT had an anti-contractile effect as exhibited in previous studies from our laboratory, dose-response curves to cromakalim (1 nM – 10 μM) were constructed in endothelium-intact and endothelium-denuded WT thoracic aorta rings either with PVAT (PVAT+) or without PVAT (PVAT-) precontracted by phenylephrine (1 μM). The results are summarised in Figure 3-6. In endothelium-intact vessels (Figure 3-6 A), the log EC50 and the Emax to cromakalim were not significantly different between PVAT-intact (70.7 ± 7.3%, *n*=7) and PVAT-removed vessels (62.5 ± 10.2%, *n*=6). In endothelium-denuded vessels (Figure 3-6 B), there was no significant difference in the log EC50, and the Emax to cromakalim in PVAT-intact vessels (49.6 ± 9.6 %, *n*=5) compared to vessels from which the PVAT had been removed (39.4 ± 15.9%, *n*=5) (*P*=0.6).

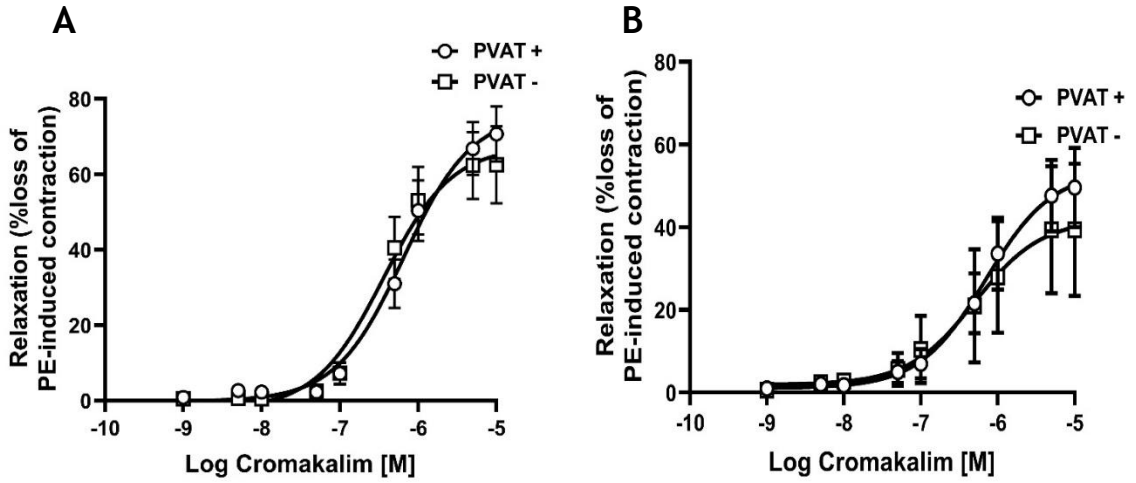

Figure 3-6 Effect of PVAT on cromakalim-induced vascular relaxation in wild-type thoracic aorta.

WT thoracic aortic rings, with PVAT (PVAT +) and without PVAT (PVAT -) were mounted in a wire myograph and preconstricted with phenylephrine (PE, 1 μM) and relaxed with increasing concentrations of cromakalim (1 nM – 10 μM). (A) endothelium-intact vessels (*n*=7 for PVAT (+) and 6 for PVAT (-). (B) endothelium -denuded vessels (*n*=5 for both groups). (Two-way ANOVA).

3.3.7 Effect of genotype on cromakalim-induced vascular relaxation in endothelium-intact abdominal aortic rings in the presence or absence of PVAT.

Having characterised the effects of endothelium, genotype and PVAT in thoracic aortic rings (sections 3.3.4 and 3.3.5), the same effects were assessed in abdominal aortic rings. Dose-response curves to cromakalim, (1 nM – 10 μM) were constructed in endothelium-intact abdominal aortic rings in the presence or absence of PVAT after preconstruction with phenylephrine (1 μM). The results are summarised in Figure 3-7. In PVAT-intact vessels (Figure 3-7 A), the Emax to cromakalim were significantly higher in WT (Emax= 71.4 ± 5.66 %, *n*=10) compared to KO vessels (Emax= 31.3 ± 3.0 %, *n*=9) (*P*<0.001 for Emax). However, the log EC50 was not significant between both groups. When PVAT was removed (Figure 3-7 B), the difference in response to cromakalim between WT and KO was still apparent. In WT vessels the Emax to cromakalim was 62.87 ± 3.9 %, (*n*=8) compared KO vessels (45.6 ± 8.4 %, *n*=7), although this difference no longer achieved statistical significance (*P*=0.09). Similarly, no significant difference in the log EC50 was found between the two groups.

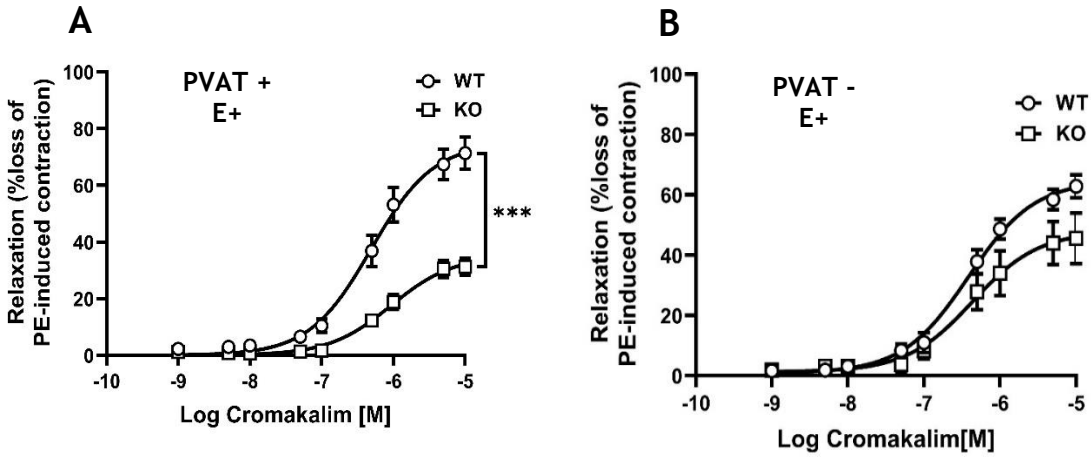

Figure 3-7 Effect of genotype on cromakalim-induced vascular relaxation in endothelium-intact abdominal aortic rings in the presence or absence of PVAT.

Abdominal aortic rings with intact-endothelium from WT and KO mice were mounted on a wire myograph and preconstricted with phenylephrine (PE, 1 μM) and relaxed with increasing concentrations of cromakalim (1 nM – 10 μM). Data shown represent the mean ± SEM % relaxation in mN. (A) PVAT-intact aortic rings (*n*= 10 for WT and 9 for KO). (B) PVAT-removed aortic rings (*n*=8 for WT and 7 for KO). ****P* < 0.001 (Two-way ANOVA).

Next, the effect of genotype was studied in PVAT-intact abdominal aortic rings either in the presence or absence of endothelium. Dose-response curves to cromakalim (1 nM – 10 μM) were constructed in PVAT-intact abdominal aortic rings precontracted by phenylephrine (1 μM). The results are summarised in Figure 3-8. In endothelium-intact vessels (Figure 3-8 A), the Emax to cromakalim were significantly higher in WT (71.4 ± 5.66 %, *n*=10) compared to KO vessels (31.3 ± 3.0 %, *n*=9; *P*<0.001). However, the log EC50 was not significant between both groups. In endothelium-denuded vessels (Figure 3-8 B), the Emax to cromakalim still significantly higher in WT vessels (78.4 ± 10.2 %, *n*=5) compared to KO vessels (30 ± 8.8 %, *n*=5) (*P*<0.05). However, the log EC50 was statistically not significantly different (*P*= 0.98).

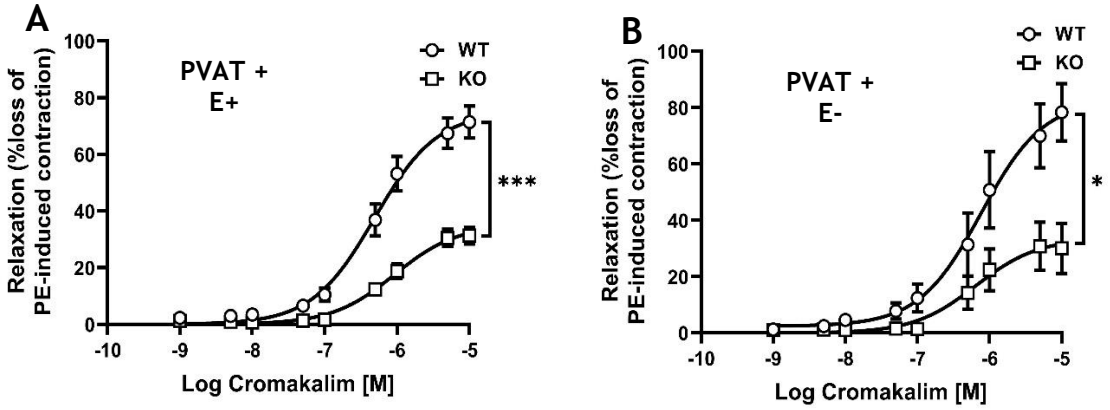

Figure 3-8 Effect of genotype on cromakalim-induced vascular relaxation in abdominal aortic rings in the presence or absence of endothelium.

Abdominal aortic rings with intact PVAT from WT and KO mice were mounted on a wire myograph and preconstricted with phenylephrine (PE, 1 μM) and relaxed with increasing concentrations of cromakalim (1 nM – 10 μM). Data shown represent the mean ± SEM % relaxation in mN. (A) Endothelium intact aortic rings (*n*= 10 for WT and 9 for KO). (B) Endothelium denuded aortic rings (*n*=5). **P* < 0.05; ****P* < 0.001 (Two-way ANOVA).

3.3.8 Effect of PVAT on cromakalim-induced vascular relaxation in abdominal aortic rings.

To examine the effect of PVAT in abdominal aortae, dose-response curves to cromakalim, (1 nM – 10 μM) were constructed in endothelium-intact WT and KO abdominal aorta rings with PVAT (PVAT+) and without PVAT (PVAT-) precontracted by phenylephrine (1 μM). The results are summarised in Figure 3-9. In WT vessels (Figure 3-9 A), the log EC50 and Emax to cromakalim were not significantly different between PVAT-intact (71.4 ± 5.6, n=10) and PVAT-removed vessels (62.8 ± 3.85, n=8). In KO mice (Figure 3-9 B), vessels without PVAT produced a higher Emax to cromakalim compared to vessels with intact PVAT (45.5 ± 8.36, *n*=7 vs 31.3 ± 3.03, *n*=9), although this difference no longer achieved statistical significance (*P*=0.1). Similarly, the log EC50 was not significantly different between the two groups.

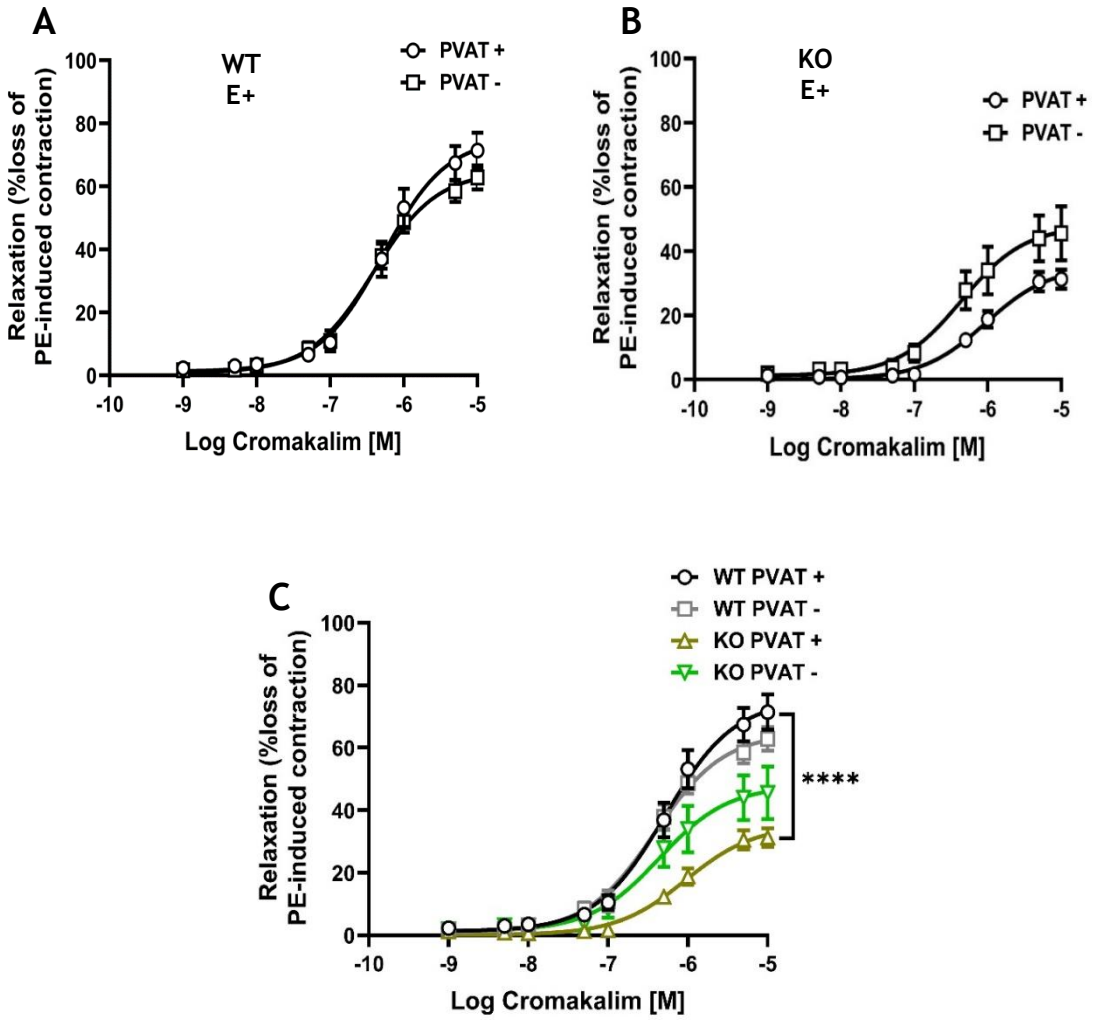

Figure 3-9 Effect of PVAT on cromakalim- induced vascular relaxation in abdominal aortic rings

Endothelium-intact abdominal aortic rings with or without PVAT from (A) WT and (B) KO mice were mounted on a wire myograph and preconstricted with phenylephrine (PE, 1 μM) and relaxed with increasing concentrations of cromakalim (1 nM – 10 μM). (C) Representative graph comparing the data in figures 3-8 A and B. Data shown represent the mean ± SEM % relaxation from (A) 8-10 or (B) 7-9 mice. ****P < 0.0001 (Two-way ANOVA).

3.3.9 Phenylephrine does not stimulate AMPK in HUVECs

To test whether phenylephrine (PE) altered basal or stimulated AMPK activity in HUVECs, cells were incubated with PE (1 μM), in the presence or absence of AICAR (2 mM) (an AMPK activator), and the extent of phosphorylation of the AMPK substrate ACC at Ser^{79} was determined by western blotting analysis of HUVECs lysates.

AICAR caused a significant (n=3, P < 0.01) stimulation of ACC Ser^{79} phosphorylation compared to vehicle (Figure 3-10). Incubation of HUVECs with PE did not alter basal or stimulated ACC Ser^{79} phosphorylation (n=3).

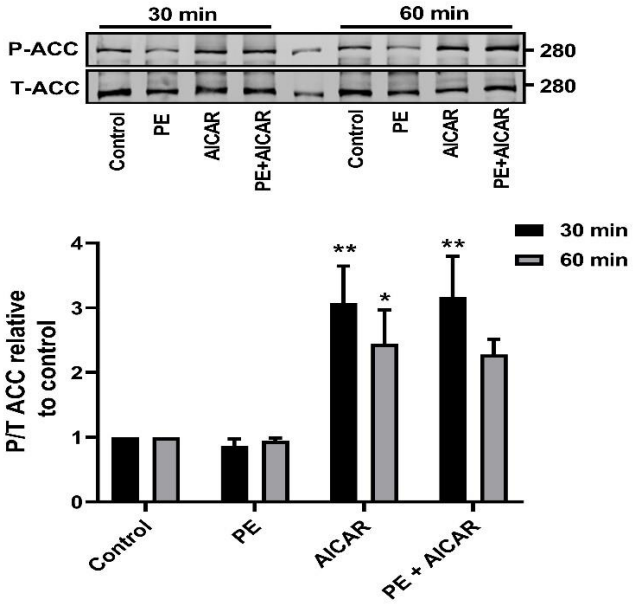

Figure 3-10 Effect of phenylephrine on basal and stimulated AMPK activity in HUVECs

HUVECs were incubated with DMSO (control), phenylephrine (PE, 1 µM), AICAR (2 mM), or both for 30- or 60-min. Lysates were prepared, resolved by SDS-PAGE and subjected to immunoblotting with the antibodies indicated. (A) Representative western blots. (B) Quantification of ACC Ser^{79} (P-ACC) phosphorylation relative to total (T-ACC) ACC. Data shown represent the mean ± SEM phosphorylation relative to control from three independent experiments. **P < 0.01, *P < 0.05 relative to lack of AICAR (one-way ANOVA).

3.3.10 Cromakalim and phenylephrine do not activate AMPK or increase eNOS phosphorylation in HUVECs.

To rule out the possibility that vasodilation to cromakalim is compromised in KO abdominal aortae because cromakalim or phenylephrine (PE) have eNOS or AMPK-dependent actions, HUVECs were incubated with cromakalim (10 µM) or PE (1 µM) for various durations. The extent of eNOS Ser^{1177} and ACC Ser^{79} phosphorylation was determined by western blotting analysis of HUVEC lysates.

Incubation of HUVECs with cromakalim or PE did not increase phosphorylation of eNOS Ser^{1177} in HUVECs (n=3, Figure 3-11 A, B). In addition, cromakalim had no effect on the phosphorylation of the AMPK substrate ACC Ser^{79} (n=3, Figure 3-11

C). The AMPK activator A769662 stimulated an increase in AMPK activity as assessed by ACC Ser^{79} phosphorylation (n=3, P<0.01).

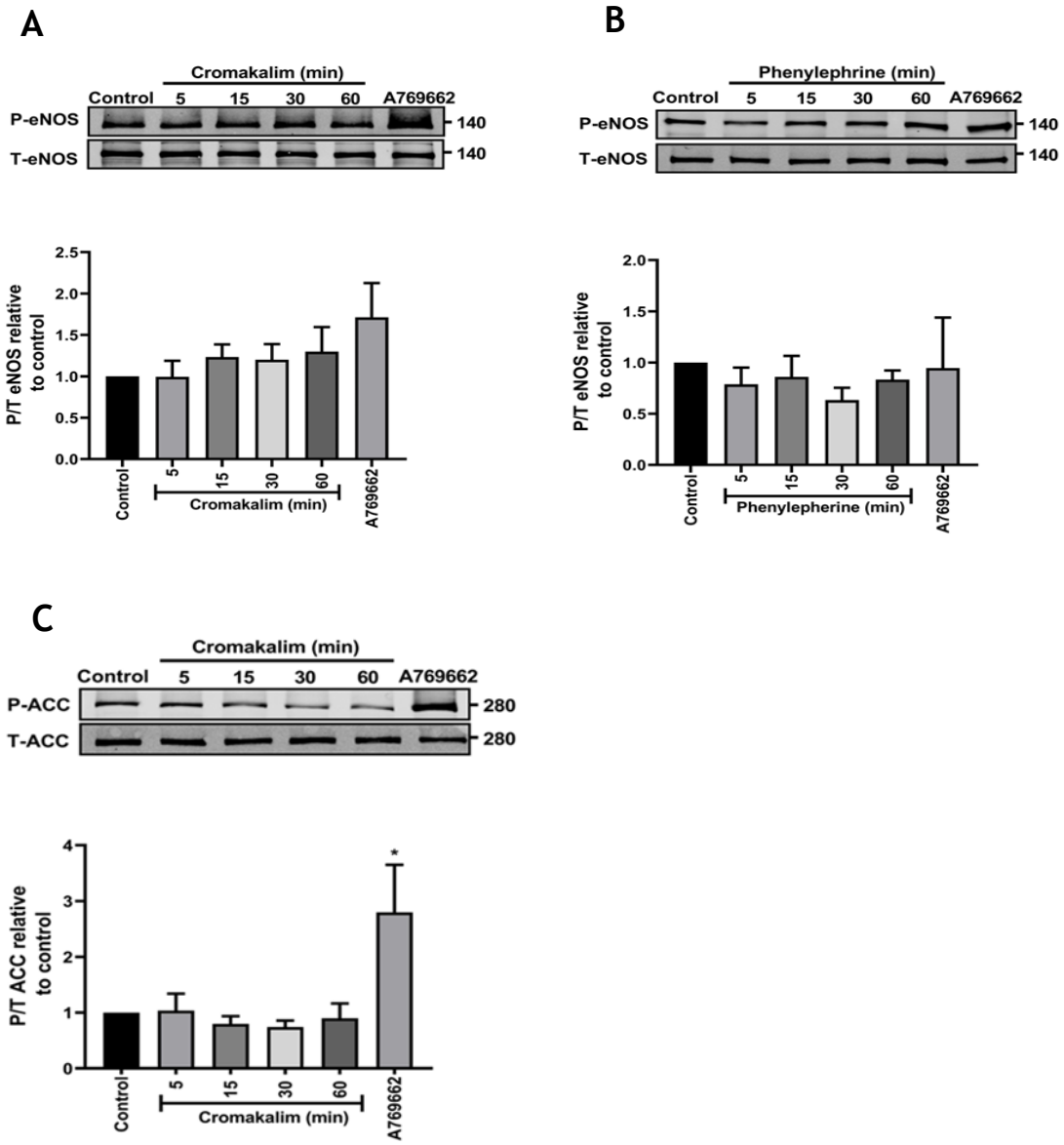

Figure 3-11 Effect of cromakalim and phenylephrine on AMPK and eNOS phosphorylation following different incubation times in HUVECs.

HUVECs were incubated with DMSO (control) or A769662 (100 µM) for 60 min or: (A,C) cromakalim (10 µM), or (B) phenylephrine (1 µM) for various durations. Lysates were prepared, resolved by SDS-PAGE and subjected to immunoblotting with the antibodies indicated. (A & B) Quantification of eNOS Ser^{1177} phosphorylation relative to total eNOS. (C) Quantification of ACC Ser^{79} phosphorylation relative to total. Representative immunoblots with molecular mass markers indicated on the right are shown on the top of each corresponding graph. Data shown represent the mean ± SEM fold phosphorylation relative to control from three independent experiments. *P < 0.05 (one-way ANOVA).

3.4 Discussion

The principal findings of this chapter highlight the compromised vasodilatory function of the perivascular adipose tissue (PVAT) of AMPKα1 knockout mice within both endothelium-intact and denuded abdominal vessels. In contrast, no discernible difference was found in the anticontractile activity of WT and KO thoracic PVAT. This observation intimates a potential functional difference between WT and KO abdominal PVAT, particularly with regard to substances released by PVAT which mediates the activation of K_{ATP} channel when using K^+ channel opener cromakalim.

Furthermore, the heightened impairment in vasorelaxation observed in KO abdominal PVAT within endothelium-intact and denuded rings suggests an influential role of PVAT-derived substances on VSMCs, potentially impacted by the deletion of the AMPKα1 subunit. Additionally, the absence of discernible effects on AMPK stimulation in HUVECs following exposure to cromakalim or phenylephrine discounts AMPK activation within endothelial cells as contributing to the observed differences in relaxation response between WT and KO abdominal PVAT. This could suggest functional differences between WT and KO abdominal PVAT which necessitates further investigations to elucidate the precise nature of which PVAT-derived substances are responsible for the observed effects.

In both endothelium-intact and -denuded thoracic aortic rings, the contraction response to phenylephrine and the relaxation response to cromakalim were not different between WT and KO mice. This suggests that the function of thoracic PVAT was not altered by deletion of AMPK α1. However, a prior study conducted in our laboratory revealed that in endothelium-denuded thoracic aortae of AMPK α1 KO mice, PVAT exhibited a reduced anticontractile and vasorelaxant effect relative to WT, which was associated with dysregulation of adipocytokine secretion, particularly adiponectin (Almabrouk *et al.*, 2017).

One notable difference between the two studies lies in the vasoconstrictor reagent used. Almabrouk *et al* employed the thromboxane A2 (TxA_2) mimetic U46619 (9,11-dideoxy-11α, 9α-epoxymethanoprostaglandin F2α), which is a more potent vasoconstrictor compared to phenylephrine used in the current study. TxA_2 is known to interact with signalling pathways typically associated with

endothelium-derived hyperpolarization and can directly modulate endothelial cell and/or vascular smooth muscle cell hyperpolarization (Ellinsworth *et al.*, 2014). Therefore, in this study, phenylephrine was used as a more physiological vasoconstrictor agent.

The role of K_{ATP} channels in the anti-contractile effect of PVAT was first proposed by Lohn *et al*. (Löhn *et al.*, 2002). It has been proposed that PVAT induces vasorelaxation through releasing PVRFs which act on the endothelium and also on VSMCs. On endothelium, PVRFs stimulate NO release, which in turn diffuses into neighbouring VSMCs, where it activates soluble guanylate cyclase (sGC). NO-induced activation of sGC leads to the production of cyclic guanosine monophosphate (cGMP) which activates protein kinase G (PKG), and this can modulate the activity of K_{ATP} channels. The interaction between K_{ATP} channels and NO is an integral part of the endothelium-dependent regulation of vascular tone. Therefore, cromakalim was used to examine the relaxing ability of PVAT.

Although both thoracic and abdominal aortae are considered as a conducting vessel, the PVAT surrounding each one differs in the gross appearance and in function. Thoracic PVAT is similar to BAT in terms of having small adipocytes with multiple small lipid droplets and abundant mitochondria (Gálvez-Prieto *et al.*, 2008; Fitzgibbons *et al.*, 2011; Almabrouk *et al.*, 2017). Abdominal and mesenteric PVAT resembles WAT, with adipocytes containing large lipid droplets with relatively few mitochondria (Police *et al.*, 2009; Fitzgibbons *et al.*, 2011). BAT plays a crucial role in heat production, in contrast with WAT which predominantly stores energy in the form of fatty acids. Both BAT and WAT secrete a wide range of adipokines which contribute to maintaining the vasculature in a normal functional state (Chang *et al.*, 2020). It has been speculated that differences in PVAT phenotype could contribute to disease susceptibility in different blood vessels, possibly through alteration of its secretory function (Chang *et al.*, 2020) or through the release of pro-inflammatory cytokines (Chatterjee *et al.*, 2009; Payne *et al.*, 2010). Given the differences in adipose tissue surrounding thoracic versus abdominal aortae, both PVAT depots were examined in the current study.

Despite the studies that have been done to attempt to understand the molecular mechanisms by which PVAT regulates vascular tone, the molecular mechanism(s) is still not clear. Several studies have reported that PVAT regulates vascular

contractility by releasing a wide variety of mediators that influence the underlying VSMC and vascular endothelium. These mediators are collectively called PVAT-derived relaxing factor (PVRF) (Löhn *et al.*, 2002). It has been reported that the direct contact of PVAT with the vessel is not necessary for PVAT to exert an anticontractile effect. Addition of a dissected PVAT or PVAT conditioned medium (CM) into the organ bath of aortic rings with no PVAT augmented the relaxation equally as effectively as when the PVAT was in contact with the artery (Almabrouk *et al.*, 2017). The identity of these factors has not been completely defined although adiponectin (Fésüs *et al.*, 2007; Almabrouk *et al.*, 2017), hydrogen sulfide (H_2S) (Fang *et al.*, 2009), nitric oxide (NO) (Gil-Ortega *et al.*, 2010), leptin (Vecchione *et al.*, 2002), and hydrogen peroxide (Gao *et al.*, 2007) have been proposed. Previous studies in our lab demonstrated that PVAT from AMPKα1 KO mice secreted less adiponectin, and incubation with globular adiponectin recovered the impaired relaxation to cromakalim in KO vessels both with and without PVAT, suggesting that adiponectin may be one of the PVRFs that induces vasorelaxation by direct action on VSMCs (Almabrouk *et al.*, 2017). The data presented in this chapter adds further information on how PVAT induces vasorelaxation, as well as the role of AMPK in the regulation of VSMCs and PVAT function.

Several studies have reported different mechanisms by which PVAT exerts an anticontractile effect on different vascular beds. In thoracic aorta of male Sprague-Dawley rats, relaxant effect of PVRFs was mediated by tyrosine kinase-dependent activation of ATP-dependent K^+ channels in vascular smooth muscle cells (Löhn *et al.*, 2002). Moreover, in the same study they found that mechanical removal of endothelium or inhibition of endothelial NO did not affect the anticontractile effect of PVRFs to serotonin. Interestingly, they found that relaxation in intact PVAT rings was abolished when rings were incubated in Ca^{2+} free solution. Therefore, they concluded that PVAT induces relaxation through release of transferable factors that act through activation of K_{ATP} channels and tyrosine kinase in a Ca^{2+} dependent and endothelium-independent manner. In thoracic aortae as well, it has also been reported that PVAT can induce an anticontractile effect on VSMC via release of H_2O_2 , as incubation of PVAT-intact and endothelium denuded (PVAT+ E-) aortic rings with catalase, a scavenger of H_2O_2, enhanced the contractile response to phenylephrine (Gao *et al.*, 2007); an

effect which was not seen in rings with PVAT removed and denuded endothelium (PVAT- E-).Furthermore, addition of SOD and the SOD mimetic (tiron) reduced the contractile response to phenylephrine in PVAT+ rings but not in PVAT- rings (Gao *et al.*, 2007). PVAT-derived H_2O_2 modulates vessel contractility via activation of soluble guanylate cyclase (sGC), because sGC inhibition counteracted the anticontractile effect of PVAT in PVAT+ E- arteries and eliminated the inhibitory effect of exogenously applied H_2O_2 on phenylephrine-induced contraction in PVAT- E- arteries (Gao *et al.*, 2007). In Wistar rats thoracic PVAT was also reported to induce endothelium-dependent relaxation through NO release and subsequent K_{Ca} channel activation (Gao *et al.*, 2007). The reason behind this diversity in K^+ channel subtypes activated by PVRF is not clear, but it may be related to differences in the distribution of these K^+ channels among different vessels or different species.

In mouse mesenteric vessels, adiponectin was found to relax VSMCs via delayed rectifier K^+ (K_v) channel opening and membrane hyperpolarisation (Fésüs *et al.*, 2007). However, another study suggested that the anticontractile effect of adiponectin on blood vessels is mediated by activation of large conductance calcium dependent potassium channels (BKca channel) on VSMCs (Lynch *et al.*, 2013). In HFD rats, chronic adiponectin treatment normalised mesenteric artery-endothelial cell function by a mechanism that involved increased eNOS phosphorylation and decreased PVAT inflammation (Sena *et al.*, 2017). It has also been reported that mesenteric PVAT regulates arterial tone of mesenteric arteries by inducing vasorelaxation via K_v channel activation in VSMCs (Verlohren *et al.*, 2004; Gálvez *et al.*, 2006).

In addition to its role in the regulation of cellular and whole-body metabolism (Salt and Hardie, 2017), several studies reported that activation of AMPK is essential for maintaining vascular homeostasis through modulation of several signalling pathways. AMPK activation is demonstrated to have vasorelaxant effects and to suppress VSMC proliferation, migration, and hypertrophy (Liang *et al.*, 2013). AMPK mediates the action of vascular endothelial growth factor (VEGF), a key regulator of endothelial cell function and angiogenesis (Reihill *et al.*, 2007). In endothelial cells, adiponectin stimulates angiogenesis by promoting cross-talk between AMP-activated protein kinase and Akt signaling (Ouchi *et al.*, 2004). It

has also been speculated that commonly used medications like metformin, rosiglitazone, and statins exert their cardiovascular protective benefits partially via AMPK activation (Davis *et al.*, 2006; Zou and Wu, 2008; Boyle *et al.*, 2008).

The predominant AMPK catalytic subunit in endothelium (Morrow *et al.*, 2003) and PVAT (Almabrouk et al., 2017) is α1, while the α2 catalytic subunit is mostly found in skeletal and cardiac muscle (Stapleton *et al.*, 1996). AMPK activation induces vasorelaxation through endothelium-dependent and independent pathways. Several studies have shown that endothelial AMPK activation results in NO release via phosphorylation of eNOS at Ser^{1177} and Ser^{633} (Zou and Wu, 2008). It has been reported that in diabetes, metformin improves vascular endothelial functions by increasing AMPKα1-dependent eNOS activation and NO bioactivity (Davis *et al.*, 2006). In human aortic endothelial cells, direct activation of AMPK with 5'-aminoimidazole-4-carboxamide ribonucleoside (AICAR) stimulates NO production (Morrow *et al.*, 2003). Moreover, activation of AMPKα1 by AICAR induces endothelium-independent aortic relaxation (Goirand *et al.*, 2007; Pyla *et al.*, 2022). In resistance arteries, activation of AMPK was shown to directly relax VSMCs by reducing intracellular Ca^{2+} levels, which was achieved by calcium sequestration via SERCA activation, as well as activation of BK_{Ca} channels (Schneider *et al.*, 2015). AMPK activation is proposed to mediate the anticontractile effect of adiponectin. Meijer et al showed that adiponectin release and AMPK activation in the vessel wall is necessary in insulin-induced vasodilation in muscle resistance arteries (Meijer *et al.*, 2013). Moreover, Almabrouk et al reported that in AMPKα1 KO mice the anticontractile effect of thoracic aortic PVAT was lost, which was associated with a reduction in adiponectin secretion by KO PVAT (Almabrouk *et al.*, 2017). This suggests that AMPKα1 has a critical role in maintaining the anticontractile actions of PVAT.

The role of AMPK in the function of PVAT and on ADRFs release has not been widely studied. We investigated the effect of AMPKα1 deficiency on the anticontractile effect of the PVAT. A previous study reported that in endothelium denuded vessels, PVAT lost its anticontractile effect in AMPKα1 KO mice (Almabrouk *et al.*, 2017). Moreover, Almabrouk *et al*, also reported that the presence of PVAT or addition of globular adiponectin enhanced the relaxation to cromakalim. This suggests that the anticontractile effect of PVAT and/or adiponectin could be

partly mediated by K_{ATP} channels. The vasorelaxant effect of cromakalim is not mediated by AMPK activation in VSMCs (Almabrouk *et al.*, 2017). The current study also reported a reduction in the vasodilatory effect of abdominal PVAT in AMPKα1 KO mice. This reduction was observed in both endothelium-intact and denuded vessels, although the effect was higher in endothelium-intact rings. This suggests that AMPK α1 could have a role on relaxation mediated via both endothelium and VSMCs mechanisms. This role could be by influencing the secretion of ADRFs which act on both endothelium and VSMCs. Furthermore, current study also reported that the difference in relaxation response between WT and AMPK α1 KO is unlikely to be due to AMPK or eNOS activation on endothelial cells as both reagents used, cromakalim and phenylephrine, had no effect on AMPK or eNOS activation on cultured endothelial cells. However, the effect of these reagents on the AMPK and eNOS phosphorylation on PVAT has not been investigated.

3.5 Conclusion

The findings presented in this study align with and extend existing evidence implicating AMPK in the modulation of the anticontractile effect of PVAT across diverse vascular beds. Specifically, our investigation revealed a compromised vasodilatory response in abdominal PVAT from AMPKα1 KO mice. Furthermore, the heightened impairment in vasorelaxation observed in KO abdominal PVAT is endothelium-independent and may reflect a difference in the physiology of VSMCs or PVAT, potentially impacted by the deletion of the AMPKα1 subunit. In light of prior research indicating that the anticontractile impact of PVAT is contingent on the release of relaxing factors, our results suggest a potential role for AMPKα1 in the regulation of the release of these factors within abdominal PVAT. The next chapter will explore the difference in the secretory activity of PVAT between WT and AMPK α1 KO mice shedding further light on the intricate mechanisms underlying the observed effects.

Chapter 4 Effect of AMPKα1 on PVAT secretory function

4.1 Introduction

Comparable to adipose tissue found in other anatomical locations, PVAT contains diverse cell types, including adipocytes, macrophages, fibroblasts, T-lymphocytes, preadipocytes, as well as vascular structures and nerve components (Grigoras *et al.*, 2019). The phenotypic characteristics of PVAT manifest as either BAT, WAT, or a combination thereof, contingent upon its specific anatomical site (Sowka and Dobrzyn, 2021). In mice, thoracic PVAT is similar to BAT in terms of having small adipocytes with multiple small lipid droplets and abundant mitochondria, as well as high expression of UCP-1 (Gálvez-Prieto *et al.*, 2008; Fitzgibbons *et al.*, 2011; Almabrouk *et al.*, 2017). Abdominal and mesenteric PVAT resembles WAT, with adipocytes containing large lipid droplets with relatively few mitochondria (Police *et al.*, 2009; Fitzgibbons *et al.*, 2011; Padilla *et al.*, 2013).

In the past, PVAT was considered as merely a passive reservoir for energy storage, as well as a supportive and thermoregulatory organ. When PVAT was shown to influence aortic responsiveness in rats (Soltis and Cassis, 1991), an important role of PVAT as an active endocrine organ was established, further characterised when adipocyte-derived relaxing factors (ADRFs) were identified (Löhn *et al.*, 2002). The direct contact of PVAT with the adventitial layer allows for humoral crosstalk between cells of the PVAT and the other cell layers within the vessel wall (VSMCs and endothelium). However, many studies have demonstrated that it is not necessary for PVAT to be in direct contact with the vessel wall to exert its anticontractile effect. Transfer of a dissected PVAT or PVAT-derived conditioned medium to a PVAT-free vessel preparation is sufficient to produce enhanced vessel relaxation (Almabrouk *et al.*, 2017). The identity of these ADRFs has not been completely defined although adiponectin (Fésüs *et al.*, 2007; Almabrouk *et al.*, 2017), hydrogen sulfide (H_2S) (Fang *et al.*, 2009), NO (Gil-Ortega *et al.*, 2010), leptin (Vecchione *et al.*, 2002), and hydrogen peroxide (Gao *et al.*, 2007) have been proposed. The mechanism(s) by which these ADRFs influence the underlying VSMCs, and endothelium has not been fully investigated. Many studies have reported various mechanisms on different vascular beds (discussed in the previous chapter).

The complexity of PVAT in terms of its different phenotypes, anatomical locations, and secretory profiles have developed into an active and expanding research field

with attempts being made to link the activity of PVAT to cardiovascular health and disease. Growing evidence has shown that the presence of normally functioning PVAT is required to maintain the vasculature in a healthy state (Chang *et al.*, 2020). Moreover, studies have illustrated that in the context of cardiovascular disease, perivascular adipose tissue (PVAT) undergoes functional impairment characterised by alterations in its inflammatory profile, shifts in cellular composition, and modifications in the release of adipocytokines (Nosalski and Guzik, 2017). Dysfunctional PVAT has the propensity to attract proinflammatory immune cells, foster dysfunction in endothelial cells, and stimulate proliferation in vascular smooth muscle cells (VSMC) (Qi *et al.*, 2018; Sowka and Dobrzyn, 2021). Previous work in our lab demonstrated that high fat diet causes an attenuation in the anticontractile effect of PVAT along with inflammatory cell infiltration and a reduction in adiponectin secretion and AMPK phosphorylation (Almabrouk *et al.*, 2018). Therefore, targeting dysfunctional PVAT may provide a new treatment strategy for prevention and treatment of cardiovascular diseases.

In addition to its role in regulating cellular and whole-body energy homeostasis, AMPK also play an important role in maintaining vascular homeostasis (Rodríguez *et al.*, 2021). In cardiac tissues, AMPK regulates metabolism and contractile function, as well as promoting antiatherogenic, anti-inflammatory, and anticontractile actions in blood vessels (Salt and Hardie, 2017). Several studies have reported that AMPK activation induces vasorelaxation via activation of endothelial NOS and increasing NO synthesis (Morrow *et al.*, 2003; Rodríguez *et al.*, 2020), and also via direct relaxation of VSMCs by reducing intracellular Ca^{2+} levels (Schneider *et al.*, 2015). In PVAT, previous work from our lab reported a diminished anticontractile effect of PVAT in AMPK α1 KO mice along with reduced adiponectin release by PVAT (Almabrouk *et al.*, 2017). In the previous chapter of this thesis, it was also reported that in AMPKα1 KO mice the vasodilatory activity of abdominal PVAT was attenuated in both endothelium-intact and denuded vessels. Therefore, the aim of the work presented in this chapter was to investigate whether AMPK may mediate the endothelium-dependent anticontractile effect of abdominal PVAT via modulating release of PVRFs.

4.2 Aims of the study

Building upon the findings outlined in Chapter 3, which elucidated the loss of the anti-contractile effect in abdominal PVAT in KO mice compared to WT mice, here the aim was to investigate disparities in the secretory profile between thoracic and abdominal PVAT derived from WT and KO mice. Secondly, since the difference in the anti-contractile effect of PVAT between WT and KO abdominal aortae was more marked in endothelium-intact vessels, the effect of PVAT CM was assessed on different signalling pathways in cultured endothelial cells. Understanding the role of AMPK in regulating PVAT function and its potential influence on vascular relaxation through the modulation of various PVRFs is essential for elucidating the comprehensive impact of AMPK on PVAT function and its implications for vascular health.

4.3 Results

4.3.1 PVAT weight in thoracic and abdominal region.

To assess the quantity of PVAT which surrounds both thoracic and abdominal aortae, PVAT from both anatomical locations was carefully dissected and weighed. As seen in Figure 4-1, abdominal aorta has significantly more PVAT compared to that surrounding the thoracic aorta (37.6 ± 4.5mg vs 12.2 ± 0.71mg, respectively) (*P*<0.0001; *n*=10/group).

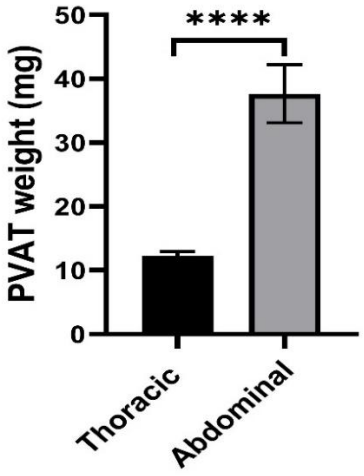

Figure 4-1 PVAT weight in thoracic and abdominal region

To measure the amount of PVAT surrounding thoracic and abdominal aortae, PVAT was carefully dissected and weighed. (*P*<0.001 unpaired t-test)

4.3.2 AMPKα1 knockout mouse PVAT has altered adipokine release.

To assess the secretion of adipokines by PVAT from WT and AMPKα1 KO mice, conditioned medium from thoracic and abdominal PVAT was prepared and assayed using a Proteome Profiler Adipokine array (R&D systems) which detects 38 different adipocytokines (as described in sections 2.6.52.6.6).

As can be seen in Figure 4-2, conditioned media derived from thoracic AMPKα1 KO PVAT released lower quantities of some adipokines in comparison with WT PVAT. However, this difference was not significant (*n*=3).

Similarly, conditioned medium derived from abdominal PVAT from AMPKα1 KO mice released lower quantities of some adipokines in comparison with WT PVAT (Figure 4-3). The release of factors including fibroblast growth factor-21 (FGF-21), intercellular adhesion molecule 1 (ICAM-1), tissue inhibitor of metalloproteinase 1 (TIMP-1), insulin-like growth factor-II (IGF-II), and leukaemia inhibitory factor (LIF) were significantly lower in AMPKα1 KO compared to wild type PVAT (n=3; $^{*}P < 0.05$).

Although statistical significance was not met, the release of the following adipokines from KO abdominal PVAT was also reduced compared to the WT PVAT: interleukin 6 (IL-6) (P= 0.07), interleukin II (IL-II) (P= 0.08), monocyte chemoattractant protein-1 (MCP-1) (P= 0.09), dipeptidyl peptidase-4 (DPPIV) (P= 0.08), hepatocyte growth factor (HGF) (P= 0.09), leptin (P= 0.059), receptor for advanced glycation end-products (RAGE (P= 0.08), regulated upon activation, normal T cell expressed and secreted (RANTES) (P= 0.07), and serpin (P= 0.053).

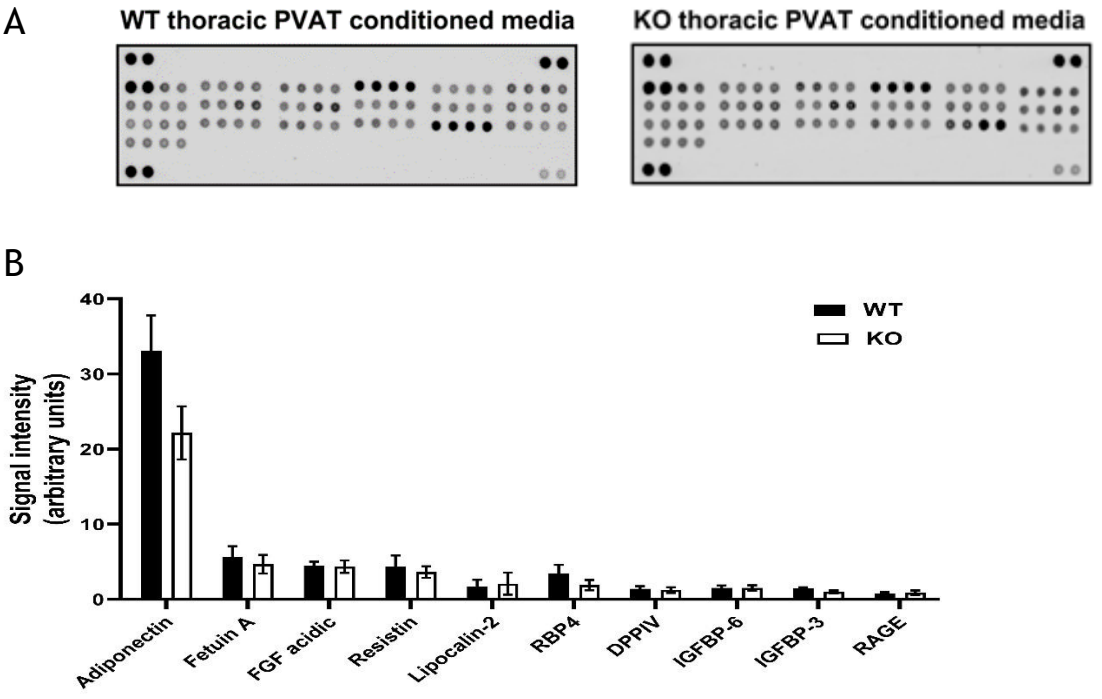

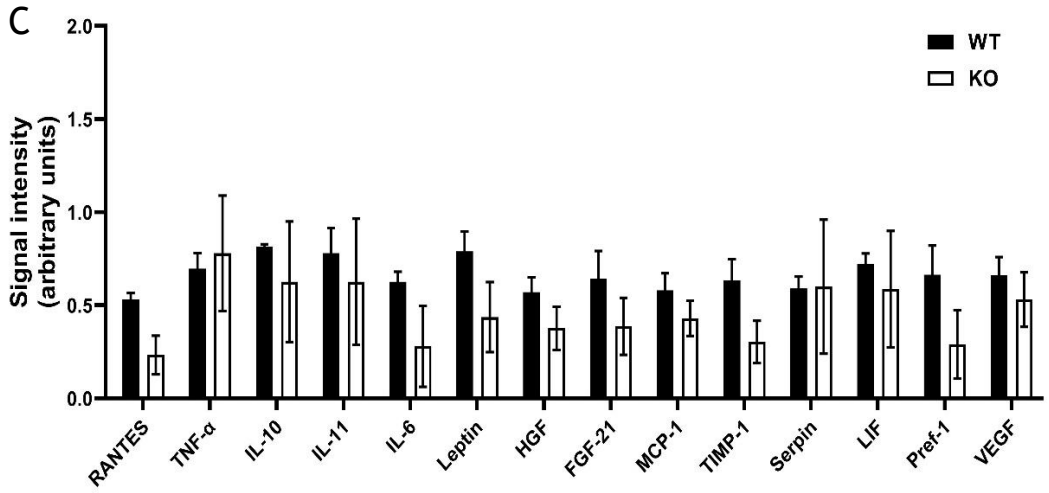

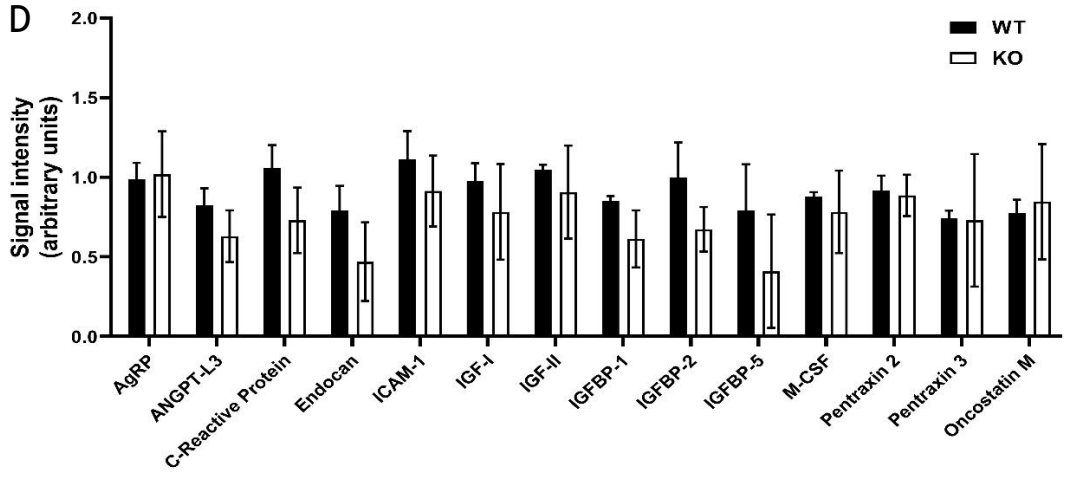

E

	1	2	3	4	5	6	7	8	9	10	11	12	13	14	15	16	17	18	19	20	21	22	23	24
A	PC																						PC	
B	Adiponectin		AgRP		ANGPT-L3		CRP		DPP-4		Endocan		Fetuin A		FGF acidic		FGF-21		HGF		ICAM-1		IGF-I	
C	IGF-II		IGFBP-1		IGFBP-2		IGFBP-3		IGFBP-5		IGFBP-6		IL-6		IL-10		IL-11		Leptin		LIF		Lipocalin-2	
D	MCP-1		M-CSF		Oncostatin M		Pentraxin 2		Pentraxin 3		Pref-1		RAGES		RANTES		RBP4		Resistin		Serpin E1		TIMP-1	
E	TNF-α		VEGF																					
F	PC																						NC	

Figure 4-2 Adipokine levels in wild type and AMPKα1 KO thoracic PVAT conditioned medium.

Thoracic PVAT from WT and KO mice was incubated in 1 mL PSS at 37ºC for 1 h with continuous oxygenation and conditioned medium was collected. Adipokine levels in conditioned medium were assessed using a Proteome Profiler Mouse Adipokine Array kit containing 38 mouse adipokine and adipokine-related antibodies in duplicate. (A) Representative arrays showing chemiluminescent reaction spots on the adipokine profiler membranes. (B, C, D) Comparative levels of adipokines released by 10 mg of PVAT (*n*=3). (E) A position map of the antibodies on the array, with FGF-21 highlighted in grey.

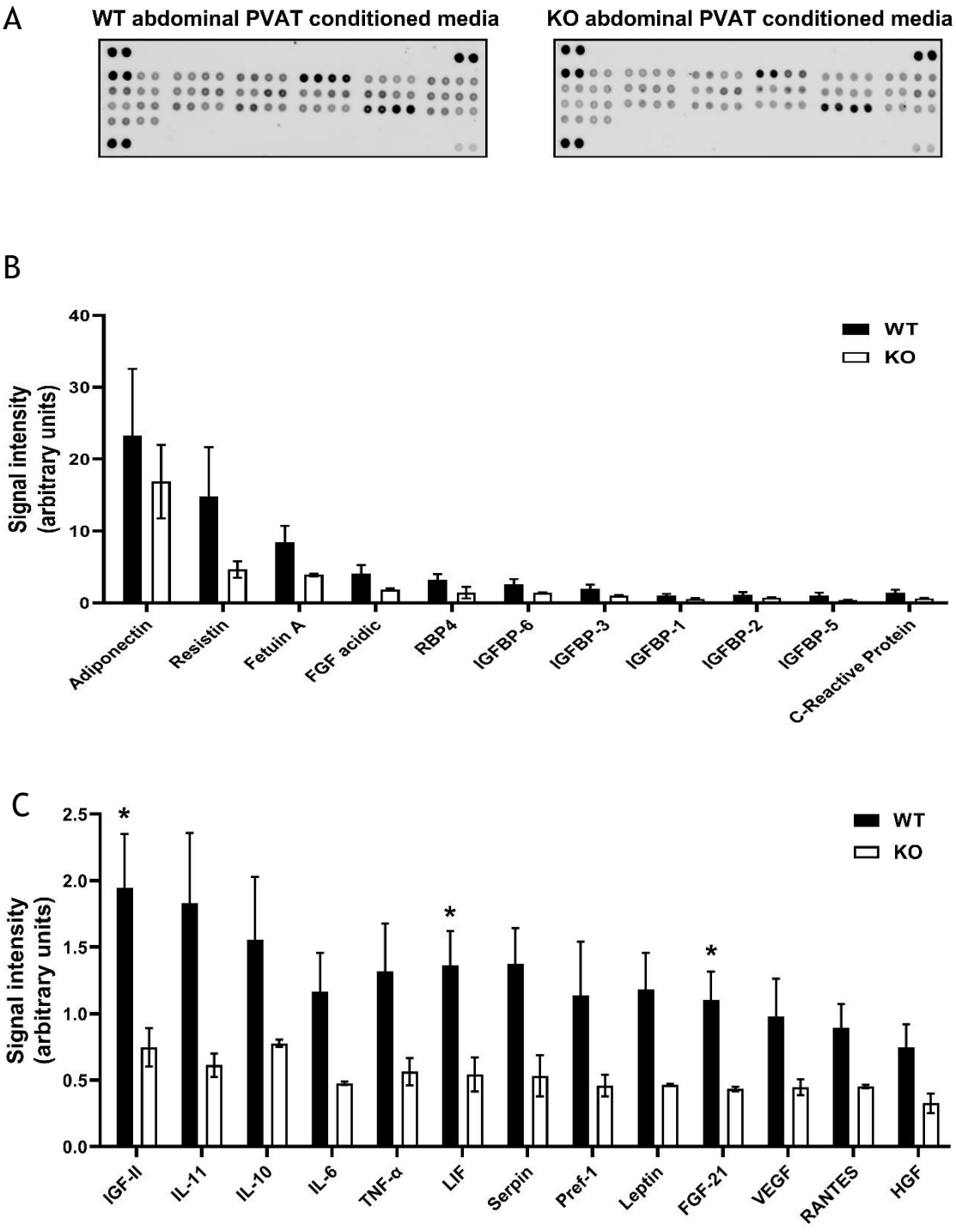
A
WT abdominal PVAT conditioned media
KO abdominal PVAT conditioned media
B
Signal intensity (arbitrary units)
WT
KO
Adiponectin
Resistin
Fetuin A
FGF acidic
RBP4
IGFBP-6
IGFBP-3
IGFBP-1
IGFBP-2
IGFBP-5
C-Reactive Protein
C
Signal intensity (arbitrary units)
WT
KO
IGF-II
IL-11
IL-10
IL-6
TNF-α
LIF
Serpin
Pref-1
Leptin
FGF-21
VEGF
RANTES
HGF

D

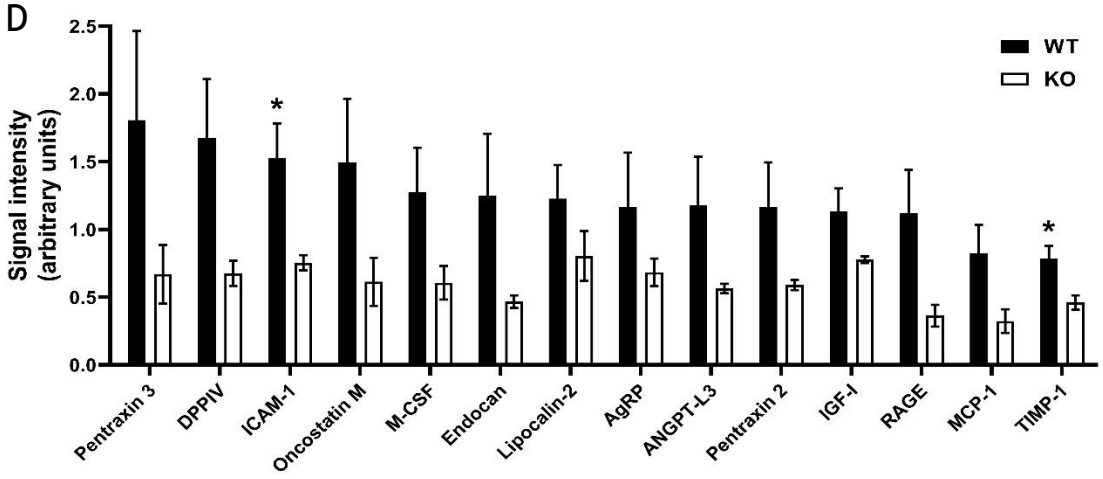

E

	1	2	3	4	5	6	7	8	9	10	11	12	13	14	15	16	17	18	19	20	21	22	23	24
A	PC																						PC	
B	Adiponectin		AgRP		ANGPT-L3		CRP		DPP-4		Endocan		Fetuin A		FGF acidic		FGF-21		HGF		ICAM-1		IGF-I	
C	IGF-II		IGFBP-1		IGFBP-2		IGFBP-3		IGFBP-5		IGFBP-6		IL-6		IL-10		IL-11		Leptin		LIF		Lipocalin-2	
D	MCP-1		M-CSF		Oncostatin M		Pentraxin 2		Pentraxin 3		Pref-1		RAGES		RANTES		RBP4		Resistin		Serpin E1		TIMP-1	
E	TNF-α		VEGF																					
F	PC																						NC	

Figure 4-3 Adipokine levels in wild type and AMPKα1 KO abdominal PVAT conditioned medium.

Abdominal PVAT from WT and KO mice was incubated in 1 mL PSS at 37ºC for 1 h with continuous oxygenation and conditioned medium was collected. Adipokine levels in conditioned medium were assessed using a Proteome Profiler Mouse Adipokine Array kit containing 38 mouse adipokine and adipokine-related antibodies in duplicate. (A) Representative arrays showing chemiluminescent reaction spots on the adipokine profiler membranes. (B, C, D) Comparative levels of some adipokines released by 10 mg of PVAT (n=3). (E) A position map of the antibodies on the array with FGF-21 highlighted in grey. *P < 0.05 relative to KO (Unpaired t-test).

4.3.3 Abdominal PVAT from AMPKα1 knockout mice releases less FGF-21

Quantification of the array data indicated reduced FGF-21 release by abdominal KO PVAT (P<0.05) (Figure 4-4 A). Recent research has emphasised a potentially beneficial protective function of FGF-21 within the vascular system, demonstrating its influence on endothelial function. Therefore, an ELISA was used to quantify this more accurately in a larger number of samples. (Experimental protocol described in section 2.6.7). As can be seen in Figure 4-4 B, the concentration of FGF-21 in abdominal KO PVAT conditioned medium was significantly (P<0.01) lower than that in WT PVAT conditioned medium (0.535 ±0.055 pg/hr/mg PVAT in WT, n = 4 vs 0.097 ± 0.02 pg/hr/mg PVAT in KO, n = 3). This result is consistent with the data from the adipokine array. Moreover, in the array experiment FGF-21 levels in abdominal WT PVAT conditioned media were

higher than in thoracic WT PVAT conditioned medium. This was also the case when assessing by ELISA where FGF-21 was undetectable in thoracic PVAT conditioned medium in both genotypes (data not shown).

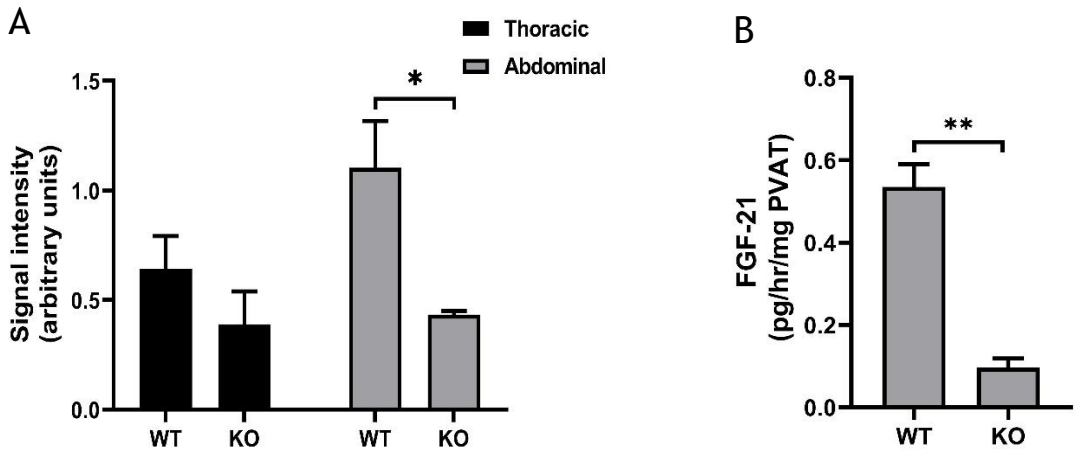

Figure 4-4 FGF-21 in wild type and AMPKα1 KO PVAT conditioned medium.

Thoracic and abdominal PVAT from both genotypes was incubated in PSS at 37ºC for 1 h with continuous oxygenation and conditioned medium collected. (A) FGF-21 levels were assessed using a Proteome Profiler Mouse Adipokine Array kit (*n*=3). (B) FGF-21 levels in conditioned media from abdominal PVAT were measured by ELISA (*n*= 3-4). Data shown represent the mean ± SEM (A) arbitrary units or (B) pg/hr/mg PVAT. **P* < 0.05, ***P* < 0.01 (Unpaired t-test).

4.3.4 AMPKα1 knockout PVAT has reduced FGF-21 levels.

To assess the tissue levels of FGF-21 in the PVAT of wild-type and AMPKα1 knockout mice, homogenised thoracic and abdominal PVAT lysates were prepared and subjected to immunoblotting with anti-FGF-21 antibodies.

As seen in Figure 4-5, FGF-21 levels in abdominal PVAT of AMPKα1 knockout mice were lower, though not significantly compared to wild-type abdominal PVAT (*P*= 0.12). However, we were unable to detect FGF-21 in thoracic PVAT lysates, even when high (40µg) protein levels were loaded.

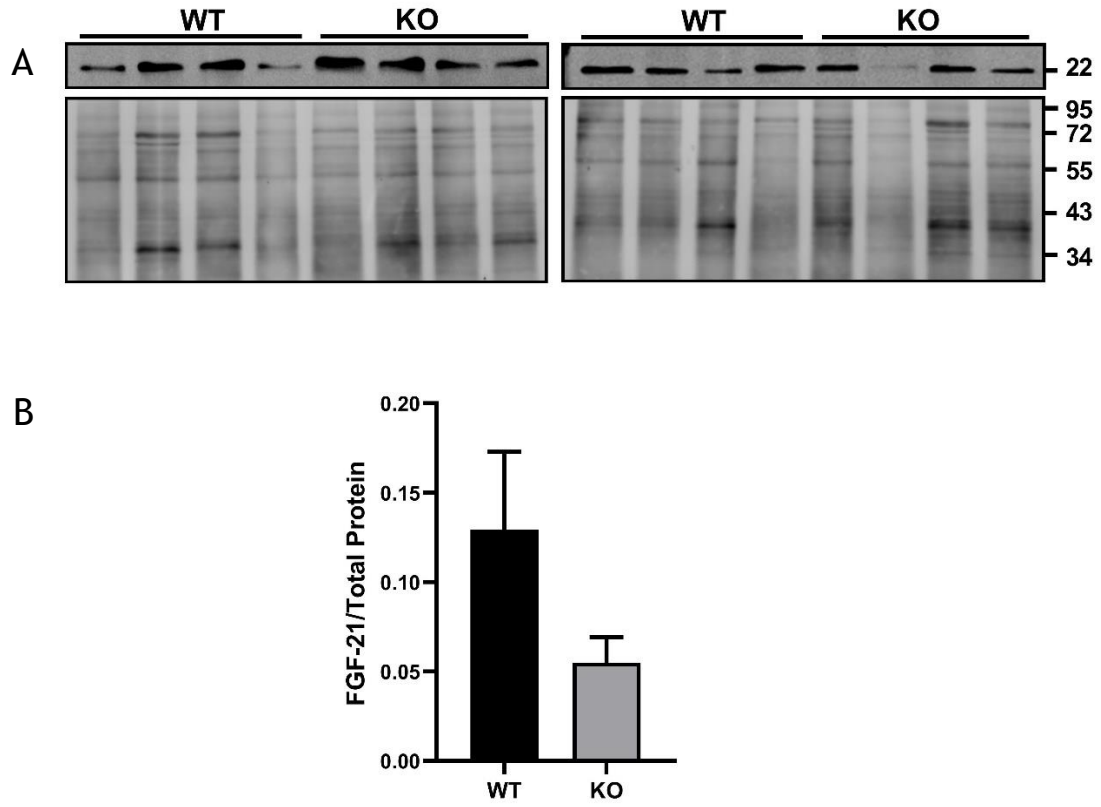

Figure 4-5 FGF-21 levels in abdominal PVAT

Lysates from both WT and KO abdominal PVAT were prepared and resolved by SDS-PAGE then subjected to immunoblotting with anti-FGF-21 antibodies. (A) Representative immunoblots with molecular mass markers indicated on the right in KDa. (B) Quantification of FGF-21 levels relative to total lysate protein levels, assessed with REVERT total protein stain (*n*= 8 per group). Data shown represent the mean ± SEM FGF21/total protein in arbitrary units.

4.3.5 *Fgf21* mRNA levels were not altered in AMPKα1 knockout mice.

To determine whether *Fgf21* gene expression was altered in AMPKα1 KO PVAT, *Fgf21* mRNA expression was measured by qPCR (methods as described in section 2.12). RNA was extracted from thoracic and abdominal PVAT of both genotypes, reverse transcribed, and the expression of *Fgf21* mRNA examined by quantitative PCR using mouse *Fgf21* TaqMan probes.

Fgf21 gene expression was higher in WT thoracic PVAT compared to KO PVAT, although it did not achieve statistical significance. In abdominal PVAT, the expression of *Fgf21* gene was very similar between both genotypes (Figure 4-6).

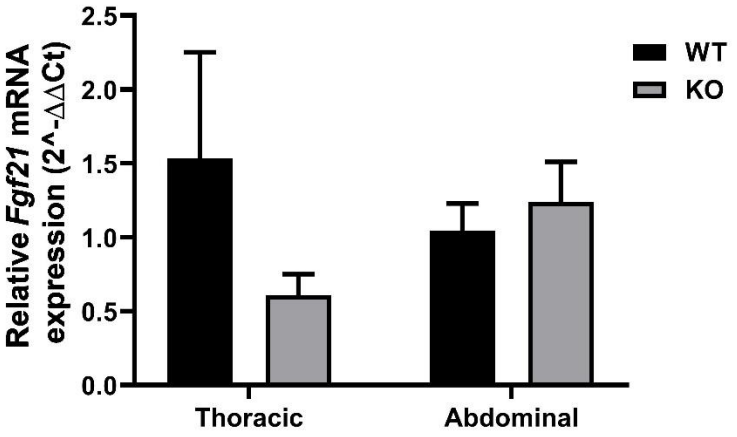

Figure 4-6 *Fgf21* mRNA expression in WT and AMPKα1 KO PVAT

Fgf21 mRNA expression was measured by qPCR normalised to TATA-box binding protein (*Tbp)* expression. Data shown represent the mean ± SEM relative expression, *n*=4.

4.3.6 Serum FGF-21 levels are not altered in AMPKα1 knockout mice.

To investigate whether FGF-21 levels in the systemic circulation are altered in AMPKα1 KO mice, blood samples from wild type and KO mice were collected immediately after euthanising and FGF-21 levels in the serum were measured by ELISA (as described previously). Serum FGF-21 levels are primary derived from the liver, especially in response to metabolic stress, fasting, or certain dietary conditions. As shown in Figure 4-7, the systemic level of FGF-21 in both genotypes was not different.

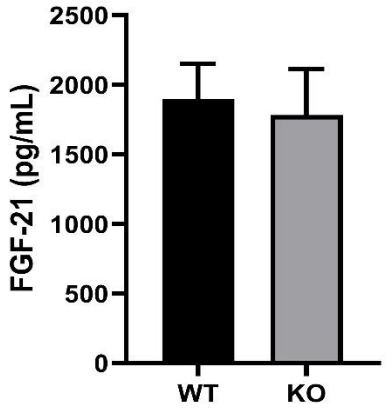

Figure 4-7 Serum FGF-21 levels in wild type and AMPKα1 KO mice

Blood samples from WT and KO mice were collected at time of dissection and allowed to clot for 2 h at room temperature before centrifuging for 20 min at 2000 x g. Serum was then aspirated and stored at -20ºC. Serum FGF-21 levels were measured using a Mouse/Rat FGF-21 Quantikine ELISA Kit. Data shown represent the mean ± SEM pg/mL FGF21 (*n*=10) (Unpaired t-test).

4.3.7 Nitric oxide release by PVAT

To assess the role of AMPKα1 on NO synthesis by PVAT, thoracic and abdominal PVAT from both genotypes was collected and incubated for 1 h in PSS at 37ºC with continuous oxygenation and conditioned medium collected. NO levels in the conditioned medium were measured using a Sievers 280 NO analyser as described in section 2.12.3.

As shown in Figure 4-8, in thoracic PVAT, the synthesis of NO was significantly reduced in AMPKα1 KO compared to WT PVAT (309.2 ± 45.3 vs 139.2 ± 48.6 nmol NOx/mg PVAT/hr; *n*=6; **P* < 0.05). However, in abdominal PVAT, the synthesis of NO was similar in WT and AMPKα1 KO mice (*n*=6). Interestingly, in both genotypes the synthesis of NO by abdominal PVAT was lower than that produced by thoracic PVAT. This difference was significant in wild type PVAT (309.2 ± 45.3 vs 43.3 ± 8.2 nmol NOx/mg PVAT/hr for thoracic and abdominal PVAT, respectively) (*n*=6; ****P* < 0.001).

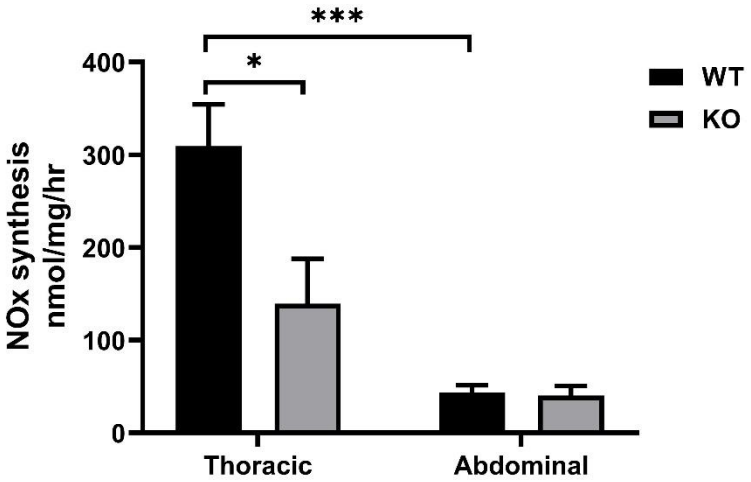

Figure 4-8 NOx production by aortic PVAT of wild type and AMPKα1 KO mice

Thoracic and abdominal PVAT from both genotypes was incubated in PSS at 37ºC for 30 min with continuous oxygenation and conditioned medium collected. NOx levels in conditioned medium were quantified using a Sievers 280 NO analyser. Data shown represent the mean ± SEM nmol NOx/mg PVAT/hr (*n*=6). **P* < 0.05, ***P* < 0.001 (Unpaired t-test). This experiment was performed by Abdmajid Hwej (University of Glasgow).

4.3.8 Effect of PVAT conditioned medium on AMPK activity in HUVECs.

To examine the effect of PVAT-derived conditioned medium on AMPK activity, cultured HUVECs were incubated for 30 min with either thoracic or abdominal PVAT conditioned medium from either KO or WT mice. AMPK activity was assessed by the degree of phosphorylation of the AMPK substrate, ACC Ser^{79} by western blotting analysis.

As shown in Figure 4-9, stimulation of HUVECs with conditioned medium from thoracic PVAT of WT or AMPKα1 KO mice caused a small increase in phosphorylation of ACC that did not achieve statistical significance. In conditioned medium from abdominal PVAT of either WT or KO mice caused a small decrease in ACC phosphorylation that also did not achieve statistical significance (*n*=4). Furthermore, in both genotypes, the conditioned medium from the thoracic region exhibited a greater stimulation of ACC compared to the abdominal counterpart, although statistical significance was not attained.

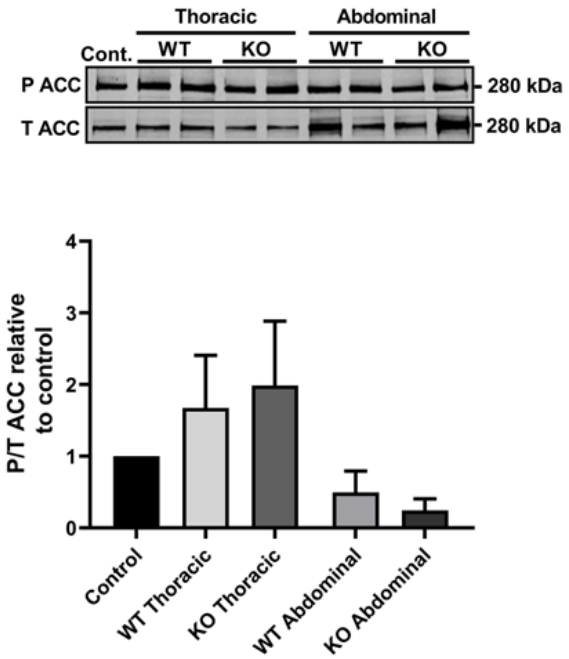

Figure 4-9 Effect of PVAT conditioned medium on AMPK activity in HUVECs.

HUVECs were incubated with thoracic and abdominal PVAT-derived conditioned medium from WT or AMPKα1 KO mice for 30 min. Lysates were prepared, resolved by SDS-PAGE and subjected to immunoblotting with the ACC antibodies (T, total, P, phospho). Representative immunoblots with

molecular mass markers (in KDa) indicated on the right are shown on the top of each corresponding graph. Data shown represent the mean ± SEM phosphorylation relative to control from four independent experiments. (one-way ANOVA).

4.3.9 Effect of PVAT conditioned medium on eNOS stimulation in HUVECs.

Phosphorylation of eNOS at Ser^{1177} by Akt, AMPK and other kinases has been reported to increase eNOS activity leading to enhanced nitric oxide (NO) production (Thors *et al.*, 2011; Liang *et al.*, 2021). To examine the effect of PVAT-derived conditioned medium on eNOS phosphorylation, cultured HUVECs were incubated for 30 min with thoracic or abdominal PVAT conditioned medium from either KO or WT mice. The extent of eNOS Ser^{1177} phosphorylation was determined by western blotting analysis of HUVEC lysates.

As shown in Figure 4-10, stimulation of HUVECs with conditioned medium from thoracic or abdominal PVAT from either genotype had no effect on eNOS phosphorylation compared to the negative control (*n*=4).

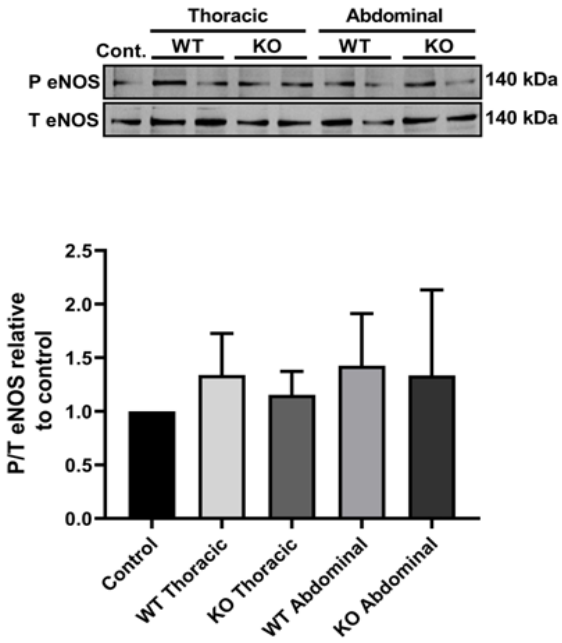

Figure 4-10 Effect of PVAT conditioned medium on eNOS stimulation in HUVECs.

HUVECs were incubated with thoracic and abdominal PVAT-derived conditioned medium from WT or AMPKα1 KO mice for 30 min. Lysates were prepared, resolved by SDS-PAGE and subjected to immunoblotting with the eNOS antibodies (T, total, P, phospho). Representative immunoblots with molecular mass markers (in KDa) indicated on the right are shown on the top of each corresponding graph. Data shown represent the mean ± SEM phosphorylation relative to control from four independent experiments. (one-way ANOVA).

4.3.10 Effect of PVAT conditioned medium on Akt stimulation in HUVECs.

The activation of Akt by various growth factors, such as IGF and VEGF, is well-documented and plays a crucial role in regulating multiple cellular processes, including endothelial function (Sun *et al.*, 2019). To examine the effect of PVAT-derived conditioned medium on Akt stimulation, cultured HUVECs were incubated for 30 min with thoracic or abdominal PVAT conditioned medium from either KO or WT mice. The extent of Akt Ser^{473} phosphorylation was determined by western blotting analysis of HUVECs lysates.

As shown in Figure 4-11, stimulation of HUVECs with conditioned medium from thoracic PVAT of wild type or AMPKα1 KO mice had no effect on Akt phosphorylation (*n*=4). In contrast, conditioned medium from abdominal PVAT of wild type or AMPKα1 KO mice caused a two-fold increase in Akt phosphorylation (*n*=4).

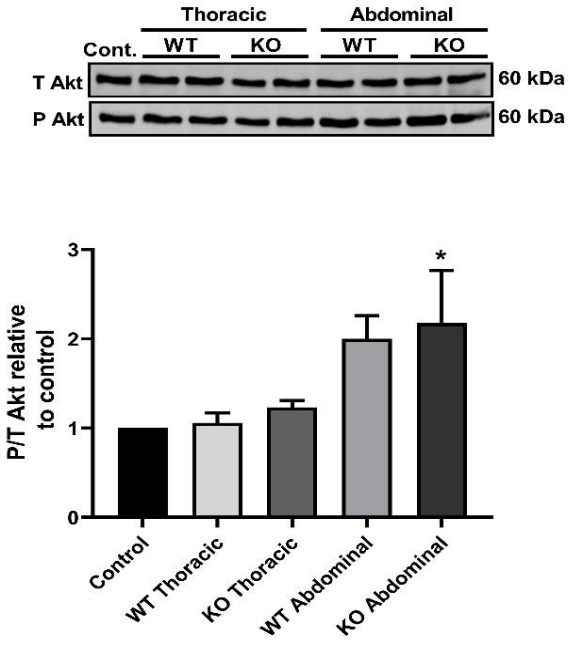

Figure 4-11 Effect of PVAT conditioned medium on Akt stimulation in HUVECs.

HUVECs were incubated with thoracic and abdominal PVAT-derived conditioned medium from WT or AMPKα1 KO mice for 30 min. Lysates were prepared, resolved by SDS-PAGE and subjected to immunoblotting with the Akt antibodies (T, total, P, phospho). Representative immunoblots with molecular mass markers (in KDa) indicated on the right are shown on the top of each corresponding graph. Data shown represent the mean ± SEM phosphorylation relative to control from four independent experiments. ($p<0.05$; one-way ANOVA).

4.3.11 Effect of PVAT conditioned medium on ERK1/2 stimulation in HUVECs.

ERK1/2 signalling is critical for the regulation of eNOS phosphorylation and nitric oxide (NO) production, impacting endothelial functions, including survival, proliferation, migration, angiogenesis, and tube formation (Wu *et al.*, 2021). To examine the effect of PVAT-derived conditioned medium on ERK1/2 stimulation, cultured HUVECs were incubated for 30 min with thoracic and abdominal PVAT conditioned medium from both WT and KO mice. The extent of ERK1/2 $Thr^{202,}$ Tyr^{204} phosphorylation was determined by western blotting analysis of HUVEC lysates. As shown in Figure 4-12, stimulation of HUVECs with conditioned medium from either thoracic or abdominal PVAT of WT or AMPKα1 KO mice increased the ERK1/2 $Thr^{202,}$ Tyr^{204} phosphorylation (*n*=4). It is also clear from the graph that ERK1/2 phosphorylation was significantly higher in response to abdominal PVAT conditioned medium than thoracic PVAT conditioned medium.

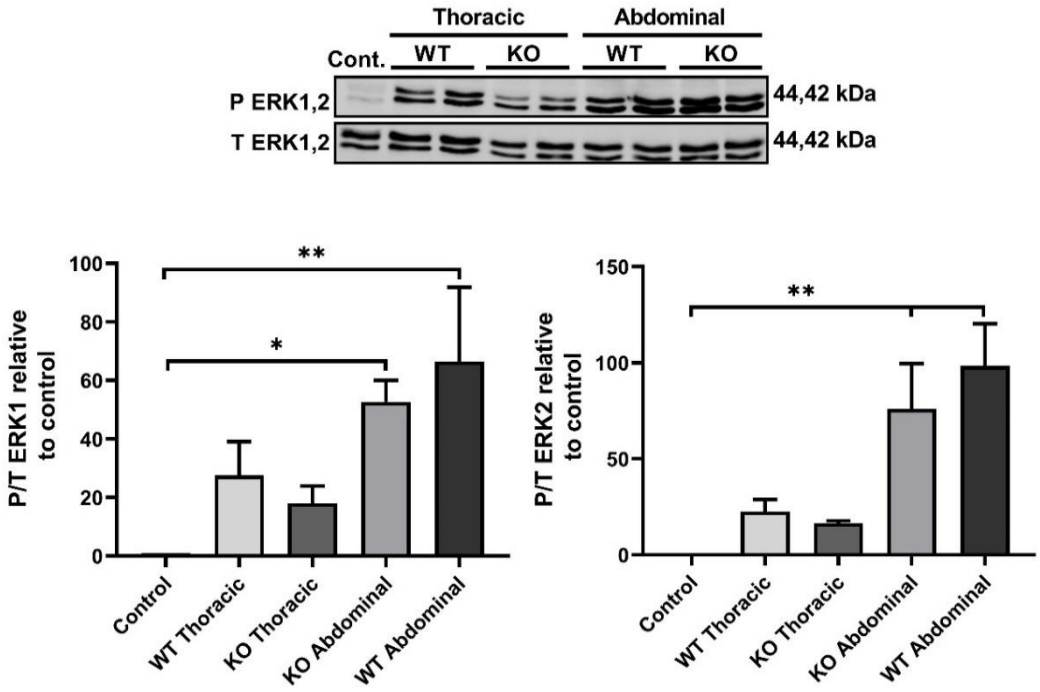

Figure 4-12 Effect of PVAT conditioned medium on ERK1/2 stimulation in HUVECs.

HUVECs were incubated with thoracic and abdominal PVAT-derived conditioned medium from WT or AMPKα1 KO mice for 30 min. Lysates were prepared, resolved by SDS-PAGE and subjected to immunoblotting with the ERK1/2 antibodies (T, total, P, phospho). Representative immunoblots with molecular mass markers (in KDa) indicated on the right are shown on the top of each corresponding graph. Data shown represent the mean ± SEM phosphorylation relative to control from four independent experiments. **P* < 0.05, ***P* < 0.01 (one-way ANOVA).

4.4 Discussion

The key finding in this chapter is that AMPKα1 plays a key role in the secretory function of aortic PVAT. In AMPKα1 KO mice, PVAT, particularly abdominal PVAT, exhibits dysregulation in the secretory function compared to WT PVAT. The striking difference was a reduction in adiponectin, FGF-21, ICAM-1, TIMP-1, IGF-II, and LIF secretion by abdominal PVAT in KO mice. Quantitative studies using ELISA further confirmed a significant reduction in FGF-21 measured in conditioned media from abdominal PVAT from KO mice. Furthermore, analysis of PVAT lysates demonstrated that KO PVAT also contained less FGF-21. These findings suggest that the impairment of adipokine secretion by abdominal KO PVAT could be responsible for the attenuation in the vasodilatory function of KO abdominal aorta reported in the previous chapter.

The aim of this chapter is to understanding the impact of AMPKα1 deletion on the secretory function of thoracic and abdominal PVAT. The research utilised a Proteome Profiler Adipokine array to assess 38 adipokines in PVAT conditioned media (CM), providing a semi-quantitative analysis. The results indicate a difference in the secretory profiles between thoracic and abdominal PVAT, with a specific reduction in FGF-21 secretion in the CM from KO abdominal PVAT. It is important to note that the study examined the secretory profile of PVAT under basal, unstimulated conditions. Comparing these results with those obtained using reagents like noradrenaline, AMPK activators, and FGF-21 would provide more comprehensive insights.

FGF-21 is member of the FGF family, and it plays a role in carbohydrate and lipid metabolism. In recent years, FGF-21 has been demonstrated to possess multiple profound cardioprotective effects and plays a role in the prediction, treatment, and improvement of prognosis in CVDs (Zhang *et al.*, 2021). Moreover, research indicates that FGF-21 can activate the AMPK pathway, either directly through FGFR1/β-klotho signalling or indirectly by stimulating the secretion of adiponectin and corticosteroids, which consequently activate AMPK signalling in their target tissues (Salminen *et al.*, 2017).

To confirm the array result, FGF-21 levels in the PVAT CM and PVAT lysates were assessed using an ELISA and immunoblotting, respectively. Both experiments

further confirmed a reduction in FGF-21 secretion by abdominal KO PVAT, as well as a reduction in the FGF-21 level in abdominal PVAT lysates of KO mice. In addition, the study went further to explore the systemic impact by measuring circulating levels of FGF-21 in serum samples from both genotypes. Results showed that both genotypes demonstrated similar levels of FGF-21 in serum samples. However, although circulating levels are the same, the paracrine effects of FGF-21 released by PVAT on blood vessels, particularly in relation to its potential involvement in the anti-contractile effects of PVAT could be altered in the KO mice and need further investigation.

PVAT consists of adipocytes and stromal cells which produce an ever-growing list of molecules, including the production of adipokines, cytokines, growth factors, gaseous compounds, and reactive oxygen species, which exert paracrine effects on vascular smooth muscle cells (VSMCs) and endothelial cells (Chang *et al.*, 2020). While PVAT across different anatomical sites may exhibit characteristics of either brown or white adipose tissues, its secretory profile markedly diverges from other fat depots. For example, compared to subcutaneous and perirenal adipose tissue, mouse aortic PVAT secretes substantially less adiponectin and leptin, whereas the secretion of pro-inflammatory cytokines including IL-6, IL-8, and MCP-1 is markedly increased (Chatterjee *et al.*, 2009). Moreover, in terms of its ability to modulate vessel-tone, PVAT is also distinguishable from classical BAT (suprascapular) and WAT (inguinal). In an experiment performed to compare the effect of mouse thoracic aortic PVAT, BAT, and WAT extracts on vessel resting tone, PVAT, but not inguinal WAT or suprascapular BAT extracts induced significant vasodilation and further attenuated phenylephrine-induced vasoconstriction (Li *et al.*, 2022). This further suggests that only substances secreted by PVAT, but not by other BAT or WAT depots can modulate vasoconstriction or dilation (Li *et al.*, 2022).

Moreover, the phenotypic discrepancies between thoracic and abdominal PVAT appear to be clinically important because abdominal aortae are more susceptible to atherosclerosis and aortic aneurysm development than thoracic aortae (Padilla *et al.*, 2013; Yap *et al.*, 2021). It has also been demonstrated that abdominal PVAT is more susceptible to inflammation, as indicated by greater expression of inflammatory genes and immune cell infiltration markers in abdominal PVAT

compared to thoracic PVAT (Padilla *et al.*, 2013). During the course of this study, as shown in Figure 4-1, it was found that abdominal aortae were always embedded in abundant PVAT, with two- to three-fold more mass compared to that surrounding the thoracic aorta when the PVAT was dissected and weighed. Taken together, this highlights the important role that PVAT plays at different anatomical locations.

In the array experiment, there was an alteration in adipokine release in KO PVAT, more notably by abdominal PVAT. It is clear from the array result that adiponectin is the most abundant adipokine released by both thoracic and abdominal PVAT. However, abdominal PVAT released less adiponectin compared to thoracic PVAT. More interestingly, adiponectin secretion was impaired in KO thoracic and abdominal PVAT. This is with an agreement with a previous study in our lab in which KO mice were demonstrated to exhibit loss of PVAT anticontractile actions along with a marked reduction in PVAT-derived adiponectin levels (Almabrouk *et al.*, 2017). Moreover, in obese WT mice, PVAT adiponectin secretion and AMPK phosphorylation was reduced, which correlated with a reduced anticontactle effect of PVAT (Almabrouk *et al.*, 2018). This indicates a crucial role for AMPK in adiponectin secretion and adiponectin-mediated vasorelaxation.

Additionally, in the array experiment, the release of several factors, including FGF-21, ICAM-1, TIMP-1, IGF-II, and LIF, was significantly lower in AMPKα1 KO compared to wild type PVAT. Although not statistically significant, the release of additional adipokines like IL-6, IL-II, MCP-1, DPPIV, HGF, leptin, RAGE, RANTES, and serpin was also reduced in KO abdominal PVAT compared to WT PVAT. FGF-21 was selected in this study due to its involvement in vascular homeostasis, while the other factors have distinct functions. FGF-21 is a member of the endocrine FGF subfamily considered to be a key metabolic regulator. In recent years, FGF-21 has also been demonstrated to have cardioprotective functions (Zhang *et al.*, 2021). In mice, FGF-21 treatment has been shown to improve post-myocardial infarction outcome through modulating cardiac remodelling and decreasing pro-inflammatory cytokine expression, an action which was mediated by adiponectin (Joki *et al.*, 2015). In endothelial cells, FGF-21 has a protective effect against high glucose-induced apoptosis (Guo *et al.*, 2018), and high glucose-induced endothelial cell damage and dysfunction (Wang *et al.*, 2014). In athero-prone

apolipoprotein E (apoE)$^{-/-}$ mice , FGF-21 has a protective effect against atherosclerosis by suppressing Fas-mediated apoptosis (Yan *et al.*, 2018). FGF-21 has also been reported to attenuate hypoxia-induced pulmonary hypertension (Liu *et al.*, 2018) and has a protective effect against angiotensin II-induced hypertension (Pan *et al.*, 2018) and angiotensin II-induced cardiac hypertrophy and dysfunction (Li *et al.*, 2019a).

It is known that FGF-21 and adiponectin share obvious functional similarity and have been linked together in multiple studies. It has been reported that FGF-21 treatment enhances the expression and secretion of adiponectin in mice adipocytes along with increasing its circulating levels (Lin *et al.*, 2013; Joki *et al.*, 2015). Moreover, it has also been demonstrated that adiponectin mediates the metabolic effect of FGF-21, and adiponectin knockout mice were resistant to several therapeutic benefits of FGF-21 (Lin *et al.*, 2013; Joki *et al.*, 2015). FGF-21 is also reported to protect against atherosclerosis via inducing adiponectin production in adipocytes (Lin *et al.*, 2015). In the same way, the cross-talk between adiponectin and AMPK has widely reported, and both AMPK and adiponectin were shown to have vasodilatory properties (Salt and Hardie, 2017; Almabrouk *et al.*, 2017).

Similarly, FGF-21 is reported to display a remarkable overlap with AMPK in their metabolic regulatory function, e.g., systemic glucose control and lipid metabolism (Salminen *et al.*, 2017). Indeed, FGF-21 administration has been revealed to stimulate AMPK signalling in several tissues. Chau *et al.* demonstrated that FGF-21 regulates mitochondrial activity and enhances oxidative capacity by activating AMPK-SIRT1-PGC-1α pathway in adipocytes (Chau *et al.*, 2010). This stimulatory action was mediated by LKB1, an upstream kinase of AMPK, which suggests that LKB1 might be one of the phosphorylation targets of FGF-21 (Chau *et al.*, 2010). In rat cultured cardiac myocytes, AICAR, an AMPK activator, induced a substantial increase in FGF-21 levels in the culture medium and in the cells (Sunaga *et al.*, 2019). Similarly, incubation of cultured cardiac myocytes with recombinant FGF-21 increased AMPK phosphorylation, along with activation of down-stream targets of AMPK such as SIRT1, PGC1α, ERK, and p38 mitogen-activated protein kinase (MAPK), which is known to have a cardioprotective function (Sunaga *et al.*, 2019). In a diabetic mouse model, treatment of cardiac cells with FGF-21 induced a

protective effect against apoptosis by activating extracellular signal-regulated kinase (ERK)1/2-dependent p38 MAPK–AMPK signalling pathway (Zhang *et al.*, 2015).

As mentioned earlier, previous studies have demonstrated that in AMPKα1 KO mice adiponectin secretion by the PVAT was markedly reduced (Almabrouk *et al.*, 2017). In this chapter, data indicate that there is a marked reduction of PVAT-FGF-21 secretion by KO abdominal PVAT, and both studies reported an attenuation in the PVAT-anticontractile effect. This suggests that AMPK-adiponectin-FGF-21 could be linked together, and this link could perhaps play a role in the PVAT-vasorelaxant function observed in the two studies. The next chapter will investigate in more detail the role of FGF-21 on vascular homeostasis, and its relation to AMPK.

To confirm the array results, FGF-21 levels in thoracic and abdominal PVAT CM was measured using FGF-21–specific ELISA. FGF-21 levels were significantly lower in KO abdominal PVAT CM compared to WT CM. Furthermore, FGF-21 levels in KO abdominal PVAT were lower than in WT abdominal PVAT, although a statistically significant difference was not achieved. However, in thoracic PVAT CM, we were unable to detect FGF-21. This could be due to the difference in the amount of PVAT which surrounds thoracic and abdominal aortae used in this experiment. When PVAT was dissected and weighed, abdominal PVAT was present in almost 3-5 times the amount of thoracic PVAT. Furthermore, FGF-21 in thoracic PVAT lysates was also undetectable. This is consistent with a previous study in which FGF-21 in mouse thoracic PVAT extract was undetectable (Li *et al.*, 2019b). Although FGF-21 targets both BAT and WAT, it has been reported that WAT is the more important target of FGF-21, where it plays a role in glucose control (Kharitonenkov *et al.*, 2005). Moreover, we also demonstrated that lack of AMPKα1 does not influence the circulatory levels of FGF-21. This could indicate that AMPKα1 mediates FGF-21 function in manner specific to fat depot.

ADRFs are not limited to adipokines, but also include gaseous compounds like nitric oxide (NO) (Gil-Ortega *et al.*, 2010; Victorio *et al.*, 2016). Although endothelial nitric oxide synthase (eNOS) is primarily expressed in endothelial cells, various groups have demonstrated the expression of eNOS in thoracic aortic PVAT (Man *et al.*, 2022). PVAT-derived NO is an important player in the protective role

of PVAT; it diffuses into the adjacent VSMCs and endothelium and induces vasodilation. Several studies have demonstrated that in obesity, PVAT-endothelial nitric oxide synthase (eNOS) expression and NO production was significantly reduced, and this could contribute to obesity-induced vascular dysfunction (Xia *et al.*, 2016; Man *et al.*, 2022). Previous studies have reported that AMPK phosphorylates and activate eNOS, leading to increased NO production (Thors *et al.*, 2011; Salt and Hardie, 2017). In PVAT, AMPK activation with various AMPK activators was reported to induce PVAT-eNOS phosphorylation and improve PVAT function (Sun *et al.*, 2014; Chen *et al.*, 2016).

Based on this link between AMPK and eNOS function, we assessed the influence of AMPKα1 on PVAT-released nitric oxide (NO). In thoracic PVAT, NO release was significantly diminished in KO compared to WT. Moreover, in both genotypes, NO release by abdominal PVAT was much lower compared to thoracic PVAT. This is in agreement with a previous study in which eNOS expression and NO production was reduced in rat abdominal PVAT compared to thoracic PVAT (Victorio *et al.*, 2016). This could indicate that the impairment in the PVAT-vasorelaxant effect observed in KO abdominal PVAT is not related to NO release, as in both genotypes NO release by abdominal PVAT was not different.

However, it is worth mentioning that although AMPK is frequently reported to phosphorylate Ser^{1177} of the eNOS, and therefore is linked with a relaxing effect, previous studies failed to consistently demonstrate a major role for AMPK on eNOS-dependent relaxation. A previous study demonstrated that *in vitro*, activation of AMPKα1 did not alter the phosphorylation of eNOS on Ser^{1177}, but increased its phosphorylation on Thr^{495} and attenuated NO production (Zippel *et al.*, 2018). In another study, AICAR was reported to impair the NO-mediated relaxations in aortic preparations induced by acetylcholine or sodium nitroprusside (SNP) (Davis *et al.*, 2012). Moreover, in mouse aortic rings, AICAR induced a dose-dependent relaxation that was independent of either the endothelium or the inhibition of eNOS, and mediated by the AMPKα1 subunit in smooth-muscle cells (Goirand *et al.*, 2007; Almabrouk *et al.*, 2017). Therefore, the link between AMPK- and NO-dependent alterations in vascular reactivity is not consistent and could depend on the model studied.

In the last experiment in this chapter the influence of PVAT CM on AMPK, eNOS, Akt and ERK1/2 activation in HUVECs was studied. AMPK, eNOS, Akt and ERK1/2 signalling pathways reportedly play an important role in the regulation of eNOS phosphorylation and nitric oxide (NO) production. The most notable effect was the phosphorylation of ERK1/2 by abdominal, and to a lesser extent thoracic PVAT CM of both genotypes. In endothelial cells, ERK1/2 signalling plays a crucial role in regulation of eNOS phosphorylation and NO production, and endothelial function including survival, proliferation, migration, and angiogenesis (Wu *et al.*, 2021). Although ERK1/2 signalling could be activated by many different mediators, both adiponectin (Ouchi *et al.*, 2004) and FGF-21 (Chen *et al.*, 2021) are reported to stimulate ERK1/2 in endothelial cells. In the array experiment, we reported more FGF-21 and less adiponectin in abdominal PVAT CM compared to thoracic PVAT CM. So, the activation of ERK1/2 by abdominal PVAT CM could be mediated more by FGF-21. However, the identity of the factor(s) responsible for this action was not assessed. Moreover, as Akt is known to phosphorylate on Ser^{1177}, the lack of Akt phosphorylation fits with the lack of eNOS Ser^{1177} phosphorylation. On the other hand, thoracic, but not abdominal, PVAT CM showed a trend toward AMPK stimulation (2-fold), as reported by phosphorylation of ACC, a downstream target of AMPK. Although, the identity of the factor(s) responsible for this action is not known, previous studies demonstrated that adiponectin stimulates AMPK in endothelial cells (Salt and Hardie, 2017). We also reported more adiponectin release by thoracic PVAT CM in the array experiment. However, AMPK stimulation is unlikely to be caused by FGF-21, as we reported more FGF-21 in abdominal than in thoracic PVAT CM. Finally, although previous studies reported that adiponectin stimulates eNOS phosphorylation in endothelial cells, via AMPK activation, in the current experiments, PVAT CM had no effect on eNOS activation.

One potential limitation of the experiments using HUVECs is that the CM used was from mice and was used to stimulate human endothelial cells. However, although the principal mechanisms are likely to be conserved between species It would be worthwhile to investigate the effect of mice CM from either genotype, on mouse endothelial cells. Furthermore, normalisation of CM was difficult since the amount of PVAT obtained from abdominal aortae was more than that obtained from thoracic aortae. Therefore, it would be better to repeat it using an equal amount of pooled PVAT.

4.5 Conclusion

In summary, this chapter highlights the important role AMPKα1 has on the secretory function of PVAT. Although we also demonstrated dysregulation in secretion of different adipokines by KO PVAT, this study focused on FGF-21 as a potential mediator of PVAT function. This was based on literature and the results of previous studies in which the AMPK-FGF-21 and adiponectin-FGF-21 link was demonstrated. Although FGF-21 has been reported to have a cardioprotective effect and plays a role in maintaining vascular function, its effect on vascular tone is not widely known. Therefore, it is worth investigating the effect of FGF-21 on endothelium and VSMC-mediated vasorelaxation.

Chapter 5 The effect of FGF-21 on cell signalling, NO analysis and vasorelaxation

5.1 Background

The fibroblast growth factor (FGF) family is composed of 23 polypeptides which act in an autocrine, paracrine or endocrine manner with a wide range of biological functions, including cell growth, cellular proliferation, survival, migration, and differentiation (Hui *et al.*, 2018). Within the FGF family, the hormonal subfamily, FGF-19, FGF-21, and FGF-23, lack heparin-binding domains and are released into the bloodstream to act in an endocrine manner (Fisher and Maratos-Flier, 2016; Degirolamo *et al.*, 2016). FGF-21 was first identified as a member of the FGF family in 2000 (Nishimura *et al.*, 2000) and has attracted global attention because of its ability to regulate energy balance and glucose and lipid metabolism (Kharitonenkov *et al.*, 2005). FGF-21 is highly expressed in liver, pancreas, testis, brown adipose tissue (BAT) and white adipose tissue (WAT) and has multiple proposed metabolic functions (Fon Tacer *et al.*, 2010; Potthoff *et al.*, 2012). FGF-21 increases insulin levels, insulin sensitivity, reducing hyperglycaemia and improving dyslipidaemia and obesity, thereby providing a therapeutic target for metabolic diseases (Chen *et al.*, 2022). Adipocytes are the primary target of FGF-21, where it modulates lipolysis, enhances mitochondrial oxidative capacity, increases glucose uptake, enhances PPARγ activity, and promotes browning of WAT (Chen *et al.*, 2011; Kleiner *et al.*, 2012).

The molecular mechanism of FGF-21 signalling in its target tissues is complex and involves several tyrosine kinase receptors (FGFRs) as well as an obligate co-receptor, ß-klotho (KLB) (Figure 5-1) (Ogawa *et al.*, 2007). FGFRs include four subtypes, namely: FGFR1, 2, 3, and 4 (Mohammadi *et al.*, 2005). FGFR1c, FGFR4, and FGFR3c receptor isoforms are the main receptors for FGF-21 (Ogawa *et al.*, 2007; Suzuki *et al.*, 2008; Kilkenny and Rocheleau, 2016). In HUVECs, in addition to FGFR1c, which is considered as the major FGF receptor in EC, similar levels of FGFR3c, detectable amounts of FGFR2c are also expressed (Antoine *et al.*, 2005). KLB is a single-transmembrane protein that is required for FGF-21 to bind FGFRs and activate FGF-21 intracellular signalling cascades (Zhang *et al.*, 2021). Knockdown of KLB expression *in vivo* (Ding *et al.*, 2012; Adams *et al.*, 2012) and *in vitro* (Ogawa *et al.*, 2007) resulted in loss of FGF-21 metabolic activity. The FGFR and Klotho protein are expressed in a tissue-specific manner which increases the specificity of the endocrine functions of FGF-21 (Kurosu *et al.*, 2007; Fon Tacer *et al.*, 2010; Salminen *et al.*, 2017). KLB is expressed at high levels in

enterohepatic tissues including liver, gall bladder, colon, pancreas, and also in both brown and white adipose tissues (Ito *et al.*, 2000; Fon Tacer *et al.*, 2010), which may determine the tissue-specific metabolic effects of FGF-21 (Kurosu *et al.*, 2007). In addition to liver, adipose tissue is considered as the predominant site for FGF-21 metabolic function and both KLB and FGFRs (especially FGFR1) are highly expressed in adipose tissue (Ogawa *et al.*, 2007). This is supported by the evidence that systemic or adipose tissue-specific deletion of KLB largely abolished the metabolic function of FGF-21 (Ogawa *et al.*, 2007; Ding *et al.*, 2012). Furthermore, in lipodystrophic mice (mice with reduced body fat), recombinant FGF-21 treatment was ineffective at improving glucose and lipid homeostasis, while white adipose tissue (WAT) transplantation from wild type mice restored FGF-21 responsiveness in these mice (Véniant *et al.*, 2012a).

In the vasculature, KLB and FGFR1c are expressed at a high level in mice aortae, suggesting that FGF-21 may affect blood vessel physiology (Antoine *et al.*, 2005; Fon Tacer *et al.*, 2010). KLB is also expressed in endothelial cells (Wang *et al.*, 2014), PVAT (Berti *et al.*, 2016) and heart and cardiac myocytes (Patel *et al.*, 2014; Wu *et al.*, 2017). This indicates a possible role of FGF-21 in the cardiovascular system.

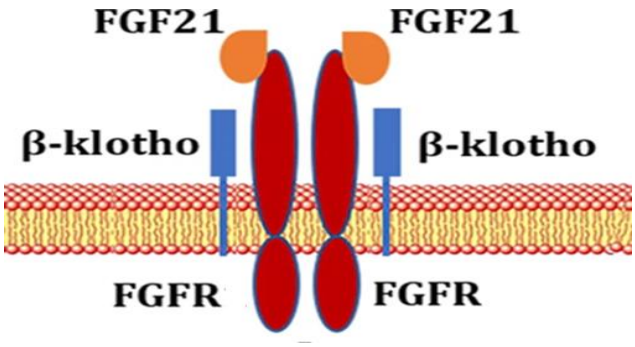

Figure 5-1 FGF-21/FGFR/β-Klotho complex

KLB is a single-transmembrane protein that is required for FGF-21 to bind FGFRs and activate FGF-21 intracellular signalling cascades (Adapted from (Ying *et al.*, 2019).

5.2 FGF-21 and AMPK:

Both FGF-21 and AMPK are fundamental regulators of energy metabolism with a remarkable overlap in their function. FGF-21 regulates systemic glucose and lipid metabolism by enhancing insulin sensitivity, increasing glucose uptake and lipid

oxidation, whilst inhibiting lipogenesis. AMPK is a major energy metabolic sensor in cells, regulating energy production by stimulating the breakdown of glucose and lipids. This similarity in the metabolic profiles of FGF-21 and AMPK could indicate that FGF-21 and AMPK might act through the same energy metabolic pathways, or that many of the metabolic effects of FGF-21 are mediated through the AMPK signalling pathways. Indeed, mounting evidence indicates that FGF-21 activates AMPK in target tissues either directly through FGFR1/KLB signalling or indirectly by stimulating the secretion of adiponectin and corticosteroids (Salminen *et al.*, 2017). For instance, Chau *et al.* demonstrated that in mouse and human adipocytes, FGF-21 enhanced mitochondrial oxidative capacity by activating peroxisome proliferator-activated receptor gamma coactivator-1α (PGC-1α), a key regulator of energy metabolism, through the activation of the AMPK-SIRT1 pathway (Chau *et al.*, 2010). They reported that FGF-21 activates AMPK through stimulation of LKB1, which phosphorylates and activates AMPK. This suggests that LKB1 might be one of the targets of FGFR1.

In the cardiovascular system, several studies demonstrated that AMPK mediates the protective function of FGF-21 in different vascular tissues. In a diabetic mouse model, FGF-21 was reported to protect the heart from palmitate-induced apoptosis by activating ERK1/2-p38 MAPK-AMPK signalling pathway (Zhang *et al.*, 2015). Similarly, in diabetic mice and cultured cardiomyocytes exposed to high glucose (HG), FGF-21 protects against diabetic cardiomyopathy and HG-induced cardiomyocyte injury by activating AMPK signalling (Wu *et al.*, 2017). It also has been demonstrated that FGF-21 protects the heart and improves cardiac function in response to myocardial ischaemia via activation of PI3K/Akt, ERK1/2, and AMPK pathways (Patel *et al.*, 2014). In endothelial cells, it has been demonstrated that the protective role of FGF-21 is partly mediated by AMPK activation. For instance, Wang *et al.* reported that FGF-21 protects against HG-induced endothelial cell damage and eNOS dysfunction partly via AMPK activation (Wang *et al.*, 2014). Similarly, in an *in vivo* study, long-term administration of FGF-21 to mice with T2DM ameliorated diabetes-induced aortic endothelial dysfunction and improved aorta relaxation by inhibiting oxidative stress via activation of the CaMKK2/AMPK signalling pathway (Ying *et al.*, 2019).

5.3 FGF-21 and adiponectin:

FGF-21 and adiponectin represent the two major hormones secreted from the liver and adipose tissues respectively, and share obvious functional similarity (Nishimura *et al.*, 2000; Yamauchi and Kadowaki, 2008). Elevation of circulating FGF-21 or adiponectin levels by pharmacological or genetic approaches or administration of the recombinant protein has been shown to increase energy expenditure, reduce adiposity, decrease insulin resistance and hyperglycaemia, and alleviate myocardial infarction, diabetic cardiomyopathy, and atherosclerosis in rodents and non-human primates (Berg *et al.*, 2001; Fruebis *et al.*, 2001; Kharitonenkov *et al.*, 2005; Véniant *et al.*, 2012b; Lin *et al.*, 2015). A number of animal-based studies have suggested that FGF-21 is a potent regulator of adiponectin secretion, and that FGF-21 critically depends on adiponectin to exert its glycaemic and insulin-sensitising effects (Holland *et al.*, 2013; Lin *et al.*, 2013; Joki *et al.*, 2015). FGF-21-deficient mice exhibited significantly lower serum adiponectin levels in lean and high fat diet-induced obese mice (Lin *et al.*, 2013). Similarly, adiponectin knockout mice are resistant to the effects of FGF-21 to alleviate obesity-associated insulin resistance, hyperglycaemia, dyslipidaemia, and liver steatosis (Lin *et al.*, 2015). However, in both animals and humans with obesity, plasma adiponectin concentrations are reduced whereas circulating FGF-21 levels are increased. This might be due to FGF-21 resistance, and suggests that a dysfunctional FGF-21-adiponectin axis may contribute to the pathogenesis of obesity-related metabolic syndrome (Lin *et al.*, 2013). It has also been shown that FGF-21 administration to WT mice with myocardial infarction attenuates cardiac dysfunction and inflammation through an adiponectin-dependent mechanism (Joki *et al.*, 2015). This suggests that adiponectin acts as an obligatory downstream mediator of FGF-21.

5.4 Association of FGF-21 with cardiovascular risk and atherosclerosis

Previous studies of FGF-21 primarily focused on its expression and metabolic function, with results showing a promising role of FGF-21 as a metabolic regulator and a potential therapeutic for various human diseases, including type 2 diabetes, and obesity. In the past decade, however, the relationship between FGF-21 and cardiovascular disease (CVD) has become the most popular research topic. CVD is

one of the leading causes of global mortality and morbidity. Recent studies have demonstrated an association between FGF-21 and CVD including carotid atherosclerosis and coronary heart disease. Indeed, FGF-21 has been shown to exert its cardiovascular protective effects on blood vessels and heart and contribute to the fine-tuning of multi-organ crosstalk under various pathophysiological conditions (Lin *et al.*, 2015; Joki *et al.*, 2015; Wu *et al.*, 2017). Additionally, numerous clinical studies reported that serum FGF-21 levels are increased in patients with diabetic cardiomyopathy and other cardiovascular diseases (Cheng *et al.*, 2016). Interestingly, increased FGF-21 serum levels have also been associated with pericardial fat accumulation, indicating that FGF-21 may be related to fat deposition and dyslipidaemia (Lee *et al.*, 2014). Pericardial fat has been previously shown to be related to cardio-metabolic risk factors and contribute to CAD. This suggests that FGF-21 could potentially be used as a biomarker to predict the occurrence of cardiovascular diseases.

5.4.1 Role of FGF-21 in atherosclerosis

Atherosclerosis is a life-threatening cardiovascular disease characterised by excessive intimal fibrosis, fatty plaque formation, the proliferation of smooth muscle cells and migration of cells such as monocytes, T cells, and platelets in response to inflammation and oxidative stress. Since FGF-21 plays an important role in the regulation of lipid metabolism, the effect of FGF-21 in atherosclerosis is of interest. Indeed, a growing body of evidence indicates a protective role of FGF-21 in atherosclerosis development and progression. In aortae, a high level of FGFR1c and KLB are expressed making it a potential target tissue for FGF-21 (Fon Tacer *et al.*, 2010). Accumulating data indicates that FGF-21 significantly increases in atherosclerosis, and that FGF-21 deficiency accelerates atherosclerotic plaque formation (Chow *et al.*, 2013; Lin *et al.*, 2015). In metabolic diseases such as diabetes, hypertension and obesity, serum levels of FGF-21 increase which may be related to initiation and promotion of atherosclerosis (Zhang *et al.*, 2008b; Semba *et al.*, 2013; Li *et al.*, 2017). Serum FGF-21 was elevated in patients with subclinical atherosclerosis and newly diagnosed type 2 diabetes (Xiao *et al.*, 2015).

In athero-prone apoE$^{-/-}$ mice, FGF-21 deficiency causes a marked exacerbation of atherosclerotic plaque formation and mortality, which was accompanied by

hypoadiponectinaemia and severe hypercholesterolaemia (Lin *et al.*, 2015). However, treatment with recombinant FGF-21 prevented the initiation and progression of atherosclerosis via inducing adipocyte-adiponectin production and reducing hepatic cholesterol synthesis and attenuation of hypercholesterolaemia (Lin *et al.*, 2015; Huang *et al.*, 2022). Moreover, administration of exogenous FGF-21 also protects $apoE^{-/-}$ mice from atherosclerosis in the aortic arch and abdominal aortae by modifying lipid profiles and downregulating CRP and TNFα expression (Wu *et al.*, 2014). In Wistar rats and $apoE^{-/-}$ mice fed high fat diet, FGF-21 dramatically improved atherosclerosis by decreasing serum TG and LDL levels and increasing serum HDL and superoxide dismutase levels, along with upregulation of eNOS mRNA expression in the aortae (Zhu *et al.*, 2014; Huang *et al.*, 2022).

In addition to its lipid lowering effects, mechanistic studies reported other mechanisms through which FGF-21 might prevent or ameliorate atherosclerosis. FGF-21 has been reported to protect against atherosclerosis by enhancing the activity of the antioxidant system and suppressing oxidative stress and endoplasmic reticulum stress (ERS). Oxidative stress is a well-known component of atherosclerosis pathogenesis, occurring in parallel with overproduction of reactive oxygen species (ROS), activation of pro-inflammatory signalling pathways and expression of cytokines/chemokines (Poznyak *et al.*, 2020). It has been shown that the disruption of endothelial cell function is recognized as an early initiating factor in the development of atherogenesis (Rajendran *et al.*, 2013). In human umbilical vein endothelial cells (HUVECs), FGF-21 treatment significantly enhanced cell viability and inhibited H_2O_2-induced cell apoptosis by preventing mitogen-activated protein kinase (MAPK) signalling pathway activation (Zhu *et al.*, 2014). FGF-21 protects against high glucose-induced endothelial cell damage and regulates nitric oxide production and endothelial nitric oxide synthase (eNOS) phosphorylation in HUVECs (Wang *et al.*, 2014). Interestingly, knockdown of AMPKα1/2 isoforms by siRNA or AMPK inhibition (using compound C) partly abolished the protective effect of FGF-21 on eNOS phosphorylation (Wang *et al.*, 2014). This suggests that AMPK is critical for the regulatory effect of FGF-21 on eNOS phosphorylation in HUVECs.

In cultured endothelial progenitor cells (EPCs), circulating cells which are essential for vascular endothelial cell repair, pre-treatment with FGF-21 restored

H_2O_2-induced EPC dysfunction including improvement of cell viability, migration and tube formation (Huang *et al.*, 2022). This protective effect of FGF-21 was mediated by the Akt/eNOS/NO pathway. Moreover, inhibition of FGF-21 in HUVECs inhibited cell proliferation, and migration, with substantial suppression of eNOS, PI3K, and AKT mRNA levels and phospho-eNOS, PI3K, and phospho-AKT protein levels (Li *et al.*, 2017). This suggests that FGF-21 plays an important role in the regulation of eNOS expression.

Taken together, these observations indicate that FGF-21 directly and indirectly inhibits key processes in the pathogenesis of atherosclerosis and therefore protects against CVD.

5.5 Aims of the study

Prior investigations have yielded promising outcomes with respect to the involvement of fibroblast growth factor-21 (FGF-21) in cardiovascular disease (CVD) and its impact on endothelial cells. However, a comprehensive exploration of FGF-21's influence on vasorelaxation is lacking. The results elucidated in Chapter 3 suggest that in vessels with an intact endothelium, the anti-contractile effect of abdominal PVAT is attenuated in AMPKα1 KO mice in comparison to their wild-type counterparts. Additionally, the data presented in Chapter 4 demonstrates a diminished secretion of FGF-21 in abdominal PVAT from AMPKα1 KO mice relative to PVAT from wild-type mice. As a consequence, the primary aim of this chapter is to assess the potential impact of FGF-21 on endothelial function, with a specific focus on examining its effects on endothelial nitric oxide synthase (eNOS) and AMPK phosphorylation in cultured human umbilical vein endothelial cells (HUVECs). Furthermore, acknowledging the pivotal role of PVAT in vascular homeostasis and recognizing adipose tissue as a recognised target of FGF-21, an assessment of the influence of FGF-21 on cultured 3T3-L1 adipocytes was undertaken. Finally, a functional study was executed to assess the effect of FGF-21 on vasorelaxation in mouse aortic rings.

5.6 Results

5.6.1 Effect of FGF-21 on AMPK activity in HUVECs

To examine the effect of FGF-21 on AMPK activity, cultured HUVECs were incubated with human FGF-21 (50 ng/mL) for various durations, insulin (1 μM, 60 min), as well as the AMPK activator compound 991 (10 μM, 60 min) as a positive control. Insulin has been previously reported to inhibit AMPK in adipose tissue (Kopietz *et al.*, 2020). While this evidence is derived from adipocytes, it provides insights into the potential regulatory effects of insulin on AMPK activity and this effect may extend to other cell types including endothelial cells. AMPK activity was assessed by the degree of phosphorylation of the AMPK substrate, ACC Ser^{79} by western blotting analysis.

As shown in Figure 5-2 A, stimulation of HUVECs with human FGF-21 and insulin had no effect on ACC phosphorylation (*n*=3). In contrast, compound 991 significantly increased ACC phosphorylation.

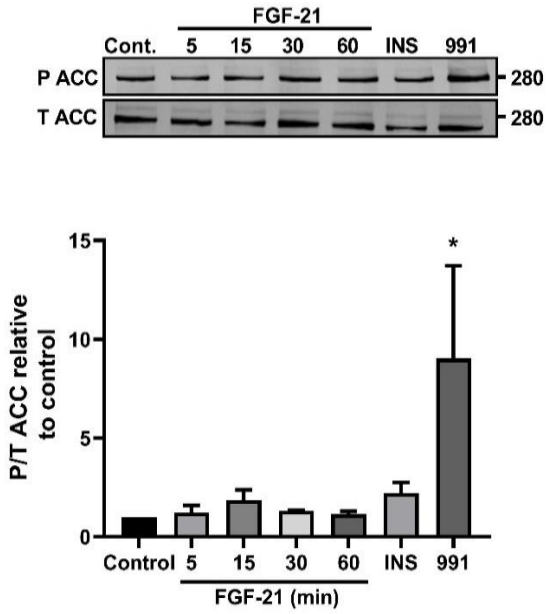

Figure 5-2 Effect of FGF-21 on AMPK activity in HUVECs

HUVECs were incubated with PBS (control), compound 991 (10 μM), or insulin (1 μM) for 60 min, and human FGF-21 (50 ng/mL) for various durations. Lysates were prepared, resolved by SDS-PAGE and subjected to immunoblotting with anti-ACC antibodies (T, total, P, phospho). The graph represents the quantification of ACC Ser^{79} phosphorylation relative to total ACC. Representative immunoblots with molecular mass markers (in KDa) indicated on the right are shown on the top of the graph. Data shown represent the mean ± SEM phosphorylation relative to control from three independent experiments. *P < 0.05 (one-way ANOVA).

5.6.2 Effect of FGF-21 on eNOS phosphorylation in HUVECs

To examine the effect of FGF-21 on eNOS phosphorylation, cultured HUVECs were incubated with PBS (control), compound 991 (10 μM), or insulin (1 μM) for 60 min, and human FGF-21 (50 ng/mL) for various durations. Insulin has been previously demonstrated to stimulate eNOS Ser^{1177} phosphorylation in HUVECs (Salt *et al.*, 2003). The extent of eNOS Ser^{1177} phosphorylation was determined by western blotting analysis of HUVEC lysates.

As shown in Figure 5-3, stimulation of HUVECs with human FGF-21 (at various time points), insulin or compound 991 had no effect on eNOS phosphorylation (*n*=3).

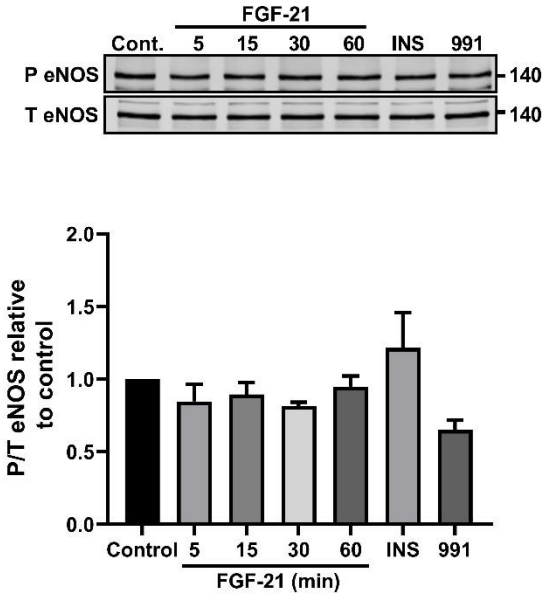

Figure 5-3 Effect of FGF-21 on eNOS phosphorylation in HUVECs

HUVECs were incubated with PBS (control), compound 991 (10 μM), or insulin (1 μM) for 60 min, and human FGF-21 (50 ng/mL) for various durations. Lysates were prepared, resolved by SDS-PAGE and subjected to immunoblotting with anti-eNOS antibodies (T, total, P, phospho). The graph represents the eNOS Ser^{1177} phosphorylation relative to total eNOS. Representative immunoblots with molecular mass markers (in KDa) indicated on the right are shown on the top of the graph. Data shown represent the mean ± SEM phosphorylation relative to control from three independent experiments (one-way ANOVA).

5.6.3 Effect of FGF-21 on Akt phosphorylation in HUVECs

Akt is a serine/threonine kinase that can influence NO production through its effects on eNOS. Akt can directly phosphorylate and activate eNOS, enhancing its enzymatic activity and promoting the production of NO. Akt is a well-described target of insulin and, therefore, insulin was used as a positive control.

To examine the effect of FGF-21 on Akt stimulation, cultured HUVECs were incubated with PBS (control), compound 991 (10 μM), or insulin (1 μM) for 60 min, and human FGF-21 (50 ng/mL) for various durations. The extent of Akt Ser^{473} phosphorylation was determined by western blotting analysis of HUVEC lysates.

As shown in Figure 5-4, stimulation of HUVECs with human FGF-21 had no effect on Akt phosphorylation over various incubation times (*n*=3). Insulin stimulated Akt, although statistical significance was not achieved (*P*= 0.08). Compound 991 inhibited Akt phosphorylation, though not significantly.

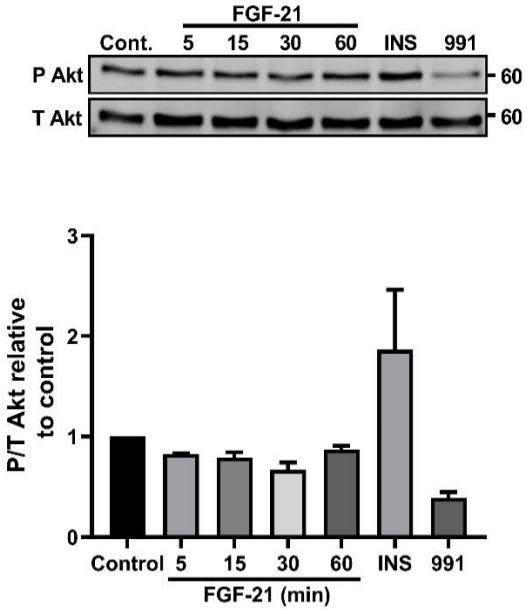

Figure 5-4 Effect of FGF-21 on Akt phosphorylation in HUVECs

HUVECs were incubated with PBS (control), compound 991 (10 μM), or insulin (1 μM) for 60 min, and human FGF-21 (50 ng/mL) for various durations. Lysates were prepared, resolved by SDS-PAGE and subjected to immunoblotting with anti-Akt antibodies (T, total, P, phospho). The graph represents Akt Ser^{473} phosphorylation relative to total Akt. Representative immunoblots with molecular mass markers (in KDa) indicated on the right are shown on the top of the graph. Data shown represent the mean ± SEM phosphorylation relative to control from three independent experiments (one-way ANOVA).

5.6.4 Effect of FGF-21 on ERK1/2 phosphorylation in HUVECs

ERK1/2, also known as extracellular signal-regulated kinase 1 and 2, are members of the mitogen-activated protein kinase (MAPK) family. ERK1/2 can phosphorylate eNOS at multiple sites, including Ser^{1177}, which is a major regulatory phosphorylation site (Wu *et al.*, 2021). Phosphorylation of eNOS at Ser^{1177} by ERK1/2 leads to the activation of eNOS and an increase in its enzymatic activity, resulting in enhanced production of NO.

To examine the effect of FGF-21 on ERK1/2 stimulation, cultured HUVECs were incubated with PBS (control), compound 991 (10 μM), or insulin (1 μM) for 60 min, and human FGF-21 (50 ng/mL) for various durations. The extent of ERK1/2 $Thr^{202,}$ Tyr^{204} phosphorylation was determined by western blotting analysis of HUVEC lysates.

As shown in Figure 5-5, stimulation of HUVECs with human FGF-21, insulin or compound 991 had no significant effect on ERK1/2 phosphorylation (*n*=3).

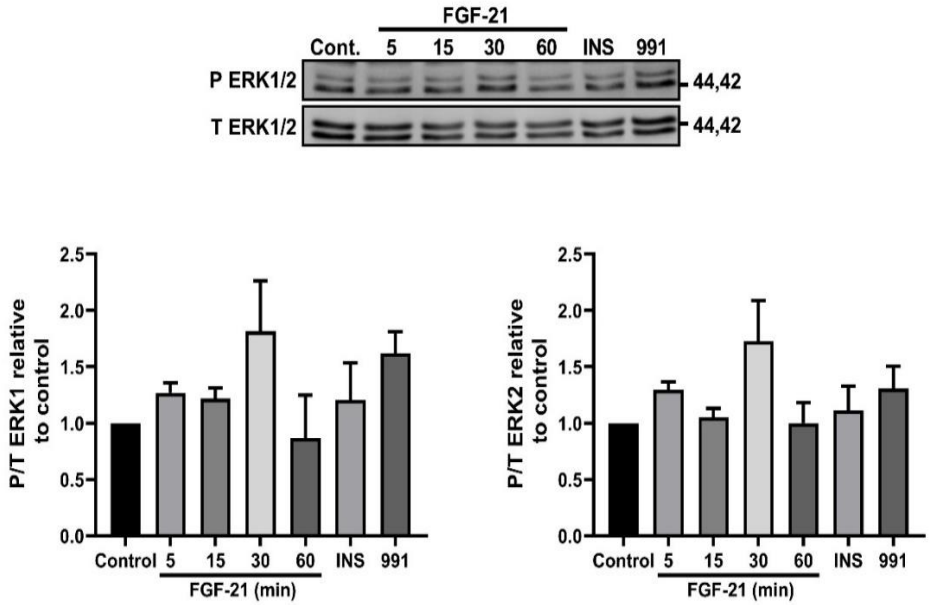

Figure 5-5 Effect of FGF-21 on ERK1/2 phosphorylation in HUVECs

HUVECs were incubated with PBS (control), compound 991 (10 μM), or insulin (1 μM) for 60 min, and human FGF-21 (50 ng/mL) for various durations. Lysates were prepared, resolved by SDS-PAGE and subjected to immunoblotting with anti-ERK1/2 antibodies (T, total, P, phospho). The graph represents ERK1/2 Thr^{202}, Tyr^{204} phosphorylation relative to total ERK1/2. Representative immunoblots with molecular mass markers (in KDa) indicated on the right are shown on the top of the graph. Data shown represent the mean ± SEM phosphorylation relative to control from three independent experiments (one-way ANOVA).

5.6.5 Effect of FGF-21 on nitric oxide release by HUVECs

To assess the role of FGF-21 on NO synthesis by HUVECs, cultured HUVECs were incubated with PBS (control) or compound 991 (10 μM) for 60 min, and human FGF-21 (50 ng/mL) for various durations. NO levels in the conditioned medium were measured using a Sievers 280 NO analyser as described in section 2.13.

As shown in Figure 5-6, FGF-21 and compound 991 had no effect on NO synthesis in HUVECs. This result was consistent with the effect of FGF-21 on eNOS phosphorylation in HUVECs described earlier.

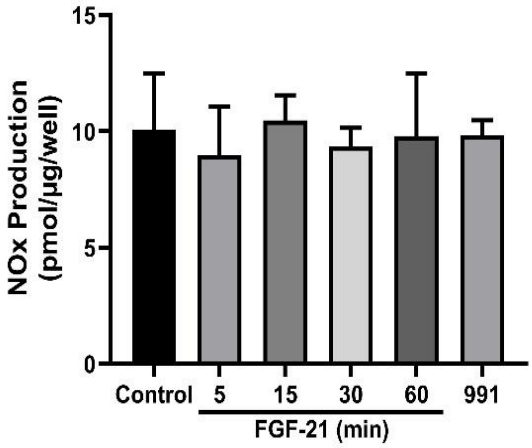

Figure 5-6 Effect of FGF21 on nitric oxide release by HUVECs

HUVECs were incubated with PBS (control) or Compound 991 (10 μM) for 60 min, and human FGF-21 (50 ng/mL) for various durations. NOx levels in conditioned medium were quantified using a Sievers 280 NO analyser. Data shown represent the mean ± SEM pmol/μg/well (*n*=3).

5.6.6 Validation of human FGF-21 protein

Given the lack of effect of FGF-21 on ACC, eNOS, Akt or ERK1/2 phosphorylation and NO synthesis in HUVECs, it was important to ensure the human FGF-21 used was active. Previous studies reported that FGF-21 can influence the ERK1/2 pathway in 3T3-L1 adipocytes (Ge *et al.*, 2011; Guo *et al.*, 2019). Therefore, to validate the human FGF-21 protein, cultured 3T3-L1 adipocytes were incubated with PBS (control), human FGF-21 (50 ng/mL), or mouse FGF-21 (50 ng/mL) for 30 min. The extent of ERK1/2 Thr^{202} and Tyr^{204} phosphorylation was determined by western blotting analysis of 3T3-L1 adipocyte lysates.

As seen in Figure 5-7, in a single experiment, stimulation of 3T3-L1 adipocytes with human or mouse FGF-21 increased ERK1/2 phosphorylation (*n*=1).

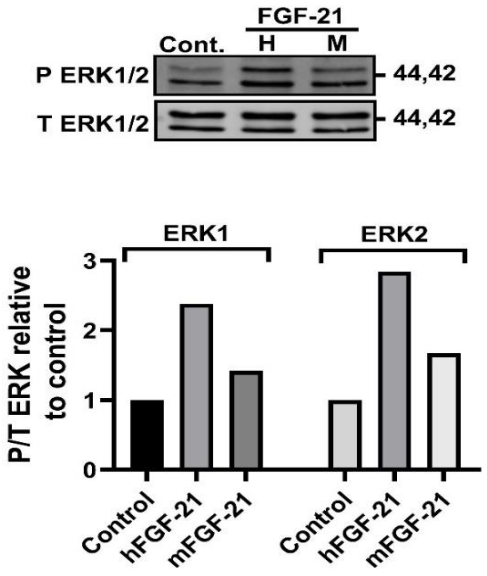

Figure 5-7 Validation of human FGF-21 protein

3T3-L1 adipocytes were incubated with PBS (control), human FGF-21 (50 ng/mL), or mouse FGF-21 (50 ng/mL) for 30 min. Lysates were prepared, resolved by SDS-PAGE and subjected to immunoblotting with anti-ERK1/2 antibodies (T, total, P, phospho). (A) Representative immunoblots with molecular mass markers indicated on the right (in KDa). (B) Quantification of ERK1/2 (Thr^{202}, Tyr^{204}) phosphorylation relative to total ERK1/2 (*n*=1).

5.6.7 Klotho level in HUVECs

To identify potential mechanisms underlying the lack of an effect of FGF-21 on HUVECs, we investigated the levels of KLB in HUVECs. Lysates from HUVECs or the human hepatocellular carcinoma cell line HepG2 (positive control) were subjected to immunoblotting with human KLB antibodies.

As seen in the Figure 5-8, KLB protein was detected in HepG2 cells but not HUVECs.

Figure 5-8 Klotho expression in HUVECs and 3T3-L1 adipocytes

HepG2 and HUVEC lysates were prepared, resolved by SDS-PAGE and subjected to immunoblotting with anti-KLB antibodies. Representative immunoblot with molecular mass markers indicated on the right.

5.6.8 Effect of FGF-21 on eNOS, AMPK, Akt, and ERK1/2 phosphorylation in 3T3-L1 adipocytes

Since FGF-21 had no significant effect on AMPK, eNOS, Akt, and ERK1/2 phosphorylation in HUVECs, its effect on cultured 3T3-L1 adipocytes was also investigated. Both 3T3-L1 adipocytes and abdominal PVAT exhibit a white adipocyte phenotype, such that the effect of FGF-21 on 3T3-L1 adipocytes will likely mimic the autocrine/endocrine effect of FGF-21 on abdominal PVAT.

5.6.8.1 Effect of FGF-21 on AMPK activity in 3T3-L1 adipocytes

To examine the effect of FGF-21 on AMPK activity, cultured 3T3-L1 adipocytes were incubated with mouse FGF-21 (50 ng/mL) for 30- or 60-min. AMPK activity was assessed by the degree of phosphorylation of the AMPK substrate, ACC Ser^{79} by western blotting analysis.

As shown in Figure 5-9 A, stimulation of 3T3-L1 adipocytes with mouse FGF-21 had no significant effect on ACC phosphorylation (*n*=3).

5.6.8.2 Effect of FGF-21 on eNOS phosphorylation in 3T3-L1 adipocytes

To examine the effect of FGF-21 on eNOS phosphorylation, cultured 3T3-L1 adipocytes were incubated with mouse FGF-21 (50 ng/mL) for 30 or 60 min. The extent of eNOS Ser^{1177} phosphorylation was determined by western blotting analysis of 3T3-L1 adipocytes lysates.

As shown in Figure 5-9 B, stimulation of 3T3-L1 adipocytes with mouse FGF-21 had no significant effect on eNOS phosphorylation at different time points (*n*=3).

5.6.8.3 Effect of FGF-21 on Akt phosphorylation in 3T3-L1 adipocytes

To examine the effect of FGF-21 on Akt stimulation, cultured 3T3-L1 adipocytes were incubated with FGF-21 (50 ng/mL) for 30 or 60 min. The extent of Akt Ser^{473} phosphorylation was determined by western blotting analysis of 3T3-L1 adipocyte lysates.

As shown in Figure 5-9 C, 30-minutes of stimulation of 3T3-L1 adipocytes with mouse FGF-21 did not significantly affect Akt phosphorylation (n=3). However, there was a trend towards Akt stimulation at 60 minutes (*P*=0.09)

5.6.8.4 Effect of FGF-21 on ERK1/2 phosphorylation in 3T3-L1 adipocytes

To examine the effect of FGF-21 on ERK1/2 stimulation, cultured 3T3-L1 adipocytes were incubated with mouse FGF-21 (50 ng/mL) for 30 or 60 min. The extent of ERK1/2 Thr^{202}, Tyr^{204} phosphorylation was determined by western blotting analysis of 3T3-L1 adipocytes.

As shown in Figure 5-9 D, stimulation of 3T3-L1 adipocytes with mouse FGF-21 caused a significant increase in ERK1 phosphorylation after 30 min incubation (*n*=3). Additionally, there was an observable tendency toward increased ERK1 activation after 60 minutes of incubation and heightened ERK2 activation after 30 minutes (*P*= 0.09).

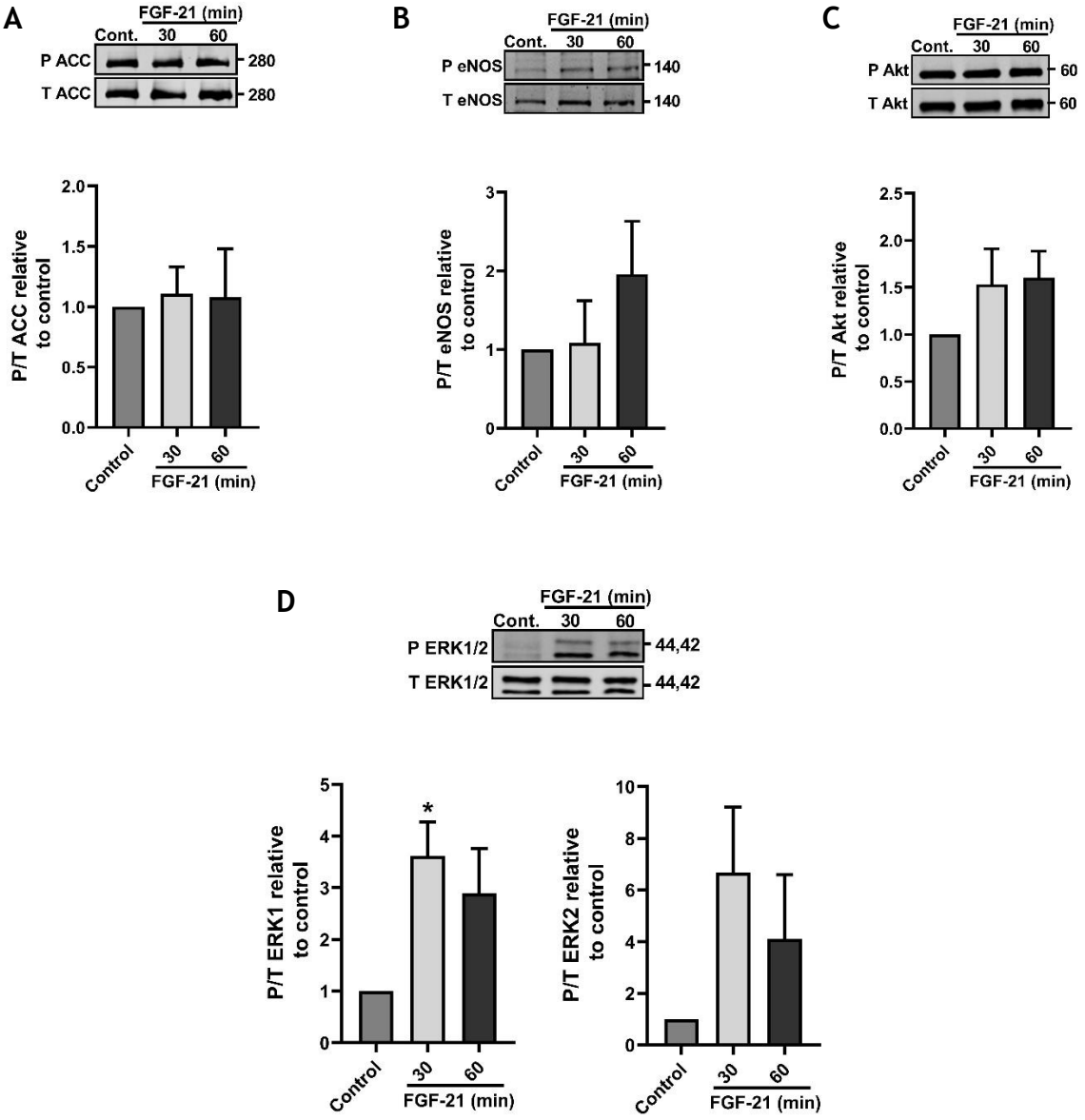

Figure 5-9 Effect of FGF-21 on eNOS, AMPK, AKT, and ERK1/2 phosphorylation in 3T3-L1 adipocytes

3T3-L1 adipocytes were incubated with PBS (control) for 60 min, and mouse FGF-21 (50 ng/mL) for 30- and 60-min. Lysates were prepared, resolved by SDS-PAGE and subjected to immunoblotting with the antibodies indicated (T, total, P, phospho). (A) Quantification of ACC Ser^{79} phosphorylation relative to total ACC. (B) Quantification of eNOS Ser^{1177} phosphorylation relative to total eNOS. (C) Quantification of Akt Ser^{473} phosphorylation relative to total Akt. (D) Quantification of ERK1/2 (Thr^{202}, Tyr^{204}) phosphorylation relative to total ERK1/2. Representative immunoblots with molecular mass markers indicated on the right are shown on the top of each corresponding graph. Data shown represent the mean ± SEM phosphorylation relative to control from three independent experiments. *P < 0.05 (Unpaired t-test).

5.6.9 Effect of FGF-21 on nitric oxide release by 3T3-L1 adipocytes

As PVAT is known to secrete PVRFs including NO, the effect of FGF-21 on NO synthesis by 3T3-L1 adipocytes was assessed. Cultured 3T3-L1 adipocytes were incubated with mouse FGF-21 (50 ng/mL) for 30 or 60 min, and NO levels in the conditioned medium were measured using a Sievers 280 NO analyser as described in section 2.13.

As shown in Figure 5-10, FGF-21 had no effect on NO synthesis in 3T3-L1 adipocytes. This result was consistent with the effect of FGF-21 on eNOS phosphorylation in 3T3-L1 adipocytes described earlier.

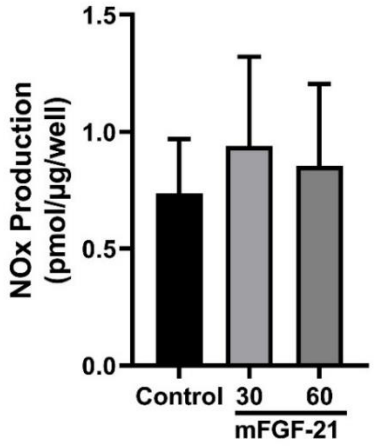

Figure 5-10 Effect of FGF-21 on nitric oxide release by 3T3-L1 adipocytes

3T3-L1 adipocytes were incubated with PBS (control) for 60 min, or mouse FGF-21 (50 ng/mL) for 30 or 60-min. NOx levels in conditioned medium were quantified using a Sievers 280 NO analyser. Data shown represent the mean ± SEM pmol/µg/well (*n*=3).

5.6.10 Effect of FGF-21 on nitric oxide release by PVAT

To assess the role of FGF-21 on NO synthesis by PVAT, pooled thoracic and abdominal PVAT from wild type mice was collected and incubated with and without mouse FGF-21 (100 ng/mL) for 60 min in 1 mL KHHB at 37ºC with continuous oxygenation and conditioned medium collected. NO levels in the conditioned medium were measured using a Sievers 280 NO analyser as described in section 2.13.

As shown in Figure 5-11, the synthesis of NO was significantly reduced when incubated with FGF-21 (**P < 0.01 and *P < 0.05, respectively) in both thoracic and

abdominal PVAT. Consistent with the results shown previously (4.3.7), abdominal PVAT released less NO compared to thoracic PVAT.

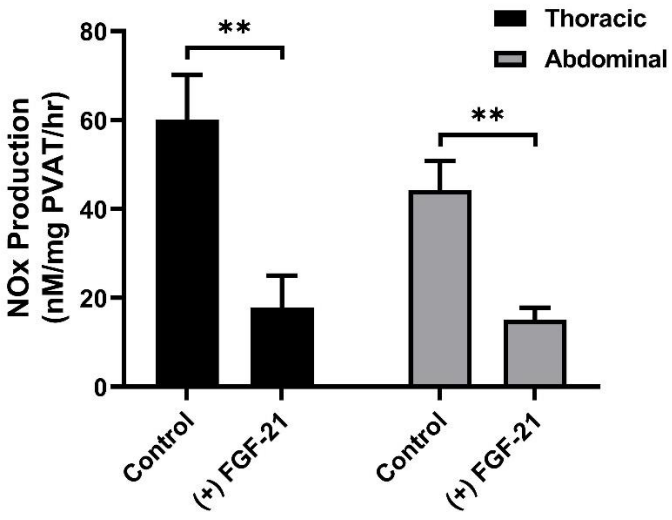

Figure 5-11 Effect of FGF-21 on nitric oxide release by PVAT

Wild type pooled thoracic and abdominal PVAT (three/sample) was incubated with and without FGF-21 (100 ng/mL) in 1 mL KHHB at 37ºC for 60 min with continuous oxygenation and conditioned medium collected. NOx levels in conditioned medium were quantified using a Sievers 280 NO analyser. Data shown represent the mean ± SEM nmol NOx/mg PVAT/hr (*n*=6). ***P* < 0.01 (Unpaired t-test).

5.6.11 Effects of FGF-21 on vascular contraction/relaxation in thoracic aortic rings.

To further investigate the role of FGF-21 in endothelium-mediated vascular responses, endothelium-intact thoracic aortic rings without PVAT from wild type mice were incubated with and without mouse FGF-21 (100 ng/mL) prior to constriction with phenylephrine (1 μM). Dose-response curves to the vasodilator acetylcholine (1 nM – 10 μM) were then constructed. The results are summarised in Figure 5-12. Incubation of aortic rings with FGF-21 did not alter the PE-induced contraction (control group= 10.13 ± 0.60 mN vs FGF-21 group= 10.24 ± 0.65 mN; *n*=7). Similarly, FGF-21 did not alter the maximal extent of acetylcholine-induced relaxation compared to the absence of added FGF-21 (44 ± 7.3%, *n*=7 vs 39 ±7.7%, *n*=7; respectively).

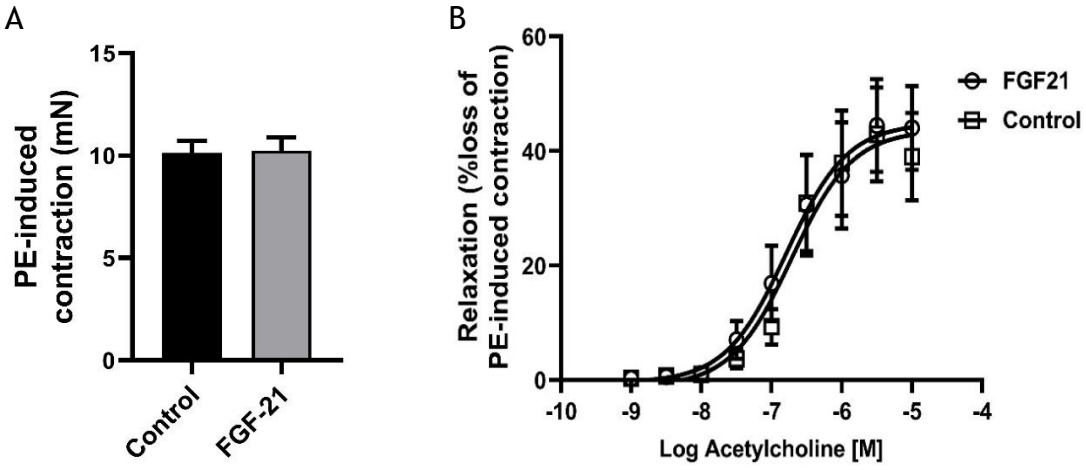

Figure 5-12 Effects of FGF-21 on vascular contraction/relaxation in thoracic aortic rings

Endothelium-intact thoracic aortic rings without PVAT from WT mice were mounted on a wire myograph, preconstricted with phenylephrine (PE, 1 μM) and relaxed with increasing concentrations of acetylcholine (1 nM – 10 μM). (A) Maximum response to PE. (B) Relaxation response to increasing concentrations of ACh (1 nM – 10 μM). Data shown represent the mean ± SEM (*n*= 7).

5.7 Discussion

The key findings of this chapter are that FGF-21 does not exhibit discernible influence on the phosphorylation of eNOS or AMPK and does not influence the release of nitric oxide (NO) in both HUVECs and 3T3-L1 adipocytes. Additionally, FGF-21 did not induce any changes in the phosphorylation of ERK1/2 and Akt in HUVECs. Moreover, the levels of the KLB cofactor were undetectable in the HUVECs used in this study. Furthermore, FGF-21 did not affect the constriction or endothelium-dependent relaxation of mouse aorta.

Moreover, the present study also revealed that compound 991 induced phosphorylation of ACC but did not elicit a corresponding effect on eNOS phosphorylation, despite earlier reports indicating AMPK phosphorylation of eNOS at Ser^{1177} and subsequent stimulation of NO production. Nonetheless, existing literature has established that AMPK activation in endothelial cells does not consistently coincide with eNOS phosphorylation or NO synthesis, as evidenced by studies conducted by (Mount *et al.*, 2005; Stahmann *et al.*, 2010). A previous study also demonstrated that *in vitro*, activation of AMPKα1 did not alter the phosphorylation of eNOS on Ser^{1177}, but increased its phosphorylation on Thr^{495} and attenuated NO production (Zippel *et al.*, 2018). Moreover, considering the pivotal role of Akt phosphorylation in eNOS phosphorylation, the absence of an observable effect of compound 991 on Akt, as reported in the current study, may contribute to the observed lack of activity of compound 991 on eNOS. This aligns with the understanding that Akt serves as a key mediator in the phosphorylation of eNOS, and alterations in Akt phosphorylation can impact the subsequent phosphorylation status of eNOS and its functional outcomes. Similarly, insulin is recognised to stimulate endothelial NO synthesis through Akt-mediated phosphorylation and activation of eNOS at Ser^{1177}, as demonstrated by (Ritchie *et al.*, 2010). Nevertheless, in the present study, the absence of insulin-stimulated Akt phosphorylation could explain the observed lack of insulin's effect on eNOS phosphorylation.

Although the current study has not shown any effect of FGF-21 in HUVECs, previous studies have suggested a potential role for FGF-21 in modulating the function of endothelial cells (Wang *et al.*, 2014; Li *et al.*, 2017; Guo *et al.*, 2018; Huang *et al.*, 2019). Notably, Wang *et al.* (2014) demonstrated that incubation of HUVECs

with FGF-21 ameliorated the detrimental effects induced by high glucose levels, including decreased cell viability, impaired migration, and associated oxidative stress (Wang *et al.*, 2014). FGF-21 also prevented the high glucose-induced decrease in eNOS phosphorylation at Ser^{1177} and Ser^{633}, as well as the decrease in NO production in HUVECs. The protective effect of FGF-21 against high glucose-induced cell damage and eNOS dysfunction was AMPK-dependent, as inhibition of the AMPK pathway using compound C or knockdown of AMPKα1/2 isoforms by siRNA abolished the protective effect of FGF-21 on eNOS phosphorylation (Wang *et al.*, 2014). This study also reported that FGF-21 activates AMPK signalling in HUVECs. In a similar study, Guo *et al.* (2018) demonstrated that pre-treatment of HUVECs with FGF-21 provided protection against high glucose-induced oxidative stress and apoptosis through the PI3K/Akt pathway (Guo *et al.*, 2018). The study also observed an increase in eNOS and Akt phosphorylation in HUVECs treated with FGF-21 alone. Similarly, in an *in vivo* study, long-term administration of FGF-21 to mice with T2DM ameliorated diabetes-induced aortic endothelial dysfunction, enhanced eNOS phosphorylation, and improved aorta relaxation by inhibiting oxidative stress via activation of the CaMKK2/AMPK signalling pathway (Ying *et al.*, 2019). In the same study, they also found that AMPKα knockdown in HUVECs markedly compromised the FGF-21-induced activation of eNOS and ACC.

Moreover, the effect of FGF-21 on eNOS and Akt expression and phosphorylation on HUVECs were also previously assessed by transfection of the cells with FGF-21 mimics or inhibitors. FGF-21 mimics led to an increase in the expression and phosphorylation of eNOS, while an FGF-21 inhibitor had the opposite effect (Li *et al.*, 2017). Similar effects were observed on Akt expression and phosphorylation. However, co-transfection with both FGF-21 inhibitors and eNOS resulted in increased Akt expression and phosphorylation. These findings suggest that FGF-21 regulates eNOS expression and phosphorylation through Akt signalling (Li *et al.*, 2017).

In human brain microvascular endothelial cells (HBMECs), Huang *et al.* (2019) demonstrated that FGF-21 promotes angiogenesis and wound healing by partially upregulating endothelial nitric oxide synthase (eNOS) (Huang *et al.*, 2019). Additionally, in endothelial progenitor cells (EPCs), pretreatment with FGF-21 was found to restore impaired function caused by H_2O_2-induced oxidative stress

through the Akt/eNOS/NO pathway (Huang *et al.*, 2022). These findings further support the potential beneficial effects of FGF-21 on various endothelial cell types.

One notable distinction between the present study and the previously cited investigations lies in the duration of FGF-21 incubation. In the present study, HUVECs were exposed to FGF-21 for a period ranging from 0 to 60 minutes, while other studies employed longer incubation periods of 12 to 48 hours. It is worth noting, however, that a prior study demonstrated the activation of ERK1/2, AMPK, and Akt in cardiomyocytes following FGF-21 treatment for 5, 15, and 20 minutes, respectively (Patel *et al.*, 2014). Furthermore, the majority of studies investigating the impact of FGF-21 on endothelial function have focused on its protective effects in pathological or abnormal metabolic conditions, such as elevated glucose or cholesterol levels. In contrast, the present study specifically examined the role of FGF-21 in endothelial function under normal culture conditions. Consequently, it would be valuable to explore the role of FGF-21 in endothelial function under pathological conditions, such as hypoxia or starvation, in order to obtain a comprehensive understanding of its potential effects.

Moreover, KLB in HUVECs was undetectable in the current study, and this likely underlies the lack of effect of FGF-21 observed in these cells. In other studies the source of endothelial cells or the different conditions they were cultured in may have induced sufficient KLB expression for FGF-21 to have an effect. KLB is essential for the binding of FGF-21 to FGFRs, initiating the signalling cascade involved in the regulation of glucose metabolism and energy expenditure (Ogawa *et al.*, 2007; Yie *et al.*, 2012). Loss of FGF-21's metabolic activity has been observed *in vivo* following knockdown of KLB expression (Ding *et al.*, 2012; Adams *et al.*, 2012) as well as *in vitro* (Ogawa *et al.*, 2007). KLB is primarily expressed in specific tissues such as the liver, WAT, BAT, pancreas, and testes (Ito *et al.*, 2000; Fon Tacer *et al.*, 2010). It was not until Wang *et al* (2014) reported the expression of KLB in endothelial cells that the possibility of FGF-21 directly acting on endothelial cells emerged (Wang *et al.*, 2014). Moreover, *in vitro* investigations revealed the presence of the KLB protein in cultured endothelial progenitor cells (EPCs), and it was observed that the expression of KLB was increased following FGF-21 incubation for 12 h (Huang *et al.*, 2022). Different passages of HUVECs

were utilised in this study, and it remains possible that *in-vitro* passaging led to loss of KLB expression, such that FGF-21 effects may only be observed in freshly isolated or lower passage HUVECs.

Given the previous findings indicating that perivascular adipose tissue (PVAT) releases various vasorelaxant molecules, including NO, the objective of this study was also to investigate the impact of FGF-21 on eNOS phosphorylation and the subsequent production of NO in 3T3-L1 adipocytes. Additionally, the study aimed to assess the involvement of AMPK, Akt, and ERK1/2 signalling pathways in mediating these effects. It is also worth mentioning that a previous study has reported that treatment of human perivascular adipocytes with FGF-21 led to a change in their secretory function (Berti *et al.*, 2016).

As shown in the results section, FGF-21 had no effect on eNOS phosphorylation after 30 or 60 min incubation in 3T3-L1 adipocytes. This could suggest that longer incubation periods might be required to assess the effect of FGF-21 on eNOS stimulation. As reported in previous studies, FGF-21 significantly stimulated ERK1/2 in 3T3-L1 adipocytes (Chau *et al.*, 2010; Jin *et al.*, 2016). While there was a trend toward FGF-21-stimulated Akt phosphorylation at 60 min, there was no noticeable effect on ACC stimulation after short 30- and 60-min incubations.

Surprisingly, 1 h PVAT incubation with FGF-21 resulted in reduced NO production, yet the mechanisms by which this inhibition occurs are unclear. It is widely recognized that adipose tissue serves as a prominent target for the actions of FGF-21. FGF-21 has been shown to have the potential to enhance the thermogenic activity of BAT and induce the browning process in WAT (Kleiner *et al.*, 2012). Moreover, FGF-21 exhibits regulatory effects on glucose and lipid metabolism in adipose tissues, thereby exerting a protective role against ectopic lipid accumulation in the liver and skeletal muscle (Kharitonenkov *et al.*, 2005; Schlein *et al.*, 2016). In mouse and human adipocytes, FGF-21 enhances mitochondrial function by activating peroxisome proliferator-activated receptor gamma coactivator-1α (PGC-1α), a key regulator of energy metabolism, through activation of the AMPK-SIRT1 pathway (Chau *et al.*, 2010). They reported that the activation of AMPK required the stimulation of LKB1, an upstream kinase of AMPK, which suggests that LKB1 might be one of the targets of FGFR1. It is noteworthy

to highlight that the incubation duration of FGF-21 in this study was 3 days, representing a notable distinction from the present investigation.

Finally, we examined the direct impact of FGF-21 on endothelium-dependent vasorelaxation using wire myography. Given the established role of PVAT in modulating vascular tone through the release of vasoactive molecules, the experiment involved the removal of PVAT to exclude the influence of other perivascular-derived factors on the vascular tone. As shown in the results section 5.6.11, addition of FGF-21 had no effect on the PE-induced contraction and did not alter acetylcholine-induced relaxation in vessels lacking PVAT. This is in agreement with the previous findings in this chapter that shows no obvious role of FGF-21 on eNOS phosphorylation and NO production in HUVECs or 3T3-L1 adipocytes. However, by removing the PVAT the PVRFs will be lost, and this includes adiponectin which is known to have vasorelaxant properties. Previous studies in our laboratory have demonstrated that PVAT from AMPKα1 KO mice secrete less adiponectin than WT, and the addition of adiponectin to vessels in the organ bath significantly augmented relaxation (Almabrouk *et al.*, 2017). Previous studies demonstrated that adiponectin acts as an obligatory downstream mediator of FGF-21. Therefore, the lack of influence of FGF-21 on vascular tone reported in the current study could be related to the lack of adiponectin when PVAT was removed.

So far, a limited number of studies have investigated the *in vitro* role of FGF-21 on vessel tension. Interestingly, Ying *et al*. showed that in diabetic mouse aorta or mouse aorta exposed to high glucose, long-term *in vivo* FGF-21 pre-treatment or 2 h incubation with FGF-21 *in vitro* improved acetylcholine-induced vasorelaxation, enhanced eNOS activity, and increased NO release (Ying *et al.*, 2019). This action was suggested to be mediated by inhibition of local oxidative stress via CaMKK2/AMPK activation. Moreover, in the same study treatment of isolated mice aorta with intact PVAT with an increasing concentration of FGF-21 induced dose-dependent relaxation in the aorta. This FGF-21 mediated relaxation was almost blocked by compound c (AMPK inhibitor) or selective CaMKK2 antagonist (STO-609) suggesting that the FGF21-CaMKK2-AMPK signalling pathway directly induces dilation in conduit arteries (Ying *et al.*, 2019). In another recent study, treatment of ApoE-deficient mice with FGF-21 improved acetylcholine-

stimulated aortic relaxation via increased eNOS mRNA expression and upregulation of antioxidant superoxide dismutase genes expression (Huang *et al.*, 2022). Both studies further highlighted the protective role of FGF-21 against vascular injury induced by different metabolic diseases. This protective effect is suggested to be either due to the role of FGF-21 in maintaining the homeostasis or due to its interaction with different cellular pathways as well as its antioxidant effect, or both. One of the notable differences between the previous studies and the current study is that the current study assessed the vasoactive role of FGF-21 on mouse aorta under normal metabolic conditions. This further highlights the protective role of FGF-21 in maintaining metabolic and cardiovascular homeostasis in different metabolic diseases.

5.8 Conclusion:

In summary, the incubation of HUVECs or 3T3-L1 adipocytes with FGF-21 did not induce alterations in eNOS activity or NO release. Potential factors contributing to this lack of effect include the absence of KLB expression on HUVECs and the relatively short incubation periods employed. Additionally, the absence of adiponectin, a crucial mediator for FGF-21, might have played a role in the observed outcomes. However, previous research has indicated a promising role for FGF-21 in mediating and protecting endothelial function in diverse metabolic disorders. This protective function is associated, at least in part, with AMPK activation or an increase in adiponectin secretion. Considering the metabolic properties of FGF-21, it is not surprising that FGF-21 and AMPK are increasingly considered as promising candidates for drug development targeting metabolic diseases, such as type 2 diabetes and metabolic syndrome.

Chapter 6 General Discussion

6.1 Summary and Discussion of Results

The research presented in this thesis has advanced our comprehension of the role of perivascular adipose tissue (PVAT) in the regulation of vascular tone, specifically examining the role of AMPK in this regard. As with any research study, the results have left some questions unanswered and do suggest some areas that require further investigation in subsequent studies.

PVAT represents a specialised form of adipose tissue enveloping most mammalian blood vessels. Recognised as an active endocrine organ, PVAT possesses the capacity to regulate diverse aspects of vascular physiology, including blood vessel tone, endothelial function, and the growth and proliferation of vascular smooth muscle cells. Under normal physiological conditions, PVAT exhibits a robust anticontractile effect by releasing a spectrum of vasoactive substances, including nitric oxide (NO), hydrogen sulfide (H_2S), hydrogen peroxide (H_2O_2), adiponectin, leptin, prostacyclin, angiotensin 1-7, palmitic acid methyl ester, and omentin (Kim *et al.*, 2019; Ahmed *et al.*, 2023). However, under some pathophysiological conditions, PVAT exhibits pro-contractile effects because the balance between anticontractile and pro-contractile factors is shifted. Some PVAT-derived pro-contractile agents include angiotensin II, superoxide anion, prostaglandins, catecholamines, resistin, visfatin, and chemerin (Ahmed *et al.*, 2023).

The acknowledgment of PVAT as a functional endocrine organ has significantly advanced our understanding of the molecular mechanisms regulating its function, particularly in the context of obesity and associated co-morbidities. In the sphere of cardiovascular health, PVAT is emerging as a critical contributor to the initiation and progression of cardiovascular diseases, potentially linking obesity, insulin resistance, and vascular disorders, particularly given its detrimental impact on blood vessel function in individuals with obesity (Valentini *et al.*, 2023). For example, studies suggest that PVAT contributes to the development of endothelial dysfunction (ED) (Houben *et al.*, 2012; Eringa *et al.*, 2012). Notably, specific adipokines produced by PVAT influence insulin sensitivity, playing a role in the aetiology of type 2 diabetes, and contributing to the exacerbation of ED in the context of this chronic condition (Yudkin *et al.*, 2005; Szasz *et al.*, 2013; Lastra and Manrique, 2015).

AMP-activated protein kinase (AMPK) is a critical cellular energy sensor and regulator that plays a pivotal role in maintaining vascular function. AMPK activation is associated with multiple beneficial effects that collectively contribute to the maintenance of vascular health. One of the key roles of AMPK in vascular function is the promotion of vasorelaxation. Activation of AMPK induces the release of vasodilatory factors, such as nitric oxide (NO), from endothelial cells (Morrow *et al.*, 2003; Rodríguez *et al.*, 2020). This effect could play a role in regulating blood flow and preventing excessive vasoconstriction.

AMPK also plays a crucial role in PVAT function, including facilitating communication between PVAT and the vascular wall, influencing the vascular endothelium and smooth muscle cells, and contributing to the regulation of vascular tone and function. AMPK activation in PVAT has been shown to regulate the secretion of adipokines, including adiponectin, which influences vascular tone and contributes to the anticontractile properties of PVAT (Almabrouk *et al.*, 2017). Furthermore, AMPK activation in PVAT has been demonstrated to have anti-inflammatory effects, thereby reducing inflammation around blood vessels and helping to maintain a healthier vascular environment (Sun *et al.*, 2014). These findings underscore the significant role of AMPK in regulating PVAT function and its impact on various aspects of vascular health, highlighting its potential as a therapeutic target for cardiovascular diseases.

Studies have demonstrated that PVAT regulates vascular tone through releasing vasorelaxant factors (PVRFs) which influence the underlying VSMCs and endothelial cells. Previous work in our lab had used vessels denuded of endothelium to study exclusively how AMPK in the PVAT regulates VSMC relaxation. The work demonstrated an attenuation in the anticontractile effect of PVAT and reduced adiponectin release in AMPKα1 knockout mice (Almabrouk *et al.*, 2017).

To further examine the role of PVAT and AMPK in modulating vascular function, the aim of the current study was to extend these findings to evaluate the role of AMPKα1 on mediating PVAT's influence on the vascular endothelium.

Chapter 3 examined the involvement of PVAT and AMPK in modulating relaxation in endothelium-intact thoracic and abdominal rings from wild-type and AMPKα1

KO mice. Cromakalim (a K_{ATP} channel opener) was used as a vasodilator. The opening of K_{ATP} channels facilitates the efflux of K^+, leading to membrane hyperpolarisation. Membrane hyperpolarisation inhibits calcium influx through voltage-gated calcium channels, resulting in relaxation of VSMCs and vasodilation.

The influence of PVAT on vascular tone was examined in two anatomical locations, thoracic and abdominal aortae. Thoracic PVAT is similar to BAT, while abdominal and mesenteric PVAT is similar to WAT. This difference in phenotype is of crucial importance, as small vessels play a major role in the regulation of blood pressure compared to large vessels. Moreover, this phenotypic discrepancy appears to be clinically important, as abdominal aortae are more susceptible to atherosclerosis and the development of aortic aneurysms than thoracic aortae (Victorio *et al.*, 2016). In conditions like obesity, abdominal PVAT, as in other WAT depots, becomes more susceptible to inflammation, as indicated by greater expression of inflammatory genes and immune cell infiltration markers in abdominal PVAT relative to thoracic PVAT (Villacorta and Chang, 2015). This may cause altered secretion of adipokines by the PVAT, potentially contributing to vascular dysfunction and inflammation. The difference between thoracic and abdominal PVAT with regard to its effect on vascular tone has not been widely investigated. Previous studies demonstrated that the anticontractile function of PVAT is lost in the abdominal aorta along with a reduction in eNOS-derived NO production compared with the thoracic aorta (Victorio *et al.*, 2016).

Taken together, this chapter highlighted the impaired anti-contractile effect of abdominal PVAT in the KO mouse in both endothelium-intact and denuded abdominal arteries. Furthermore, the heightened impairment in vasorelaxation observed in KO abdominal rings with PVAT and an intact endothelium suggests an influential role of PVAT-derived substances on endothelial function, potentially impacted by the deletion of the AMPKα1 subunit. Moreover, since addition of cromakalim or phenylephrine to human umbilical vein endothelial cells (HUVECs) did not activate AMPK, it suggests that AMPK activation within endothelial cells is unlikely to be the causative factor for the observed variations in relaxation response between WT and KO abdominal aorta with intact PVAT. While the specific cause(s) for these effects remains unclear at this point, the potential

involvement of AMPK in regulating inflammation within WAT and influencing the secretion of adipokines seems to be a plausible contributory factor.

AMPK plays a significant role in regulating inflammation in WAT. Investigations have revealed that AMPK activation reduces inflammation in adipocytes by suppressing pro-inflammatory pathways (Lihn *et al.*, 2004). AMPK has been reported to inhibit the expression and secretion of pro-inflammatory cytokines in adipose tissue, and its activation has been associated with the inhibition of IL-1ß-stimulated IRAK4 phosphorylation and TNF-α-stimulated IKK/IκB/NF-κB signalling in cultured adipocytes (Mancini *et al.*, 2017). Moreover, a previous study in our lab demonstrated that high-fat diet (HFD) causes an inflammatory infiltrate, reduced AMPK phosphorylation and attenuates the anticontractile effect of murine aortic PVAT (Almabrouk *et al.*, 2018). Interestingly, the study also reported that aortic PVAT in mice lacking AMPKα1 has a similar phenotype to wild-type aortic PVAT after HFD, indicating that AMPK may safeguard the vessel against adverse alterations in response to HFD.

Additionally, AMPK has been identified as a potential regulator of PVAT and a target of PVAT action in the blood vessel. Indeed, our previous work also demonstrated that AMPK may regulate adiponectin secretion by PVAT either directly by targeting its release from adipocytes and/or indirectly by its anti-inflammatory function which would limit the suppression of adiponectin expression, thereby influencing the anticontractile activity of PVAT(Almabrouk *et al.*, 2018). The role of AMPK in regulating PVAT function might also involve the modulation of other PVRFs, including nitric oxide (NO), which in turn affects vascular relaxation. This could potentially be through regulating various metabolic and inflammatory pathways.

Taken together, the differences between WT and KO abdominal PVAT necessitates further investigations to elucidate the precise mechanism(s) and to characterise the nature of PVAT-derived substances responsible for the observed effects. For instance, this could include studying the histological and secretory differences between them.

In contrast to the abdominal aorta, both endothelium-intact and denuded thoracic aortic rings from WT and KO mice showed no differences in response to the

vasoconstrictor phenylephrine and the vasodilator cromakalim. This could indicate that the function of thoracic PVAT remained unaffected by the deletion of AMPK α1. However, a previous study from our laboratory reported that in denuded thoracic aortae of AMPK α1 KO mice, PVAT exhibited a diminished anticontractile effect compared to WT, correlating with disruptions in adiponectin secretion (Almabrouk *et al.*, 2017). One of the difference between the two studies is the vasocostrictor reagents used. PE was used in the current study, while U46619 was used in the previous study. Although both reagents are involved in signaling pathways that regulate vascular tone by increasing intracellular calcium, they act on different receptors. PE is a sympathomimetic drug which selectively binds to and activates alpha-1 adrenergic receptors on the surface of VSMCs activating a signalling cascade that ultimately increases intracellular calcium, leading to MLCK activation and VSMC contraction. Whereas U46619 mimics the action of thromboxane A2 and binds to thromboxane receptors, initiating a cascade of intracellular signaling events that ultimately increases intracellular calcium levels, leading to activation of the contractile machinery and contraction of VSMCs (Jiang *et al.*, 2021).

These findings underscore the complex and context-dependent role of AMPK in modulating PVAT function and its impact on vascular tone regulation, highlighting the need for further research to elucidate the specific mechanisms and substances involved in the observed effects. This might include studying the role of AMPK in regulating the secretory function of PVAT as well as regulating the cellular components.

The potential functional differences between thoracic and abdominal PVAT warrant continued investigation to enhance our understanding of the intricate interplay between AMPK, PVAT, and vascular function.

Chapter 4

Expanding on the above findings, the objective in chapter 4 was to further understand the role of AMPK in regulating PVAT function and its potential influence on vascular relaxation and to perhaps understand what underlies the differences between abdominal and thoracic PVAT. Therefore, the study investigated the potential differences in the secretory profile between thoracic

and abdominal PVAT derived from WT and KO mice. Additionally, the study aimed to assess the impact of PVAT conditioned media (CM) on different signalling pathways in cultured endothelial cells, given the more pronounced difference in the anti-contractile effect of PVAT between WT and KO abdominal aortae in endothelium-intact vessels.

In AMPKα1 KO mice, abdominal PVAT demonstrated a disruption in its secretory function compared to WT abdominal PVAT. Notably, there was a significant decrease in the release of adiponectin, FGF-21, ICAM-1, TIMP-1, IGF-II, and LIF by abdominal PVAT in KO mice.

The role of AMPK in influencing the release of ADRFs has been investigated in a limited number of studies. Within adipose tissue, AMPK plays a pivotal role in regulating adipokine secretion through both direct and indirect mechanisms. Directly, AMPK activation affects the expression and release of adiponectin by modulating intracellular signalling pathways. Notably, a study by Lihn *et al.* revealed that the AMPK activator AICAR reduced TNF-α and IL-6 production while concurrently increasing adiponectin gene expression and AMPKα1 activity in adipose tissue (Lihn *et al.*, 2004). Given that TNF-α and IL-6 can inhibit adiponectin gene expression, this suggests a direct regulatory role of AMPK in mitigating inflammation and enhancing adiponectin release. Consistent with this, previous research in our laboratory demonstrated a significant reduction in adiponectin release from thoracic aortic PVAT lacking AMPKα1. Therefore, it is proposed that AMPK, either by directly modulating adiponectin secretion from PVAT or indirectly by alleviating PVAT inflammation, plays a crucial role in the regulation of adiponectin release (Almabrouk *et al.*, 2018). Similarly, the PPARγ agonist troglitazone which also activates AMPK has a positive effect on adiponectin expression in mature adipocytes (Achari and Jain, 2017). Additionally, the present study aligns with prior research indicating that adiponectin is the predominant peptide secreted by adipocytes and that its release is impaired in the absence of AMPKα1 (Almabrouk *et al.*, 2017).

The effect of adiponectin released by PVAT on vasorelaxation has been studied in the past. Hence, the current work investigated a different PVAT-released adipokine as a possible explanation for the findings reported in Chapter 3. In recent years, FGF-21 has been demonstrated to play a pivotal role in promoting

vascular homeostasis through its regulatory effects on endothelial function and nitric oxide production. Furthermore, studies suggest that FGF-21 can activate the AMPK pathway (Salminen *et al.*, 2017). This activation could occur either directly through FGFR1/ß-klotho signalling or indirectly by triggering the secretion of adiponectin, subsequently leading to the activation of AMPK signalling in their respective target tissues (Yamauchi *et al.*, 2002; Zhou *et al.*, 2009). The concentration of FGF-21 within abdominal KO PVAT and its release by PVAT were significantly diminished compared to that seen in WT abdominal PVAT. Consequently, the present investigation focused on FGF-21 as a potential PVRF responsible for the differences observed in chapter 3.

The findings indicate a notable influence of PVAT conditioned media (PVAT CM) on the activation of signalling pathways in HUVECs, particularly in the phosphorylation of ERK1/2 (Thr^{202}, Tyr^{204}) induced by abdominal PVAT CM. ERK1/2 signalling in endothelial cells is known to play a role in regulating eNOS phosphorylation, nitric oxide (NO) production and overall endothelial function, impacting processes such as survival, proliferation, migration, and angiogenesis (Kong *et al.*, 2017). However, the data revealed no effect of PVAT CM from either WT or KO mice on eNOS activation in endothelial cells.

A similar trend was observed in Akt phosphorylation in response to abdominal PVAT CM, although statistical significance was not reached. Akt, a protein kinase, serves as a central node in several signal transduction pathways, phosphorylating numerous downstream targets. It is a critical regulator of endothelial cell function, including cell growth, migration, survival, and vascular tone. Akt directly phosphorylates eNOS on Ser^{1177}, leading to the activation of the enzyme and subsequent NO production. Together with the lack of a statistically significant effect on Akt phosphorylation, this could also explain the lack of eNOS activation observed in the same experiment.

Although the precise causes of the observed effects are yet unknown, previous studies have linked the activation of ERK1/2 and Akt in endothelial cells to adiponectin and FGF-21. PVAT activity is known to be complex, and its possible role in vascular homeostasis may be influenced by the varied effects of adiponectin and FGF-21 on cellular signalling pathways. Further research is necessary to elucidate the precise elements and mechanisms underlying the

complex interactions between PVAT and endothelial cell signalling pathways, as it is possible that other variables or factors in the experimental setup are influencing the reported outcomes. For instance, future experiments could add individual PVAT-derived substances to test the effect on the Akt and ERK1/2 pathways or study the effect of PVAT CM in mouse endothelial cells which may differ in their response compared to HUVECs. Understanding these complexities may help illuminate the more general effects of PVAT on vascular function and offer suggestions for potential vascular therapy routes.

Chapter 5

The findings in Chapter 3 suggest that the anti-contractile effect of abdominal PVAT is diminished in vessels with an intact endothelium in AMPKα1 KO mice compared to WT mice. Furthermore, the data presented in Chapter 4 indicates a reduction in FGF-21 secretion in abdominal PVAT from AMPKα1 KO mice relative to PVAT from wild-type mice. Given the positive effects of FGF-21 on metabolic regulation, anti-inflammatory responses, endothelial protection, and angiogenesis, FGF-21 was selected as the focus for the research presented in this chapter. The primary objective was to evaluate the potential impact of FGF-21 on endothelial function, specifically examining its effects on eNOS and AMPK phosphorylation in HUVECs, cells which were readily available in our lab. Acknowledging the significance of PVAT in vascular homeostasis and the known targeting of adipose tissue by FGF-21, the study also assessed FGF-21's influence on cultured 3T3-L1 adipocytes. Finally, a functional study was conducted in mouse aortic rings to assess the effect of FGF-21 on vasorelaxation.

FGF-21 is a member of the fibroblast growth factor (FGF) family, which act in an autocrine, paracrine, or endocrine manner with a wide range of biological functions, including cell growth, cellular proliferation, survival, migration, and differentiation (Hui *et al.*, 2018). It is expressed in several metabolically active tissues, including the liver, adipose tissue, pancreas, and brain (Fon Tacer *et al.*, 2010). FGF-21 is well-known for its role in metabolic regulation. It plays a crucial part in glucose and lipid metabolism, which are intimately linked to vascular health (Chen *et al.*, 2022). FGF-21 has been demonstrated to possess anti-inflammatory properties, mitigating the detrimental effects of inflammation on endothelial cells. FGF-21 has also been shown to positively regulate NO

production, and to protect endothelial cells from various stressors, including oxidative stress and inflammatory stimuli.

Both FGF-21 and AMPK play fundamental roles in energy metabolism, sharing significant functional overlap. FGF-21 regulates systemic glucose and lipid metabolism by enhancing insulin sensitivity, increasing glucose uptake, and inhibiting lipogenesis. AMPK, a crucial metabolic sensor, regulates energy production by stimulating glucose and lipid breakdown. The similarities in their metabolic profiles suggest that FGF-21 and AMPK may act through similar metabolic pathways. Evidence suggests that FGF-21 activates AMPK directly through FGFR1/KLB signalling or indirectly by stimulating the secretion of adiponectin and corticosteroids (Salminen *et al.*, 2017).

Recent research has shifted the focus on FGF-21 from its metabolic role to its association with cardiovascular disease (CVD). While previous studies highlighted its metabolic regulation and therapeutic potential for conditions like type 2 diabetes and obesity, more recent investigations emphasise its cardiovascular protective effects. Studies indicate a connection between FGF-21 and CVD, including carotid atherosclerosis and coronary heart disease (Lin *et al.*, 2015; Wu *et al.*, 2017). Clinical studies show elevated serum FGF-21 levels in patients with diabetic cardiomyopathy and other cardiovascular diseases (Chen *et al.*, 2016), suggesting its potential as a biomarker for predicting cardiovascular events. Interestingly, increased FGF-21 levels are associated with pericardial fat accumulation (Lee *et al.*, 2014), indicating a potential link between FGF-21, fat deposition, and dyslipidaemia, with implications for cardiovascular risk assessment. As the FGF-21 has beneficial effects on glucose and lipid metabolism, the elevated levels of FGF-21 in conditions like diabetic cardiomyopathy may reflect underlying metabolic dysregulation and stress on the body.

In the cardiovascular system, AMPK mediates the protective functions of FGF-21 in various vascular tissues. Studies show that FGF-21 protects the heart from apoptosis and diabetic cardiomyopathy by activating the ERK1/2-p38 MAPK-AMPK signalling pathway (Zhang *et al.*, 2015). FGF-21 also improves cardiac function in response to myocardial ischaemia via activation of PI3K/Akt, ERK1/2, and AMPK pathways (Patel *et al.*, 2014). In endothelial cells, FGF-21's protective role involves AMPK activation, shielding against endothelial cell damage and

dysfunction induced by high glucose (Wang *et al.*, 2014). Long-term FGF-21 administration to diabetic mice ameliorates aortic endothelial dysfunction and improves aorta relaxation through the CaMKK2/AMPK signalling pathway, inhibiting oxidative stress (Ying *et al.*, 2019). Overall, these findings highlight the interconnected roles of FGF-21 and AMPK in regulating energy metabolism and exerting protective effects in cardiovascular and metabolic contexts.

Moreover, FGF-21 and adiponectin, major hormones from the liver and adipose tissues, respectively, share functional similarities and exhibit therapeutic potential in various metabolic and cardiovascular conditions. Elevating their levels, either through pharmacological/genetic means or recombinant protein administration, has shown benefits such as increasing energy expenditure, reducing adiposity, improving insulin sensitivity, and protecting against myocardial infarction, diabetic cardiomyopathy and atherosclerosis in rodents and non-human primates. Studies suggest a reciprocal relationship between FGF-21 and adiponectin, with FGF-21 influencing adiponectin secretion. FGF-21's effects on glycaemic control and insulin sensitivity may depend on adiponectin, as seen in animal models. In obesity, a dysfunctional FGF-21-adiponectin axis, possibly due to FGF-21 resistance, may contribute to metabolic syndrome. Notably, FGF-21 administration in mice with myocardial infarction attenuates cardiac dysfunction and inflammation through an adiponectin-dependent mechanism, suggesting adiponectin acts as a crucial downstream mediator of FGF-21.

The main findings of chapter 5 indicate that FGF-21 does not have a measurable impact on the phosphorylation of eNOS or AMPK and nor does it affect the release of nitric oxide (NO) by both HUVECs and 3T3-L1 adipocytes. Additionally, FGF-21 does not induce any changes in the phosphorylation of ERK1/2 and Akt in HUVECs. Moreover, the levels of the KLB cofactor were undetectable in the HUVECs used in this study. Functionally, FGF-21 did not affect the contraction or endothelium-dependent relaxation of mouse aorta.

Although the current study did not reveal any effect of FGF-21 on the phosphorylation of eNOS or AMPK or on the release of NO in both HUVECs and 3T3-L1 adipocytes, prior research has suggested a potential role for FGF-21 in modulating the function of endothelial cells. Previous studies demonstrated that FGF-21 protects HUVECs from detrimental effects induced by high glucose,

including impaired cell viability, migration, and oxidative stress (Wang *et al.*, 2014; Li *et al.*, 2017). FGF-21 also prevented high glucose-induced decrease in eNOS phosphorylation and NO production in HUVECs (Wang *et al.*, 2014). The protective effect of FGF-21 against high glucose-induced cell damage and eNOS dysfunction was AMPK-dependent. Similarly, Guo *et al.* (2018) showed that pre-treatment of HUVECs with FGF-21 provided protection against high glucose-induced oxidative stress and apoptosis through the PI3K/Akt pathway (Guo *et al.*, 2018). In an *in vivo* study, long-term administration of FGF-21 to mice with T2DM ameliorated diabetes-induced aortic endothelial dysfunction, enhanced eNOS phosphorylation, and improved aorta relaxation by inhibiting oxidative stress via activation of the CaMKK2/AMPK signalling pathway (Ying *et al.*, 2019). These findings suggest that while the current study did not demonstrate a direct influence of FGF-21 on endothelial cells, previous research has indicated potential beneficial effects of FGF-21 on endothelial function through various signalling pathways.

The effect of FGF-21 on eNOS and Akt expression and phosphorylation in HUVECs has been reported in previous studies. Li *et al.* demonstrated that FGF-21 mimics led to an increase in the expression and phosphorylation of eNOS, while FGF-21 inhibitors had the opposite effect (Li *et al.*, 2017). Similar effects were observed on Akt expression and phosphorylation. Co-transfection with both FGF-21 inhibitors and eNOS resulted in increased Akt expression and phosphorylation, suggesting that FGF-21 regulates eNOS expression and phosphorylation through Akt signaling. Additionally, in human brain microvascular endothelial cells, Huang *et al.* showed that FGF-21 promotes angiogenesis and wound healing by partially upregulating eNOS (Huang *et al.*, 2019). Furthermore, in endothelial progenitor cells (EPCs), pretreatment with FGF-21 was found to restore impaired function caused by H_2O_2-induced oxidative stress through the Akt/eNOS/NO pathway (Huang *et al.*, 2022). These findings support the potential beneficial effects of FGF-21 on various endothelial cell types, despite the current study not demonstrating any influence of FGF-21 on the phosphorylation of eNOS or Akt in HUVECs.

So, what could account for the lack of effect of FGF in the current study? The present study differs from previous research in the duration of endothelial cell

exposure to FGF-21. While this study exposed HUVECs to FGF-21 for 0 to 60 min, other studies utilised much longer incubation periods of between 12 and 48 hours. However, one study did use a shorter incubation time and did demonstrate the activation of ERK1/2, AMPK, and Akt in cardiomyocytes following FGF-21 treatment for 5, 15, and 20 minutes, respectively (Patel *et al.*, 2014). Furthermore, most investigations into the impact of FGF-21 on endothelial function have focused on its protective effects in pathological metabolic conditions, such as elevated glucose or cholesterol levels. In contrast, the present study specifically examined the role of FGF-21 in endothelial function under normal culture conditions. Therefore, it would be valuable to explore the role of FGF-21 in endothelial function under pathological conditions, such as hypoxia or starvation, or in endothelial cells lacking AMPK to obtain a comprehensive understanding of its potential effects. Additionally, the undetectable levels of KLB in the HUVECs used in the current study may underlie the lack of observed effects, as KLB is essential for the binding of FGF-21 to FGFRs. The expression of KLB in endothelial cells, including HUVECs, has been reported in other studies (Wang *et al.*, 2014; Huang *et al.*, 2022), and its absence in the HUVECs utilised in this study may have contributed to the lack of observed effects. It might be possible that *in-vitro* passaging led to loss of KLB expression, such that FGF-21 effects may only be observed in freshly isolated HUVECs. Therefore, the study underscores the importance of considering the duration of FGF-21 exposure, culture conditions, and the expression of the KLB cofactor in endothelial cells when interpreting its effects.

The study also aimed to investigate the impact of FGF-21 on eNOS phosphorylation and subsequent NO production in 3T3-L1 adipocytes, with a focus on the involvement of AMPK, Akt, and ERK1/2 signalling pathways. The investigation was motivated by previous findings indicating that PVAT releases vasorelaxant molecules, including NO. The study also noted prior research that reported changes in the secretory function of human perivascular adipocytes with FGF-21 treatment (Berti *et al.*, 2016). However, the study's results revealed no significant effect of FGF-21 on eNOS phosphorylation after short incubation periods of 30 or 60 minutes in 3T3-L1 adipocytes. As kinases act quickly, this suggests that shorter incubation periods may be necessary to fully assess the impact of FGF-21 on eNOS stimulation. The study also found that FGF-21 significantly stimulated ERK1/2 in

3T3-L1 adipocytes, and while there was a trend toward FGF-21-stimulated Akt phosphorylation at 60 minutes, no noticeable effect on ACC phosphorylation was observed after the short 30- and 60-minute incubation periods. The study concluded that the cellular response to FGF-21, especially regarding eNOS phosphorylation and ACC stimulation, may require a shorter exposure time. The results also highlighted the importance of considering incubation duration in investigating the effects of FGF-21 on adipocytes and suggested potential signalling pathways involved in its actions, such as the ERK1/2 pathway. The study recommended further exploration with extended incubation periods and in the context of physiological or pathological conditions to provide a more comprehensive understanding of FGF-21's impact on adipocyte function.

The surprising observation that a 1-hour PVAT incubation with FGF-21 resulted in reduced NO production raises intriguing questions about the underlying mechanisms. Adipose tissue is recognised as a significant target for FGF-21 actions, with known effects on enhancing the thermogenic activity of BAT and inducing the browning process in WAT (Kleiner *et al.*, 2012). FGF-21 also plays a regulatory role in glucose and lipid metabolism in adipose tissues, contributing to the prevention of ectopic lipid accumulation in the liver and skeletal muscle.

Previous studies in mouse and human adipocytes have demonstrated that FGF-21 enhances mitochondrial function by activating Peroxisome Proliferator-Activated Receptor Gamma Coactivator-1α (PGC-1α), a key regulator of energy metabolism (Chau *et al.*, 2010). This activation occurs through the AMP-activated protein kinase (AMPK)-Sirtuin 1 (SIRT1) pathway. The study reports that the activation of AMPK required the stimulation of Liver Kinase B1 (LKB1), an upstream kinase of AMPK, suggesting that LKB1 might be a target of FGF-21. It's crucial to note that the incubation duration of FGF-21 in this study was 3 days, which differs significantly from the shorter incubation periods in the present investigation. This distinction in duration could account for the observed differences in NO production. Longer exposure to FGF-21 might trigger regulatory mechanisms or downstream effects that are not evident with shorter incubation periods.

The findings underscore the complexity of FGF-21's actions in adipose tissue and highlight the importance of considering incubation duration in understanding its effects on NO production. Further research exploring the time-dependent effects

of FGF-21 on adipose tissue function and NO regulation could provide additional insights into the intricate molecular mechanisms involved.

The study also aimed to investigate the direct impact of FGF-21 on endothelium-dependent vasorelaxation in WT thoracic aortae using wire myography. The experiment involved removing PVAT to investigate the influence of exogenous addition of FGF-21 on vascular tone without influence of other PVAT-derived factors. The results indicated that the addition of FGF-21 had no effect on PE-induced contraction and did not alter acetylcholine-induced relaxation in vessels lacking PVAT. This finding aligns with earlier observations in the study that showed no significant role of FGF-21 on eNOS phosphorylation and NO production in HUVECs or 3T3-L1 adipocytes.

However, the removal of PVAT will also have led to the loss of perivascular-derived factors, including adiponectin, which is known to have vasorelaxant properties. Prior studies indicated that adiponectin acts as an obligatory downstream mediator of FGF-21 (Lin *et al.*, 2013; Hui *et al.*, 2016). Previous research from our laboratory demonstrated that PVAT from mice lacking AMPKα1 secreted less adiponectin, and the addition of adiponectin to vessels enhanced relaxation (Almabrouk *et al.*, 2017). Therefore, the lack of influence of FGF-21 on vascular tone reported in the current study could be related to the absence of adiponectin when PVAT was removed.

In contrast, other studies have reported positive effects of FGF-21 on vasorelaxation under diabetic or high-glucose conditions. These studies suggested that in PVAT-intact vessels, FGF-21 may improve acetylcholine-induced vasorelaxation, enhance eNOS activity, and increase NO release, potentially mediated by inhibition of local oxidative stress through CaMKK2/AMPK activation (Ying *et al.*, 2019). Another recent study in ApoE-deficient mice demonstrated that FGF-21 improved aortic relaxation via increased eNOS mRNA expression and upregulation of antioxidant superoxide dismutase gene expression (Huang *et al.*, 2022).

The notable difference between these previous studies and the current one lies in the metabolic conditions under examination. The current study assessed the vasoactive role of FGF-21 on mouse aorta under normal metabolic conditions,

emphasising the potential protective role of FGF-21 in maintaining metabolic and cardiovascular homeostasis in different metabolic diseases.

In summary, the study indicates that, under normal metabolic conditions, FGF-21 did not directly influence vasorelaxation in mouse aorta lacking PVAT, potentially due to the absence of adiponectin. However, other studies suggest a positive role for FGF-21 in vasorelaxation under specific pathological conditions, emphasising the multifaceted nature of FGF-21's effects on vascular function and the need for further exploration in diverse metabolic contexts.

6.2 Limitations:

There are several noteworthy limitations within the current study that warrant attention. Firstly, the utilisation of global AMPKα1 KO models makes it more difficult to identify the precise role that AMPK plays in controlling vascular function inside the PVAT. This limitation arises from the absence of AMPKα1 not only in PVAT but also in the endothelium and VSMCs, coupled with its association with metabolic and physiological irregularities. This limitation underscores the importance of refining experimental models to isolate the specific contributions of PVAT-AMPK to vascular function. By employing more targeted knockout models that selectively exclude AMPKα1 in PVAT while preserving its expression in endothelial cells and VSMCs, future studies could provide a clearer understanding of the distinct role played by PVAT-AMPK in vascular regulation. It is worth mentioning that a previous study had sought to investigate the role of AMPK in lipolysis and fatty acid metabolism within adipose tissue under normal physiological conditions, employing more targeted approaches through the utilisation of newly developed adipose tissue specific AMPKα1 and α2 knockout mouse models (Kim *et al.*, 2016). So, establishing a mouse model with selective deletion of AMPKα1 and α2 in PVAT will help to understand the *in vivo* role of AMPK in mediating the function of PVAT in vascular homeostasis. Furthermore, it is important to acknowledge the possibility of adaptive cellular and molecular changes arising from the absence of AMPKα1, which may influence the observed outcomes. However, this aspect was not explored in the current study.

The reliance on phenylephrine and cromakalim as the sole vasoconstrictor and vasodilator reagents, respectively, could restrict the applicability of the findings. To enhance the robustness of the thesis, future experiments could employ a more diverse array of physiological agents for vascular function experiments. This approach would facilitate a more comprehensive evaluation of whether PVAT from WT and KO animals exhibits consistent effects across various stimuli.

The present work underscores the regulatory function of AMPK in PVAT function via modulating FGF-21 secretion. This regulation might not be limited to PVAT but could also involve other adipose tissue. Therefore, it is worth investigating the role of AMPK in FGF-21 secretion and function in other fat depots. Given the

metabolic function of FGF-21. this could have an important role in some metabolic diseases like obesity and diabetes.

6.3 Conclusion:

The results presented in this thesis have highlighted the crucial involvement of perivascular adipose tissue in vascular function, mediated by the release of diverse bioactive molecules that modulate vascular smooth muscle cells and endothelial function. Additionally, the data presented herein further support the regulatory role of AMPK in PVAT's vascular function by modulating the secretion of adipokines. Although the impact of FGF-21 on endothelial function and vascular tone was not demonstrated in this study, the regulation of its secretion by PVAT via AMPK represents a novel discovery. Given the beneficial effects of AMPK and FGF-21 on metabolic and cardiovascular health, exploring their interaction holds clinical significance, warranting further investigation in future study.

List of References

Aaronson, P. I., Ward, J. P. T. & Connolly, M. J. 2020. *The cardiovascular system at a glance,* Hoboken, NJ, Wiley-Blackwell.

Achari, A. E. & Jain, S. K. 2017. Adiponectin, a Therapeutic Target for Obesity, Diabetes, and Endothelial Dysfunction. *Int J Mol Sci,* 18.

Adams, A. C., Cheng, C. C., Coskun, T. & Kharitonenkov, A. 2012. FGF21 requires ßklotho to act in vivo. *PLoS One,* 7**,** e49977.

Agabiti-Rosei, C., Paini, A., De Ciuceis, C., Withers, S., Greenstein, A., Heagerty, A. M. & Rizzoni, D. 2018. Modulation of vascular reactivity by perivascular adipose tissue (PVAT). *Current Hypertension Reports,* 20**,** 1-11.

Aghamohammadzadeh, R., Greenstein, A. S., Yadav, R., Jeziorska, M., Hama, S., Soltani, F., Pemberton, P. W., Ammori, B., Malik, R. A., Soran, H. & Heagerty, A. M. 2013. Effects of bariatric surgery on human small artery function: evidence for reduction in perivascular adipocyte inflammation, and the restoration of normal anticontractile activity despite persistent obesity. *J Am Coll Cardiol,* 62**,** 128-135.

Ahmed, A., Bibi, A., Valoti, M. & Fusi, F. 2023. Perivascular Adipose Tissue and Vascular Smooth Muscle Tone: Friends or Foes? *Cells,* 12.

Ahwazi, D., Neopane, K., Markby, G. R., Kopietz, F., Ovens, A. J., Dall, M., Hassing, A. S., Gräsle, P., Alshuweishi, Y., Treebak, J. T., Salt, I. P., Göransson, O., Zeqiraj, E., Scott, J. W. & Sakamoto, K. 2021. Investigation of the specificity and mechanism of action of the ULK1/AMPK inhibitor SBI-0206965. *Biochem J,* 478**,** 2977-2997.

Akoumianakis, I., Tarun, A. & Antoniades, C. 2017. Perivascular adipose tissue as a regulator of vascular disease pathogenesis: identifying novel therapeutic targets. *British journal of pharmacology,* 174**,** 3411-3424.

Almabrouk, T. A., Ugusman, A. B., Katwan, O. J., Salt, I. P. & Kennedy, S. 2017. Deletion of AMPKα1 attenuates the anticontractile effect of perivascular adipose tissue (PVAT) and reduces adiponectin release. *British journal of pharmacology,* 174**,** 3398-3410.

Almabrouk, T. A., White, A. D., Ugusman, A. B., Skiba, D. S., Katwan, O. J., Alganga, H., Guzik, T. J., Touyz, R. M., Salt, I. P. & Kennedy, S. 2018. High fat diet attenuates the anticontractile activity of aortic PVAT via a mechanism involving AMPK and reduced adiponectin secretion. *Frontiers in physiology,* 9**,** 51.

Antoine, M., Wirz, W., Tag, C. G., Mavituna, M., Emans, N., Korff, T., Stoldt, V., Gressner, A. M. & Kiefer, P. 2005. Expression pattern of fibroblast growth factors (FGFs), their receptors and antagonists in primary endothelial cells and vascular smooth muscle cells. *Growth Factors,* 23**,** 87-95.

Ayala-Lopez, N., Martini, M., Jackson, W. F., Darios, E., Burnett, R., Seitz, B., Fink, G. D. & Watts, S. W. 2014. Perivascular adipose tissue contains functional catecholamines. *Pharmacol Res Perspect,* 2**,** e00041.

Baker, A. R., Silva, N. F., Quinn, D. W., Harte, A. L., Pagano, D., Bonser, R. S., Kumar, S. & Mcternan, P. G. 2006. Human epicardial adipose tissue expresses a pathogenic profile of adipocytokines in patients with cardiovascular disease. *Cardiovasc Diabetol,* 5**,** 1.

Basatemur, G. L., Jørgensen, H. F., Clarke, M. C., Bennett, M. R. & Mallat, Z. 2019. Vascular smooth muscle cells in atherosclerosis. *Nature reviews cardiology,* 16**,** 727-744.

Berbée, J. F., Boon, M. R., Khedoe, P. P., Bartelt, A., Schlein, C., Worthmann, A., Kooijman, S., Hoeke, G., Mol, I. M., John, C., Jung, C., Vazirpanah, N., Brouwers, L. P., Gordts, P. L., Esko, J. D., Hiemstra, P. S., Havekes, L. M., Scheja, L., Heeren, J. & Rensen, P. C. 2015. Brown fat activation reduces hypercholesterolaemia and protects from atherosclerosis development. *Nat Commun,* 6**,** 6356.

Berg, A. H., Combs, T. P., Du, X., Brownlee, M. & Scherer, P. E. 2001. The adipocyte-secreted protein Acrp30 enhances hepatic insulin action. *Nature medicine,* 7**,** 947-953.

Berryman, D. E. & List, E. O. 2017. Growth hormone's effect on adipose tissue: quality versus quantity. *International journal of molecular sciences,* 18**,** 1621.

Berti, L., Hartwig, S., Irmler, M., Rädle, B., Siegel-Axel, D., Beckers, J., Lehr, S., Al-Hasani, H., Häring, H.-U. & Hrabě De Angelis, M. 2016. Impact of fibroblast growth factor 21 on the secretome of human perivascular preadipocytes and adipocytes: a targeted proteomics approach. *Archives of Physiology and Biochemistry,* 122**,** 281-288.

Bijland, S., Mancini, S. J. & Salt, I. P. 2013. Role of AMP-activated protein kinase in adipose tissue metabolism and inflammation. *Clin Sci (Lond),* 124**,** 491-507.

Boyle, J. G., Logan, P. J., Ewart, M. A., Reihill, J. A., Ritchie, S. A., Connell, J. M., Cleland, S. J. & Salt, I. P. 2008. Rosiglitazone stimulates nitric oxide synthesis in human aortic endothelial cells via AMP-activated protein kinase. *Journal of Biological Chemistry,* 283**,** 11210-11217.

Brown, N. K., Zhou, Z., Zhang, J., Zeng, R., Wu, J., Eitzman, D. T., Chen, Y. E. & Chang, L. 2014. Perivascular adipose tissue in vascular function and disease: a review of current research and animal models. *Arterioscler Thromb Vasc Biol,* 34**,** 1621-30.

Brozovich, F. V., Nicholson, C. J., Degen, C. V., Gao, Y. Z., Aggarwal, M. & Morgan, K. G. 2016. Mechanisms of Vascular Smooth Muscle Contraction and the Basis for Pharmacologic Treatment of Smooth Muscle Disorders. *Pharmacol Rev,* 68**,** 476-532.

Bussey, C. E., Withers, S. B., Aldous, R. G., Edwards, G. & Heagerty, A. M. 2016. Obesity-Related Perivascular Adipose Tissue Damage Is Reversed by Sustained Weight Loss in the Rat. *Arterioscler Thromb Vasc Biol,* 36**,** 1377-85.

Cacanyiova, S., Majzunova, M., Golas, S. & Berenyiova, A. 2019. The role of perivascular adipose tissue and endogenous hydrogen sulfide in vasoactive responses of isolated mesenteric arteries in normotensive and spontaneously hypertensive rats. *J Physiol Pharmacol,* 70.

Calabrese, M. F., Rajamohan, F., Harris, M. S., Caspers, N. L., Magyar, R., Withka, J. M., Wang, H., Borzilleri, K. A., Sahasrabudhe, P. V., Hoth, L. R., Geoghegan, K. F., Han, S., Brown, J., Subashi, T. A., Reyes, A. R., Frisbie, R. K., Ward, J., Miller, R. A., Landro, J. A., Londregan, A. T., Carpino, P. A., Cabral, S., Smith, A. C., Conn, E. L., Cameron, K. O., Qiu, X. & Kurumbail, R. G. 2014. Structural basis for AMPK activation: natural and synthetic ligands regulate kinase activity from opposite poles by different molecular mechanisms. *Structure,* 22**,** 1161-1172.

Carling, D. 2017. AMPK signalling in health and disease. *Curr Opin Cell Biol,* 45**,** 31-37.

Chang, L., Garcia-Barrio, M. T. & Chen, Y. E. 2020. Perivascular adipose tissue regulates vascular function by targeting vascular smooth muscle cells. *Arteriosclerosis, thrombosis, and vascular biology,* 40**,** 1094-1109.

Chang, L., Villacorta, L., Li, R., Hamblin, M., Xu, W., Dou, C., Zhang, J., Wu, J., Zeng, R. & Chen, Y. E. 2012a. Loss of perivascular adipose tissue on peroxisome proliferator–activated receptor-γ deletion in smooth muscle cells impairs intravascular thermoregulation and enhances atherosclerosis. *Circulation,* 126**,** 1067-1078.

Chang, L., Villacota, L., Dou, C., Chen, E. & Zhang, J. 2012b. Perivascular adipose tissue-derived prostaglandins constrict vessel. Am Heart Assoc.

Chatterjee, T. K., Stoll, L. L., Denning, G. M., Harrelson, A., Blomkalns, A. L., Idelman, G., Rothenberg, F. G., Neltner, B., Romig-Martin, S. A. & Dickson, E. W. 2009. Proinflammatory phenotype of perivascular adipocytes: influence of high-fat feeding. *Circulation research,* 104**,** 541-549.

Chau, M. D., Gao, J., Yang, Q., Wu, Z. & Gromada, J. 2010. Fibroblast growth factor 21 regulates energy metabolism by activating the AMPK–SIRT1–PGC-1α pathway. *Proceedings of the National Academy of Sciences,* 107**,** 12553-12558.

Chaudhry, R., Miao, J. H. & Rehman, A. 2023. Physiology, Cardiovascular. *StatPearls*. Treasure Island (FL): StatPearls Publishing

Copyright © 2023, StatPearls Publishing LLC.

Chen, H., Vanhoutte, P. M. & Leung, S. W. S. 2019. Acute activation of endothelial AMPK surprisingly inhibits endothelium-dependent hyperpolarization-like relaxations in rat mesenteric arteries. *Br J Pharmacol,* 176**,** 2905-2921.

Chen, W., Hoo, R. L.-C., Konishi, M., Itoh, N., Lee, P.-C., Ye, H.-Y., Lam, K. S.-L. & Xu, A. 2011. Growth hormone induces hepatic production of fibroblast growth factor 21 through a mechanism dependent on lipolysis in adipocytes. *Journal of Biological Chemistry,* 286**,** 34559-34566.

Chen, W., Shen, Z., Cai, S., Chen, L. & Wang, D. 2021. FGF21 promotes wound healing of rat brain microvascular endothelial cells through facilitating TNF-α-mediated VEGFA and ERK1/2 signaling pathway. *Advances in Clinical and Experimental Medicine,* 30**,** 711-720.

Chen, Y., Xu, X., Zhang, Y., Liu, K., Huang, F., Liu, B. & Kou, J. 2016. Diosgenin regulates adipokine expression in perivascular adipose tissue and ameliorates endothelial dysfunction via regulation of AMPK. *The Journal of Steroid Biochemistry and Molecular Biology,* 155**,** 155-165.

Chen, Z., Peng, I. C., Sun, W., Su, M. I., Hsu, P. H., Fu, Y., Zhu, Y., Defea, K., Pan, S., Tsai, M. D. & Shyy, J. Y. 2009. AMP-activated protein kinase functionally phosphorylates endothelial nitric oxide synthase Ser633. *Circ Res,* 104**,** 496-505.

Chen, Z., Yang, L., Liu, Y., Huang, P., Song, H. & Zheng, P. 2022. The potential function and clinical application of FGF21 in metabolic diseases. *Front Pharmacol,* 13**,** 1089214.

Cheng, K. K., Lam, K. S., Wang, Y., Huang, Y., Carling, D., Wu, D., Wong, C. & Xu, A. 2007. Adiponectin-induced endothelial nitric oxide synthase activation and nitric oxide production are mediated by APPL1 in endothelial cells. *Diabetes,* 56**,** 1387-94.

Cheng, P., Zhang, F., Yu, L., Lin, X., He, L., Li, X., Lu, X., Yan, X., Tan, Y. & Zhang, C. 2016. Physiological and pharmacological roles of FGF21 in cardiovascular diseases. *Journal of Diabetes Research,* 2016.

Cheung, P. C., Salt, I. P., Davies, S. P., Hardie, D. G. & Carling, D. 2000. Characterization of AMP-activated protein kinase γ-subunit isoforms and their role in AMP binding. *Biochemical journal,* 346**,** 659-669.

Chow, W. S., Xu, A., Woo, Y. C., Tso, A. W., Cheung, S. C., Fong, C. H., Tse, H. F., Chau, M. T., Cheung, B. M. & Lam, K. S. 2013. Serum fibroblast growth factor-21 levels are associated with carotid atherosclerosis independent of established cardiovascular risk factors. *Arterioscler Thromb Vasc Biol,* 33**,** 2454-9.

Cinti, S. 2011. Between brown and white: novel aspects of adipocyte differentiation. *Annals of medicine,* 43**,** 104-115.

Coelho, M., Oliveira, T. & Fernandes, R. 2013. Biochemistry of adipose tissue: an endocrine organ. *Arch Med Sci,* 9**,** 191-200.

Colombo, S. L. & Moncada, S. 2009. AMPKalpha1 regulates the antioxidant status of vascular endothelial cells. *Biochem J,* 421**,** 163-9.

Cool, B., Zinker, B., Chiou, W., Kifle, L., Cao, N., Perham, M., Dickinson, R., Adler, A., Gagne, G. & Iyengar, R. 2006. Identification and characterization of a small molecule AMPK activator that treats key components of type 2 diabetes and the metabolic syndrome. *Cell metabolism,* 3**,** 403-416.

Daly, C. J. 2019. Examining Vascular Structure and Function Using Confocal Microscopy and 3D Imaging Techniques. *Adv Exp Med Biol,* 1120**,** 97-106.

Davies, S. P., Helps, N. R., Cohen, P. T. & Hardie, D. G. 1995. 5′-AMP inhibits dephosphorylation, as well as promoting phosphorylation, of the AMP-activated protein kinase. Studies using bacterially expressed human protein phosphatase-2Cα and native bovine protein phosphatase-2AC. *FEBS letters,* 377**,** 421-425.

Davis, B., Rahman, A. & Arner, A. 2012. AMP-activated kinase relaxes agonist induced contractions in the mouse aorta via effects on PKC signaling and inhibits NO-induced relaxation. *Eur J Pharmacol,* 695**,** 88-95.

Davis, B. J., Xie, Z., Viollet, B. & Zou, M.-H. 2006. Activation of the AMP-activated kinase by antidiabetes drug metformin stimulates nitric oxide synthesis in vivo by promoting the association of heat shock protein 90 and endothelial nitric oxide synthase. *Diabetes,* 55**,** 496-505.

Degirolamo, C., Sabbà, C. & Moschetta, A. 2016. Therapeutic potential of the endocrine fibroblast growth factors FGF19, FGF21 and FGF23. *Nature reviews Drug discovery,* 15**,** 51-69.

Ding, X., Boney-Montoya, J., Owen, B. M., Bookout, A. L., Coate, K. C., Mangelsdorf, D. J. & Kliewer, S. A. 2012. βKlotho is required for fibroblast growth factor 21 effects on growth and metabolism. *Cell Metab,* 16**,** 387-93.

Dolinsky, V. W., Chakrabarti, S., Pereira, T. J., Oka, T., Levasseur, J., Beker, D., Zordoky, B. N., Morton, J. S., Nagendran, J. & Lopaschuk, G. D. 2013. Resveratrol prevents hypertension and cardiac hypertrophy in hypertensive rats and mice. *Biochimica et Biophysica Acta (BBA)-Molecular Basis of Disease,* 1832**,** 1723-1733.

Dong, Y., Zhang, M., Wang, S., Liang, B., Zhao, Z., Liu, C., Wu, M., Choi, H. C., Lyons, T. J. & Zou, M. H. 2010. Activation of AMP-activated protein kinase inhibits oxidized LDL-triggered endoplasmic reticulum stress in vivo. *Diabetes,* 59**,** 1386-96.

Dubrovska, G., Verlohren, S., Luft, F. C. & Gollasch, M. 2004. Mechanisms of ADRF release from rat aortic adventitial adipose tissue. *Am J Physiol Heart Circ Physiol,* 286**,** H1107-13.

Eelen, G., De Zeeuw, P., Simons, M. & Carmeliet, P. 2015. Endothelial cell metabolism in normal and diseased vasculature. *Circ Res,* 116**,** 1231-44.

Ellinsworth, D. C., Shukla, N., Fleming, I. & Jeremy, J. Y. 2014. Interactions between thromboxane A2, thromboxane/prostaglandin (TP) receptors, and endothelium-derived hyperpolarization. *Cardiovascular research,* 102**,** 9-16.

Eringa, E. C., Bakker, W. & Van Hinsbergh, V. W. 2012. Paracrine regulation of vascular tone, inflammation and insulin sensitivity by perivascular adipose tissue. *Vascul Pharmacol,* 56**,** 204-9.

Ewart, M.-A., Kohlhaas, C. F. & Salt, I. P. 2008. Inhibition of tumor necrosis factor α–stimulated monocyte adhesion to human aortic endothelial cells by AMP-activated protein kinase. *Arteriosclerosis, Thrombosis, and Vascular Biology,* 28**,** 2255-2257.

Fang, L., Zhao, J., Chen, Y., Ma, T., Xu, G., Tang, C., Liu, X. & Geng, B. 2009. Hydrogen sulfide derived from periadventitial adipose tissue is a vasodilator. *Journal of hypertension,* 27**,** 2174-2185.

Ferland, D. J., Darios, E. S., Neubig, R. R., Sjögren, B., Truong, N., Torres, R., Dexheimer, T. S., Thompson, J. M. & Watts, S. W. 2017. Chemerin-induced arterial contraction is G(i)- and calcium-dependent. *Vascul Pharmacol,* 88**,** 30-41.

Fésüs, G., Dubrovska, G., Gorzelniak, K., Kluge, R., Huang, Y., Luft, F. C. & Gollasch, M. 2007. Adiponectin is a novel humoral vasodilator. *Cardiovascular research,* 75**,** 719-727.

Fisher, F. M. & Maratos-Flier, E. 2016. Understanding the physiology of FGF21. *Annual review of physiology,* 78**,** 223-241.

Fitzgibbons, T. P., Kogan, S., Aouadi, M., Hendricks, G. M., Straubhaar, J. & Czech, M. P. 2011. Similarity of mouse perivascular and brown adipose tissues and their resistance to diet-induced inflammation. *American Journal of Physiology-Heart and Circulatory Physiology,* 301**,** H1425-H1437.

Fon Tacer, K., Bookout, A. L., Ding, X., Kurosu, H., John, G. B., Wang, L., Goetz, R., Mohammadi, M., Kuro-O, M. & Mangelsdorf, D. J. 2010. Research resource: comprehensive expression atlas of the fibroblast growth factor system in adult mouse. *Molecular endocrinology,* 24**,** 2050-2064.

Ford, R. J. & Rush, J. W. 2011. Endothelium-dependent vasorelaxation to the AMPK activator AICAR is enhanced in aorta from hypertensive rats and is NO and EDCF dependent. *American Journal of Physiology-Heart and Circulatory Physiology,* 300**,** H64-H75.

Friederich-Persson, M., Nguyen Dinh Cat, A., Persson, P., Montezano, A. C. & Touyz, R. M. 2017. Brown adipose tissue regulates small artery function through NADPH oxidase 4–derived hydrogen peroxide and redox-sensitive protein kinase G-1α. *Arteriosclerosis, thrombosis, and vascular biology,* 37**,** 455-465.

Fruebis, J., Tsao, T.-S., Javorschi, S., Ebbets-Reed, D., Erickson, M. R. S., Yen, F. T., Bihain, B. E. & Lodish, H. F. 2001. Proteolytic cleavage product of 30-kDa adipocyte complement-related protein increases fatty acid oxidation in muscle and causes weight loss in mice. *Proceedings of the National Academy of Sciences,* 98**,** 2005-2010.

Furchgott, R. F. & Zawadzki, J. V. 1980. The obligatory role of endothelial cells in the relaxation of arterial smooth muscle by acetylcholine. *Nature,* 288**,** 373-6.

Gallo, G., Volpe, M. & Savoia, C. 2021. Endothelial Dysfunction in Hypertension: Current Concepts and Clinical Implications. *Front Med (Lausanne),* 8**,** 798958.

Gálvez-Prieto, B., Bolbrinker, J., Stucchi, P., De Las Heras, A., Merino, B., Arribas, S., Ruiz-Gayo, M., Huber, M., Wehland, M. & Kreutz, R. 2008. Comparative expression analysis of the renin-angiotensin system components between white and brown perivascular adipose tissue. *Journal of Endocrinology,* 197**,** 55-64.

Gálvez-Prieto, B., Somoza, B., Gil-Ortega, M., García-Prieto, C. F., De Las Heras, A. I., González, M. C., Arribas, S., Aranguez, I., Bolbrinker, J. & Kreutz, R. 2012. Anticontractile effect of perivascular adipose tissue and leptin are reduced in hypertension. *Frontiers in pharmacology,* 3**,** 103.

Gálvez, B., De Castro, J., Herold, D., Dubrovska, G., Arribas, S., González, M. C., Aranguez, I., Luft, F. C., Ramos, M. P. & Gollasch, M. 2006. Perivascular adipose tissue and mesenteric vascular function in spontaneously hypertensive rats. *Arteriosclerosis, thrombosis, and vascular biology,* 26**,** 1297-1302.

Gao, Y. J. & Lee, R. M. 2001. Hydrogen peroxide induces a greater contraction in mesenteric arteries of spontaneously hypertensive rats through thromboxane A(2) production. *Br J Pharmacol,* 134**,** 1639-46.

Gao, Y. J. & Lee, R. M. 2005. Hydrogen peroxide is an endothelium-dependent contracting factor in rat renal artery. *Br J Pharmacol,* 146**,** 1061-8.

Gao, Y. J., Lu, C., Su, L. Y., Sharma, A. & Lee, R. 2007. Modulation of vascular function by perivascular adipose tissue: the role of endothelium and hydrogen peroxide. *British journal of pharmacology,* 151**,** 323-331.

Gao, Y. J., Takemori, K., Su, L. Y., An, W. S., Lu, C., Sharma, A. M. & Lee, R. M. 2006. Perivascular adipose tissue promotes vasoconstriction: the role of superoxide anion. *Cardiovasc Res,* 71**,** 363-73.

Gao, Y. J., Zeng, Z. H., Teoh, K., Sharma, A. M., Abouzahr, L., Cybulsky, I., Lamy, A., Semelhago, L. & Lee, R. M. 2005. Perivascular adipose tissue modulates vascular function in the human internal thoracic artery. *J Thorac Cardiovasc Surg,* 130**,** 1130-6.

Ge, X., Chen, C., Hui, X., Wang, Y., Lam, K. S. & Xu, A. 2011. Fibroblast growth factor 21 induces glucose transporter-1 expression through activation of the serum response factor/Ets-like protein-1 in adipocytes. *J Biol Chem,* 286**,** 34533-41.

Gil-Ortega, M., Stucchi, P., Guzman-Ruiz, R., Cano, V., Arribas, S., Gonzalez, M. C., Ruiz-Gayo, M., Fernandez-Alfonso, M. S. & Somoza, B. 2010. Adaptative nitric oxide overproduction in perivascular adipose tissue during early diet-induced obesity. *Endocrinology,* 151**,** 3299-3306.

Giri, S., Rattan, R., Haq, E., Khan, M., Yasmin, R., Won, J. S., Key, L., Singh, A. K. & Singh, I. 2006. AICAR inhibits adipocyte differentiation in 3T3L1 and restores metabolic alterations in diet-induced obesity mice model. *Nutr Metab (Lond),* 3**,** 31.

Goirand, F., Solar, M., Athea, Y., Viollet, B., Mateo, P., Fortin, D., Leclerc, J., Hoerter, J., Ventura-Clapier, R. & Garnier, A. 2007. Activation of AMP kinase alpha1 subunit induces aortic vasorelaxation in mice. *J Physiol,* 581**,** 1163-71.

Gómez-Galeno, J. E., Dang, Q., Nguyen, T. H., Boyer, S. H., Grote, M. P., Sun, Z., Chen, M., Craigo, W. A., Van Poelje, P. D. & Mackenna, D. A. 2010. A potent and selective AMPK activator that inhibits de novo lipogenesis. *ACS medicinal chemistry letters,* 1**,** 478-482.

Grahame Hardie, D. 2016. Regulation of AMP-activated protein kinase by natural and synthetic activators. *Acta Pharm Sin B,* 6**,** 1-19.

Greenstein, A. S., Khavandi, K., Withers, S. B., Sonoyama, K., Clancy, O., Jeziorska, M., Laing, I., Yates, A. P., Pemberton, P. W., Malik, R. A. & Heagerty, A. M. 2009. Local inflammation and hypoxia abolish the protective anticontractile properties of perivascular fat in obese patients. *Circulation,* 119**,** 1661-70.

Grigoras, A., Amalinei, C., Balan, R. A., Giusca, S. E. & Caruntu, I. D. 2019. Perivascular adipose tissue in cardiovascular diseases-an update. *Anatolian Journal of Cardiology,* 22**,** 219.

Guo, D., Xiao, L., Hu, H., Liu, M., Yang, L. & Lin, X. 2018. FGF21 protects human umbilical vein endothelial cells against high glucose-induced apoptosis via PI3K/Akt/Fox3a signaling pathway. *Journal of Diabetes and its Complications,* 32**,** 729-736.

Guo, X., Wang, X., Yuan, Q., Wu, C., Gao, H., Xu, P., Liu, M., Wang, N., Li, D. & Ren, G. 2019. Evaluation of a cell model expressing ßKlotho for screening FGF21 analogues. *Cytotechnology,* 71**,** 1033-1041.

Hardie, D. G. 2011. AMP-activated protein kinase: an energy sensor that regulates all aspects of cell function. *Genes & development,* 25**,** 1895-1908.

Hardie, D. G. 2018. Keeping the home fires burning: AMP-activated protein kinase. *J R Soc Interface,* 15.

Hattori, Y., Suzuki, K., Hattori, S. & Kasai, K. 2006. Metformin inhibits cytokine-induced nuclear factor kappaB activation via AMP-activated protein kinase activation in vascular endothelial cells. *Hypertension,* 47**,** 1183-1188.

Hawley, S. A., Pan, D. A., Mustard, K. J., Ross, L., Bain, J., Edelman, A. M., Frenguelli, B. G. & Hardie, D. G. 2005. Calmodulin-dependent protein kinase kinase-beta is an alternative upstream kinase for AMP-activated protein kinase. *Cell Metab,* 2**,** 9-19.

Hayabuchi, Y., Nakaya, Y., Matsuoka, S. & Kuroda, Y. 1998. Hydrogen peroxide-induced vascular relaxation in porcine coronary arteries is mediated by Ca2+-activated K+ channels. *Heart Vessels,* 13**,** 9-17.

Herzig, S. & Shaw, R. J. 2018. AMPK: guardian of metabolism and mitochondrial homeostasis. *Nature reviews Molecular cell biology,* 19**,** 121-135.

Hillock-Watling, C. & Gotlieb, A. I. 2022. The pathobiology of perivascular adipose tissue (PVAT), the fourth layer of the blood vessel wall. *Cardiovasc Pathol,* 61**,** 107459.

Holland, W. L., Adams, A. C., Brozinick, J. T., Bui, H. H., Miyauchi, Y., Kusminski, C. M., Bauer, S. M., Wade, M., Singhal, E. & Cheng, C. C. 2013. An FGF21-adiponectin-ceramide axis controls energy expenditure and insulin action in mice. *Cell metabolism,* 17**,** 790-797.

Horman, S., Morel, N., Vertommen, D., Hussain, N., Neumann, D., Beauloye, C., El Najjar, N., Forcet, C., Viollet, B., Walsh, M. P., Hue, L. & Rider, M. H. 2008. AMP-activated protein kinase phosphorylates and desensitizes smooth muscle myosin light chain kinase. *J Biol Chem,* 283**,** 18505-12.

Houben, A. J., Eringa, E. C., Jonk, A. M., Serne, E. H., Smulders, Y. M. & Stehouwer, C. D. 2012. Perivascular Fat and the Microcirculation: Relevance to Insulin Resistance, Diabetes, and Cardiovascular Disease. *Curr Cardiovasc Risk Rep,* 6**,** 80-90.

Huang, W., Shao, M., Liu, H., Chen, J., Hu, J., Zhu, L., Liu, F., Wang, D., Zou, Y. & Xiong, Y. 2019. Fibroblast growth factor 21 enhances angiogenesis

and wound healing of human brain microvascular endothelial cells by activating PPARγ. *Journal of Pharmacological Sciences,* 140**,** 120-127.

Huang, W. P., Chen, C. Y., Lin, T. W., Kuo, C. S., Huang, H. L., Huang, P. H. & Lin, S. J. 2022. Fibroblast growth factor 21 reverses high-fat diet-induced impairment of vascular function via the anti-oxidative pathway in ApoE knockout mice. *Journal of Cellular and Molecular Medicine,* 26**,** 2451-2461.

Hui, Q., Jin, Z., Li, X., Liu, C. & Wang, X. 2018. FGF Family: From Drug Development to Clinical Application. *Int J Mol Sci,* 19.

Hui, X., Feng, T., Liu, Q., Gao, Y. & Xu, A. 2016. The FGF21-adiponectin axis in controlling energy and vascular homeostasis. *J Mol Cell Biol,* 8**,** 110-9.

Iacobellis, G., Pistilli, D., Gucciardo, M., Leonetti, F., Miraldi, F., Brancaccio, G., Gallo, P. & Di Gioia, C. R. 2005. Adiponectin expression in human epicardial adipose tissue in vivo is lower in patients with coronary artery disease. *Cytokine,* 29**,** 251-5.

Ibrahim, M. M. 2010. Subcutaneous and visceral adipose tissue: structural and functional differences. *Obesity reviews,* 11**,** 11-18.

Ito, S., Kinoshita, S., Shiraishi, N., Nakagawa, S., Sekine, S., Fujimori, T. & Nabeshima, Y.-I. 2000. Molecular cloning and expression analyses of mouse βklotho, which encodes a novel Klotho family protein. *Mechanisms of development,* 98**,** 115-119.

Jansen, T., Kvandová, M., Daiber, A., Stamm, P., Frenis, K., Schulz, E., Münzel, T. & Kröller-Schön, S. 2020. The AMP-Activated Protein Kinase Plays a Role in Antioxidant Defense and Regulation of Vascular Inflammation. *Antioxidants (Basel),* 9.

Jiang, R. S., Zhang, L., Yang, H., Zhou, M. Y., Deng, C. Y. & Wu, W. 2021. Signalling pathway of U46619-induced vascular smooth muscle contraction in mouse coronary artery. *Clin Exp Pharmacol Physiol,* 48**,** 996-1006.

Jin, L., Lin, Z. & Xu, A. 2016. Fibroblast Growth Factor 21 Protects against Atherosclerosis via Fine-Tuning the Multiorgan Crosstalk. *Diabetes Metab J,* 40**,** 22-31.

Joki, Y., Ohashi, K., Yuasa, D., Shibata, R., Ito, M., Matsuo, K., Kambara, T., Uemura, Y., Hayakawa, S. & Hiramatsu-Ito, M. 2015. FGF21 attenuates pathological myocardial remodeling following myocardial infarction through the adiponectin-dependent mechanism. *Biochemical and biophysical research communications,* 459**,** 124-130.

Juszczak, F., Caron, N., Mathew, A. V. & Declèves, A. E. 2020. Critical Role for AMPK in Metabolic Disease-Induced Chronic Kidney Disease. *Int J Mol Sci,* 21.

Katerelos, M., Mudge, S. J., Stapleton, D., Auwardt, R. B., Fraser, S. A., Chen, C. G., Kemp, B. E. & Power, D. A. 2010. 5-aminoimidazole-4-carboxamide ribonucleoside and AMP-activated protein kinase inhibit signalling through NF-κB. *Immunology and cell biology,* 88**,** 754-760.

Khaddaj Mallat, R., Mathew John, C., Kendrick, D. J. & Braun, A. P. 2017. The vascular endothelium: A regulator of arterial tone and interface for the immune system. *Critical reviews in clinical laboratory sciences,* 54**,** 458-470.

Kharitonenkov, A., Shiyanova, T. L., Koester, A., Ford, A. M., Micanovic, R., Galbreath, E. J., Sandusky, G. E., Hammond, L. J., Moyers, J. S. & Owens, R. A. 2005. FGF-21 as a novel metabolic regulator. *The Journal of clinical investigation,* 115**,** 1627-1635.

Khedoe, P. P., Hoeke, G., Kooijman, S., Dijk, W., Buijs, J. T., Kersten, S., Havekes, L. M., Hiemstra, P. S., Berbée, J. F., Boon, M. R. & Rensen, P. C. 2015. Brown adipose tissue takes up plasma triglycerides mostly after lipolysis. *J Lipid Res,* 56**,** 51-9.

Kilkenny, D. M. & Rocheleau, J. V. 2016. The FGF21 Receptor Signaling Complex: Klothoß, FGFR1c, and Other Regulatory Interactions. *Vitam Horm,* 101**,** 17-58.

Kim, H. W., Belin De Chantemèle, E. J. & Weintraub, N. L. 2019. Perivascular Adipocytes in Vascular Disease. *Arterioscler Thromb Vasc Biol,* 39**,** 2220-2227.

Kim, H. W., Shi, H., Winkler, M. A., Lee, R. & Weintraub, N. L. 2020. Perivascular adipose tissue and vascular perturbation/atherosclerosis. *Arteriosclerosis, thrombosis, and vascular biology,* 40**,** 2569-2576.

Kim, J. E., Song, S. E., Kim, Y. W., Kim, J. Y., Park, S. C., Park, Y. K., Baek, S. H., Lee, I. K. & Park, S. Y. 2010. Adiponectin inhibits palmitate-induced apoptosis through suppression of reactive oxygen species in endothelial cells: involvement of cAMP/protein kinase A and AMP-activated protein kinase. *J Endocrinol,* 207**,** 35-44.

Kim, S. J., Tang, T., Abbott, M., Viscarra, J. A., Wang, Y. & Sul, H. S. 2016. AMPK Phosphorylates Desnutrin/ATGL and Hormone-Sensitive Lipase To Regulate Lipolysis and Fatty Acid Oxidation within Adipose Tissue. *Mol Cell Biol,* 36**,** 1961-76.

Kleiner, S., Douris, N., Fox, E. C., Mepani, R. J., Verdeguer, F., Wu, J., Kharitonenkov, A., Flier, J. S., Maratos-Flier, E. & Spiegelman, B. M. 2012. FGF21 regulates PGC-1α and browning of white adipose tissues in adaptive thermogenesis. *Genes & development,* 26**,** 271-281.

Koenen, M., Hill, M. A., Cohen, P. & Sowers, J. R. 2021. Obesity, Adipose Tissue and Vascular Dysfunction. *Circ Res,* 128**,** 951-968.

Kong, X., Qu, X., Li, B., Wang, Z., Chao, Y., Jiang, X., Wu, W. & Chen, S. L. 2017. Modulation of low shear stress-induced eNOS multi-site phosphorylation and nitric oxide production via protein kinase and ERK1/2 signaling. *Mol Med Rep,* 15**,** 908-914.

Kopietz, F., Alshuweishi, Y., Bijland, S., Alghamdi, F., Degerman, E., Sakamoto, K., Salt, I. P. & Göransson, O. 2021. A-769662 inhibits adipocyte glucose uptake in an AMPK-independent manner. *Biochem J,* 478**,** 633-646.

Kopietz, F., Rupar, K., Berggreen, C., Säll, J., Vertommen, D., Degerman, E., Rider, M. H. & Göransson, O. 2020. Inhibition of AMPK activity in response to insulin in adipocytes: involvement of AMPK pS485, PDEs, and cellular energy levels. *Am J Physiol Endocrinol Metab,* 319**,** E459-e471.

Krawutschke, C., Koesling, D. & Russwurm, M. 2015. Cyclic GMP in Vascular Relaxation: Export Is of Similar Importance as Degradation. *Arterioscler Thromb Vasc Biol,* 35**,** 2011-9.

Kumar, R. K., Darios, E. S., Burnett, R., Thompson, J. M. & Watts, S. W. 2019. Fenfluramine-induced PVAT-dependent contraction depends on norepinephrine and not serotonin. *Pharmacol Res,* 140**,** 43-49.

Kurosu, H., Choi, M., Ogawa, Y., Dickson, A. S., Goetz, R., Eliseenkova, A. V., Mohammadi, M., Rosenblatt, K. P., Kliewer, S. A. & Kuro-O, M. 2007. Tissue-specific expression of ßKlotho and fibroblast growth factor (FGF) receptor isoforms determines metabolic activity of FGF19 and FGF21. *Journal of Biological Chemistry,* 282**,** 26687-26695.

Kwaifa, I. K., Bahari, H., Yong, Y. K. & Noor, S. M. 2020. Endothelial Dysfunction in Obesity-Induced Inflammation: Molecular Mechanisms and Clinical Implications. *Biomolecules,* 10.

Lastra, G. & Manrique, C. 2015. Perivascular adipose tissue, inflammation and insulin resistance: link to vascular dysfunction and cardiovascular disease. *Horm Mol Biol Clin Investig,* 22**,** 19-26.

Lee, H.-Y., Després, J.-P. & Koh, K. K. 2013. Perivascular adipose tissue in the pathogenesis of cardiovascular disease. *Atherosclerosis,* 230**,** 177-184.

Lee, K. Y. & Choi, H. C. 2013. Acetylcholine-induced AMP-activated protein kinase activation attenuates vasoconstriction through an LKB1-dependent mechanism in rat aorta. *Vascul Pharmacol,* 59**,** 96-102.

Lee, R. M., Lu, C., Su, L.-Y. & Gao, Y.-J. 2009. Endothelium-dependent relaxation factor released by perivascular adipose tissue. *Journal of hypertension,* 27**,** 782-790.

Lee, Y., Lim, S., Hong, E. S., Kim, J. H., Moon, M. K., Chun, E. J., Choi, S. I., Kim, Y. B., Park, Y. J., Park, K. S., Jang, H. C. & Choi, S. H. 2014. Serum FGF 21 concentration is associated with hypertriglyceridaemia, hyperinsulinaemia and pericardial fat accumulation, independently of obesity, but not with current coronary artery status. *Clinical endocrinology,* 80**,** 57-64.

Lee, Y. C., Chang, H. H., Chiang, C. L., Liu, C. H., Yeh, J. I., Chen, M. F., Chen, P. Y., Kuo, J. S. & Lee, T. J. 2011. Role of perivascular adipose tissue-derived methyl palmitate in vascular tone regulation and pathogenesis of hypertension. *Circulation,* 124**,** 1160-71.

Li, H.-F., Liu, H.-T., Chen, P.-Y., Lin, H. & Tseng, T.-L. 2022. Role of PVAT in obesity-related cardiovascular disease through the buffering activity of ATF3. *Iscience,* 25**,** 105631.

Li, S., Zhu, Z., Xue, M., Yi, X., Liang, J., Niu, C., Chen, G., Shen, Y., Zhang, H. & Zheng, J. 2019a. Fibroblast growth factor 21 protects the heart from angiotensin II-induced cardiac hypertrophy and dysfunction via SIRT1. *Biochimica et Biophysica Acta (BBA)-Molecular Basis of Disease,* 1865**,** 1241-1252.

Li, W., Jin, D., Takai, S., Hayakawa, T., Ogata, J., Yamanishi, K., Yamanishi, H. & Okamura, H. 2019b. Impaired function of aorta and perivascular adipose tissue in IL-18-deficient mice. *American Journal of Physiology-Heart and Circulatory Physiology,* 317**,** H1142-H1156.

Li, Y., Huang, J., Jiang, Z., Jiao, Y. & Wang, H. 2017. FGF21 inhibitor suppresses the proliferation and migration of human umbilical vein endothelial cells through the eNOS/PI3K/AKT pathway. *American Journal of Translational Research,* 9**,** 5299.

Lian, X. & Gollasch, M. 2016. A clinical perspective: contribution of dysfunctional perivascular adipose tissue (PVAT) to cardiovascular risk. *Current hypertension reports,* 18**,** 1-9.

Liang, B., Wang, S., Wang, Q., Zhang, W., Viollet, B., Zhu, Y. & Zou, M.-H. 2013. Aberrant endoplasmic reticulum stress in vascular smooth muscle increases vascular contractility and blood pressure in mice deficient of AMP-activated protein kinase-α2 in vivo. *Arteriosclerosis, thrombosis, and vascular biology,* 33**,** 595-604.

Liang, X. X., Wang, R. Y., Guo, Y. Z., Cheng, Z., Lv, D. Y., Luo, M. H., He, A., Luo, S. X. & Xia, Y. 2021. Phosphorylation of Akt at Thr308 regulates p-eNOS Ser1177 during physiological conditions. *FEBS Open Bio,* 11**,** 1953-1964.

Lidell, M. E., Betz, M. J., Leinhard, O. D., Heglind, M., Elander, L., Slawik, M., Mussack, T., Nilsson, D., Romu, T. & Nuutila, P. 2013. Evidence for two types of brown adipose tissue in humans. *Nature medicine,* 19**,** 631-634.

Lihn, A. S., Jessen, N., Pedersen, S. B., Lund, S. & Richelsen, B. 2004. AICAR stimulates adiponectin and inhibits cytokines in adipose tissue. *Biochem Biophys Res Commun,* 316**,** 853-8.

Lin, Z., Pan, X., Wu, F., Ye, D., Zhang, Y., Wang, Y., Jin, L., Lian, Q., Huang, Y. & Ding, H. 2015. Fibroblast growth factor 21 prevents atherosclerosis by suppression of hepatic sterol regulatory element-binding protein-2 and induction of adiponectin in mice. *Circulation,* 131**,** 1861-1871.

Lin, Z., Tian, H., Lam, K. S., Lin, S., Hoo, R. C., Konishi, M., Itoh, N., Wang, Y., Bornstein, S. R. & Xu, A. 2013. Adiponectin mediates the metabolic effects of FGF21 on glucose homeostasis and insulin sensitivity in mice. *Cell metabolism,* 17**,** 779-789.

Liu, J., Cai, G., Li, M., Fan, S., Yao, B., Ping, W., Huang, Z., Cai, H., Dai, Y. & Wang, L. 2018. Fibroblast growth factor 21 attenuates hypoxia-induced pulmonary hypertension by upregulating PPARγ expression and suppressing inflammatory cytokine levels. *Biochemical and biophysical research communications,* 504**,** 478-484.

Liu, X.-Y., Qian, L.-L. & Wang, R.-X. 2022. Hydrogen sulfide-induced vasodilation: the involvement of vascular potassium channels. *Frontiers in Pharmacology,* 13**,** 911704.

Löhn, M., Dubrovska, G., Lauterbach, B., Luft, F. C., Gollasch, M. & Sharma, A. M. 2002. Periadventitial fat releases a vascular relaxing factor. *The FASEB Journal,* 16**,** 1057-1063.

Luscher, T. F. & Vanhoutte, P. M. 2020. *The endothelium: modulator of cardiovascular function*, CRC press.

Lynch, F. M., Withers, S. B., Yao, Z., Werner, M. E., Edwards, G., Weston, A. H. & Heagerty, A. M. 2013. Perivascular adipose tissue-derived adiponectin activates BK(Ca) channels to induce anticontractile responses. *Am J Physiol Heart Circ Physiol,* 304**,** H786-95.

Ma, Y., Li, L., Shao, Y., Bai, X., Bai, T. & Huang, X. 2017. Methotrexate improves perivascular adipose tissue/endothelial dysfunction via activation of AMPK/eNOS pathway. *Mol Med Rep,* 15**,** 2353-2359.

Man, A. W., Zhou, Y., Xia, N. & Li, H. 2022. Endothelial Nitric Oxide Synthase in the Perivascular Adipose Tissue. *Biomedicines,* 10**,** 1754.

Man, A. W. C., Zhou, Y., Xia, N. & Li, H. 2020. Perivascular Adipose Tissue as a Target for Antioxidant Therapy for Cardiovascular Complications. *Antioxidants (Basel),* 9.

Mancini, S. J., Boyd, D., Katwan, O. J., Strembitska, A., Almabrouk, T. A., Kennedy, S., Palmer, T. M. & Salt, I. P. 2018. Canagliflozin inhibits interleukin-1β-stimulated cytokine and chemokine secretion in vascular endothelial cells by AMP-activated protein kinase-dependent and-independent mechanisms. *Scientific reports,* 8**,** 5276.

Mancini, S. J., White, A. D., Bijland, S., Rutherford, C., Graham, D., Richter, E. A., Viollet, B., Touyz, R. M., Palmer, T. M. & Salt, I. P. 2017. Activation of AMP-activated protein kinase rapidly suppresses multiple pro-inflammatory pathways in adipocytes including IL-1 receptor-associated kinase-4 phosphorylation. *Mol Cell Endocrinol,* 440**,** 44-56.

Meijer, R. I., Bakker, W., Alta, C.-L. A., Sipkema, P., Yudkin, J. S., Viollet, B., Richter, E. A., Smulders, Y. M., Van Hinsbergh, V. W. & Serné, E. H. 2013.

Perivascular adipose tissue control of insulin-induced vasoreactivity in muscle is impaired in db/db mice. *Diabetes,* 62**,** 590-598.

Mendizábal, Y., Llorens, S. & Nava, E. 2013. Vasoactive effects of prostaglandins from the perivascular fat of mesenteric resistance arteries in WKY and SHROB rats. *Life sciences,* 93**,** 1023-1032.

Meyer, M. R., Fredette, N. C., Barton, M. & Prossnitz, E. R. 2013. Regulation of vascular smooth muscle tone by adipose-derived contracting factor. *PLoS One,* 8**,** e79245.

Mohammadi, M., Olsen, S. K. & Ibrahimi, O. A. 2005. Structural basis for fibroblast growth factor receptor activation. *Cytokine Growth Factor Rev,* 16**,** 107-37.

Morrow, V. A., Foufelle, F., Connell, J. M., Petrie, J. R., Gould, G. W. & Salt, I. P. 2003. Direct activation of AMP-activated protein kinase stimulates nitric-oxide synthesis in human aortic endothelial cells. *Journal of Biological Chemistry,* 278**,** 31629-31639.

Mount, P. F., Hill, R. E., Fraser, S. A., Levidiotis, V., Katsis, F., Kemp, B. E. & Power, D. A. 2005. Acute renal ischemia rapidly activates the energy sensor AMPK but does not increase phosphorylation of eNOS-Ser1177. *Am J Physiol Renal Physiol,* 289**,** F1103-15.

Murakami, H., Murakami, R., Kambe, F., Cao, X., Takahashi, R., Asai, T., Hirai, T., Numaguchi, Y., Okumura, K. & Seo, H. 2006. Fenofibrate activates AMPK and increases eNOS phosphorylation in HUVEC. *Biochemical and biophysical research communications,* 341**,** 973-978.

Nagata, D., Mogi, M. & Walsh, K. 2003. AMP-activated protein kinase (AMPK) signaling in endothelial cells is essential for angiogenesis in response to hypoxic stress. *J Biol Chem,* 278**,** 31000-6.

Nishimura, T., Nakatake, Y., Konishi, M. & Itoh, N. 2000. Identification of a novel FGF, FGF-21, preferentially expressed in the liver. *Biochimica et Biophysica Acta (BBA)-Gene Structure and Expression,* 1492**,** 203-206.

Nosalski, R. & Guzik, T. J. 2017. Perivascular adipose tissue inflammation in vascular disease. *British journal of pharmacology,* 174**,** 3496-3513.

Ogawa, Y., Kurosu, H., Yamamoto, M., Nandi, A., Rosenblatt, K. P., Goetz, R., Eliseenkova, A. V., Mohammadi, M. & Kuro-O, M. 2007. βKlotho is required for metabolic activity of fibroblast growth factor 21. *Proceedings of the National Academy of Sciences,* 104**,** 7432-7437.

Ouchi, N., Kobayashi, H., Kihara, S., Kumada, M., Sato, K., Inoue, T., Funahashi, T. & Walsh, K. 2004. Adiponectin stimulates angiogenesis by promoting cross-talk between AMP-activated protein kinase and Akt signaling in endothelial cells. *Journal of Biological Chemistry,* 279**,** 1304-1309.

Owen, M. K., Witzmann, F. A., Mckenney, M. L., Lai, X., Berwick, Z. C., Moberly, S. P., Alloosh, M., Sturek, M. & Tune, J. D. 2013. Perivascular adipose tissue potentiates contraction of coronary vascular smooth muscle: influence of obesity. *Circulation,* 128**,** 9-18.

Padilla, J., Jenkins, N. T., Vieira-Potter, V. J. & Laughlin, M. H. 2013. Divergent phenotype of rat thoracic and abdominal perivascular adipose tissues. *American Journal of Physiology-Regulatory, Integrative and Comparative Physiology,* 304**,** R543-R552.

Palmer, T. M. & Salt, I. P. 2021. Nutrient regulation of inflammatory signalling in obesity and vascular disease. *Clin Sci (Lond),* 135**,** 1563-1590.

Pan, X., Shao, Y., Wu, F., Wang, Y., Xiong, R., Zheng, J., Tian, H., Wang, B., Wang, Y. & Zhang, Y. 2018. FGF21 prevents angiotensin II-induced

hypertension and vascular dysfunction by activation of ACE2/angiotensin-(1–7) axis in mice. *Cell metabolism,* 27**,** 1323-1337. e5.

Park, S. Y., Kim, K. H., Seo, K. W., Bae, J. U., Kim, Y. H., Lee, S. J., Lee, W. S. & Kim, C. D. 2014. Resistin derived from diabetic perivascular adipose tissue up-regulates vascular expression of osteopontin via the AP-1 signalling pathway. *The Journal of Pathology,* 232**,** 87-97.

Patel, V., Adya, R., Chen, J., Ramanjaneya, M., Bari, M. F., Bhudia, S. K., Hillhouse, E. W., Tan, B. K. & Randeva, H. S. 2014. Novel insights into the cardio-protective effects of FGF21 in lean and obese rat hearts. *PLoS One,* 9**,** e87102.

Payne, G. A., Borbouse, L. N., Kumar, S., Neeb, Z., Alloosh, M., Sturek, M. & Tune, J. D. 2010. Epicardial perivascular adipose-derived leptin exacerbates coronary endothelial dysfunction in metabolic syndrome via a protein kinase C-β pathway. *Arteriosclerosis, thrombosis, and vascular biology,* 30**,** 1711-1717.

Pilkington, A. C., Paz, H. A. & Wankhade, U. D. 2021. Beige Adipose Tissue Identification and Marker Specificity-Overview. *Front Endocrinol (Lausanne),* 12**,** 599134.

Police, S. B., Thatcher, S. E., Charnigo, R., Daugherty, A. & Cassis, L. A. 2009. Obesity promotes inflammation in periaortic adipose tissue and angiotensin II-induced abdominal aortic aneurysm formation. *Arteriosclerosis, thrombosis, and vascular biology,* 29**,** 1458-1464.

Potthoff, M. J., Kliewer, S. A. & Mangelsdorf, D. J. 2012. Endocrine fibroblast growth factors 15/19 and 21: from feast to famine. *Genes Dev,* 26**,** 312-24.

Poznyak, A. V., Grechko, A. V., Orekhova, V. A., Chegodaev, Y. S., Wu, W.-K. & Orekhov, A. N. 2020. Oxidative stress and antioxidants in atherosclerosis development and treatment. *Biology,* 9**,** 60.

Pyla, R., Hartney, T. J. & Segar, L. 2022. AICAR promotes endothelium-independent vasorelaxation by activating AMP-activated protein kinase via increased ZMP and decreased ATP/ADP ratio in aortic smooth muscle. *Journal of Basic and Clinical Physiology and Pharmacology,* 33**,** 759-768.

Qi, X.-Y., Qu, S.-L., Xiong, W.-H., Rom, O., Chang, L. & Jiang, Z.-S. 2018. Perivascular adipose tissue (PVAT) in atherosclerosis: a double-edged sword. *Cardiovascular diabetology,* 17**,** 1-20.

Quehenberger, P., Exner, M., Sunder-Plassmann, R., Ruzicka, K., Bieglmayer, C., Endler, G., Muellner, C., Speiser, W. & Wagner, O. 2002. Leptin induces endothelin-1 in endothelial cells in vitro. *Circ Res,* 90**,** 711-8.

Rajendran, P., Rengarajan, T., Thangavel, J., Nishigaki, Y., Sakthisekaran, D., Sethi, G. & Nishigaki, I. 2013. The vascular endothelium and human diseases. *International journal of biological sciences,* 9**,** 1057.

Reihill, J. A., Ewart, M. A., Hardie, D. G. & Salt, I. P. 2007. AMP-activated protein kinase mediates VEGF-stimulated endothelial NO production. *Biochemical and biophysical research communications,* 354**,** 1084-8.

Reynés, B., Van Schothorst, E. M., Keijer, J., Ceresi, E., Oliver, P. & Palou, A. 2019. Cold induced depot-specific browning in ferret aortic perivascular adipose tissue. *Frontiers in Physiology,* 10**,** 1171.

Richard, A. J., White, U., Elks, C. M. & Stephens, J. M. 2020. Adipose tissue: physiology to metabolic dysfunction. *Endotext [Internet].*

Ritchie, S. A., Kohlhaas, C. F., Boyd, A. R., Yalla, K. C., Walsh, K., Connell, J. M. & Salt, I. P. 2010. Insulin-stimulated phosphorylation of endothelial

nitric oxide synthase at serine-615 contributes to nitric oxide synthesis. *Biochem J,* 426**,** 85-90.

Rittig, K., Dolderer, J. H., Balletshofer, B., Machann, J., Schick, F., Meile, T., Küper, M., Stock, U. A., Staiger, H., Machicao, F., Schaller, H. E., Königsrainer, A., Häring, H. U. & Siegel-Axel, D. I. 2012. The secretion pattern of perivascular fat cells is different from that of subcutaneous and visceral fat cells. *Diabetologia,* 55**,** 1514-25.

Rodríguez, C., Contreras, C., Sáenz-Medina, J., Muñoz, M., Corbacho, C., Carballido, J., García-Sacristán, A., Hernandez, M., López, M., Rivera, L. & Prieto, D. 2020. Activation of the AMP-related kinase (AMPK) induces renal vasodilatation and downregulates Nox-derived reactive oxygen species (ROS) generation. *Redox Biol,* 34**,** 101575.

Rodríguez, C., Muñoz, M., Contreras, C. & Prieto, D. 2021. AMPK, metabolism, and vascular function. *Febs j,* 288**,** 3746-3771.

Ross, F. A., Jensen, T. E. & Hardie, D. G. 2016. Differential regulation by AMP and ADP of AMPK complexes containing different γ subunit isoforms. *Biochem J,* 473**,** 189-99.

Rossoni, L. V., Wareing, M., Wenceslau, C. F., Al-Abri, M., Cobb, C. & Austin, C. 2011. Acute simvastatin increases endothelial nitric oxide synthase phosphorylation via AMP-activated protein kinase and reduces contractility of isolated rat mesenteric resistance arteries. *Clin Sci (Lond),* 121**,** 449-58.

Salminen, A., Kauppinen, A. & Kaarniranta, K. 2017. FGF21 activates AMPK signaling: impact on metabolic regulation and the aging process. *Journal of molecular medicine,* 95**,** 123-131.

Salt, I. P. & Hardie, D. G. 2017. AMP-activated protein kinase: an ubiquitous signaling pathway with key roles in the cardiovascular system. *Circ Res,* 120**,** 1825-1841.

Salt, I. P., Morrow, V. A., Brandie, F. M., Connell, J. M. & Petrie, J. R. 2003. High glucose inhibits insulin-stimulated nitric oxide production without reducing endothelial nitric-oxide synthase Ser1177 phosphorylation in human aortic endothelial cells. *J Biol Chem,* 278**,** 18791-7.

Sandoo, A., Van Zanten, J. J., Metsios, G. S., Carroll, D. & Kitas, G. D. 2010. The endothelium and its role in regulating vascular tone. *Open Cardiovasc Med J,* 4**,** 302-12.

Saxton, S. N., Clark, B. J., Withers, S. B., Eringa, E. C. & Heagerty, A. M. 2019. Mechanistic Links Between Obesity, Diabetes, and Blood Pressure: Role of Perivascular Adipose Tissue. *Physiol Rev,* 99**,** 1701-1763.

Schlein, C., Talukdar, S., Heine, M., Fischer, A. W., Krott, L. M., Nilsson, S. K., Brenner, M. B., Heeren, J. & Scheja, L. 2016. FGF21 lowers plasma triglycerides by accelerating lipoprotein catabolism in white and brown adipose tissues. *Cell metabolism,* 23**,** 441-453.

Schneider, H., Schubert, K. M., Blodow, S., Kreutz, C.-P., Erdogmus, S., Wiedenmann, M., Qiu, J., Fey, T., Ruth, P. & Lubomirov, L. T. 2015. AMPK dilates resistance arteries via activation of SERCA and BKCa channels in smooth muscle. *Hypertension,* 66**,** 108-116.

Semba, R. D., Crasto, C., Strait, J., Sun, K., Schaumberg, D. A. & Ferrucci, L. 2013. Elevated serum fibroblast growth factor 21 is associated with hypertension in community-dwelling adults. *Journal of human hypertension,* 27**,** 397-399.

Sena, C. M., Pereira, A., Fernandes, R., Letra, L. & Seiça, R. M. 2017. Adiponectin improves endothelial function in mesenteric arteries of rats

fed a high-fat diet: role of perivascular adipose tissue. *British journal of pharmacology,* 174**,** 3514-3526.

Shaw, R. J., Kosmatka, M., Bardeesy, N., Hurley, R. L., Witters, L. A., Depinho, R. A. & Cantley, L. C. 2004. The tumor suppressor LKB1 kinase directly activates AMP-activated kinase and regulates apoptosis in response to energy stress. *Proceedings of the National Academy of Sciences,* 101**,** 3329-3335.

Shimokawa, H. & Godo, S. 2020. Nitric oxide and endothelium-dependent hyperpolarization mediated by hydrogen peroxide in health and disease. *Basic & Clinical Pharmacology & Toxicology,* 127**,** 92-101.

Siegel-Axel, D. I., Ullrich, S., Stefan, N., Rittig, K., Gerst, F., Klingler, C., Schmidt, U., Schreiner, B., Randrianarisoa, E., Schaller, H. E., Stock, U. A., Weigert, C., Königsrainer, A. & Häring, H. U. 2014. Fetuin-A influences vascular cell growth and production of proinflammatory and angiogenic proteins by human perivascular fat cells. *Diabetologia,* 57**,** 1057-66.

Soltis, E. E. & Cassis, L. A. 1991. Influence of perivascular adipose tissue on rat aortic smooth muscle responsiveness. *Clinical and Experimental Hypertension. Part A: Theory and Practice,* 13**,** 277-296.

Sowka, A. & Dobrzyn, P. 2021. Role of perivascular adipose tissue-derived adiponectin in vascular homeostasis. *Cells,* 10**,** 1485.

Stahmann, N., Woods, A., Carling, D. & Heller, R. 2006. Thrombin activates AMP-activated protein kinase in endothelial cells via a pathway involving Ca2+/calmodulin-dependent protein kinase kinase β. *Molecular and cellular biology,* 26**,** 5933-5945.

Stahmann, N., Woods, A., Spengler, K., Heslegrave, A., Bauer, R., Krause, S., Viollet, B., Carling, D. & Heller, R. 2010. Activation of AMP-activated protein kinase by vascular endothelial growth factor mediates endothelial angiogenesis independently of nitric-oxide synthase. *Journal of Biological Chemistry,* 285**,** 10638-10652.

Stanek, A., Brożyna-Tkaczyk, K. & Myśliński, W. 2021. The Role of Obesity-Induced Perivascular Adipose Tissue (PVAT) Dysfunction in Vascular Homeostasis. *Nutrients,* 13**,** 3843.

Stapleton, D., Mitchelhill, K. I., Gao, G., Widmer, J., Michell, B. J., Teh, T., House, C. M., Fernandez, C. S., Cox, T. & Witters, L. A. 1996. Mammalian AMP-activated protein kinase subfamily (∗). *Journal of Biological Chemistry,* 271**,** 611-614.

Su, Y. 2014. Regulation of endothelial nitric oxide synthase activity by protein-protein interaction. *Curr Pharm Des,* 20**,** 3514-20.

Sun, W., Lee, T.-S., Zhu, M., Gu, C., Wang, Y., Zhu, Y. & Shyy, J. Y. 2006. Statins activate AMP-activated protein kinase in vitro and in vivo. *Circulation,* 114**,** 2655-2662.

Sun, X., Meng, L., Qiao, W., Yang, R., Gao, Q., Peng, Y. & Bian, Z. 2019. Vascular endothelial growth factor A/Vascular endothelial growth factor receptor 2 axis promotes human dental pulp stem cell migration via the FAK/PI3K/Akt and p38 MAPK signalling pathways. *International Endodontic Journal,* 52**,** 1691-1703.

Sun, Y., Li, J., Xiao, N., Wang, M., Kou, J., Qi, L., Huang, F., Liu, B. & Liu, K. 2014. Pharmacological activation of AMPK ameliorates perivascular adipose/endothelial dysfunction in a manner interdependent on AMPK and SIRT1. *Pharmacological Research,* 89**,** 19-28.

Sunaga, H., Koitabashi, N., Iso, T., Matsui, H., Obokata, M., Kawakami, R., Murakami, M., Yokoyama, T. & Kurabayashi, M. 2019. Activation of

cardiac AMPK-FGF21 feed-forward loop in acute myocardial infarction: Role of adrenergic overdrive and lipolysis byproducts. *Scientific reports,* 9**,** 1-13.

Suzuki, M., Uehara, Y., Motomura-Matsuzaka, K., Oki, J., Koyama, Y., Kimura, M., Asada, M., Komi-Kuramochi, A., Oka, S. & Toru, T. 2008. βKlotho is required for fibroblast growth factor (FGF) 21 signaling through FGF receptor (FGFR) 1c and FGFR3c. *Molecular endocrinology,* 22**,** 1006-1014.

Szasz, T., Bomfim, G. F. & Webb, R. C. 2013. The influence of perivascular adipose tissue on vascular homeostasis. *Vasc Health Risk Manag,* 9**,** 105-16.

Szasz, T. & Webb, R. C. 2012. Perivascular adipose tissue: more than just structural support. *Clinical science,* 122**,** 1-12.

Thengchaisri, N. & Kuo, L. 2003. Hydrogen peroxide induces endothelium-dependent and -independent coronary arteriolar dilation: role of cyclooxygenase and potassium channels. *Am J Physiol Heart Circ Physiol,* 285**,** H2255-63.

Thors, B., Halldórsson, H. & Thorgeirsson, G. 2011. eNOS activation mediated by AMPK after stimulation of endothelial cells with histamine or thrombin is dependent on LKB1. *Biochim Biophys Acta,* 1813**,** 322-31.

Touyz, R. M., Alves-Lopes, R., Rios, F. J., Camargo, L. L., Anagnostopoulou, A., Arner, A. & Montezano, A. C. 2018. Vascular smooth muscle contraction in hypertension. *Cardiovascular Research,* 114**,** 529-539.

Towler, M. C. & Hardie, D. G. 2007. AMP-activated protein kinase in metabolic control and insulin signaling. *Circ Res,* 100**,** 328-41.

Valentini, A., Cardillo, C., Della Morte, D. & Tesauro, M. 2023. The Role of Perivascular Adipose Tissue in the Pathogenesis of Endothelial Dysfunction in Cardiovascular Diseases and Type 2 Diabetes Mellitus. *Biomedicines,* 11.

Van Dam, A. D., Boon, M. R., Berbée, J. F. P., Rensen, P. C. N. & Van Harmelen, V. 2017. Targeting white, brown and perivascular adipose tissue in atherosclerosis development. *Eur J Pharmacol,* 816**,** 82-92.

Vecchione, C., Maffei, A., Colella, S., Aretini, A., Poulet, R., Frati, G., Gentile, M. T., Fratta, L., Trimarco, V. & Trimarco, B. 2002. Leptin effect on endothelial nitric oxide is mediated through Akt–endothelial nitric oxide synthase phosphorylation pathway. *Diabetes,* 51**,** 168-173.

Véniant, M. M., Hale, C., Helmering, J., Chen, M. M., Stanislaus, S., Busby, J., Vonderfecht, S., Xu, J. & Lloyd, D. J. 2012a. FGF21 promotes metabolic homeostasis via white adipose and leptin in mice. *PLoS One,* 7**,** e40164.

Véniant, M. M., Komorowski, R., Chen, P., Stanislaus, S., Winters, K., Hager, T., Zhou, L., Wada, R., Hecht, R. & Xu, J. 2012b. Long-acting FGF21 has enhanced efficacy in diet-induced obese mice and in obese rhesus monkeys. *Endocrinology,* 153**,** 4192-4203.

Verlohren, S., Dubrovska, G., Tsang, S.-Y., Essin, K., Luft, F. C., Huang, Y. & Gollasch, M. 2004. Visceral periadventitial adipose tissue regulates arterial tone of mesenteric arteries. *Hypertension,* 44**,** 271-276.

Victorio, J. A., Fontes, M. T., Rossoni, L. V. & Davel, A. P. 2016. Different anti-contractile function and nitric oxide production of thoracic and abdominal perivascular adipose tissues. *Frontiers in physiology,* 7**,** 295.

Villacorta, L. & Chang, L. 2015. The role of perivascular adipose tissue in vasoconstriction, arterial stiffness, and aneurysm. *Horm Mol Biol Clin Investig,* 21**,** 137-47.

Wang, J., Alexanian, A., Ying, R., Kizhakekuttu, T. J., Dharmashankar, K., Vasquez-Vivar, J., Gutterman, D. D. & Widlansky, M. E. 2012. Acute

exposure to low glucose rapidly induces endothelial dysfunction and mitochondrial oxidative stress: role for AMP kinase. *Arterioscler Thromb Vasc Biol,* 32, 712-20.

Wang, L., Cheng, C. K., Yi, M., Lui, K. O. & Huang, Y. 2022. Targeting endothelial dysfunction and inflammation. *J Mol Cell Cardiol,* 168, 58-67.

Wang, P., Xu, T.-Y., Guan, Y.-F., Su, D.-F., Fan, G.-R. & Miao, C.-Y. 2009. Perivascular adipose tissue-derived visfatin is a vascular smooth muscle cell growth factor: role of nicotinamide mononucleotide. *Cardiovascular research,* 81, 370-380.

Wang, S., Zhang, M., Liang, B., Xu, J., Xie, Z., Liu, C., Viollet, B., Yan, D. & Zou, M. H. 2010. AMPKalpha2 deletion causes aberrant expression and activation of NAD(P)H oxidase and consequent endothelial dysfunction in vivo: role of 26S proteasomes. *Circ Res,* 106, 1117-28.

Wang, X.-M., Song, S.-S., Xiao, H., Gao, P., Li, X.-J. & Si, L.-Y. 2014. Fibroblast growth factor 21 protects against high glucose induced cellular damage and dysfunction of endothelial nitric-oxide synthase in endothelial cells. *Cellular physiology and biochemistry,* 34, 658-671.

Watts, S. W., Dorrance, A. M., Penfold, M. E., Rourke, J. L., Sinal, C. J., Seitz, B., Sullivan, T. J., Charvat, T. T., Thompson, J. M. & Burnett, R. 2013. Chemerin connects fat to arterial contraction. *Arteriosclerosis, thrombosis, and vascular biology,* 33, 1320-1328.

Weston, A., Egner, I., Dong, Y., Porter, E., Heagerty, A. & Edwards, G. 2013. Stimulated release of a hyperpolarizing factor (ADHF) from mesenteric artery perivascular adipose tissue: involvement of myocyte BKCa channels and adiponectin. *British journal of pharmacology,* 169, 1500-1509.

Willows, R., Navaratnam, N., Lima, A., Read, J. & Carling, D. 2017. Effect of different γ-subunit isoforms on the regulation of AMPK. *Biochem J,* 474, 1741-1754.

Woods, A., Dickerson, K., Heath, R., Hong, S. P., Momcilovic, M., Johnstone, S. R., Carlson, M. & Carling, D. 2005. Ca2+/calmodulin-dependent protein kinase kinase-beta acts upstream of AMP-activated protein kinase in mammalian cells. *Cell Metab,* 2, 21-33.

Wu, F., Wang, B., Zhang, S., Shi, L., Wang, Y., Xiong, R., Pan, X., Gong, F., Li, X. & Lin, Z. 2017. FGF21 ameliorates diabetic cardiomyopathy by activating the AMPK-paraoxonase 1 signaling axis in mice. *Clinical Science,* 131, 1877-1893.

Wu, J., Kong, M., Lou, Y., Li, L., Yang, C., Xu, H., Cui, Y., Hao, H. & Liu, Z. 2021. Simultaneous activation of Erk1/2 and Akt signaling is critical for formononetin-induced promotion of endothelial function. *Frontiers in Pharmacology,* 11, 608518.

Wu, X., Lü, Y., Fu, K., Wang, S., Zhao, D., Peng, H., Fan, Q., Lü, Y., Xin, M. & Liu, J. 2014. [Impact of exogenous fibroblast growth factor 21 on atherosclerosis in apolipoprotein E deficient mice]. *Zhonghua Xin Xue Guan Bing Za Zhi,* 42, 126-31.

Xia, N., Horke, S., Habermeier, A., Closs, E. I., Reifenberg, G., Gericke, A., Mikhed, Y., Münzel, T., Daiber, A. & Förstermann, U. 2016. Uncoupling of endothelial nitric oxide synthase in perivascular adipose tissue of diet-induced obese mice. *Arteriosclerosis, thrombosis, and vascular biology,* 36, 78-85.

Xia, N. & Li, H. 2017. The role of perivascular adipose tissue in obesity-induced vascular dysfunction. *British journal of pharmacology,* 174, 3425-3442.

Xiao, B., Sanders, M. J., Carmena, D., Bright, N. J., Haire, L. F., Underwood, E., Patel, B. R., Heath, R. B., Walker, P. A., Hallen, S., Giordanetto, F., Martin, S. R., Carling, D. & Gamblin, S. J. 2013. Structural basis of AMPK regulation by small molecule activators. *Nat Commun,* 4**,** 3017.

Xiao, Y., Liu, L., Xu, A., Zhou, P., Long, Z., Tu, Y., Chen, X., Tang, W., Huang, G. & Zhou, Z. 2015. Serum fibroblast growth factor 21 levels are related to subclinical atherosclerosis in patients with type 2 diabetes. *Cardiovascular diabetology,* 14**,** 1-8.

Xie, Z., Dong, Y., Zhang, M., Cui, M. Z., Cohen, R. A., Riek, U., Neumann, D., Schlattner, U. & Zou, M. H. 2006. Activation of protein kinase C zeta by peroxynitrite regulates LKB1-dependent AMP-activated protein kinase in cultured endothelial cells. *J Biol Chem,* 281**,** 6366-75.

Yamauchi, T. & Kadowaki, T. 2008. Physiological and pathophysiological roles of adiponectin and adiponectin receptors in the integrated regulation of metabolic and cardiovascular diseases. *International journal of obesity,* 32**,** S13-S18.

Yamauchi, T., Kamon, J., Minokoshi, Y., Ito, Y., Waki, H., Uchida, S., Yamashita, S., Noda, M., Kita, S., Ueki, K., Eto, K., Akanuma, Y., Froguel, P., Foufelle, F., Ferre, P., Carling, D., Kimura, S., Nagai, R., Kahn, B. B. & Kadowaki, T. 2002. Adiponectin stimulates glucose utilization and fatty-acid oxidation by activating AMP-activated protein kinase. *Nat Med,* 8**,** 1288-95.

Yan, X., Gou, Z., Li, Y., Wang, Y., Zhu, J., Xu, G. & Zhang, Q. 2018. Fibroblast growth factor 21 inhibits atherosclerosis in apoE−/− mice by ameliorating Fas-mediated apoptosis. *Lipids in health and disease,* 17**,** 1-8.

Yang, S. & Wang, J. 2015. Estrogen Activates AMP-Activated Protein Kinase in Human Endothelial Cells via ERß/Ca(2+)/Calmodulin-Dependent Protein Kinase Kinase ß Pathway. *Cell Biochem Biophys,* 72**,** 701-7.

Yap, Z. J., Sharif, M. & Bashir, M. 2021. Is there an immunogenomic difference between thoracic and abdominal aortic aneurysms? *Journal of Cardiac Surgery,* 36**,** 1520-1530.

Yie, J., Wang, W., Deng, L., Tam, L. T., Stevens, J., Chen, M. M., Li, Y., Xu, J., Lindberg, R. & Hecht, R. 2012. Understanding the Physical Interactions in the FGF21/FGFR/ß-Klotho Complex: Structural Requirements and Implications in FGF21 Signaling. *Chemical biology & drug design,* 79**,** 398-410.

Ying, L., Li, N., He, Z., Zeng, X., Nan, Y., Chen, J., Miao, P., Ying, Y., Lin, W. & Zhao, X. 2019. Fibroblast growth factor 21 Ameliorates diabetes-induced endothelial dysfunction in mouse aorta via activation of the CaMKK2/AMPKα signaling pathway. *Cell death & disease,* 10**,** 665.

Yu, J. W., Deng, Y. P., Han, X., Ren, G. F., Cai, J. & Jiang, G. J. 2016. Metformin improves the angiogenic functions of endothelial progenitor cells via activating AMPK/eNOS pathway in diabetic mice. *Cardiovasc Diabetol,* 15**,** 88.

Yudkin, J. S., Eringa, E. & Stehouwer, C. D. 2005. "Vasocrine" signalling from perivascular fat: a mechanism linking insulin resistance to vascular disease. *Lancet,* 365**,** 1817-20.

Zhang, C., Huang, Z., Gu, J., Yan, X., Lu, X., Zhou, S., Wang, S., Shao, M., Zhang, F. & Cheng, P. 2015. Fibroblast growth factor 21 protects the heart from apoptosis in a diabetic mouse model via extracellular signal-regulated kinase 1/2-dependent signalling pathway. *Diabetologia,* 58**,** 1937-1948.

Zhang, M., Dong, Y., Xu, J., Xie, Z., Wu, Y., Song, P., Guzman, M., Wu, J. & Zou, M.-H. 2008a. Thromboxane receptor activates the AMP-activated protein kinase in vascular smooth muscle cells via hydrogen peroxide. *Circulation research,* 102**,** 328-337.

Zhang, X., Yeung, D. C., Karpisek, M., Stejskal, D., Zhou, Z.-G., Liu, F., Wong, R. L., Chow, W.-S., Tso, A. W. & Lam, K. S. 2008b. Serum FGF21 levels are increased in obesity and are independently associated with the metabolic syndrome in humans. *Diabetes,* 57**,** 1246-1253.

Zhang, Y., Lee, T. S., Kolb, E. M., Sun, K., Lu, X., Sladek, F. M., Kassab, G. S., Garland, T., Jr. & Shyy, J. Y. 2006. AMP-activated protein kinase is involved in endothelial NO synthase activation in response to shear stress. *Arterioscler Thromb Vasc Biol,* 26**,** 1281-7.

Zhang, Y., Liu, D., Long, X.-X., Fang, Q.-C., Jia, W.-P. & Li, H.-T. 2021. The role of FGF21 in the pathogenesis of cardiovascular disease. *Chinese Medical Journal,* 134**,** 2931-2943.

Zhao, L., Fu, Z., Wu, J., Aylor, K. W., Barrett, E. J., Cao, W. & Liu, Z. 2015a. Globular adiponectin ameliorates metabolic insulin resistance via AMPK-mediated restoration of microvascular insulin responses. *J Physiol,* 593**,** 4067-79.

Zhao, Y., Vanhoutte, P. M. & Leung, S. W. 2015b. Vascular nitric oxide: Beyond eNOS. *J Pharmacol Sci,* 129**,** 83-94.

Zhou, L., Deepa, S. S., Etzler, J. C., Ryu, J., Mao, X., Fang, Q., Liu, D. D., Torres, J. M., Jia, W., Lechleiter, J. D., Liu, F. & Dong, L. Q. 2009. Adiponectin activates AMP-activated protein kinase in muscle cells via APPL1/LKB1-dependent and phospholipase C/Ca2+/Ca2+/calmodulin-dependent protein kinase kinase-dependent pathways. *J Biol Chem,* 284**,** 22426-22435.

Zhu, W., Wang, C., Liu, L., Li, Y., Li, X., Cai, J. & Wang, H. 2014. Effects of fibroblast growth factor 21 on cell damage in vitro and atherosclerosis in vivo. *Canadian journal of physiology and pharmacology,* 92**,** 927-935.

Zippel, N., Loot, A. E., Stingl, H., Randriamboavonjy, V., Fleming, I. & Fisslthaler, B. 2018. Endothelial AMP-Activated Kinase α1 Phosphorylates eNOS on Thr495 and Decreases Endothelial NO Formation. *Int J Mol Sci,* 19.

Zou, M. H. & Wu, Y. 2008. AMP-activated protein kinase activation as a strategy for protecting vascular endothelial function. *Clinical and Experimental Pharmacology and Physiology,* 35**,** 535-545.